

NIST GCR 14-917-25



Recommendations for Seismic Design of Reinforced Concrete Wall Buildings Based on Studies of the 2010 Maule, Chile Earthquake

NEHRP Consultants Joint Venture
*A partnership of the Applied Technology Council and the
Consortium of Universities for Research in Earthquake Engineering*



NIST
National Institute of
Standards and Technology
U.S. Department of Commerce

Disclaimers

This report was prepared for the Engineering Laboratory of the National Institute of Standards and Technology (NIST) under the National Earthquake Hazards Reduction Program (NEHRP) Earthquake Structural and Engineering Research Contract SB134107CQ0019, Task Order 10303. The contents of this publication do not necessarily reflect the views and policies of NIST or the U.S. Government.

This report was produced by the NEHRP Consultants Joint Venture, a joint venture of the Applied Technology Council (ATC) and the Consortium of Universities for Research in Earthquake Engineering (CUREE). While endeavoring to provide practical and accurate information, the NEHRP Consultants Joint Venture, the authors, and the reviewers assume no liability for, nor express or imply any warranty with regard to, the information contained herein. Users of information contained in this report assume all liability arising from such use.

Unless otherwise noted, photos, figures, and data presented in this report have been developed or provided by NEHRP Consultants Joint Venture staff or consultants engaged under contract to provide information as works for hire. Any similarity with other published information is coincidental. Photos and figures cited from outside sources have been reproduced in this report with permission. Any other use requires additional permission from the copyright owners.

NEHRP Consultants Joint Venture has made substantial efforts to obtain permissions for all copyright-protected images, drawings, text, and figures in this report. Materials available in this report that do not have a copyright attribution may nonetheless be protected by copyrights owned by private individuals or organizations, and may be subject to restrictions on use. Where known by NEHRP Consultants Joint Venture, the copyright owner is identified with the image. The reader may want to obtain legal advice prior to further dissemination.

Certain commercial software, equipment, instruments, or materials may have been used in the preparation of information contributing to this report. Identification in this report is not intended to imply recommendation or endorsement by NIST, nor is it intended to imply that such software, equipment, instruments, or materials are necessarily the best available for the purpose.

NIST policy is to use the International System of Units (metric units) in all its publications. In this report, however, information is presented in both metric units and U.S. Customary Units (inch-pound), as the inch-pound system is the preferred system of units in the U.S. earthquake engineering industry.

Cover illustration – Cracking, spalling, crushing, and bar buckling in a reinforced concrete shear wall of a building located in Viña del Mar, Chile (photo courtesy of Patricio Bonelli).

NIST GCR 14-917-25

Recommendations for Seismic Design of Reinforced Concrete Wall Buildings Based on Studies of the 2010 Maule, Chile Earthquake

Prepared for
*U.S. Department of Commerce
National Institute of Standards and Technology
Engineering Laboratory
Gaithersburg, MD 20899*

By
NEHRP Consultants Joint Venture
*A partnership of the Applied Technology Council and the
Consortium of Universities for Research in Earthquake Engineering*

March 2014



U.S. Department of Commerce
Penny Pritzker, Secretary

National Institute of Standards and Technology
*Patrick D. Gallagher, Under Secretary of Commerce
for Standards and Technology and Director*

Participants

National Institute of Standards and Technology

John (Jack) R. Hayes, Jr., Director, National Earthquake Hazards Reduction Program
Steven L. McCabe, Deputy Director, National Earthquake Hazards Reduction Program
www.NEHRP.gov

NEHRP Consultants Joint Venture

Applied Technology Council
201 Redwood Shores Parkway, Suite 240
Redwood City, California 94065
www.ATCouncil.org

Consortium of Universities for
Research in Earthquake Engineering
1301 S. 46th Street, Building 420
Richmond, California 94804
www.CUREE.org

Joint Venture Management Committee

James R. Harris
Robert Reitherman
Christopher Rojahn
Andrew Whittaker

Joint Venture Program Committee

Jon A. Heintz (Program Manager)
Michael Constantinou
C.B. Crouse
James R. Harris
William T. Holmes
Jack Moehle
Andrew Whittaker

Project Technical Committee

Joseph Maffei (Project Director)
Patricio Bonelli
Dominic J. Kelly
Dawn E. Lehman
Laura N. Lowes
Jack Moehle
Karl Telleen
John W. Wallace
Michael Willford

Project Review Panel

S.K. Ghosh
Tara Hutchinson
Derrick Roorda
Meté Sozen

Working Group Members

Begoña Aguirre
Ady Aviram
Anna Birely
Chris Hilson
Yuli Huang
Pablo Parra

Preface

The NEHRP Consultants Joint Venture is a partnership between the Applied Technology Council (ATC) and the Consortium of Universities for Research in Earthquake Engineering (CUREE). In 2007, the National Institute of Standards and Technology (NIST) awarded the NEHRP Consultants Joint Venture a National Earthquake Hazards Reduction Program (NEHRP) “Earthquake Structural and Engineering Research” task order contract (SB1341-07-CQ-0019) to conduct a variety of tasks. On February 27, 2010, a magnitude 8.8 earthquake occurred off the coast near the Maule region of central Chile. In September 2010, NIST initiated Task Order 10303 entitled “Analysis of Seismic Performance of Reinforced Concrete Buildings in the 2010 Chile Earthquake.”

Most mid-rise and high-rise buildings in the earthquake-affected regions were constructed with seismic-force-resisting systems consisting of reinforced concrete structural walls. Similar construction is also prevalent in regions of high seismicity in the Western United States. In response to the earthquake, several U.S. organizations sent reconnaissance teams to Chile to gather information that could be used to study implications for U.S. design and construction practice. The purpose of this project was to evaluate critical issues in the performance of reinforced concrete wall structures in the 2010 Maule earthquake, and to develop recommendations for improved shear wall design requirements for incorporation into U.S. practice.

Work on this project involved: (1) the collection of available reconnaissance information to identify trends in concrete building performance; (2) the conduct of focused studies on key issues including bar buckling and concrete crushing in wall boundary elements, overall wall buckling behaviors, discontinuities in building configuration, and advanced simulation techniques for concrete walls; and (3) interpretation of results for improvement in U.S. practice. In a separate project, NIST commissioned a study comparing U.S. and Chilean building codes and construction practices. Results are contained in NIST GCR 12-917-18, *Comparison of U.S. and Chilean Building Code Requirements and Seismic Design Practice 1985-2010* (NIST, 2012), and are intended to provide context for interpretation of findings and recommendations presented herein.

The NEHRP Consultants Joint Venture is indebted to the leadership of Joe Maffei, Project Director, and to the members of the Project Technical Committee, consisting of Patricio Bonelli, Dominic Kelly, Dawn Lehman, Laura Lowes, Jack Moehle, Karl Telleen, John Wallace, and Michael Willford, for their planning, conduct, and

oversight of the work. This report and the resulting recommendations are based on problem-focused analytical studies that were conducted by Begoña Aguirre, Ady Aviram, Anna Birely, Chris Hilson, Yuli Huang, and Pablo Parra under the direction of the Project Technical Committee. Technical review and comment at key developmental stages of the project were provided by the Project Review Panel consisting of S.K. Ghosh, Tara Hutchinson, Derrick Roorda, and Mete Sozen. The names and affiliations of all who contributed to this project are included in the list of Project Participants at the end of this report.

NEHRP Consultants Joint Venture also gratefully acknowledges Jack Hayes (Director, NEHRP), and Steve McCabe (Deputy Director, NEHRP), for their input and guidance in the conduct of this work, Ayse Hortacsu (ATC Associate Director of Projects) for assistance in the preparation of this report, and Amber Houchen for ATC report production services.

Jon A. Heintz
Program Manager

Table of Contents

Preface	v
List of Figures	xiii
List of Tables.....	xxvii
1. Introduction	1-1
1.1 Background and Objectives	1-1
1.2 Chilean Seismic Design and Construction Practice	1-2
1.2.1 Chilean Seismic Design Standards	1-2
1.2.2 Chilean Design Practice.....	1-3
1.3 The 2010 Maule Earthquake.....	1-4
1.3.1 Strong-Motion Recordings	1-5
1.4 Observed Performance of Buildings.....	1-8
1.5 Project Approach and Problem-Focused Studies.....	1-10
1.5.1 Case Study Buildings.....	1-11
1.5.2 Study Area 1: Investigation of Wall Boundary Elements	1-12
1.5.3 Study Area 2: Investigation of Overall Wall Buckling....	1-13
1.5.4 Study Area 3: Investigation of Building Configuration.....	1-13
1.5.5 Study Area 4: Analysis and Advanced Simulation of Reinforced Concrete Wall Behavior.....	1-13
1.6 Report Organization and Content	1-13
2. Investigation of Wall Boundary Elements	2-1
2.1 Description of Observed Damage to Wall Boundary Elements.....	2-1
2.2 Relevant U.S. Code Requirements and Design Practice.....	2-3
2.3 Comparison of ACI 318 Special Boundary Element Requirements and Observed Building Damage	2-4
2.3.1 Approach.....	2-4
2.3.2 Results.....	2-5
2.3.3 Potential Changes to ACI 318 Boundary Element Triggers.....	2-6
2.4 Investigation of Plastic Hinge Length.....	2-7
2.4.1 Potential Changes to ACI 318 Plastic Hinge Length, Minimum Thickness, and Confinement Requirements....	2-10
2.5 Investigation of Longitudinal Bar Buckling in Wall Boundary Elements.....	2-12
2.5.1 Approach.....	2-12
2.5.2 Results.....	2-12
2.6 Potential Changes to ACI 318 Special Boundary Element Detailing Requirements	2-14

2.6.1	Changes to Required Area of Transverse Reinforcement	2-15
2.6.2	Changes to Horizontal Spacing of Ties	2-17
2.7	Findings and Recommendations	2-19
3.	Investigation of Overall Wall Buckling	3-1
3.1	Description of Overall Wall Buckling Behavior	3-1
3.2	Relevant U.S. Code Requirements and Design Practice	3-2
3.3	Theoretical Model for Wall Instability	3-3
3.4	Comparison of Theoretical Wall Instability Model and Observed Building Damage	3-5
3.4.1	Alto Huerto Building	3-5
3.4.2	Undisclosed Building B	3-10
3.5	Findings and Recommendations	3-13
4.	Investigation of Building Configuration Issues	4-1
4.1	Description of Observed Damage due to Building Configuration Issues	4-1
4.2	Relevant U.S. Code Requirements and Design Practice	4-7
4.3	Investigation of Walls Above or Below Vertically Aligned Openings	4-9
4.3.1	Characteristic Design Practice and Observed Damage	4-9
4.3.2	Local Stress Distribution	4-11
4.3.3	Case Study Buildings	4-13
4.3.4	Findings and Recommendations	4-13
4.4	Investigation of Vertical Discontinuities	4-14
4.4.1	Case Study Buildings	4-15
4.4.2	Summary of Observed Damage	4-15
4.4.3	ASCE/SEI 31-03 Tier 1 Evaluations	4-16
4.4.4	Summary of Tier 1 Evaluation Results	4-19
4.4.5	ASCE/SEI 31-03 Tier 2 Evaluations	4-19
4.4.6	Summary of Tier 2 Evaluation Results	4-27
4.4.7	ASCE/SEI 31-03 Tier 3 Evaluations	4-27
4.4.8	Summary of Tier 3 Evaluation Results	4-35
4.4.9	Study of Coupled Wall Response	4-35
4.4.10	Study of Local Wall Discontinuities	4-40
4.5	Investigation of Pier-Spandrel Systems	4-41
4.5.1	Approach	4-41
4.5.2	Findings and Recommendations	4-42
5.	Analytical Modeling of Concrete Wall Buildings	5-1
5.1	Approaches for Analytical Modeling of Concrete Wall Buildings	5-1
5.1.1	Shell Elements	5-1
5.1.2	Beam Elements	5-2
5.1.3	Damping	5-2
5.2	Calibration of Analysis Models Based on Experimental Tests	5-3
5.2.1	Simulation of Overall Wall Buckling	5-3
5.2.2	Studies on Reinforcement Buckling	5-4
5.2.3	Simulation of Walls with Boundary Elements	5-8
5.3	Modeling Case Study of the Alto Rio Building	5-12

5.3.1	LS-DYNA Model Using Shell Elements	5-14
5.3.2	Nonlinear Seismic Response Analyses	5-15
5.4	Other Analyses of the Alto Rio Building	5-22
5.4.1	Tuna and Wallace (2014).....	5-22
5.5	Findings and Recommendations	5-24
6.	Summary of Findings and Recommendations	6-1
6.1	Overview	6-1
6.2	Wall Boundary Element Studies	6-2
6.2.1	Findings	6-2
6.2.2	Recommendations.....	6-3
6.3	Overall Wall Buckling Studies	6-4
6.3.1	Findings	6-4
6.3.2	Recommendations.....	6-5
6.4	Building Configuration Studies	6-5
6.4.1	Findings	6-6
6.4.2	Recommendations.....	6-7
6.5	Analytical Modeling Studies.....	6-9
6.5.1	Findings and Recommendations	6-10
6.6	Recommendations for Further Study	6-11
Appendix A:	Wall Boundary Element Studies	A-1
A.1	Building Descriptions	A-1
A.1.1	Alto Rio (Building No. 1).....	A-2
A.1.2	Plaza del Rio Building B (Building No. 2).....	A-4
A.1.3	Concepto Urbano (Building No. 3).....	A-6
A.1.4	Toledo (Building No. 4).....	A-7
A.1.5	Undisclosed Building A (Building No. 5)	A-9
A.1.6	Undisclosed Building B (Building No. 6).....	A-11
A.1.7	Mongolio (Building No. 7)	A-13
A.1.8	Gravity Load Calculations	A-14
A.1.9	Material Properties.....	A-16
A.3	Estimation of Building Displacements	A-17
A.3.1	Nearby Recording Stations	A-18
A.3.2	Building Period Estimates and Spectral Displacement Results.....	A-20
A.4	ACI 318 Special Boundary Element Trigger Checks	A-24
A.4.1	Moment-Curvature Neutral Axis Depth Results.....	A-24
A.5	Review of Plastic Hinge Lengths.....	A-28
A.5.1	Literature Review	A-28
A.6	Longitudinal Bar Buckling Assessments	A-29
A.6.1	Criterion for Bar Buckling Assessment	A-30
A.6.2	Assessment of Bar Buckling at Wall Boundaries in Chilean Buildings	A-31
A.6.3	Building-Specific Results	A-34
A.6.4	Calibration of Bar Buckling Approach with Past Experimental Test Results	A-52
Appendix B:	Derivation of Overall Wall Buckling Relationships	B-1
B.1	Derivation of Theoretical Model for Wall Instability	B-1
B.2	Comparison of Theoretical Model and Laboratory Tests	B-4

B.3	Comparison of Theoretical Model to Wall Thickness Requirements in Codes and Standards	B-6
Appendix C: Study of Solid Walls Above or Below Vertically Aligned Openings..... C-1		
C.1	Introduction	C-1
C.2	Simulation of Response in Discontinuity Region	C-4
C.3	Calculation of Shear Stress in Discontinuity Region	C-7
C.4	Comparison of Shear Demand and Capacity in Discontinuity Region	C-10
C.4.1	Findings.....	C-11
C.4.2	Discussion	C-13
Appendix D: Study of Vertical Discontinuities..... D-1		
D.1	Building Descriptions.....	D-1
D.1.1	Plaza del Rio Building A.....	D-2
D.1.2	Plaza del Rio Building B.....	D-3
D.1.3	Centro Mayor	D-4
D.1.4	Alto Huerto.....	D-7
D.1.5	Concepto Urbano	D-7
D.2	ASCE/SEI 31-03 Tier 1 Evaluations.....	D-8
D.2.1	Summary of Tier 1 Evaluation Results	D-9
D.3	ASCE/SEI 31-03 Tier 2 Evaluations.....	D-10
D.3.1	Summary of Tier 2 Evaluation Results	D-10
D.4	ASCE/SEI 31-03 Tier 3 Evaluations.....	D-19
D.4.1	Nonlinear Modeling and Analysis.....	D-20
D.4.2	OpenSees Nonlinear Analysis Model	D-22
D.4.3	PERFORM-3D Nonlinear Analysis Models	D-23
D.4.4	Analysis Results	D-30
D.4.5	OpenSees Nonlinear Dynamic Analysis Results.....	D-31
D.4.6	PERFORM-3D Nonlinear Dynamic Analysis Results....	D-38
D.5	Investigation of Local Vertical Discontinuities in Walls	D-41
Appendix E: Study of a Pier-Spandrel System E-1		
E.1	Case Study Building.....	E-1
E.2	Identification of Controlling Behavior.....	E-2
E.3	Plastic Analysis	E-3
Appendix F: Analysis of Wall Buildings..... F-1		
F.1	Simulation of Acevedo and Moehle (2010) Tests.....	F-1
F.2	Simulation of Rodriguez et al. (1999) Tests.....	F-2
F.3	Simulation of Lowes et al. (2011) Specimen PW4	F-3
F.3.1	Model Geometry and Material Properties	F-3
F.3.2	Loading Protocol.....	F-6
F.3.3	Simulation with Bar Buckling.....	F-6
F.4	Alto Rio Building.....	F-8
F.4.1	Building Information.....	F-8
F.4.2	Material Properties	F-9
F.4.3	Ground Motions	F-10
F.4.4	Gravity Loads.....	F-11
F.4.5	Natural Period	F-12

F.4.6	Intrinsic Damping	F-13
F.5	Alto Rio Building Simulation Results	F-13
F.5.1	Nonlinear Analysis Results for Expected and Measured Material Properties.....	F-13
F.5.2	Simulation Results with Basement Assumptions	F-14
F.6	Other Analyses of the Alto Rio Building.....	F-15
F.6.1	Tuna and Wallace (2012).....	F-15
F.6.2	Song et al. (2012).....	F-16
F.6.3	Kohrangi et al. (2012).....	F-16
References		G-1
Project Participants		H-1

List of Figures

Figure 1-1	Typical mid-rise and high-rise buildings in Santiago, Chile	1-4
Figure 1-2	Isoseismal map of the 2010 Maule earthquake	1-5
Figure 1-3	Locations of selected RENADIC and GUC recording stations in relation to major cities and the earthquake epicenter.....	1-7
Figure 1-4	Acceleration response spectra based on recordings from RENADIC stations in the 2010 Maule earthquake.....	1-7
Figure 1-5	Concrete crushing and buckling of longitudinal reinforcement initiating at wall boundaries and propagating along the length of wall segments.....	1-8
Figure 1-6	Shear failures in vertical and horizontal wall segments.....	1-9
Figure 1-7	Overall wall buckling behavior.....	1-9
Figure 1-8	Concentrated damage at: (a) wall discontinuities; and (b) structural irregularities	1-10
Figure 1-9	Concentrated damage at: (a) coupling beams; and (b) cast-in-place concrete stair elements.....	1-10
Figure 2-1	Typical reinforced concrete shear wall damage in the 2010 Maule earthquake: (a) first subterranean level of an 18-story building in Santiago; and (b) ground floor level of a 10-story building in Viña del Mar.....	2-2
Figure 2-2	Typical detailing and observed damage to wall boundary regions: (a) ground floor level of a 23-story building in Coronel; and (b) first subterranean level of a 20-story building in Santiago	2-2
Figure 2-3	Response spectra from recent large earthquakes: (a) displacement spectra for 2010 Maule earthquake; and (b) acceleration spectra for 2011 Christchurch earthquake.	2-6
Figure 2-4	Comparison of various plastic hinge length models available in the literature	2-8
Figure 2-5	Roof drift ratio versus wall curvature relations for various plastic hinge lengths for a wall with an L-shaped cross-section	2-9
Figure 2-6	Drift ratio versus limiting concrete compressive strain for various plastic hinge lengths.....	2-9
Figure 2-7	Differences in longitudinal reinforcement strain levels at each end of a flanged wall.....	2-13

Figure 2-8	Tests on conventional reinforced concrete walls: (a) test specimen details; and (b) observed damage2-15
Figure 2-9	Effect of requiring that wall boundary elements satisfy ACI 318 Equation 21-4, illustrated for boundary elements with a length-to-thickness aspect ratio of 2:12-16
Figure 2-10	Effect of requiring that wall boundary elements satisfy ACI 318 Equation 21-4, illustrated for boundary elements with a length-to-thickness aspect ratio of 3:1, and assuming that vertical spacing of hoops is maximized.....2-17
Figure 2-11	Confinement of thin wall sections and arching action between ties2-17
Figure 2-12	Impact of reduced horizontal spacing of boundary element crossties for 2:1 aspect ratio boundary elements.....2-18
Figure 2-13	Impact of reduced horizontal spacing of boundary element crossties for 3:1 aspect ratio boundary elements.....2-18
Figure 2-14	Summary of boundary element crosstie configurations for 2:1 and 3:1 aspect ratio boundary elements with maximum horizontal spacing taken as the smaller of one wall thickness or 14 inches...2-19
Figure 3-1	Examples of overall wall lateral buckling from the 2010 Maule earthquake: (a) Alto Huerto building, Concepción; and (b) Undisclosed Building B, Santiago 3-2
Figure 3-2	Lateral instability of wall boundary that has been previously yielded in tension3-4
Figure 3-3	Critical slenderness ratio as a function of maximum tensile strain3-5
Figure 3-4	Alto Huerto building: (a) East elevation; and (b) wall crushing and apparent wall buckling along Line Ñ3-6
Figure 3-5	Alto Huerto building – typical floor plans3-7
Figure 3-6	Ground acceleration and response spectra from the Concepción-San Pedro de la Paz recording station3-7
Figure 3-7	Alto Huerto building – wall Line Ñ elevation, cross-section, and nonlinear analysis models3-8
Figure 3-8	Alto Huerto building – wall Line K elevation and cross-section3-10
Figure 3-9	Undisclosed Building B: (a) exterior elevations; and (b) wall buckling in the first subterranean level along transverse Line O.....3-11
Figure 3-10	Undisclosed Building B – typical floor plan3-11
Figure 3-11	Undisclosed Building B – elevation of wall Line O3-12

Figure 3-12	Ground acceleration and response spectra from the Santiago-Centro recording station.....	3-12
Figure 4-1	Wall configuration issues associated with observed damage in Chile.....	4-1
Figure 4-2	Photograph and sketch of damage below stacked openings where coupled walls above frame into solid wall below at the Centro Mayor building, Concepción	4-2
Figure 4-3	Earthquake damage photographs illustrating a geometric wall discontinuity at the Centro Mayor building, Concepción	4-3
Figure 4-4	Earthquake damage photographs illustrating a geometric wall discontinuity at the Rio Petrohue building, Viña del Mar	4-3
Figure 4-5	Earthquake damage photographs illustrating a geometric discontinuity and geometry change resulting in a wall partially supported on a column in the Centro Mayor building, Concepción	4-3
Figure 4-6	Sketch of building section, including the region shown in Figure 4-5, showing location and severity of damage	4-4
Figure 4-7	Three-dimensional sketch of a wall configuration illustrating geometry change resulting in a wall partially supported on a column at the location of damage shown in Figure 4-5.....	4-4
Figure 4-8	Photographs of damage at discontinuities in Z-shaped walls at the south end of Plaza del Rio Building A.....	4-5
Figure 4-9	Sketch of damaged region in Plaza del Rio Building A	4-5
Figure 4-10	Photographs of the damaged section illustrated in Figure 4-9 at wall discontinuity in Plaza del Rio Building A.....	4-6
Figure 4-11	Two examples showing termination of reinforcement: (a) photograph of damage in a reinforced concrete beam at the face of a connection where lap splices were used in the plastic hinge region of the beam; and (b) wall elevation showing termination of boundary element reinforcement in the O'Higgins building in Concepción.....	4-6
Figure 4-12	Damage observed at non-seismic force-resisting components such as stairs, indicating the possibility of coupling of seismic force-resisting components by non-seismic force-resisting components	4-7
Figure 4-13	Photograph of damage to the O'Higgins building, Concepción. Damage was attributed, in part, to vertical discontinuities in the building configuration.....	4-7
Figure 4-14	Coupled walls with a vertically aligned stack of openings terminating in a solid wall panel above and below	4-9

Figure 4-15	Typical reinforcement layout around stacks of openings terminating in a solid wall, Torre Mayor building, Chillán	4-10
Figure 4-16	Damage observed in a solid wall panel above a stack of openings in the Torre Mayor building, Chillán	4-10
Figure 4-17	Damage observed in a solid wall panel below a stack of openings in the Torre Mayor building, Chillán	4-11
Figure 4-18	Assumed panel zone forces in walls below stacks of vertically aligned openings.....	4-12
Figure 4-19	Recommended details for reinforcement in wall panels beneath stacks of vertically aligned openings in coupled walls	4-14
Figure 4-20	Exterior elevation and typical floor plan of Plaza del Rio Buildings A and B	4-17
Figure 4-21	Layout of walls in the lower two stories of Plaza del Rio Building A.....	4-18
Figure 4-22	Response spectra used in Tier 2 analyses.....	4-21
Figure 4-23	Maximum DCR_u values in first story walls of Plaza del Rio Building A.....	4-22
Figure 4-24	Controlling mechanisms in first story walls of Plaza del Rio Building A.....	4-23
Figure 4-25	Tier 2 evaluation results for first story walls in Plaza del Rio Building A subjected to the Concepción ground motion record.....	4-25
Figure 4-26	Number of walls in Plaza del Rio Building A that meet (or do not meet) various performance categories.....	4-26
Figure 4-27	Shear failures in first and second story walls of Plaza del Rio Building A, as predicted using OpenSees, Perform Basic, and Perform SSI models	4-31
Figure 4-28	Tier 3 evaluation results for first story walls in Plaza del Rio Building A subjected to the Concepción ground motion record.....	4-33
Figure 4-29	Number of walls in Plaza del Rio Building A meeting (or exceeding) acceptance criteria for different performance measures and different models.....	4-34
Figure 4-30	Idealized load distribution in a coupled wall system	4-36
Figure 4-31	Damage to coupling beam in the Centro Mayor building, Concepción.....	4-36
Figure 4-32	Ratio of maximum axial compression (gravity plus seismic) to gravity load in the walls of Plaza del Rio Building A, calculated using elastic analysis.....	4-38

Figure 4-33	Maximum axial compression (gravity plus seismic) as a percentage of axial strength in the walls of Plaza del Rio Building A, calculated using elastic analysis.....	4-38
Figure 4-34	Maximum axial compression (gravity plus seismic) as a percentage of axial strength in the walls of Plaza del Rio Building A, calculated using nonlinear analysis for the unscaled Concepción record	4-39
Figure 4-35	Illustration of local wall discontinuities.....	4-40
Figure 5-1	Displaced shape of wall: (a) at end of test; (b) in simulation; and (c) force deflection hysteresis	5-4
Figure 5-2	Comparison of predicted and experimental cyclic stress-strain in the absence of buckling.....	5-5
Figure 5-3	Simulated effect of loading history for bars with s/d ratios of 2.5 and 8.....	5-6
Figure 5-4	Axial force versus compressive strain in the boundary element components of specimen PW4.....	5-7
Figure 5-5	Total axial force versus compressive strain in the boundary element components of specimen PW4	5-7
Figure 5-6	Schematic representation of a multi-layer shell element	5-8
Figure 5-7	Comparison of specimen PW4 cyclic test and simulation results without bar buckling	5-9
Figure 5-8	Failed toe of specimen PW4 at 0.75% drift	5-10
Figure 5-9	Simulation of reinforcement cage buckling in specimen PW4.....	5-10
Figure 5-10	Comparison of specimen PW4 cyclic test and simulation results with bar buckling	5-11
Figure 5-11	Comparison of cyclic and monotonic simulation results	5-12
Figure 5-12	Alto Rio Building: (a) before the earthquake; and (b) after the earthquake.....	5-13
Figure 5-13	Alto Rio Building: (a) longitudinal section; and (b) transverse section	5-13
Figure 5-14	Plan view of LS-DYNA model slice for the Alto Rio building	5-14
Figure 5-15	LS-DYNA model showing elevations	5-14
Figure 5-16	LS-DYNA shell element model showing: (a) first floor plan; and (b) second floor plan	5-15
Figure 5-17	Vertical strain and stress distributions in the wall on Grid 13 before and after concrete crushing	5-17

Figure 5-18	Shear stress distribution in the wall on Grid 13 before and after concrete crushing.....	5-17
Figure 5-19	Total axial force in the wall on Grid 13 under uniaxial, biaxial (no vertical component), and tri-axial simulation cases.....	5-18
Figure 5-20	Roof deflection relative to ground and corresponding roof drift ratio showing period elongation prior to collapse	5-19
Figure 5-21	Shear force time-history of the wall on Grid 13.....	5-19
Figure 5-22	Moment time-history of the wall on Grid 13	5-19
Figure 5-23	Total base shear ratio history at grade level of the wall on Grid 13	5-19
Figure 5-24	Predicted damage: (a) overall view; (b) close-up of damage pattern; and (c) alternate view of damage pattern	5-20
Figure 5-25	Vertical strain and stress distributions in the wall on Grid 13 before and after concrete crushing	5-21
Figure 5-26	PERFORM-3D slice model used by Tuna and Wallace (2014)....	5-22
Figure 5-27	Roof drift ratio time-history with slabs (blue) and without slabs (green)	5-23
Figure 5-28	Base shear ratio time-history.....	5-23
Figure A-1	Alto Rio (Building No. 1) – typical floor plan with case study walls highlighted	A-2
Figure A-2	Alto Rio (Building No. 1) – longitudinal section showing floor plate reductions in the upper three stories	A-3
Figure A-3	Alto Rio (Building No. 1) – typical wall setback and discontinuous flanges in the first story	A-3
Figure A-4	Plaza del Rio Building B (Building No. 2) – typical floor plan with case study walls highlighted.....	A-5
Figure A-5	Plaza del Rio Building B (Building No. 2) – hoop reinforcement at wall boundaries.....	A-5
Figure A-6	Concepto Urbano (Building No. 3) – typical floor plans with case study walls highlighted: (a) ground through the tenth floor; and (b) eleventh floor through the roof	A-7
Figure A-7	Concepto Urbano (Building No. 3) – plan section of Wall 3.2, showing horizontal wall reinforcement detailing	A-7
Figure A-8	Toledo (Building No. 4) – typical floor plan with case study walls highlighted.....	A-8
Figure A-9	Toledo (Building No. 4) – typical setback and reduced web in the first story walls	A-8

Figure A-10	Undisclosed Building A (Building No. 5) – typical floor plan with case study walls highlighted	A-10
Figure A-11	Undisclosed Building A (Building No. 5) – wall reinforcing details and observed damage at the wall boundary	A-10
Figure A-12	Undisclosed Building B (Building No. 6) – typical floor plan with case study walls highlighted	A-11
Figure A-13	Undisclosed Building B (Building No. 6) – typical wall boundary detail and photo of exposed reinforcement in the boundary of a damaged wall	A-12
Figure A-14	Undisclosed Building B (Building No. 6) – typical setback and reduced web in the first subterranean level.....	A-12
Figure A-15	Mongolio (Building No. 7) – typical floor plan with case study walls highlighted.....	A-13
Figure A-16	Mongolio (Building No. 7) – elevation of Wall 7.1 and details of barbell sections at each end	A-14
Figure A-17	BIAX program material models for: (a) H25 and H30 unconfined concrete; and (b) elasto-plastic and strain hardening reinforcing steel	A-17
Figure A-18	Summary of building orientations, nearest recording stations, and station orientations	A-18
Figure A-19	Linear displacement response spectra for the Concepción station.....	A-19
Figure A-20	Linear displacement response spectra for Viña del Mar-Centro station.....	A-19
Figure A-21	Linear displacement response spectra for the Santiago-Centro station and Santiago-Penalolen station	A-19
Figure A-22	Spectral displacements for Alto Rio (Building No. 1).....	A-21
Figure A-23	Spectral displacements for Plaza del Rio Building B (Building No. 2) and Concepto Urbano (Building No. 3).....	A-21
Figure A-24	Spectral displacements for Toledo (Building No. 4)	A-22
Figure A-25	Spectral displacements for Undisclosed Building A (Building No. 5), Undisclosed Building B (Building No. 6), and Mongolio (Building No. 7).....	A-22
Figure A-26	Illustration of damage reported in walls of Alto Rio (Building No. 1)	A-25
Figure A-27	Definition of parameter ε_p^* , which measures the amount of bar strain from the point of reloading bars in compression to the point when the bars begin to buckle	A-30

Figure A-28	Parameter ϵ_p^* versus ratios of unbraced length to bar diameter (S_h/D).....	A-31
Figure A-29	Illustration of process for estimating ϵ_p^* in the web of a flanged wall.....	A-32
Figure A-30	Illustration of the use of Rodriguez et al. (1999) to determine the drift ratio associated with concrete crushing and bar buckling	A-33
Figure A-31	Moment capacity and buckling strain indicator relations versus roof drift ratio for Wall 1.1.....	A-35
Figure A-32	Moment capacity and buckling strain indicator relations versus roof drift ratio for Wall 1.2.....	A-36
Figure A-33	Moment capacity and buckling strain indicator relations versus roof drift ratio for Wall 1.3.....	A-36
Figure A-34	Moment capacity and buckling strain indicator relations versus roof drift ratio for Wall 1.4.....	A-37
Figure A-35	Moment capacity and buckling strain indicator relations versus roof drift ratio for Wall 1.5.....	A-37
Figure A-36	Moment capacity and buckling strain indicator relations versus roof drift ratio for Wall 1.6.....	A-38
Figure A-37	Moment capacity and buckling strain indicator relations versus roof drift ratio for Wall 2.1.....	A-39
Figure A-38	Moment capacity and buckling strain indicator relations versus roof drift ratio for Wall 2.2.....	A-39
Figure A-39	Moment capacity and buckling strain indicator relations versus roof drift ratio for Wall 2.3.....	A-40
Figure A-40	Moment capacity and buckling strain indicator relations versus roof drift ratio for Wall 3.1.....	A-41
Figure A-41	Moment capacity and buckling strain indicator relations versus roof drift ratio for Wall 3.2.....	A-41
Figure A-42	Moment capacity and buckling strain indicator relations versus roof drift ratio for Wall 4.1.....	A-43
Figure A-43	Moment capacity and buckling strain indicator relations versus roof drift ratio for Wall 4.2.....	A-43
Figure A-44	Moment capacity and buckling strain indicator relations versus roof drift ratio for Wall 4.3.....	A-44
Figure A-45	Moment capacity and buckling strain indicator relations versus roof drift ratio for Wall 4.4.....	A-44
Figure A-46	Moment capacity and buckling strain indicator relations versus roof drift ratio for Wall 4.5.....	A-45

Figure A-47	Moment capacity and buckling strain indicator relations versus roof drift ratio for Wall 4.6	A-45
Figure A-48	Moment capacity and buckling strain indicator relations versus roof drift ratio for Wall 5.1	A-46
Figure A-49	Moment capacity and buckling strain indicator relations versus roof drift ratio for Wall 5.2	A-47
Figure A-50	Moment capacity and buckling strain indicator relations versus roof drift ratio for Wall 5.3	A-47
Figure A-51	Moment capacity and buckling strain indicator relations versus roof drift ratio for Wall 5.4	A-48
Figure A-52	Moment capacity and buckling strain indicator relations versus roof drift ratio for Wall 6.1	A-49
Figure A-53	Moment capacity and buckling strain indicator relations versus roof drift ratio for Wall 6.2	A-50
Figure A-54	Moment capacity and buckling strain indicator relations versus roof drift ratio for Wall 6.3	A-50
Figure A-55	Moment capacity and buckling strain indicator relations versus roof drift ratio for Wall 7.1	A-51
Figure A-56	Moment capacity and buckling strain indicator relations versus roof drift ratio for Wall 7.2	A-52
Figure A-57	Bar buckling analysis of wall specimen TW1	A-53
Figure A-58	Bar buckling analysis of wall specimen RW1	A-54
Figure A-59	Bar buckling analysis of wall specimen RW2	A-55
Figure A-60	Bar buckling analysis of wall specimen TW2	A-56
Figure B-1	Examples of wall lateral buckling: (a) 2010 Maule earthquake; and (b) 2011 Christchurch earthquake	B-1
Figure B-2	Lateral instability of a wall boundary that is previously yielded in tension.....	B-2
Figure B-3	Comparison between the theoretical relation for wall instability and test results for buckling of prismatic sections reinforced as rectangular wall boundaries: (a) test specimen; and (b) plot of data.....	B-5
Figure B-4	Configuration and detailing of T-shaped wall specimen TW2: (a) isometric; (b) cross-section; and (c) detail	B-5
Figure B-5	Out-of-plane buckling observed in T-shaped wall specimen TW2	B-6

Figure C-1	Damage map from a building in Northern California damaged in the 1989 Loma Prieta earthquake.....	C-2
Figure C-2	Damage map of the Alto Rio Building in Concepción, Chile following the 2010 Maule earthquake at Grid 8.....	C-2
Figure C-3	Damage observed in solid panels at the top and bottom of a stack of openings in the Torre Mayor building in Chillán, Chile following the 2010 Maule earthquake.....	C-3
Figure C-4	Damage observed in solid panel at the bottom of a stack of openings in the Centro Mayor building in Concepción, Chile following the 2010 Maule earthquake.....	C-3
Figure C-5	Damage observed in solid panel at the bottom of a stack of openings in the Marina del Sol building in Viña del Mar, Chile following the 2010 Maule earthquake.....	C-4
Figure C-6	Plan view of PERFORM-3D model slice for the Alto Rio building	C-4
Figure C-7	Relationship of shear stress to roof drift ratio of discontinuity region (solid line) and of average for entire wall (dashed line), using a linear model for the discontinuity region.....	C-6
Figure C-8	Shear stress–strain relationship of the discontinuity region, using an inelastic shear material	C-6
Figure C-9	Illustrations of: (a) minimum development length for wall boundary reinforcement; and (b) resulting shear stresses in the discontinuity region.....	C-7
Figure C-10	Panel zone shear and tension/compression chords.....	C-8
Figure C-11	Idealized resolution of basement wall forces beneath coupled walls	C-8
Figure C-12	Effective width of flanged wall loading a discontinuity region below a stack of openings	C-10
Figure C-13	Torre Mayor building reinforcement details around panel zone of interest.....	C-12
Figure C-14	Centro Mayor building reinforcement details around panel zone of interest.....	C-12
Figure C-15	Marina del Sol building reinforcement details around panel zone of interest.....	C-13
Figure D-1	Overview of Plaza del Rio Buildings A and B.....	D-2
Figure D-2	Layout of first and second story walls of Plaza del Rio Building A	D-3
Figure D-3	Layout of walls for lower two floors of Plaza del Rio Building B (beams and slabs are not shown)	D-4

Figure D-4	Overview of Centro Mayor building.....	D-5
Figure D-5	Layout of walls for the lower four floors of Centro Mayor building (beams and slabs are not shown)	D-6
Figure D-6	Overview of Alto Huerto building	D-7
Figure D-7	Overview of Concepto Urbano	D-8
Figure D-8	Layout of walls for a typical floor of Concepto Urbano building (beams and slabs are not shown)	D-8
Figure D-9	Maximum DCR_u values for first story walls at Plaza del Rio Building B.....	D-11
Figure D-10	Controlling response determined by largest DCR_u value for first story walls at Plaza del Rio Building B	D-12
Figure D-11	Maximum DCR_u values for first story walls at Centro Mayor building	D-13
Figure D-12	Controlling response determined by largest DCR_u value for first story walls at Centro Mayor building	D-14
Figure D-13	First story walls of Plaza del Rio Building B expected to achieve ASCE/SEI 41-06 performance levels for the Design Earthquake	D-16
Figure D-14	Second story walls of the Centro Mayor building expected to achieve ASCE/SEI 41-06 performance levels for the Design Earthquake	D-17
Figure D-15	Number of first story walls in Plaza del Rio Building B meeting and not meeting various performance objectives; colors indicate the severity of observed damage for walls in each category.....	D-18
Figure D-16	Number of second story walls in the Centro Mayor building meeting and not meeting various performance objectives; colors indicate the severity of observed damage for walls in each category.....	D-19
Figure D-17	SRSS response spectra of selected ground motion records from the 2010 Maule earthquake: (a) scaled; and (b) unscaled ...	D-21
Figure D-18	Shear strength versus strain model employed in OpenSees analyses	D-23
Figure D-19	Isometric view of PERFORM-3D model highlighting: (a) shear wall; and (b) coupling beams.....	D-23
Figure D-20	Shear backbone curves shown as shear strength versus shear strain	D-26
Figure D-21	Cyclic shear stress-strain model used in PERFORM-3D analysis	D-27

Figure D-22	Possible foundation models in PERFORM-3D.....	D-28
Figure D-23	Foundation level of building Plaza del Rio Building A modeled in PERFORM-3D (Perform SSI model): (a) wall elements are added to extend walls to centerline of mat foundation and wall elements used to model grade beams are highlighted; and (b) mat foundation elements are shown and soil springs are highlighted	D-29
Figure D-24	Building period versus foundation flexibility, k	D-31
Figure D-25	Response of first and second story walls in Plaza del Rio Building A to unscaled San Pedro de la Paz ground motion.....	D-35
Figure D-26	Response of first and second story walls in Plaza del Rio Building A to unscaled San Pedro de la Paz ground motion.....	D-36
Figure D-27	Response of first and second story walls in Plaza del Rio Building A to unscaled San Pedro de la Paz ground motion.....	D-37
Figure D-28	Number of walls in Plaza del Rio Building A exceeding acceptance criteria for each performance measure.....	D-38
Figure D-29	Perform Basic model results showing damage exceeding Collapse Prevention limits in shear walls (shear and flexure models) and coupling beams for the Concepción record.....	D-40
Figure D-30	Perform SSI model results showing damage exceeding Collapse Prevention limits in shear walls (shear and flexure models) and coupling beams for the Concepción record.....	D-41
Figure D-31	Typical local wall discontinuities observed in case study buildings.....	D-42
Figure D-32	The number of local discontinuities at each quality ranking in each of the four case study buildings	D-43
Figure D-33	Magnitude of discontinuity measure for each discontinuity ID ...	D-45
Figure E-1	Exterior elevation of the O'Higgins building after the 2010 Maule earthquake, and idealized pier spandrel system	E-1
Figure E-2	Sample plastic mechanisms studied: (a) mechanism validated by calculation and post-earthquake observations; and (b) mechanism considered and shown by calculation not to govern.....	E-3
Figure F-1	Specimen dimension and detailing.....	F-1
Figure F-2	Illustrations of: (a) test specimen; and (b) fiber beam model.....	F-2
Figure F-3	Average strain loading history applied in Rodriguez et al. (1999)	F-2
Figure F-4	Stress-strain hysteresis: (a) measured on one side of bar; and (b) measured on opposite side of bar.....	F-3
Figure F-5	Applied strain protocols 2 to 7	F-3

Figure F-6	Wall specimen PW4: (a) cross-section; and (b) boundary element.....	F-4
Figure F-7	Material properties of: (a) unconfined and confined concrete; and (b) reinforcing steel #4 bars in wall specimen PW4	F-4
Figure F-8	Elevations of: (a) PW4 test specimen; and (b) LS-DYNA shell model	F-5
Figure F-9	LS-DYNA sandwich shell for confined zones of wall	F-5
Figure F-10	LS-DYNA sandwich shell for central unconfined zone of wall	F-6
Figure F-11	Simulation of reinforcement cage buckling at PW4 wall specimen	F-7
Figure F-12	Comparison of shell element reinforcing bar model to match stress-strain hysteresis of fiber-beam model of reinforcing bar cage of PW4 wall specimen.....	F-8
Figure F-13	Alto Rio Building longitudinal section	F-9
Figure F-14	Spectra of triaxial Concepción records	F-10
Figure F-15	Acceleration time histories of the Concepción record.....	F-11
Figure F-16	Gravity stresses (MPa) in LS-DYNA model (1 MPa = 145 psi): (a) perspective view; (b) close-up of basement, first, and second floors; (c) elevation at Grid 13; and (d) elevation at Grid 17.....	F-11
Figure F-17	Roof drift ratio time-history of Grid 13 wall with expected (black) and measured (red) properties	F-13
Figure F-18	Base shear ratio time-history of Grid 13 wall with expected (black) and measured (red) properties	F-13
Figure F-19	Axial force time-history of Grid 13 wall with expected (black) and measured (red) properties.....	F-14
Figure F-20	Shear force time-history of Grid 13 wall with expected (black) and measured (red) properties.....	F-14
Figure F-21	Moment time-history of Grid 13 wall with expected (black) and measured (red) properties	F-14
Figure F-22	Roof drift ratio time-history of Grid 13 wall with (black) and without (red) basement constraint.....	F-14
Figure F-23	Base shear ratio time-history of Grid 13 wall with (black) and without (red) basement constraint.....	F-14
Figure F-24	Shear model used by Tuna and Wallace (2012)	F-15

List of Tables

Table 1-1	Ground Motion Recordings from the 2010 Maule Earthquake	1-6
Table 1-2	Summary of Case Study Building Information.....	1-12
Table 4-1	Summary of Tier 1 Checklist Items Identified as Non-Compliant for Plaza del Rio Building A.....	4-17
Table 4-2	Effective Stiffness Values for Tier 2 Analysis Models.....	4-20
Table 4-3	Plaza del Rio Building A – Tier 3 Analysis Maximum and Residual Drifts Predicted for the Concepción Ground Motion.....	4-30
Table A-1	Alto Rio (Building No. 1) – Geometry of Critical Wall Sections.....	A-4
Table A-2	Plaza del Rio Building B (Building No. 2) – Geometry of Critical Wall Sections	A-6
Table A-3	Concepto Urbano (Building No. 3) – Geometry of Critical Wall Sections.....	A-7
Table A-4	Toledo (Building No. 4) – Geometry of Critical Wall Sections	A-9
Table A-5	Undisclosed Building A (Building No. 5) – Geometry of Critical Wall Sections	A-11
Table A-6	Undisclosed Building B (Building No. 6) – Geometry of Critical Wall Sections	A-13
Table A-7	Mongolio (Building No. 7) – Geometry of Critical Wall Sections.....	A-14
Table A-8	Typical Gravity Load Assumptions (Alto Rio – Building No. 1).....	A-15
Table A-9	Design Strengths Corresponding to Cube Test Strengths	A-16
Table A-10	Summary of Estimated Periods, Spectral Displacements, and Roof Drift Ratios	A-23
Table A-11	Alto Rio (Building No. 1) Special Boundary Element Trigger Evaluation	A-25
Table A-12	Plaza del Rio Building B (Building No. 2) Special Boundary Element Trigger Evaluation.....	A-25
Table A-13	Concepto Urbano (Building No. 3) Special Boundary Element Trigger Evaluation	A-26

Table A-14	Toledo (Building No. 4) Special Boundary Element Trigger Evaluation	A-26
Table A-15	Undisclosed Building A (Building No. 5) Special Boundary Element Trigger Evaluation	A-27
Table A-16	Undisclosed Building B (Building No. 6) Special Boundary Element Trigger Evaluation	A-27
Table A-17	Mongolio (Building No. 7) Special Boundary Element Trigger Evaluation	A-28
Table A-18	Alto Rio (Building No. 1) Bar Buckling Assessment	A-35
Table A-19	Plaza del Rio Building B (Building No. 2) Bar Buckling Assessment	A-38
Table A-20	Concepto Urbano (Building No. 3) Bar Buckling Assessment....	A-40
Table A-21	Toledo (Building No. 4) Bar Buckling Assessment.....	A-42
Table A-22	Undisclosed Building A (Building No. 5) Bar Buckling Assessment.....	A-46
Table A-23	Undisclosed Building B (Building No. 6) Bar Buckling Assessment.....	A-48
Table A-24	Mongolio (Building No. 7) Bar Buckling Assessment	A-51
Table A-25	Summary of Bar Buckling Analysis Results for Wall Specimen Tests	A-56
Table C-1	Estimated Shear Demand and Capacity at Discontinuity Region	C-11
Table D-1	Descriptions of Identified Damage Levels.....	D-1
Table D-2	Summary of ASCE/SEI 31-03 Checklist Items Identified as Non-Compliant (NC).....	D-9
Table D-3	Summary of Modal Periods for Plaza del Rio Building A.....	D-30
Table D-4	Maximum and Residual Roof Drifts for Plaza del Rio Building A from OpenSees Analyses.....	D-32
Table D-5	Summary of Roof Drifts for Plaza del Rio Building A from OpenSees Analyses	D-32
Table D-6	Maximum and Residual First and Second Story Drifts for Plaza del Rio Building A from OpenSees Analyses	D-33
Table D-7	Summary of Predicted and Observed Performance Levels for Primary Lateral Load-Carrying Walls using Different Performance Criteria	D-34

Table D-8	Plaza del Rio Building A Maximum and Residual Drifts for the Concepción Ground Motion	D-39
Table E-1	Wall Pier and Spandrel Beam Shear Strength and Expected Behavior Mode	E-2
Table F-1	Natural Periods of the LS-DYNA Alto Rio Building Model Based on Stiffness Assumptions	F-12

1.1 Background and Objectives

On February 27, 2010, a magnitude 8.8 earthquake occurred off the coast near the Maule region of central Chile. In terms of magnitude, this earthquake is the eighth largest event ever recorded worldwide. Within Chile, it is one of more than 20 earthquakes exceeding magnitude 7.0 that have occurred since 1730, eight of which have exceeded magnitude 8.0, and two of which have exceeded magnitude 9.0. It is the most significant event to occur in Chile since the magnitude 7.8 earthquake offshore of Valparaíso on March 3, 1985, which affected areas including Santiago, Valparaíso, and Viña del Mar. [Data from *Historic World Earthquakes* (USGS, 2013a).]

As a result of frequent historic seismic activity, building codes in Chile have included consideration of seismic effects, and building practice has included earthquake-resistant construction. Modern Chilean practice has been modeled after U.S. practice, and Chilean design standards are comparable to U.S. codes and standards that were in effect during the mid-1990s. Building construction in both Chile and the United States covers a wide range of building types and structural systems, but typical Chilean mid-rise and high-rise design practice favors reinforced concrete bearing wall construction that is similar to construction prevalent in regions of high seismicity in the Western United States.

Although the collective performance of buildings in the 2010 Maule earthquake was generally considered to be very good, a number of mid-rise and high-rise buildings experienced heavy damage, and a few collapsed, as a result of the earthquake. In response, several U.S. organizations sent reconnaissance teams to Chile to gather information that could be used to study implications for U.S. design and construction practice. These teams observed many instances of structural damage in reinforced concrete walls that appeared to warrant further investigation. Observed damage included concrete crushing and buckling of longitudinal reinforcement at wall boundaries, out-of-plane buckling of walls, damage from coupling of walls through slabs and other elements, and damage concentrated at wall discontinuities.

Similarities between U.S. and Chilean seismic design and construction practices presented a unique opportunity to investigate the observed performance of buildings subjected to strong ground shaking, and to extract lessons for improving design and construction of reinforced concrete buildings that will be subjected to future

earthquakes. Recognizing the potential value to U.S. practice, the National Institute of Standards and Technology (NIST) initiated a series of projects intended to study the effects of the earthquake and document lessons learned. As one of the projects in this series, the objectives of this project were: (1) to evaluate critical issues in the design of reinforced concrete walls; and (2) to develop recommendations for improving wall design requirements. Work included the documentation of wall failure modes and observed damage, and the conduct of problem-focused studies to investigate the potential causes of observed behavior. This report presents the findings, conclusions, and recommendations from these studies.

1.2 Chilean Seismic Design and Construction Practice

Since 1985, Chilean seismic design and construction practice has been largely modeled after U.S. practice (with some important differences). To provide context for studies of earthquake effects, NIST commissioned a study comparing U.S. and Chilean building codes and construction practices. Detailed comparisons are contained in NIST GCR 12-917-18, *Comparison of U.S. and Chilean Building Code Requirements and Seismic Design Practice 1985-2010* (NIST, 2012). Key points from this comparison are summarized in the sections that follow.

1.2.1 Chilean Seismic Design Standards

Two primary standards govern seismic-resistant design of reinforced concrete structures in Chile:

- NCh433 – *Earthquake Resistant Design of Buildings*
- NCh430 – *Reinforced Concrete Design and Analysis Requirements*

NCh433 encompasses requirements for calculating seismic loads for design of structures, comparable to Chapters 11 through 22 of ASCE/SEI 7, *Minimum Design Loads for Buildings and Other Structures*, in the United States. In 2010, the version in effect was NCh433.Of96, *Earthquake Resistant Design of Buildings* (INN, 1996). NCh433.Of96 is closely related to seismic design requirements contained in various editions of the *Uniform Building Code*, which were used throughout the Western United States during the period between 1988 and 2000.

NCh430 sets the criteria for design and detailing of reinforced concrete structures, comparable to ACI 318, *Building Code Requirements for Structural Concrete*, in the United States. In 2010, the version in effect was NCh430.Of2008, *Reinforced Concrete Design and Analysis Requirements* (INN, 2008). NCh430.Of2008 adopted the 2005 version of ACI 318 as its fundamental basis, but with important Chilean exceptions.

Overall, seismic design requirements in Chile and the United States are similar. In spite of some notable differences, it can be shown that a typical Chilean mid-rise to

high-rise residential building would be designed for an equivalent strength-level base shear coefficient that is nearly identical to U.S. base shear coefficients. Although requirements are similar overall, certain specific enhancements to U.S. seismic design requirements have occurred since the 1990s, but have not been reflected in Chilean standards:

- Requirements for confinement in shear wall boundary zones and plastic hinge regions.
- Requirements for ductile detailing of coupling beams.
- Limitations on the use of certain irregular structural configurations.

Differences between U.S. and Chilean standards related to the above requirements are likely to have had an effect on the performance of buildings in the 2010 Maule earthquake.

1.2.2 Chilean Design Practice

Low-rise construction in Chile has traditionally consisted of masonry or concrete bearing wall buildings with relatively short spans and many walls. As building practices evolved, and mid-rise and high-rise construction became more prevalent, engineers continued these same practices, employing relatively short spans in floor systems and providing many load-bearing walls for both gravity and seismic force resistance.

Chilean mid-rise and high-rise construction favors reinforced concrete bearing wall systems, with floors consisting of flat slab construction. Configurations are mostly rectangular in plan, although non-rectangular configurations are also used. High-rise construction often has extensive glazing with few exterior walls. Setbacks in building elevation occur, but are less common.

In residential construction, most interior walls are reinforced concrete structural walls. These include corridor walls, party walls between individual units, and walls around stair and elevator cores. Walls observed in apartment buildings are typically 200mm (8 inches) thick for buildings up to 16 stories, and 250mm (10 inches) thick for buildings up to 25 stories (Cowan et al., 2011) with two curtains of reinforcing steel. Office buildings utilize similar construction, but generally have fewer, thicker structural walls, longer spans in the floor plate, and moment-resisting frames on the building perimeter. Typical mid-rise and high-rise construction in Santiago is shown in Figure 1-1.

The use of redundant wall systems and relatively good performance of these systems in past earthquakes are the primary reasons why Chilean design standards evolved without provisions for confined boundaries. Although the use of unconfined

boundary elements was permitted, not all Chilean engineers universally implemented this in practice. Some Chilean engineers have reported that partial confinement of boundary zones has been routinely provided using cross ties with alternating 90-degree and 135-degree hooks.



Figure 1-1 Typical mid-rise and high-rise buildings in Santiago, Chile (photo courtesy of Renè Lagos).

In the time leading up to the 2010 Maule earthquake, modern building codes had been in effect in Chile for some time, and U.S. design concepts were embodied in Chilean seismic design practice. At the time of the earthquake, the affected building stock included a significant number of engineered buildings with designs rooted in U.S. seismic design practice.

1.3 The 2010 Maule Earthquake

The Maule earthquake occurred at 3:34 am local time on February 27, 2010, in the Bio-Bio/Maule region of Central Chile (USGS, 2013b). The earthquake had a moment magnitude, M_w , of 8.8, with a duration of shaking that lasted more than 120 seconds in some areas. The epicenter was located at 35.909° South latitude, 72.733° West longitude, or approximately 105 kilometers (65 miles) north-northeast of Concepción, and 335 kilometers (210 miles) southwest of Santiago. The focal depth was estimated to be 35 kilometers (22 miles).

The fault slip generated significant ground shaking that was felt in cities including Santiago, Valparaíso, Viña del Mar, Talca, Concepción, Temuco, and Valdivia. Deformations in the ocean floor generated a tsunami that was severe in the cities of Constitución and Talcahuano near the fault-rupture zone. An isoseismal map from USGS Pager, showing the epicentral location and distribution of estimated intensity

throughout the affected region, is shown in Figure 1-2. Much of Chile’s central plain, including Santiago, experienced a Modified Mercalli Intensity (MMI) of VII, while communities closer to the coast experienced intensities of VIII to IX.

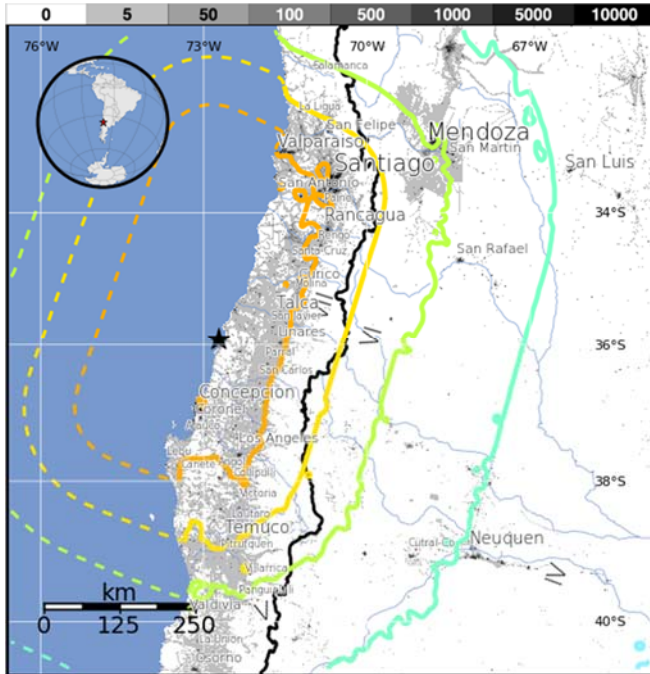


Figure 1-2 Isoseismal map of the 2010 Maule earthquake (USGS, 2013b).

1.3.1 Strong-Motion Recordings

The University of Chile maintains a network of strong-motion instruments in central and southern Chile. These instruments are organized in two arrays: (1) the National Accelerograph Network at the Department of Civil Engineering (RENADIC); and (2) the Seismological Service at the Department of Geophysics (GUC) (Boroschek et al., 2012). In the 2010 Maule earthquake, 31 stations from these two arrays recorded strong ground motions. Table 1-1 summarizes ground motion recordings from this network, as provided in Boroschek et al. (2012) and GUC (2010).

Figure 1-3 shows the locations of selected RENADIC recording stations in relation to the major cities of Santiago, Viña del Mar, and Concepción, as well as the epicenter of the earthquake. Also plotted is the location of the selected GUC Concepción-San Pedro de la Paz station. Other records available through GUC were not used in this study, and are not shown in the figure.

Figure 1-4 shows 5% damped, elastic acceleration response spectra for the RENADIC ground motion recordings. Recorded motions exceeded the Chilean elastic design spectrum at several locations. At sites around Viña del Mar and Concepción, peaks in the spectra were observed to occur

Table 1-1 Ground Motion Recordings from the 2010 Maule Earthquake (Boroschek et al., 2012)

No.	Station	Owner	Latitude	Longitude	Station Type ¹	Peak Ground Acceleration, g	
						Dir.	Value
1	Angol ²	RENADIC	-37.7947° (S)	-72.7081° (W)	QDR	NS	0.928
2	Concepción	RENADIC	-36.8261° (S)	-73.0547° (W)	SMA-1	Long.	0.402
3	Constitución	RENADIC	-35.3401° (S)	-72.4057° (W)	SMA-1	Trans.	0.640
4	Copiapo	RENADIC	-27.355° (S)	-70.3413° (W)	QDR	NS	0.030
5	Curico	RENADIC	-34.9808° (S)	-71.2364° (W)	QDR	NS	0.470
6	Hualane	RENADIC	-34.95° (S)	-71.80° (W)	SMA-1	Trans.	0.461
7	Llolleo	RENADIC	-33.6167° (S)	-71.6176° (W)	SMA-1	Trans.	0.564
8	Matanzas	RENADIC	-33.9593° (S)	-71.8727° (W)	SMA-1	Long.	0.342
9	Papudo	RENADIC	-32.5114° (S)	-71.4471° (W)	SMA-1	Trans.	0.421
10	Santiago-Centro	RENADIC	-33.46° (S)	-70.69° (W)	SSA-2	Trans.	0.309
11	Santiago-La Florida	RENADIC	-33.5248° (S)	-70.5383° (W)	K2	NS	0.236
12	Santiago-Maipu	RENADIC	-33.5167° (S)	-70.7667° (W)	QDR	NS	0.562
13	Santiago-Penalolen	RENADIC	-33.50° (S)	-70.579° (W)	QDR	NS	0.295
14	Santiago-Puente Alto	RENADIC	-33.5769° (S)	-70.5811° (W)	QDR	NS	0.265
15	Talca	RENADIC	-35.4233° (S)	-71.66° (W)	SMA-1	Long.	0.477
16	Vallenar	RENADIC	-28.5716° (S)	-70.759° (W)	QDR	NS	0.020
17	Valparaíso-UTFSM	RENADIC	-33.0356° (S)	-71.5953° (W)	SMA-1	Trans.	0.304
18	Valparaíso-Almendral	RENADIC	-33.0458° (S)	-71.6068° (W)	SMA-1	Trans.	0.265
19	Valdivia	RENADIC	-39.8244° (S)	-73.2133° (W)	QDR	EW	0.138
20	Viña del Mar-Centro	RENADIC	-33.0253° (S)	-71.5508° (W)	QDR	EW	0.334
21	Viña del Mar-El Salto	RENADIC	-33.0469° (S)	-71.51° (W)	Etna	NS	0.351
22	Cerro El Roble	GUC	-32.9759° (S)	-71.0156° (W)	FBA ES-T	NS	0.19
23	Olmué-Casa Particular	GUC	-32.9940° (S)	-71.1730° (W)	QDR	NS	0.35
24	Casablanca-Teatro Municipal	GUC	-33.3208° (S)	-71.4108° (W)	QDR	EW	0.33
25	Las Condes-Cerro Calán	GUC	-33.3961° (S)	-70.5369° (W)	SSA-120SLN	EW	0.23
26	Santiago-Cerro Santa Lucia	GUC	-33.4405° (S)	-70.6428° (W)	Makalu	EW	0.34
27	La Reina-Colegio Las Américas	GUC	-33.4518° (S)	-70.5308° (W)	Makalu	NS	0.31
28	La Pintana-Antumapu	GUC	-33.5691° (S)	-70.6335° (W)	FBA ES-T	EW	0.27
29	San José de Maipo-Municipalidad	GUC	-33.6407° (S)	-70.3538° (W)	Makalu	EW	0.48
30	Melipilla-Campanía de Bomberos	GUC	-33.6874° (S)	-71.2138° (W)	QDR	EW	0.78
31	Concepción-San Pedro de la Paz	GUC	-36.8442° (S)	-73.1087° (W)	Etna	NS	0.65

¹ QDR: Free-field analog, U. Chile; SMA-1: Free-field analog, U. Chile; SSA-2: Free-field digital, U. Chile; K2: Free-field digital, METRO S.A.; Etna: Free-field digital, U. Chile

² Station soil-structure interaction under evaluation.

at longer periods, presumably because of soil effects (Boroschek and Contreras, 2012). In particular, the Concepción record had a spectral peak at a period of about 1.5 seconds.



Figure 1-3 Locations of selected RENADIC and GUC recording stations in relation to major cities and the earthquake epicenter (image from Google Earth).

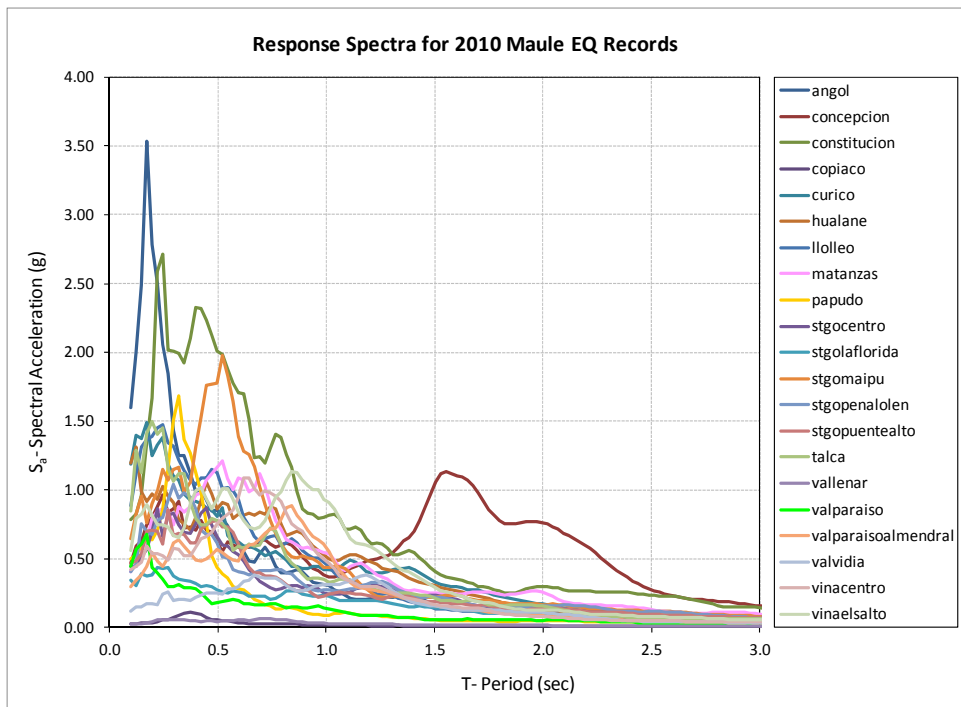


Figure 1-4 Acceleration response spectra based on recordings from RENADIC stations in the 2010 Maule earthquake (data from University of Chile, 2012).

1.4 Observed Performance of Buildings

Losses from the earthquake were estimated to be \$30 billion (\$U.S.), with more than 520 fatalities (USGS, 2013b; EERI, 2010). From various sources, damage estimates included: over 370,000 houses damaged or destroyed (Comerio, 2013); more than 4,000 schools significantly damaged (USGS, 2013b); approximately 300 highway bridges damaged, including 20 collapsed spans (Buckle et al., 2012), and 80 hospitals needing repairs (Elnashai et al., 2012).

Given the intensity of shaking, most buildings were generally considered to have performed well in the earthquake. Based on building surveys in selected metropolitan regions in Chile, the Engineers Association of Chile (2010) estimated that approximately 2% of engineered buildings experienced severe damage or collapse; 12% were damaged such that they were not usable until repaired; and 86% were usable immediately following the earthquake.

Approximately 50 multi-story reinforced concrete buildings were severely damaged, and four experienced partial or total collapse (EERI, 2010). Immediately following the earthquake, reconnaissance teams began observing recurring patterns of damage in shear walls and other elements of mid-rise and high-rise reinforced concrete buildings (Westenenk et al., 2012). There were many instances of concrete crushing and buckling of longitudinal reinforcement at wall boundaries, with failures that propagated along the entire length of the wall segment (Figure 1-5).

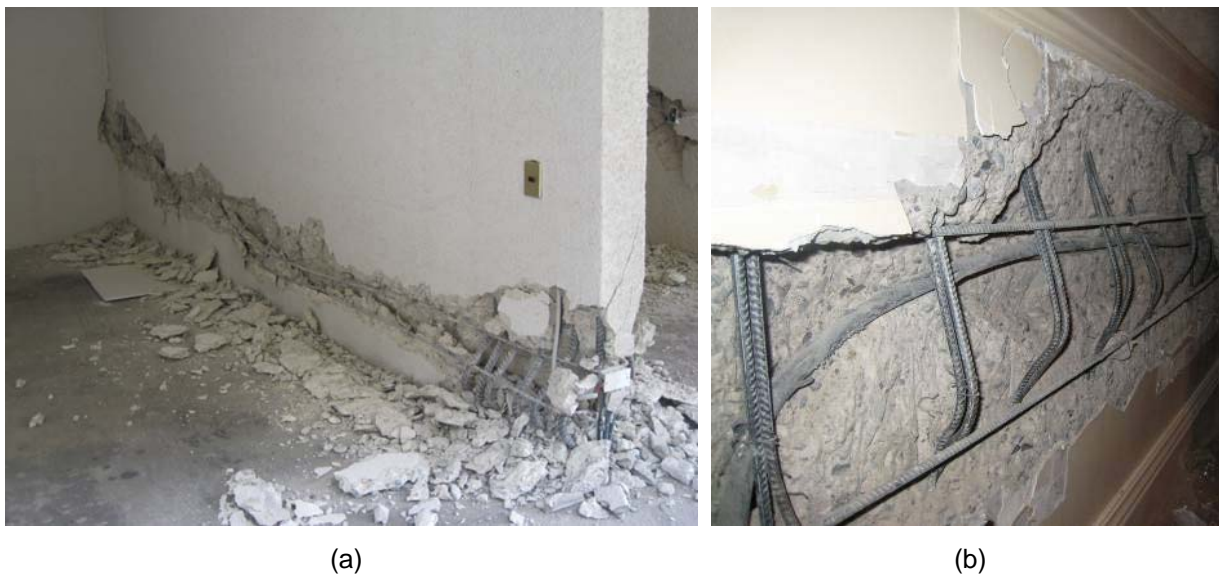


Figure 1-5 Concrete crushing and buckling of longitudinal reinforcement initiating at wall boundaries and propagating along the length of wall segments: (a) photo courtesy of Patricio Bonelli; (b) photo courtesy of Joseph Maffei.

Other vertical and horizontal wall segments experienced shear failures (Figure 1-6). A few walls exhibited apparent out-of-plane lateral instability that was reminiscent of

overall wall buckling behavior (Figure 1-7). Localized damage attributed to building configuration issues was concentrated at locations of wall discontinuities and structural system irregularities (Figure 1-8), or unintended coupling of walls through slabs and other elements (Figure 1-9).

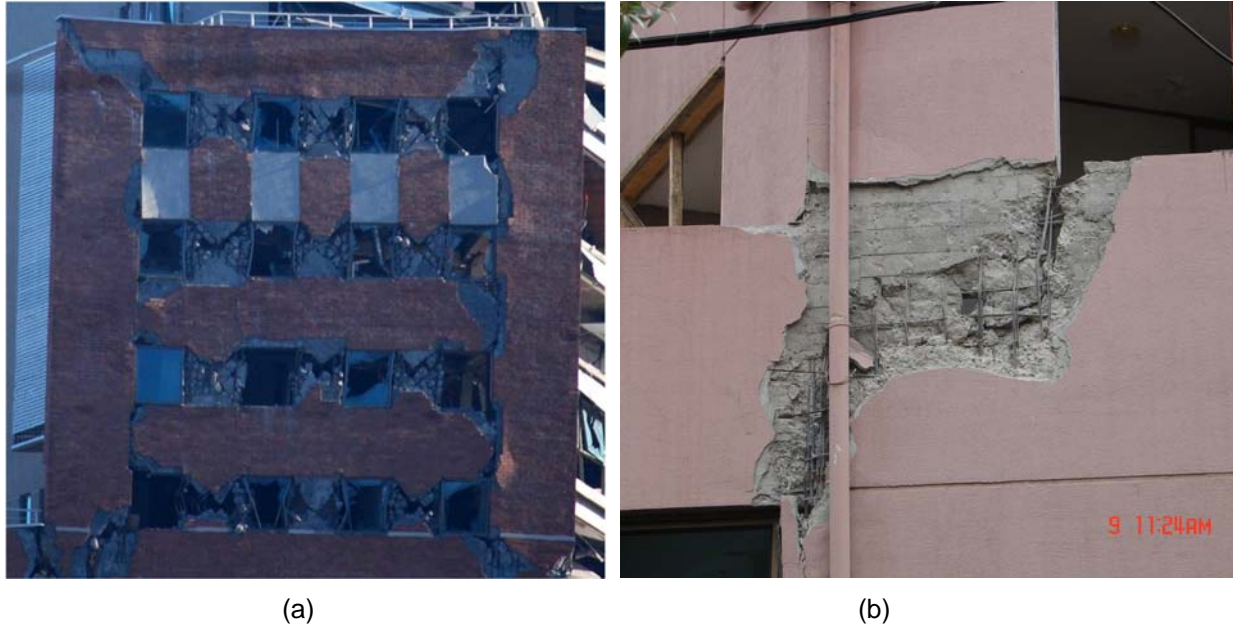


Figure 1-6 Shear failures in vertical and horizontal wall segments: (a) photo courtesy of PEER; (b) photo courtesy of ASCE.



Figure 1-7 Overall wall buckling behavior (DICTUC, 2010e).



(a)

(b)

Figure 1-8 Concentrated damage at: (a) wall discontinuities (photo courtesy of Joseph Maffei); and (b) structural irregularities (photo courtesy of Joseph Maffei).



(a)

(b)

Figure 1-9 Concentrated damage at: (a) coupling beams (photo courtesy of ASCE); and (b) cast-in-place concrete stair elements (photo courtesy of ASCE).

1.5 Project Approach and Problem-Focused Studies

Although many different building types and occupancy classes were affected by the earthquake, damage observed in mid-rise and high-rise reinforced concrete bearing wall structures, typically used in high-density, multi-family residential construction, was targeted for further study. This type of construction was chosen because:

- Structures of this type are common in both Chile and the United States, and many are located in regions of high seismicity in the United States.

- Structures of this type are designed using sophisticated engineering techniques and typify the application of sophisticated building design and construction practices in both countries.
- Chilean practice in the design of these structures is based on U.S. building codes and standards (with some modifications), enabling lessons from observed performance to be applicable to design in both countries.
- Structural drawings for many of these buildings were available for use in detailed studies.

Studies were organized around the recurring patterns of damage that were observed in shear walls and other elements of mid-rise and high-rise reinforced concrete buildings, and teams were assigned to investigate. Studies were grouped into the following areas for detailed investigation:

- Study Area 1: Investigation of concrete crushing and longitudinal bar buckling in wall boundary elements.
- Study Area 2: Investigation of overall wall buckling behavior.
- Study Area 3: Investigation of building configuration issues related to discontinuities, irregularities, and coupling.
- Study Area 4: Analysis and advanced simulation of reinforced concrete wall behavior.

1.5.1 Case Study Buildings

Potential case study buildings were identified through a review of available reconnaissance data from a variety of sources, including: American Society of Civil Engineers (ASCE), Applied Technology Council (ATC), Earthquake Engineering Research Institute (EERI), Geotechnical Extreme Events Reconnaissance (GEER), Los Angeles Tall Buildings Structural Design Council (LATBSDC), National Institute of Standards and Technology (NIST), National Science Foundation (NSF), Pacific Earthquake Engineering Research Center (PEER), and many other individual firms and research institutions who sent teams to investigate.

Buildings selected for study were buildings known to have exhibited the targeted behaviors (e.g., boundary element crushing and bar buckling, overall wall buckling, and localized damage at discontinuities and irregularities), and known to have sufficient information in terms of drawings and ground motion recordings to conduct detailed studies. Case study buildings are summarized in Table 1-2. Details on the design and construction of each building, and the damage observed in each building as a result of the earthquake, are described as part of the problem-focused studies in the chapters that follow.

Table 1-2 Summary of Case Study Building Information

Building	Location	Design Date	Number of Stories	Study Area	Characteristic Damage
Alto Huerto	Concepción	2007	15 above grade; 2 basement	2, 3	Concrete crushing at wall boundaries; overall wall buckling; localized damage at wall discontinuities
Alto Rio	Concepción	2007	15 above grade; 2 basement	1, 3	Collapsed
Centro Mayor	Concepción	2005	17 above grade; 2 basement	3	Concrete crushing; shear failure; localized damage at discontinuities and irregularities
Concepto Urbano	Concepción	2007	22 above grade; 2 basement	1, 3	Relatively undamaged
Marina del Sol	Viña del Mar	2003	20 above grade	3	Localized shear failure in a first story wall panel below a stack of opening
Mongolio	Santiago	2007	10 above grade; 1 basement	1	Shear failure; localized wall damage due to slab coupling
O'Higgins	Concepción	2008	21 above grade; 2 basement	3	Shear failure; localized damage and partial collapse at wall discontinuities and irregularities
Plaza del Rio (Building A)	Concepción	2004	12 above grade; no basement	3	Concrete crushing and bar buckling at wall boundaries; localized damage at wall discontinuities
Plaza del Rio (Building B)	Concepción	2004	13 above grade; no basement	1, 3	Relatively undamaged
Toledo	Viña del Mar	1996	10 above grade; 1 basement	1	Severe concrete crushing and bar buckling at wall boundaries
Undisclosed Building A ¹	Santiago	2005	12 above grade; 2 basement	1	Concrete crushing and bar buckling at wall boundaries; overall wall buckling in the first subterranean level
Undisclosed Building B ¹	Santiago	2006	20 above grade; 4 basement	1, 2	Overall wall buckling in the first subterranean level

¹ Detailed engineering information for Undisclosed Building A and Undisclosed Building B was provided for use in this study on condition that the building identity would not be disclosed. Detailed information on other buildings identified by name has been included with permission.

1.5.2 Study Area 1: Investigation of Wall Boundary Elements

Using the response of the Alto Rio, Concepto Urbano, Mongolio, Toledo, Undisclosed Building A, Undisclosed Building B, and Plaza del Rio buildings as a basis, this study area focuses on the behaviors and issues related to flexure-governed walls including: confinement triggers for special boundary elements, plastic hinge length, and bar buckling. It is intended to determine if observed damage was consistent with expectations, and to investigate the effect of axial load, cross-section shape, and spacing of transverse reinforcement on the resulting damage. It is also

intended to investigate whether or not current requirements for special boundary elements in ACI 318 are a reliable indicator of potential wall damage.

1.5.3 Study Area 2: Investigation of Overall Wall Buckling

Using observations from the Alto Huerto building and Undisclosed Building A, supplemented with a theoretical model for wall instability and laboratory tests on prisms, this study area investigates overall wall buckling behavior. Examples of buckled and non-buckled walls are analyzed for sensitivity to building characteristics such as wall slenderness, wall axial stress level, and wall configuration.

1.5.4 Study Area 3: Investigation of Building Configuration

This study area focuses on three overarching building configuration issues associated with observed damage, and presents recommendations for avoiding such issues or accounting for them in analysis and design. Using observations from the Alto Rio, Torre Mayor, Centro Mayor, and Marina del Sol buildings, the first study investigates behavior in discontinuity regions located above or below vertically aligned openings. A method of calculation of shear stress in this panel zone is proposed and recommendations for design of such panel zones are developed.

Additionally, using observations from the Plaza del Rio (A and B), Centro Mayor, Alto Huerto, and Concepto Urbano buildings, a second study investigates vertical irregularities and strength and stiffness discontinuities, and explores the extent to which evaluation tools commonly used in the United States capture these types of building configuration issues.

Lastly, using observations from the O'Higgins building, a third study investigates expected failure mechanisms in pier-spandrel systems.

1.5.5 Study Area 4: Analysis and Advanced Simulation of Reinforced Concrete Wall Behavior

Using the response of the Alto Rio building, supplemented with calibrated simulations of experimental tests on shear wall panels, this study investigates the ability of advanced analytical methods to simulate overall behavior and predict locations and types of damage. It includes simulation of advanced component behaviors including overall wall buckling and bar buckling observed in experimental tests, as well as a three-dimensional, full-building engineering assessment of the Alto Rio building in an attempt to simulate the likely mode of failure that precipitated collapse of the building.

1.6 Report Organization and Content

This report summarizes the studies of reinforced concrete wall buildings in Chile, and the resulting recommendations for U.S. design and construction practice. It is

organized around four problem-focused study areas targeting recurring patterns of damage observed in shear walls and other elements of mid-rise and high-rise reinforced concrete buildings.

Chapter 2 summarizes detailing practices and observed damage to boundary elements in reinforced concrete walls in Chile, investigates the ability of current ACI 318 requirements to capture or predict that damage, and identifies potential changes that could be considered for U.S. shear wall design requirements that are suggested by the results.

Chapter 3 investigates lateral wall instability in which the overall concrete wall section (as opposed to individual reinforcing bars) buckles laterally out-of-plane over a portion of the wall length and height, and provides design recommendations for minimizing this potential behavior.

Chapter 4 investigates building configuration issues associated with the damage related to wall discontinuities and structural irregularities, and provides recommendations for avoiding such issues or considering them in analysis and design.

Chapter 5 discusses approaches for analytical modeling of concrete wall buildings, and presents a series of studies using these models to capture behaviors observed in experimental tests of concrete wall specimens and buildings damaged in the 2010 Maule earthquake.

Chapter 6 synthesizes findings and recommendations from studies on wall boundary elements, wall buckling, discontinuities in building configuration, and wall simulation techniques presented in Chapters 2 through 5.

Appendix A presents detailed information on the approaches and assumptions used in modeling reinforced concrete shear walls and assessing boundary element behavior as discussed in Chapter 2. Design loads, material properties, seismic demands, and other parameters that were considered are described and summarized for each building.

Appendix B presents the derivation of wall instability relationships used in the discussion of overall wall buckling in Chapter 3.

Appendix C examines the basic mechanism for damage occurring in reinforced concrete wall sections above or below a series of stacked wall openings discussed in Chapter 4, considers case studies from Chile, and proposes a design solution.

Appendix D summarizes studies exploring the extent to which commonly used evaluation tools capture building configuration issues discussed in Chapter 4 that contributed to concrete wall damage observed in the 2010 Maule earthquake.

Appendix E illustrates an approach for gaining an understanding of building response through consideration of the relative strengths of various structural components and actions in a pier-spandrel system discussed in Chapter 4.

Appendix F presents detailed information regarding testing configuration, material properties, and loading protocols used in the experiments selected for calibration of analytical models presented in Chapter 5.

The references cited in the preparation of this report are provided in Appendix G.

Investigation of Wall Boundary Elements

This chapter summarizes the results of an investigation of damage observed in boundary elements of reinforced concrete shear walls in the 2010 Maule earthquake, and what changes, if any, should be considered for U.S. shear wall design requirements. Relevant U.S. requirements include provisions in ACI 318-11, *Building Code Requirements for Structural Concrete and Commentary* (ACI, 2011) related to: (1) triggers for determining if special boundary elements are required; (2) assumptions on plastic hinge lengths used as a basis for code provisions; and (3) relationships between the quantity and distribution of transverse reinforcement and section failure (i.e., concrete crushing and reinforcing bar buckling).

In this chapter, the observed damage to wall boundary elements is described, ACI 318 triggers for special boundary elements are applied to Chilean buildings, a method for estimating the susceptibility of walls to buckling of longitudinal reinforcement is developed and tested, and the implications of potential changes to ACI 318 shear wall detailing (and how such changes would affect wall design) are investigated.

2.1 Description of Observed Damage to Wall Boundary Elements

Widespread and significant damage to reinforced concrete structural walls, particularly at or near the ground level, was observed in buildings in Santiago, Viña del Mar, and Concepción following the 2010 Maule earthquake (Figure 2-1). In general, crushing and spalling of concrete and buckling of vertical reinforcement were observed, often extending over nearly the entire length of the wall. Damage was typically concentrated over a short height equal to one to three times the wall thickness, but was also observed at other locations over the height of the wall.

Closer inspection of wall boundary regions (Figure 2-2) revealed that non-existent hoops or relatively large spacing of hoops (e.g., 200 mm; 8 inches), large spacing of horizontal web reinforcement (e.g., 200 mm; 8 inches), and 90-degree hooks on horizontal reinforcement were common details present in damaged walls (Massone et al., 2012).

Because traditional Chilean practice often uses thin structural walls (e.g., 150 mm to 200 mm; 6 inches to 8 inches thick), spalling of approximately 20 mm (0.75 inches)

of cover concrete on each side results in about a 25% reduction in wall thickness. Once the cover concrete spalls, 90-degree hooks used to anchor transverse reinforcement at the wall boundaries are susceptible to opening, which makes them ineffective at confining the concrete core and providing stability to the vertical bars. Large spacing of transverse reinforcement and the use of 90-degree hooks likely contributed to buckling of vertical reinforcement, which led to the observed concentration of damage in shear walls.



Figure 2-1 Typical reinforced concrete shear wall damage in the 2010 Maule earthquake: (a) first subterranean level of an 18-story building in Santiago (photo courtesy of Jack Moehle); and (b) ground floor level of a 10-story building in Viña del Mar (photo courtesy of Patricio Bonelli).

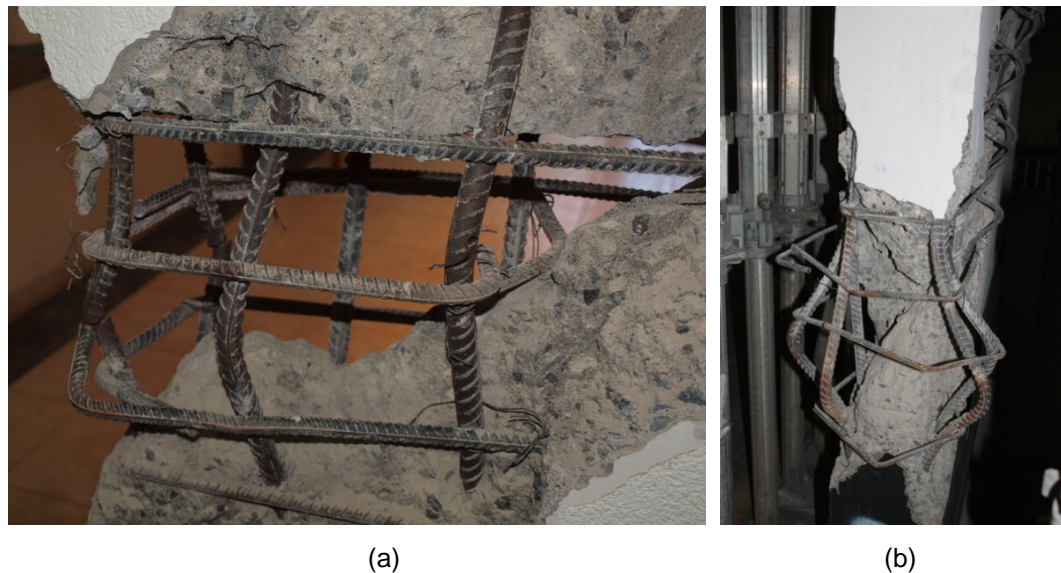


Figure 2-2 Typical detailing and observed damage to wall boundary regions: (a) ground floor level of a 23-story building in Coronel (photo courtesy of John Wallace); and (b) first subterranean level of a 20-story building in Santiago (photo courtesy of Jack Moehle).

2.2 Relevant U.S. Code Requirements and Design Practice

Current U.S. provisions for special structural walls are contained in Section 21.9 of ACI 318-11, including provisions for reinforcement (Section 21.9.2), shear strength (Section 21.9.4), design for flexural and axial loads (Section 21.9.5), and boundary elements of special structural walls (Section 21.9.6). This section focuses on the provisions of Section 21.9.6.

In ACI 318 Section 21.9.6, neutral axis depths (Section 21.9.6.2) or wall compressive stresses (Section 21.9.6.3) are compared to specified limits to determine if special boundary elements are required at wall boundaries. If special boundary elements are required, the quantity and distribution of transverse reinforcement is based on Section 21.9.6.4; otherwise the requirements of Section 21.9.6.5 apply.

In ACI 318 Section 21.9.6.2, a displacement-based approach is used to develop requirements for neutral axis depth. The design displacement, δ_u , is related to local plastic hinge rotation, θ_p , and extreme fiber compressive strain, ε_c , as:

$$\theta_p = \frac{\delta_u}{h_w}; \quad \theta_p = \left(\phi_u = \frac{\varepsilon_c}{c} \right) \left(l_p = \frac{l_w}{2} \right) \quad \therefore \quad \varepsilon_c = 2 \left[\frac{\delta_u}{h_w} \right] \left[\frac{c}{l_w} \right] \quad (2-1)$$

where h_w is the wall height, l_p is the plastic hinge length, c is the neutral axis depth for the nominal moment and the largest axial load for the specified load combinations ($M_n, P_{u,max}$), and l_w is the wall length. The plastic hinge length is assumed to be half the length of the wall (i.e., $l_p = 0.5l_w$). If the compressive strain exceeds a limiting value, assumed to be 0.003, then special transverse reinforcement is required. In ACI 318 Equation 21-8, this approach is rearranged to define a limiting neutral axis depth instead of a limiting concrete compressive strain as:

$$c_{limit} = \frac{0.003l_w}{2(\delta_u/h_w)} = \frac{l_w}{667(\delta_u/h_w)} \approx \frac{l_w}{600(\delta_u/h_w)} \quad (2-2)$$

In this approach, it is obvious that the need for special boundary elements is sensitive to the values used for the design displacement, δ_u , plastic hinge length, l_p , and the value assumed for limiting concrete compressive strain. If the largest computed neutral axis depth, c , computed for ($M_n, P_{u,max}$) is less than c_{limit} , then special boundary elements are not required. For the purpose of checking neutral axis depth, the value of δ_u/h_w shall not be taken less than 0.007. This approach was originally added in the 1999 edition of ACI 318 based on research following the 1985 Chile earthquake (Wallace and Moehle, 1992; Wallace, 1996; Wallace and Orakcal, 2002).

Alternatively, the stress-based approach of ACI 318 Section 21.9.6.3 may be used, in which the maximum compressive stress at the extreme fiber (wall edge) is used to determine the need for special boundary elements. The compressive stress is computed as:

$$f_c = \frac{P_u}{A_g} + \frac{M_u c}{I_g} \leq 0.2 f'_c \quad (2-3)$$

where P_u and M_u are the design (factored) axial load and moment, respectively, A_g is the wall gross area, I_g is the gross concrete moment of inertia, and c is the distance from the elastic centroid to the wall edge. ACI 318 Commentary Section R21.9.6.3 notes that stresses calculated using Equation 2-3 are index values, and are not intended to describe the actual state of stress in the wall at the critical section.

If special boundary elements are required, the quantity and distribution of required transverse reinforcement is defined in Section 21.9.6.4, which refers to requirements for special moment frame columns (ACI 318 Section 21.6.4), and provides transverse reinforcement that is intended to prevent bar buckling and concrete crushing at large deformation demands. If special boundary elements are not required, the requirements of Section 21.9.6.5 apply, which provide a moderate amount of transverse reinforcement to prevent bar buckling at smaller deformation demands. Where special boundary elements are not required, the region at the wall boundary is referred to as an ordinary or typical boundary condition. The height of the wall over which special boundary elements are required is defined in Section 21.9.6.2 for the displacement-based approach and Section 21.9.6.3 for the stress-based approach.

2.3 Comparison of ACI 318 Special Boundary Element Requirements and Observed Building Damage

Although Chilean codes have referenced ACI 318 as a basis for reinforced concrete design requirements since the 1990s, Chilean implementation of ACI 318 has omitted requirements for special boundary elements. As a result, the majority of buildings that experienced the 2010 Maule earthquake did not have special boundary element detailing, which provides an opportunity to assess if the provisions of ACI 318 Section 21.9.6.2 effectively identify the susceptibility of wall boundaries to the observed damage.

2.3.1 Approach

A total of seven mid-rise and high-rise buildings in Santiago, Viña del Mar, and Concepción were selected for study. These included Alto Rio, Plaza del Rio Building B, Concepto Urbano, Toledo, Undisclosed Building A, Undisclosed Building B, and Mongolio. In these buildings, the provisions of ACI 318 Section 21.9.6.2 were applied to determine if the walls would have required special boundary elements, and the results were cross-referenced with the level of damage observed in the walls. The requirements of ACI 318 Section 21.9.6.3 were not applied as they tend to be conservative (i.e., a special boundary element is almost always required per these requirements).

A range of building heights (e.g., 10 to 22 stories) was selected, because wall height plays a significant role in axial load and roof drift ratio demands. Various wall cross-sections (e.g., T-shaped, L-shaped, and rectangular) were selected to investigate differences in the behavior of flanged versus planar walls. Detailed information on building design, construction, material properties, and loading is provided in Appendix A.

Expected roof drift ratios were calculated using a simplified approach based on an estimate of building period and spectral displacements obtained from displacement response spectra from nearby recording stations. Response spectra, estimated periods, and drift ratio calculations for each building are provided in Appendix A. Alternative approaches of estimating building periods, when available, were used for comparison.

Moment-curvature analyses were performed on critical wall sections to determine neutral axis depths corresponding to the factored axial load and estimated roof drift ratios on each wall. Calculated neutral axis depths were compared to ACI 318 triggers for special boundary elements. For asymmetric wall cross sections (e.g., T-shaped and L-shaped walls), moment-curvature analyses were performed for both bending with the flange in tension and bending with the flange in compression. Moment-curvature analysis results for each wall cross-section are provided in Appendix A.

2.3.2 Results

The results of special boundary element trigger evaluations for case study walls in each building are provided in Appendix A. In general, end zones of planar walls, and end zones opposite the flange of T-shaped and L-shaped walls would have required ACI 318 special boundary element detailing based on the requirements of Section 21.9.6.2.

Wall axial load ratios varied between $0.05A_gf'_c$ and $0.45A_gf'_c$, with most walls having moderate axial demands on the order of $0.10A_gf'_c$ to $0.15A_gf'_c$. Walls with higher axial load ratios (on the order of $0.20A_gf'_c$ to $0.45A_gf'_c$) generally exceeded ACI 318 triggers and would have required special boundary element detailing based on Section 21.9.6.2.

Calculated roof drift ratios typically ranged between 0.4% and 1.0%, with the exception of one building, which had the highest drift ratio at nearly 3%. In general, walls with higher drift ratios exceeded ACI 318 triggers, and walls with lower drift ratios did not. ACI 318 requires a minimum drift ratio of 0.7% for the purpose of checking special boundary element requirements. Three buildings had estimated drift ratios less than 0.7%. In these three cases, most walls exceeded ACI 318 triggers and would have required special boundary elements regardless of whether the checks

were made using the actual estimated drift ratio or the code-specified minimum drift ratio.

Overall, correlation between ACI 318 special boundary element triggers and observed damage in the case study buildings was good. In most cases, the need for special boundary elements corresponded with damage at the wall boundary. Similarly, wall sections that did not need special boundary elements were undamaged at the wall boundary. Notable exceptions include the Concepto Urbano building, in which the wall sections significantly exceeded special boundary element triggers at the estimated roof drift ratio, but were relatively undamaged in the earthquake. The drift ratio for this building was significantly higher than the other buildings, at 3%. A possible explanation for this discrepancy is that the approximate building drift ratio was overestimated in the case of this building. Other exceptions occurred in the Alto Rio building in which wall flanges did not exceed special boundary element triggers, yet were noted as damaged. It is possible that the impending collapse of the degrading building resulted in extensive damage across all walls, masking individual cases where wall boundaries otherwise might not have been damaged.

Results support the need for special boundary element detailing in walls with: (1) asymmetric flanged cross-sections (e.g., L-shaped and T-shaped); (2) high axial load ratios; and (3) large displacement demands. All of these factors can lead to deep neutral axis depths and excessive demands at the extreme compression fiber.

2.3.3 Potential Changes to ACI 318 Boundary Element Triggers

As shown in Figure 2-3, response spectra computed using ground motions recorded in recent large earthquakes have, in many cases, significantly exceeded design response spectra.

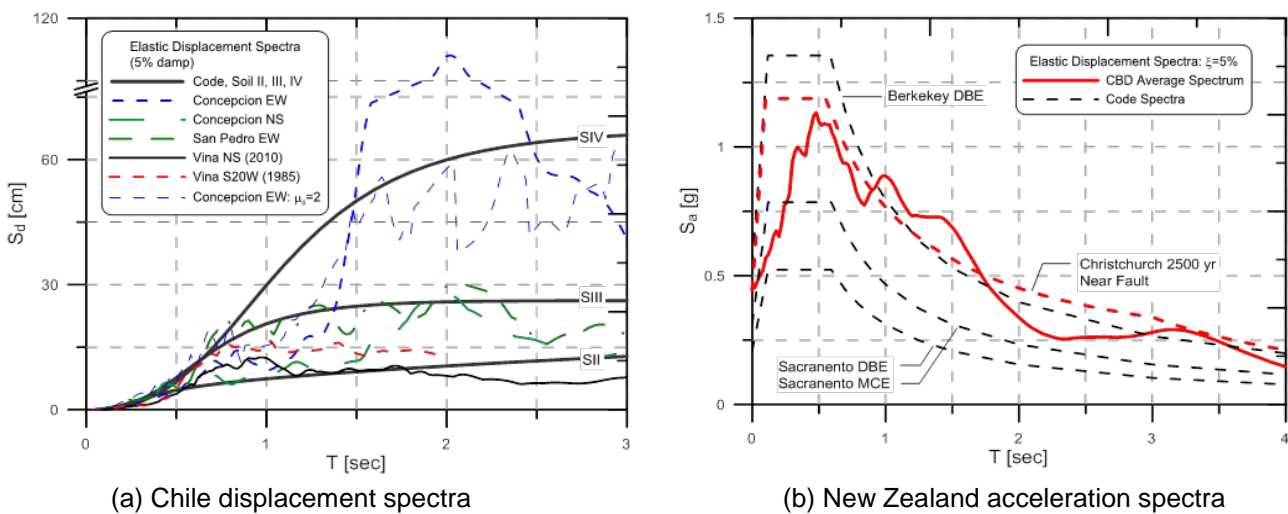


Figure 2-3 Response spectra from recent large earthquakes: (a) displacement spectra for 2010 Maule earthquake; and (b) acceleration spectra for 2011 Christchurch earthquake.

In Chile, for example, the vast majority of buildings were designed for the Soil Type II response spectrum (in accordance with NCh433.Of96 (INN, 1996)). Ordinates for elastic response spectra from motions recorded in the 2010 Maule earthquake were generally 2 to 6 times the values for the Soil Type II spectrum at periods between 0.5 and 2.0 seconds.

The trigger for special boundary elements in ACI 318 is directly related to the estimate of design displacement. Given such large potential differences between design and actual demand, it is important to recognize how displacement demands influence design requirements for structural walls. Response spectra used for design must be appropriate for the earthquake hazard and soil profile at the site. Since the earthquake, Chilean design response spectra have been revised, particularly for soft-soil sites. This change is not specific to concrete wall buildings, so it is not discussed in detail here, but soft-soil sites can increase displacement demand, and therefore deformation demands on wall boundary elements.

Recent developments in U.S. codes have focused on performance-based targets for design, and on providing an acceptably low probability of collapse given earthquake shaking at the Maximum Considered Earthquake (MCE) hazard level (FEMA, 2009). In contrast, current ACI 318 triggers for special boundary elements are based on evaluation of the concrete crushing limit at the Design Earthquake (DE) hazard level, which is defined as two-thirds of the MCE hazard level in ASCE/SEI 7-10, *Minimum Design Loads for Buildings and Other Structures* (ASCE, 2010).

A potential change has been considered by ACI technical committees to adjust special boundary element requirements to consider demands associated with the MCE hazard level. One approach involves adjusting Equation 2-2 (ACI 318 Equation 21-8), which defines the limiting neutral axis depth, to include a factor of about two on the drift ratio, δ_u / h_w , in the denominator (see Equation 2-4):

$$c_{limit} = \frac{l_w}{600(2\delta_u / h_w)} \quad (2-4)$$

This factor is based on a combination of two factors: 1.5, which is the relationship between MCE spectra and DE spectra; and 1.25, which is an adjustment for the potential for damping to be in the range of 2.0% to 2.5% (ATC, 2010). The intent of such a change would be to relax detailing requirements only when the estimated displacement, taken as twice the design displacement, has a low probability of being exceeded.

2.4 Investigation of Plastic Hinge Length

The provisions of ACI 318 Section 21.9.6.2 are based on an assumed plastic hinge length equal to half the length of the wall (i.e., $l_p = 0.5l_w$). ASCE/SEI 41-06, *Seismic*

Rehabilitation of Existing Buildings (ASCE, 2007), also recommends using a plastic hinge length equal to half the length of the wall. Wall damage observed in Chile, however, tended to concentrate over a relatively short height (e.g., 2 to 3 wall thicknesses). The following study was undertaken to reassess the assumption of $l_p = 0.5l_w$.

A review of various plastic hinge models available in the literature is provided in Appendix A. Recommended values for wall plastic hinge length vary widely, although typical values are in the range between $0.5l_w$ and $1.0l_w$, but less than one story height. Figure 2-4 illustrates results obtained from various relations used to estimate plastic hinge length. Most of the models in the figure were developed from tests on concrete columns and beams subjected to a variety of loading conditions. The horizontal black line at 0.5 represents the relationship implicit in ACI 318 Section 21.9.6.2 and ASCE/SEI 41-06.

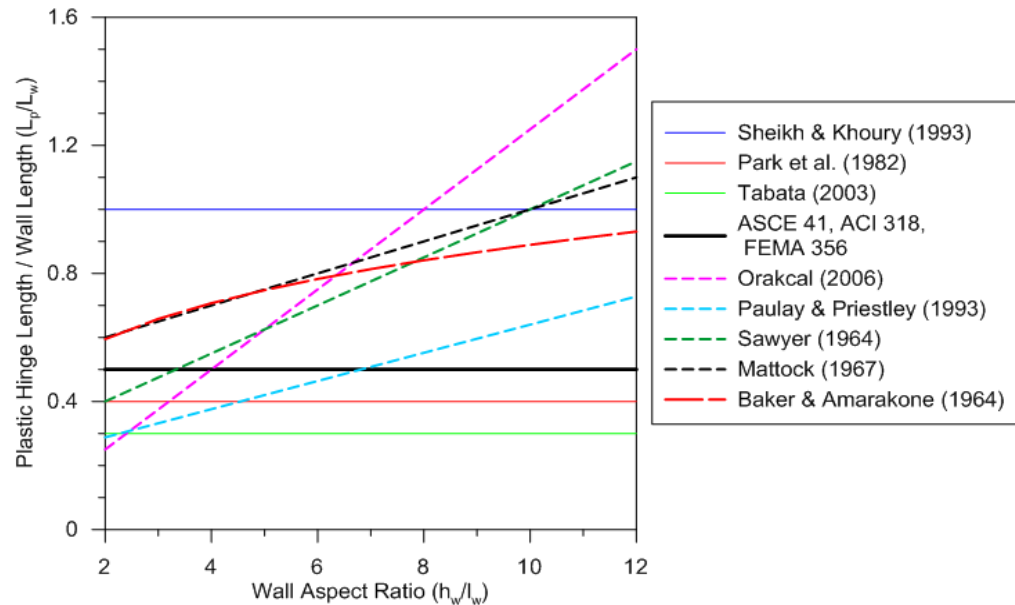


Figure 2-4 Comparison of various plastic hinge length models available in the literature.

The value selected for plastic hinge length may have a significant impact on the results computed using Equation 2-2, or with the following relation, which includes both elastic and inelastic displacements (Wallace and Moehle, 1992):

$$\frac{\delta_u}{h_w} = \frac{11}{40} \phi_y h_w + l_p (\phi_u - \phi_y) \quad (2-5)$$

Figure 2-5, which presents drift versus curvature relations for various plastic hinge lengths for a wall with an L-shaped cross section, demonstrates that computed curvature values obtained using Equation 2-5 are sensitive to the assumed plastic hinge length. For small estimates of plastic hinge length, damage concentrates over a

short height, and strength loss occurs at relatively low deformation (drift) demands. Improved behavior (i.e., strength loss at higher inelastic deformations) occurs where inelastic deformations are spread out over greater heights. Figure 2-6 relates drift ratio, δ_u / h_w , to the limiting concrete compressive strain ($\epsilon_c = 0.003$) for various plastic hinge lengths, and shows that the drift ratio at which the limiting compressive strain is reached is significantly impacted by the assumed plastic hinge length.

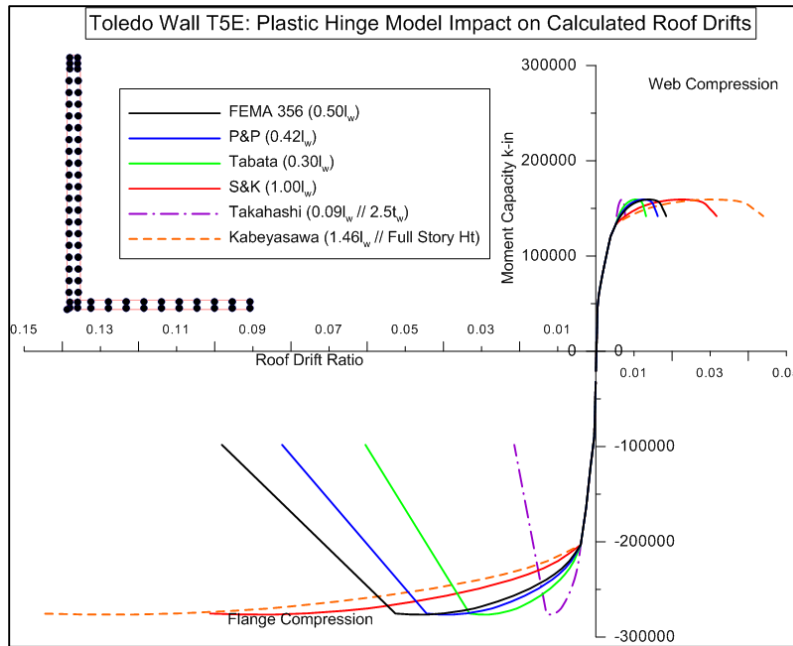


Figure 2-5 Roof drift ratio versus wall curvature relations for various plastic hinge lengths for a wall with an L-shaped cross-section.

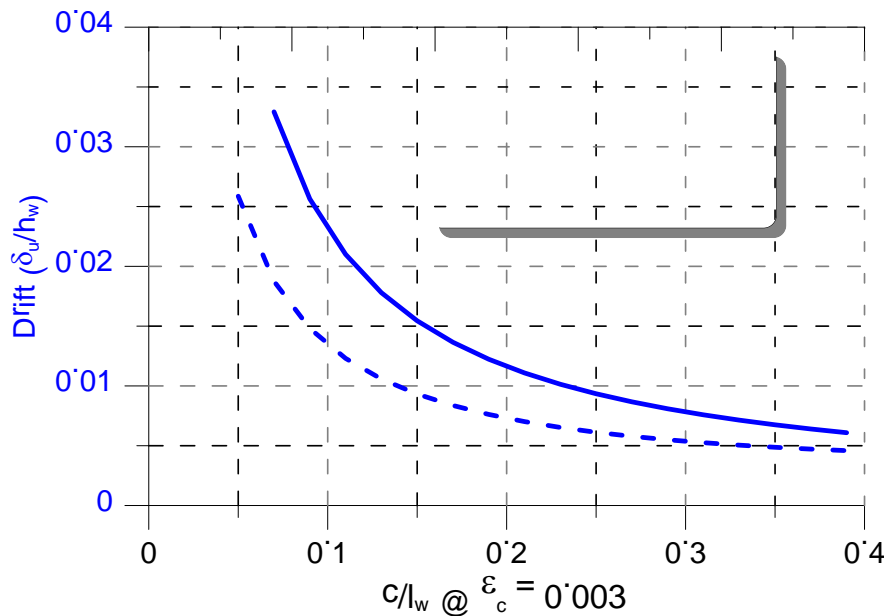


Figure 2-6 Drift ratio versus limiting concrete compressive strain for various plastic hinge lengths.

2.4.1 Potential Changes to ACI 318 Plastic Hinge Length, Minimum Thickness, and Confinement Requirements

Potential changes to ACI 318 were studied to investigate the continued use of $l_p = 0.5l_w$. Section 10.3 of ACI 318 defines tension-controlled and compression-controlled sections for beams; however, no guidance is provided on how these requirements should be applied to special (or ordinary) structural walls. In addition, ACI 318 does not place limits on the axial stress in walls.

The performance of walls in Chile suggests that higher axial stresses coupled with asymmetric wall cross-sections (e.g., T-shaped) may lead to compression-controlled behavior in which the concrete compressive strain reaches 0.003 prior to yielding in the tension reinforcement. Such behavior was also observed in wall specimens tested by Thomsen and Wallace (2004), which have similar detailing to walls in Chile.

One way to avoid compression-controlled behavior is to place a limit on axial load. In the 1997 *Uniform Building Code* (ICBO, 1997), for example, wall axial load was limited to $0.35P_o$, where P_o is the nominal axial strength of the wall at zero eccentricity. At higher axial loads, the lateral strength and stiffness of the wall could not be considered in resisting seismic forces. As a possible alternative to neglecting the seismic resistance of walls that are not tension-controlled, more stringent detailing requirements could be considered, such as:

- Requiring tension-controlled walls to use $l_p = 0.5l_w$.
- Requiring special boundary elements on walls that are not tension-controlled.
- Requiring increased wall thickness for improved lateral stability under large compressive loads.
- Requiring the application of ACI 318 Equation 21-4 (for column confinement) in the design of special boundary elements.

Checking that a wall is tension-controlled can be accomplished using the following relation:

$$\frac{c}{l_w} < \frac{\varepsilon_c}{\varepsilon_c + \varepsilon_s} l_w = \frac{0.003}{0.003 + 0.005} l_w = 0.375l_w \quad (2-6)$$

where ε_c is the extreme fiber compressive concrete strain and ε_s is the tensile strain in the boundary longitudinal reinforcement located closest to the edge of the wall (furthest from the neutral axis). In Equation 2-6, ε_c is taken as 0.003 and ε_s is taken as 0.005 to be consistent with values used to define tension-controlled beam sections according to ACI 318 Section 10.3.4.

The minimum drift ratio of $\delta_u / h_w = 0.007$ for boundary element checks in Section 21.9.6.2 has the effect of always requiring special boundary elements where:

$$\frac{c}{l_w} > \frac{c_{limit}}{l_w} = \frac{1}{600(\delta_u/h_w = 0.007)} = 0.238 \quad (2-7)$$

Current ACI 318 provisions already require special boundary elements if walls are not tension-controlled (i.e., the walls are compression-controlled), and also require special boundary elements if the tensile strain in the boundary reinforcement furthest from the neutral axis is less than 0.0096. A change to require boundary elements on compression-controlled walls is not required.

Whether or not current ACI 318 requirements provide an adequate amount of transverse reinforcement in special boundary elements of thin walls, however, is not clear. Current requirements for transverse reinforcement do not address the effect of loss of cover in wall boundaries. In the case of thin walls, concrete cover over the primary longitudinal reinforcement accounts for a large percentage of total wall thickness. Loss of cover in thin walls results in a correspondingly larger reduction in the total cross-section, and a reduction in ductile behavior.

Based on a review of data from Thomsen and Wallace (2004) and Tran (2012), limiting the ratio of concrete cover to approximately 10% of the wall thickness has been shown to result in ductile wall behavior up to drift ratios of 2.5% for walls with boundary transverse reinforcement satisfying (or nearly satisfying) current ACI 318 requirements for A_{sh} , which are based on ACI 318 Equation 21-5. For cover of 0.75 inches to 1.5 inches, this would translate to minimum wall thicknesses of 7.5 inches and 15 inches, respectively.

Given values in ACI 117-10, *Specification for Tolerances for Concrete Construction and Materials* (ACI, 2010), for members with depth (or thickness) over 4 inches but less than 12 inches, reinforcement tolerance is $\pm 3/8$ inch, concrete cover tolerance is $-3/8$ inch, and reduction in concrete cover cannot exceed one-third the specified cover. The critical case is for larger cover; therefore, one approach for restricting the use of thin walls would be to prescribe minimum wall thickness that is 10 times the cover, including an allowance for cover tolerance.

For example, minimum wall thickness values for 0.75 inches and 1.5 inches of cover, including tolerance, would be $10 \times (0.75 + 0.375) = 11.25$ inches, and $10 \times (1.5 + 0.375) = 18.75$ inches, respectively. A specified minimum wall thickness in the range of 12 inches to 18 inches would be consistent with this approach.

An alternative to increasing wall thickness using current transverse reinforcement requirements (e.g., based on ACI 318 Equation 21-5) would be to require more transverse reinforcement in thin walls (e.g., use of ACI 318 Equation 21-4), which is discussed in Section 2.6, below.

2.5 Investigation of Longitudinal Bar Buckling in Wall Boundary Elements

Typical vertical spacing of transverse reinforcement in the boundary zones of structural walls in Chile is approximately 150 mm to 200 mm (6 inches to 8 inches). For longitudinal bar diameters in the range of 18 mm to 25 mm (#6 to #8), ratios of hoop (or tie) spacing to longitudinal bar diameter, s/d_b , ranged between 8 and 11. For comparison, requirements for spacing of transverse reinforcement in ACI 318 Section 21.6.4.3 include a ratio of $s/d_b = 6$ as one of a series of limits. Larger s/d_b ratios result in limited confinement of concrete, and leave longitudinal reinforcement more susceptible to buckling instability.

The following study was undertaken to assess whether or not buckling of vertical reinforcement should have been expected at the boundaries of concrete walls in Chilean buildings, and to explore the relationship between the phenomena of concrete crushing and bar buckling. Issues relevant to detailing of concrete walls include: (1) to what extent does concrete cover restrain bar buckling; (2) to what extent does bar buckling induce spalling of cover concrete; and (3) in what configurations is bar buckling likely to precede crushing of the concrete core. This information can be used to determine if current ACI detailing provisions and limitations on s/d_b ratios are adequate to prevent bar buckling under design displacements.

2.5.1 Approach

This section summarizes the approach used to assess the likelihood of bar buckling in Chilean walls, and to compare results with observed behavior. Assessment of the onset of bar buckling was based on the parameter ε_p^* introduced in Rodriguez et al. (1999). As defined, the parameter ε_p^* measures the amount of bar strain from the point of reloading bars in compression to the point when bars begin to buckle (background and derivation is provided in Appendix A).

In this investigation, approximate analyses were used to estimate the roof displacement (and drift ratios) in each building. Moment-curvature analyses at critical wall sections were used to calculate tensile and compressive strains associated with the estimated roof drift ratios, and these values were used to approximate the strain histories in the longitudinal boundary reinforcement. From the approximate strain histories, values of the parameter ε_p^* were estimated for each wall, and then the likelihood of longitudinal bar buckling at wall boundaries in Chilean case study buildings was assessed.

2.5.2 Results

Assessments for each wall cross-section in each case study building are provided in Section A.6. In tension-controlled wall sections, bar buckling analyses at the

expected roof drift ratios produced relatively large longitudinal bar strains at wall boundaries without a flange (e.g., rectangular cross-sections, and T-shaped or L-shaped sections opposite the flange). In many such wall sections, onset of bar buckling was expected to occur prior to concrete crushing at the expected roof drift ratios.

At flanges of tension-controlled walls, buckling analyses generally produced much lower strains such that the onset of bar buckling was unlikely. This result is not unexpected. For flanged wall sections, a relatively deep neutral axis depth for compression occurs in the web when the flange is in tension, which limits the tensile strain in the longitudinal reinforcement in the flange. Similarly, a very shallow neutral axis depth occurs when the flange is in compression, limiting the compressive strains in the longitudinal reinforcement in the flange. Figure 2-7 illustrates the difference in reinforcing strains at different ends of a flanged wall for equal but opposite roof drifts.

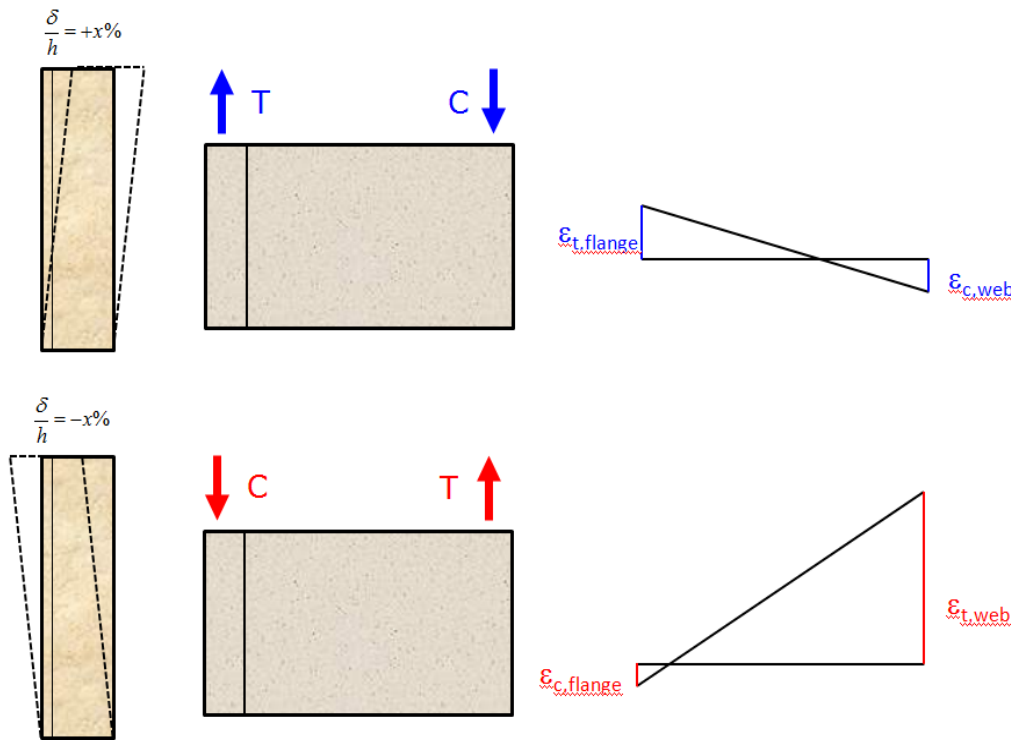


Figure 2-7 Differences in longitudinal reinforcement strain levels at each end of a flanged wall.

Analyses of several compression-controlled wall sections with high axial loads (i.e., $\geq 0.20A_gf'_c$) indicated that neither the onset of bar buckling nor strength loss due to concrete crushing was likely at the expected roof drift ratios. Because of the relatively large neutral axis depths in compression-controlled walls, moment-curvature analyses revealed that extreme fiber strains in tension would not significantly exceed yield strains, which would, in turn, minimize reloading strains,

and ultimately reduce the cumulative strain history in the reinforcement of such walls. Because the magnitude of the tension and compression strain cycles contributes to the calculation of the bar buckling parameter ε_p^* , compression-controlled walls reacted differently in the bar buckling evaluation.

Results from bar buckling assessments had some correlation with observed damage in that many walls with high longitudinal reinforcement strain demands exhibited bar buckling behavior, and walls with low demands did not. However, in some buildings that were heavily damaged (e.g., Toledo), wall damage did not correlate with the assessed potential for onset of bar buckling. In this case, it is possible that the use of horizontal web reinforcement as transverse reinforcement in the absence of hoops (or ties) overestimated the stability of the longitudinal reinforcement.

Post-earthquake damage assessments also indicated that compression-controlled wall sections were damaged near the base of the wall. It is possible that discrepancies between analyses and observed damage could be due to limitations in the simplified analysis and drift-curvature relationship approach used in the bar buckling assessment, and the assumption that plane sections remain plane after loading. It also is noted that the use of an assumed plastic hinge length equal to half of the wall length is probably not appropriate for compression-controlled walls, since significant spread of plasticity is unlikely to occur in walls that do not include special boundary element detailing. Furthermore, damage was often noted at locations where horizontal setbacks occurred in the wall section. Stress (and strain) concentrations at wall setbacks would be expected to cause higher strain levels than predicted by the drift-curvature relationship used in this study.

2.6 Potential Changes to ACI 318 Special Boundary Element Detailing Requirements

ACI 318 detailing requirements for special boundary elements are based on requirements that were developed for columns. A review of recent wall damage in earthquakes and laboratory tests has raised questions related to detailing of thin walls and whether current detailing requirements are adequate to provide the code-intended performance. ACI technical committees have considered changes to the requirements for special boundary elements including:

1. Requiring the area of transverse reinforcement, A_{sh} , in special boundary elements to satisfy both ACI 318 Equation 21-4 and ACI 318 Equation 21-5 (current provisions only require that ACI 318 Equation 21-5 be satisfied).
2. Adding a requirement that the horizontal spacing of hoops (or tie) legs along the length of the wall be limited to $2/3 \times t_w$, or alternatively t_w .

This section presents an evaluation of the effects that such changes would have on concrete wall designs, if adopted.

2.6.1 Changes to Required Area of Transverse Reinforcement

The intent of requiring that wall boundary elements satisfy ACI 318 Equation 21-4 would be to discourage the use of thin wall sections with large cover and to increase the amount (area) of confining steel in order to help maintain core stability if the cover were to spall.

Tests of conventional reinforced concrete wall sections are shown in Figure 2-8. In these tests, the transverse reinforcement provided at the wall boundaries was 1.4 and 2.1 times that required by ACI 318-11 Section 21.9.6.4, however, concrete crushing and lateral instability (Figure 2-8b) were observed to occur early in the tests. Inspection of the damaged boundary zone revealed that relatively large clear cover was used, on the order of 40 mm (1.5 inches), which is larger than ACI 318 code minimum of 19 mm (0.75 inches), suggesting that the amount of transverse reinforcement provided was incapable of maintaining stability of the compression zone following loss of concrete cover.

ACI 318 Equation 21-4, which is based on maintaining column axial load capacity after spalling of concrete cover, typically governs the selection of transverse reinforcement where cover makes up a larger percentage of the gross concrete section (e.g., in smaller column sections). This equation was also required for special boundary elements in walls prior to the 1999 edition of ACI 318, but it was dropped because it did not control for the thicker wall sections that were commonly used at the time. For the conventional reinforced concrete walls in Figure 2-8, the provided transverse reinforcement was only 0.34 and 0.45 times that required by ACI 318 Equation 21-4, suggesting that improved performance may have resulted if more transverse reinforcement had been provided. Additional testing is needed to determine appropriate requirements to ensure ductile behavior of thin boundary elements.

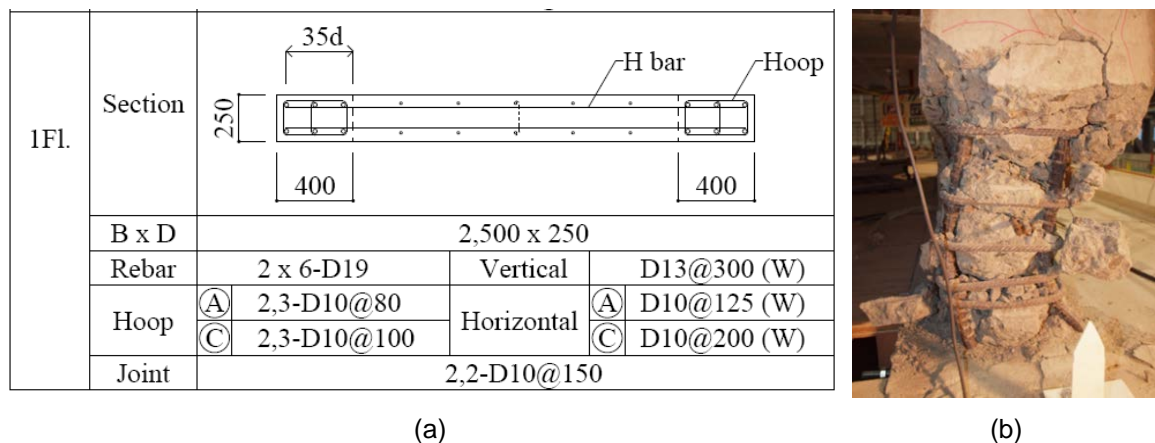


Figure 2-8 Tests on conventional reinforced concrete walls: (a) test specimen details; and (b) observed damage (Nagae et al., 2011). Note that in the table dimensions are given in mm.

In Figure 2-9, results for different thicknesses of concrete cover are presented to illustrate the impact of reinstating ACI 318 Equation 21-4 on transverse hoop and crosstie area, A_{sh} , for special boundary elements. In the figure, ACI 318 Equation 21-5 is provided as a baseline for comparison. Larger concrete cover thickness constitutes more of the gross section area, which significantly increases the required area of transverse reinforcement (relative to ACI 318 Equation 21-5), especially in smaller sections. Thicker wall sections see little to no increase in area because the relative percentage of cover is small. Also, as the boundary element gets longer (i.e., extends deeper into the wall web), the ratio of confined concrete section area to gross section area increases, and the additional area of transverse reinforcement required by ACI 318 Equation 21-4 decreases.

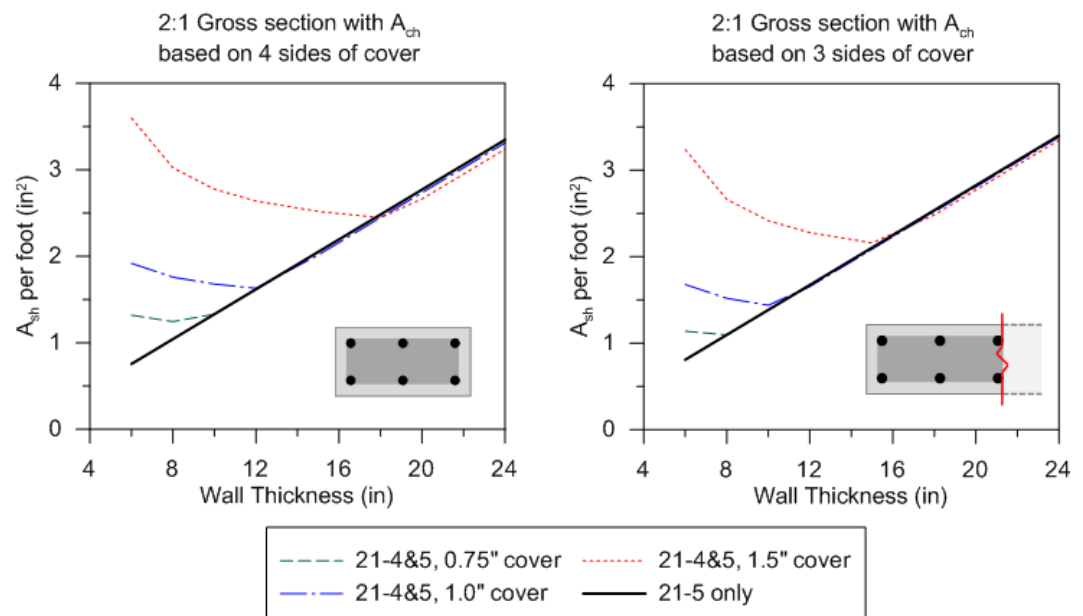


Figure 2-9 Effect of requiring that wall boundary elements satisfy ACI 318 Equation 21-4, illustrated for boundary elements with a length-to-thickness aspect ratio of 2:1.

Figure 2-9 also demonstrates the difference in required area of transverse reinforcement per ACI 318 Equation 21-4 when calculating the area of the confined core, A_{ch} , with three sides of cover (i.e., a wall boundary) as opposed to four sides of cover (i.e., a column). Considering only three sides of cover reduces the overall percentage of cover as a fraction of gross area, and results in a smaller calculated area of transverse reinforcement. Figure 2-10 presents similar information for a 3:1 aspect ratio, and shows the required area per hoop interval assuming the vertical spacing is maximized to the largest spacing allowed by ACI 318 special boundary element detailing requirements.

2.6.2 Changes to Horizontal Spacing of Ties

The intent of decreasing the maximum horizontal spacing of ties would be to improve confinement by decreasing the span of arching action of the confined core, as shown in Figure 2-11. ACI 318-11 Section 21.6.4.2 currently allows a horizontal distance, h_x , of 14 inches between adjacent hoops or ties. Use of such a large spacing in special boundary elements of thin walls is unlikely to provide sufficient confinement, and is inconsistent with the ACI 318 Section 21.9.6.4 requirement limiting vertical spacing of ties to no greater than one-third the wall thickness.

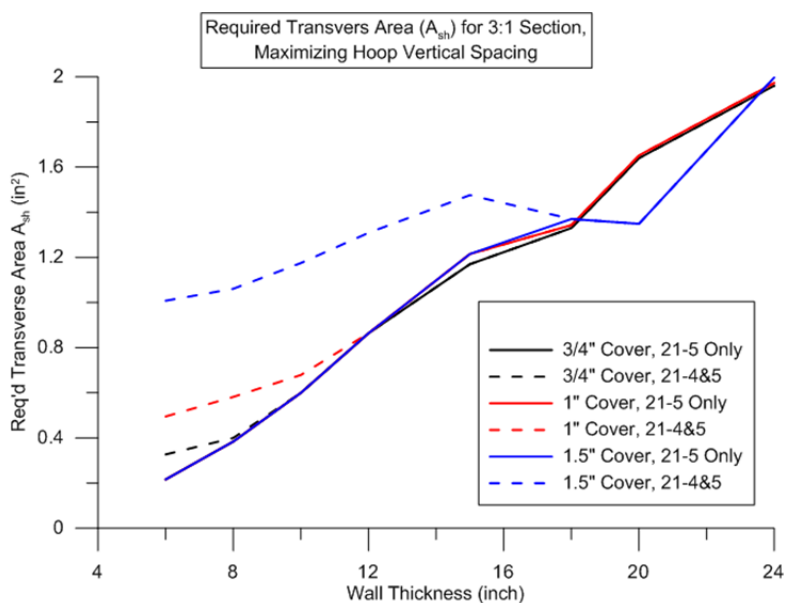


Figure 2-10 Effect of requiring that wall boundary elements satisfy ACI 318 Equation 21-4, illustrated for boundary elements with a length-to-thickness aspect ratio of 3:1, and assuming that vertical spacing of hoops is maximized.

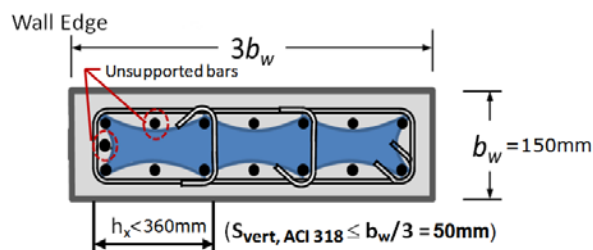


Figure 2-11 Confinement of thin wall sections and arching action between ties.

For example, in a 10-inch thick wall, vertical spacing along the height of the wall is limited to one-third the wall thickness, or 3.33 inches; however, horizontal spacing along the length of the wall can be 14 inches. An additional limit should be considered for special boundary elements, similar to that used for vertical spacing (e.g., the horizontal distance between legs of hoops or ties should be limited to some

factor times the wall thickness, such as $2/3 \times t_w$ or t_w). Also, not permitting intermediate, unsupported bars at the wall edge (as shown in Figure 2-11), should be considered. The potential impact of reducing the horizontal spacing, h_x , for crossies to t_w or $2/3 \times t_w$ is shown for 2:1 aspect ratio boundary elements in Figure 2-12, and for 3:1 aspect ratio boundary elements in Figure 2-13.

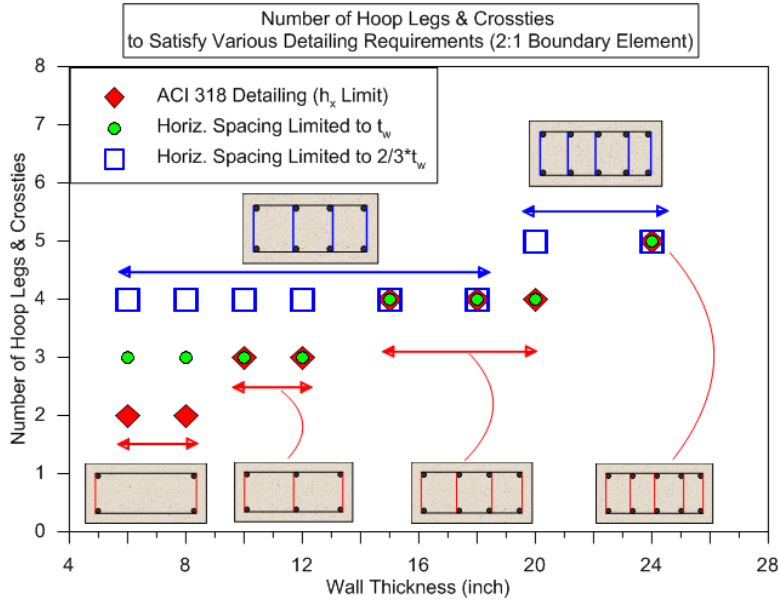


Figure 2-12 Impact of reduced horizontal spacing of boundary element crossies for 2:1 aspect ratio boundary elements.

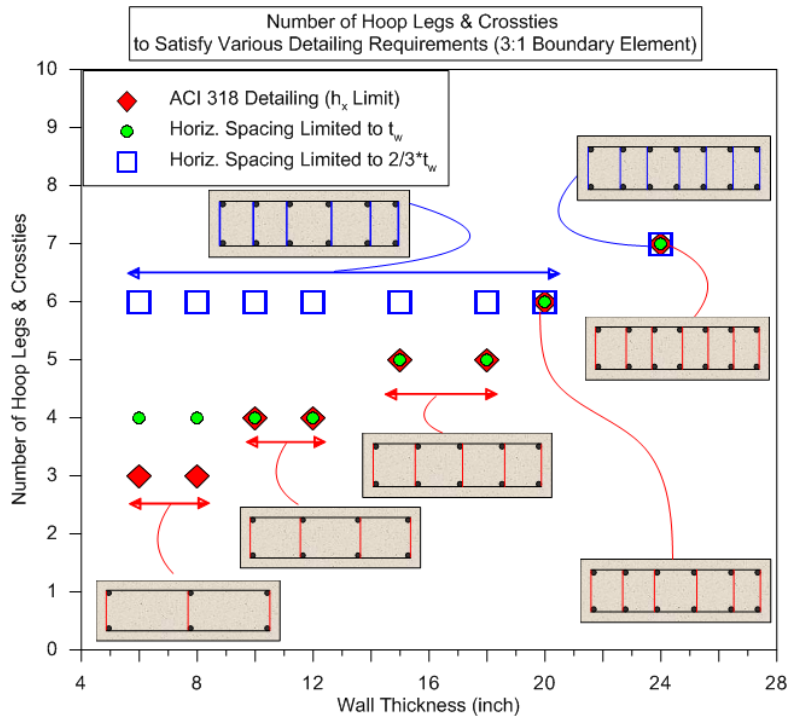


Figure 2-13 Impact of reduced horizontal spacing of boundary element crossies for 3:1 aspect ratio boundary elements.

In the figures, cross-section configurations are provided to illustrate the minimum reinforcement pattern for various wall thicknesses. Current ACI 318 requirements are represented by the cross-sections along the bottom of the figure. Hollow squares indicate the number of hoop legs or crosssties that are necessary to satisfy $h_x = 2/3 \times t_w$. Circles represent the number of hoop legs or crosssties needed to satisfy horizontal spacing of $h_x = t_w$, or no more than the wall thickness.

Current requirements allow thin walls (e.g. 6 inches to 8 inches thick) with 2:1 aspect ratio boundary elements to have a single hoop 14 inches long confining the boundary. Although this satisfies the code, it is unlikely to provide reliable confinement to the core of the boundary element, and is inconsistent with the requirement for vertical spacing to be no more than one-third the least dimension of the boundary element.

Reducing horizontal spacing to one wall thickness (t_w) requires even the thinnest walls to have at least one crossstie within the special boundary element (for 2:1 aspect ratio boundary elements). Further reduction of spacing to $2/3 \times t_w$ requires all 2:1 aspect ratio boundary elements to have at least four transverse bars (e.g., two crosssties, two hoop legs) confining the boundary element.

Figure 2-14 summarizes potential changes in boundary element crossstie configurations based on a maximum horizontal spacing of no more than the smaller of one wall thickness or 14 inches. If this limit is used, only boundary elements less than 10 inches thick will require additional crosssties.

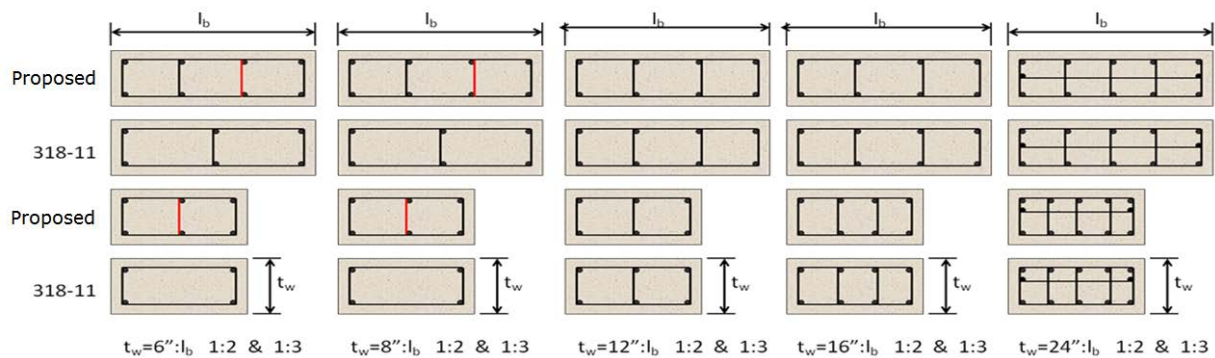


Figure 2-14 Summary of boundary element crossstie configurations for 2:1 and 3:1 aspect ratio boundary elements with maximum horizontal spacing taken as the smaller of one wall thickness or 14 inches.

2.7 Findings and Recommendations

In the 2010 Maule earthquake, reinforced concrete walls exhibited crushing and spalling of concrete and buckling of vertical reinforcement at wall boundaries, which often extended over the entire length of the wall. Damage was typically concentrated over a short height equal to one to three times the wall thickness, but was also

observed at other locations over the height of the wall. Thin wall sections, non-existent hoops or crossties, relatively large spacing of horizontal web reinforcement, and use of 90-degree hooks were common details present in damaged walls.

Investigation of observed damage in wall boundary elements included study of ACI 318 boundary element triggers, study of plastic hinge length, and study of concrete crushing and bar buckling behaviors. These studies resulted in the following findings:

- Application of ACI 318 boundary element triggers to walls in Chilean buildings indicated that most walls would have required special boundary element detailing in accordance with ACI 318. In general, observed damage correlated well with the need for special boundary elements. Results support the need for special boundary element detailing in walls with: (1) asymmetric flanged cross-sections (e.g., L-shaped and T-shaped); (2) high axial load ratios; and (3) large displacement demands.
- Investigation of plastic hinge length revealed that ACI 318 triggers for special boundary elements are very sensitive to the assumed plastic hinge length, and that observed wall damage in Chile occurred over much shorter heights (e.g., one to three times the wall thickness) than traditional assumptions on the order of half the wall length (e.g., $l_p = 0.5l_w$), especially in compression-controlled walls.
- Investigation of potential concrete crushing and bar buckling behaviors at the boundaries of Chilean structural walls revealed that some walls would have been expected to exhibit bar buckling behavior, while other walls would have been expected to exhibit concrete crushing prior to bar buckling. There was some correlation between observed damage and the expected onset of bar buckling, but correlation was better in tension-controlled walls, and worse in compression-controlled walls.

ACI 318 requirements for boundary elements in reinforced concrete walls have evolved over many code cycles, and ACI technical committees have recently considered several changes that have not yet been implemented. In some cases, requirements that were removed in prior code cycles should be considered for reinstatement. Based on the observed damage to concrete walls in Chile and the findings from wall boundary element investigations conducted herein, the following impacts to ACI 318 requirements for design of reinforced concrete walls can be considered (or reconsidered):

- The limiting neutral axis depth trigger for special boundary elements can be adjusted to provide improved performance at MCE-level ground shaking hazards. One approach would be to adjust ACI 318 Equation 21-8 to include a factor of about two in the denominator, as shown in Equation 2-4.

- The assumed plastic hinge length of $l_p = 0.5l_w$ can be maintained in the case of tension-controlled walls.
- Current provisions, which essentially require special boundary elements in walls that are not tension-controlled (i.e., compression-controlled walls), should be maintained.
- Increased minimum wall thickness should be considered for improved lateral stability under large compressive loads and potential spalling of concrete cover. One approach would be to prescribe a minimum wall thickness that is 10 times the cover, including an allowance for cover tolerance, which has demonstrated improved ductility in tests of concrete wall specimens.
- Observed damage correlated well with the need for special boundary elements, but the lack of special boundary element detailing in Chilean walls does not provide data to directly confirm or refute the adequacy of current ACI 318 requirements for the amount and spacing of transverse reinforcement in special boundary elements. However, knowledge gained from damage to walls that exhibited spalling of concrete cover and loss of confinement, supplemented with results from wall tests by others, indicate that requiring the amount of transverse reinforcement in wall boundaries to satisfy ACI 318 Equation 21-4 (in addition to ACI 318 Equation 21-5) should be considered.
- The current maximum horizontal spacing of hoops or crossties in wall boundary elements is inconsistent with requirement for vertical spacing, which is limited to one-third the wall thickness. An additional limit should be considered for special boundary elements such that the horizontal distance between legs of hoops or ties is limited to a factor (e.g., two-thirds or one) times the wall thickness. In addition, intermediate, unsupported bars at the wall edge should not be permitted.
- The buckling indicator, ε_p^* , proposed by Rodriguez et al. (1999) merits further investigation as a tool for evaluating the susceptibility of longitudinal bars to buckling in concrete walls subjected to flexure. Calibration of this approach with a larger set of test data is recommended.

Investigation of Overall Wall Buckling

This chapter presents the results of an investigation on lateral wall instability in which the overall concrete wall section buckles laterally out-of-plane over a portion of the wall length and height. This behavior was observed in some buildings following the 2010 Maule earthquake (EERI, 2010) and in one building following the 2011 Christchurch earthquake (EERI, 2011).

Overall wall buckling is differentiated from individual bar buckling, but overall wall buckling damage was most apparent in the end regions of walls where vertical tension and compression strains from in-plane wall flexure were the greatest. As a result, it can be difficult to differentiate between damage that was initiated by bar buckling or concrete crushing, versus overall wall buckling. In this chapter, the factors contributing to overall wall buckling are investigated as a separate and distinct behavior. The observed out-of-plane buckling behavior is described, a theoretical buckling model is developed, and the model is applied to two buildings that were damaged in the 2010 Maule earthquake. The chapter concludes with recommendations for design.

3.1 Description of Overall Wall Buckling Behavior

Overall wall buckling refers to the lateral instability of the entire wall section over a portion of the wall length and height. Figure 3-1 illustrates two examples from buildings investigated after the 2010 Maule earthquake. Prior to this earthquake, overall wall buckling had been observed in experimental tests (Chai and Elayer, 1999; Thomsen and Wallace, 2004), but had not been reported in an actual earthquake. Since the 2010 Maule earthquake, overall wall buckling has been observed in at least one building (following the 2011 Christchurch earthquake in New Zealand). Relative to other types of wall damage that occurred in the 2010 Maule earthquake, cases of documented overall wall buckling behavior are relatively few, and were often associated with significant residual drift in the building.

Wall buckling is a phenomenon that has generally been associated with wall slenderness. In recent years, design practice in Chile (and in other countries) has resulted in wall sections that are more slender than was common practice in prior years. For example, rectangular wall sections with edge thicknesses $b = 150$ mm to 200 mm (6 inches to 8 inches), and floor-to-floor slenderness ratios $h_u/b = 16$ or

greater, are not unusual. According to one theory (Corley et al., 1981; Paulay and Priestley, 1993), wall buckling is exacerbated by reduced sectional stiffness due to residual tensile strains in previously yielded walls. Alternatively, buckling may simply be an outcome of increased slenderness and eccentricities introduced when a thin boundary crushes under moment and axial force.



Figure 3-1 Examples of overall wall lateral buckling from the 2010 Maule earthquake: (a) Alto Huerto building, Concepción (DICTUC, 2010d); and (b) Undisclosed Building B, Santiago (DICTUC, 2010e).

In this chapter, two possible behavior modes are considered that can lead to overall wall buckling:

- Tensile strain and cracking in concrete followed by compression buckling of the overall wall section, in which one curtain of vertical reinforcement yields before the other (or in the case of walls with a single curtain of reinforcement, cracks that close on one side of the wall before the other).
- Compression strain and subsequent spalling of concrete cover, which leads directly to buckling instability and out-of-plane deformation, or results in a reduced wall section that is more susceptible to tensile strain followed by compression buckling (as described above).

3.2 Relevant U.S. Code Requirements and Design Practice

Provisions governing the slenderness of structural walls designed as compression members are contained in Chapter 14 of ACI 318-11, *Building Code Requirements for Structural Concrete and Commentary* (ACI, 2011). For a given unsupported wall height, h_u , an empirical method limits wall slenderness ratios to $h_u/b \leq 25$, and corresponding wall thicknesses to $b \geq 4$ inches, in which b is the thickness of the extreme flexural compression fiber. Alternatively, walls can be designed by the

slenderness provisions of ACI 318 Chapter 10, in which case there is no prescriptive limit on wall slenderness. ACI 318 Chapter 21 does not address slenderness of wall boundaries. Previously, the 1997 *Uniform Building Code* (ICBO, 1997) required $h_u/b \leq 16$, but this provision was not carried forward into the *International Building Code* (ICC, 2000) and subsequent editions.

ACI 318 Chapter 14 requires two curtains of reinforcement for walls thicker than 10 inches. Additionally, ACI 318 Chapter 21 requires two curtains of reinforcement in walls having a factored design shear $V_u \geq 2A_{cv}\lambda\sqrt{f'_c}$, where A_{cv} is the web area (equal to wall length, l_w , times wall thickness, b_w), λ is a modification factor for lightweight aggregate concrete, and f'_c is the specified compressive strength of the concrete (psi). Otherwise one curtain of reinforcement is permitted.

Prior to the 1990s, common design and construction practice used enlarged boundary elements that provided inherent stability against overall wall buckling. Current practice embeds the boundary element within the rectangular cross-section.

According to NIST GCR 11-917-11, *Seismic Design of Cast-in-Place Concrete Special Structural Walls and Coupling Beams: A Guide for Practicing Engineers* (NIST, 2011), 8 inches is a practical lower limit on thickness for special structural walls; however, construction quality and wall performance are generally improved if the thickness is at least 12 inches where special boundary elements are used, and at least 10 inches elsewhere. Thinner wall sections are permitted by ACI 318, and are not uncommon in the United States or other countries that use ACI 318 as a basis. For reference, Appendix B compares wall thickness requirements in codes and standards from other countries.

3.3 Theoretical Model for Wall Instability

Although global wall buckling occurs when the wall boundary is in compression, buckling may be influenced by residual tensile strain in the wall due to prior loading in the opposite direction (Corley et al., 1981; Paulay and Priestley, 1993; Chai and Elayer, 1999). The basic phenomenon of buckling as affected by prior tensile strains is described below, and a strain-based approach for assessing buckling vulnerability is introduced. A complete derivation of theoretical wall instability relationships is presented in Appendix B.

A multistory wall is shown in Figure 3-2. The foundation, floor diaphragms, and roof diaphragm provide lateral support at each level, so the unsupported height of the wall boundary can be taken equal to the story clear height, h_u . An effective length, kh_u , can be defined based on the rotational restraint provided at each floor. For slender walls, k can be taken as 0.5, representing an idealized condition of full fixity at the top and bottom of the wall unsupported length.

A typical wall boundary is subjected to alternating tension and compression as a building responds to an earthquake. If the boundary yields in tension, a cracked section is produced, with crack widths dependent on the amplitude of the reinforcement tensile strain, ε_{sm} , during the tension excursion. In a previously yielded wall, crack closure under deformation reversal may require yielding of the longitudinal reinforcement in compression.

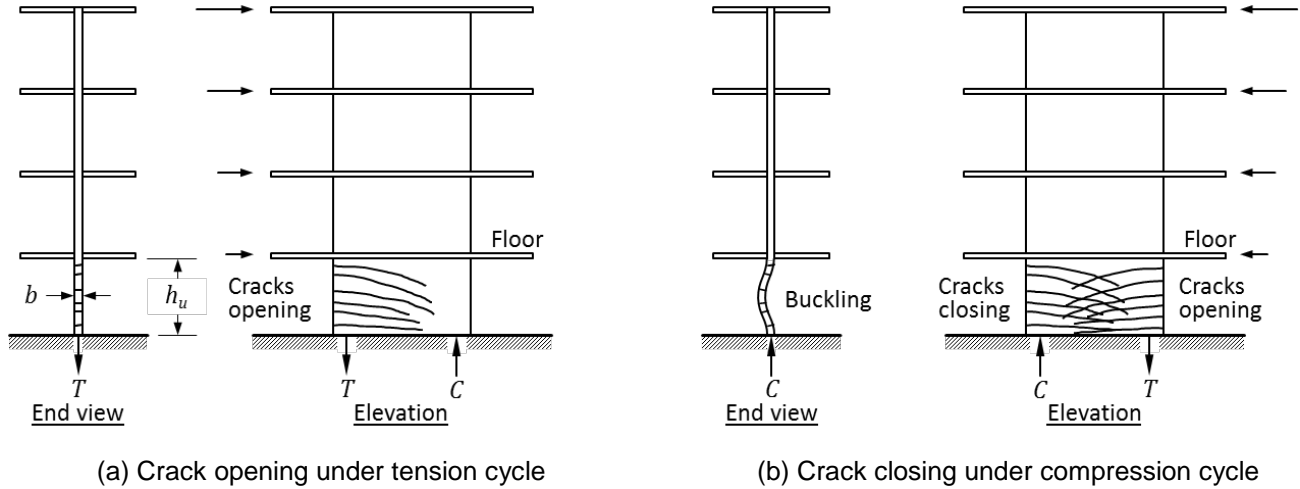


Figure 3-2 Lateral instability of wall boundary that has been previously yielded in tension (after Chai and Elayer, 1999).

In a wall with two curtains of reinforcement, any asymmetry in the reinforcement will result in one curtain yielding before the other, leading to out-of-plane curvature and a tendency to buckle out of plane. In a wall with one curtain of reinforcement, out-of-plane curvature occurs even more readily. Whether or not the wall remains stable depends on the amplitude of the prior tensile strain, ε_{sm} , and the slenderness ratio of the wall, kh_u/b , where b is the thickness of the wall (or the wall boundary). Based on the derivation of theoretical wall instability relationships presented in Appendix B, the critical slenderness ratio can be related to the maximum prior tensile strain, ε_{sm} , using Equation 3-1:

$$\frac{b}{kh_u} = \frac{1}{\pi} \sqrt{\frac{\varepsilon_{sm} - 0.005}{\kappa \xi}} \quad (3-1)$$

where κ is a factor for the effective depth for out-of-plane bending of the wall. Typical values of κ are 0.8 for walls with two curtains of reinforcement and 0.5 for walls with one curtain of reinforcement. The parameter ξ is given by Equation 3-2:

$$\xi \leq 0.5 \left(1 + \frac{2m}{0.85} - \sqrt{\left(\frac{2m}{0.85} \right)^2 + \frac{4m}{0.85}} \right) \quad (3-2)$$

in which $m = \rho f_y / f'_c$ is the mechanical reinforcement ratio. For practical construction, values of ξ are in the range of $0.4 \leq \sqrt{\xi} \leq 0.6$. As a design approximation for walls

with two curtains of reinforcement, substituting values of $\kappa = 0.8$ and $\sqrt{\xi} = 0.5$ into Equation 3-1, and inverting, gives:

$$\frac{h_u}{b} = \frac{1}{0.7k\sqrt{\epsilon_{sm} - 0.005}} \quad (3-3)$$

Equation 3-3 is plotted in Figure 3-3, showing the relation between the critical slenderness ratio, h_u/b , and the maximum tensile strain, ϵ_{sm} , for a value of $k = 0.5$ (i.e., fixed-fixed boundary conditions). The strain corresponding to fracture of the boundary element longitudinal reinforcement represents a practical upper bound for strain in the reinforcement. Considering the effects of low-cycle fatigue, the maximum usable tensile strain is approximately 0.05, so the practical range indicated in Figure 3-3 is limited by this value. Also shown in the figure is the limiting slenderness ratio of $h_u/b = 16$, as specified in the 1997 *Uniform Building Code*.

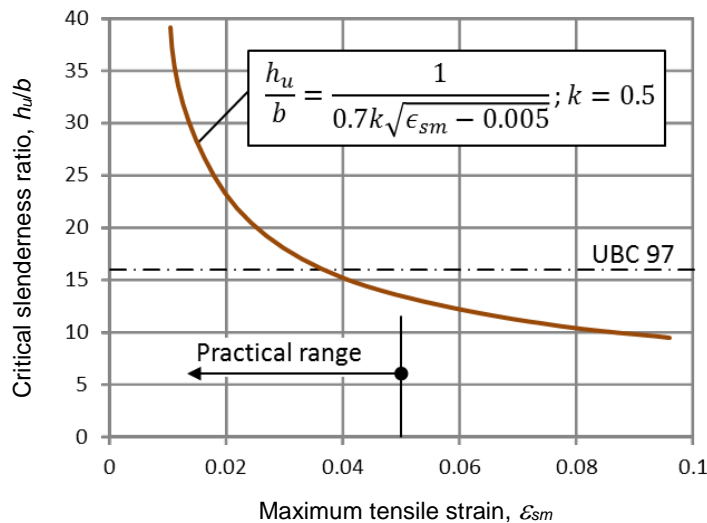


Figure 3-3 Critical slenderness ratio as a function of maximum tensile strain.

3.4 Comparison of Theoretical Wall Instability Model and Observed Building Damage

Detailed studies were carried out on two buildings in which apparent out-of-plane buckling was observed following the 2010 Maule earthquake. Results are compared to theoretical wall instability relationships, and the results are summarized in the sections that follow. More detailed information on these studies is available in Parra and Moehle (2013).

3.4.1 Alto Huerto Building

The Alto Huerto building is a 15-story structure with two basement levels below grade located in Concepción (Figure 3-4a). The building sustained damage as a result of the 2010 Maule earthquake that was characterized by wall crushing in the

first story and in the basement levels. Some walls exhibited apparent out-of-plane buckling (Figure 3-4b).



(a) (b)
Figure 3-4 Alto Huerto building: (a) East elevation; and (b) wall crushing and apparent wall buckling along Line Ñ (DICTUC, 2010d).

The building was designed in 2007 and constructed in 2009. The seismic force-resisting system consists of reinforced concrete walls with a typical thickness of 200 mm (8 inches). The gravity system includes the walls as bearing walls, along with interior reinforced concrete columns. First floor and typical plans are shown in Figure 3-5.

The typical story height is 2.55 m (8 feet 4 inches). There are some vertical discontinuities in the walls in the first story. For example, the walls on Lines K and Ñ (and other wall lines) are set back from the face of the building by approximately 2 m (6 feet), resulting in reduced wall length in the first story with respect to the upper stories. This configuration has been referred to as a “flag-shaped” wall configuration.

Instruments recorded the ground acceleration at a nearby station (Concepción-San Pedro de la Paz) owned by the Seismological Service at the Department of Geophysics at the University of Chile (GUC). Figure 3-6 presents the corrected ground acceleration record as a function of time (East-West component) and the 2% damped linear response spectra from this station.

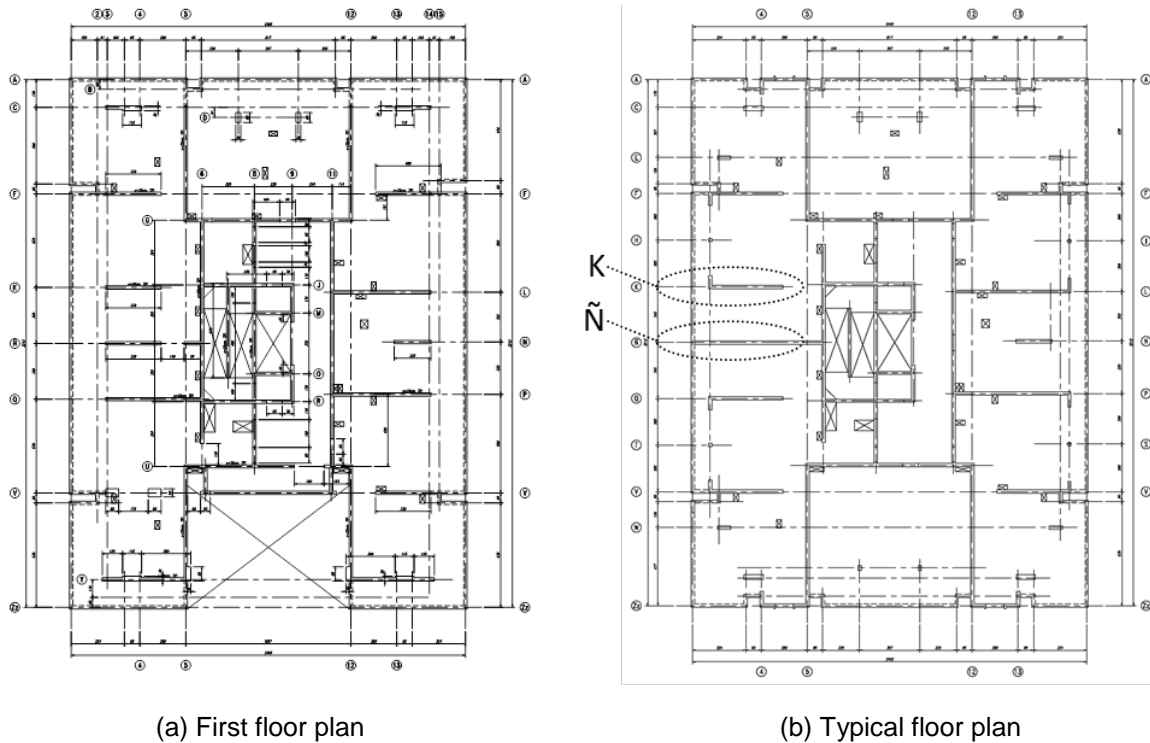


Figure 3-5 Alto Huerto building – typical floor plans (Westenenk et al., 2012).

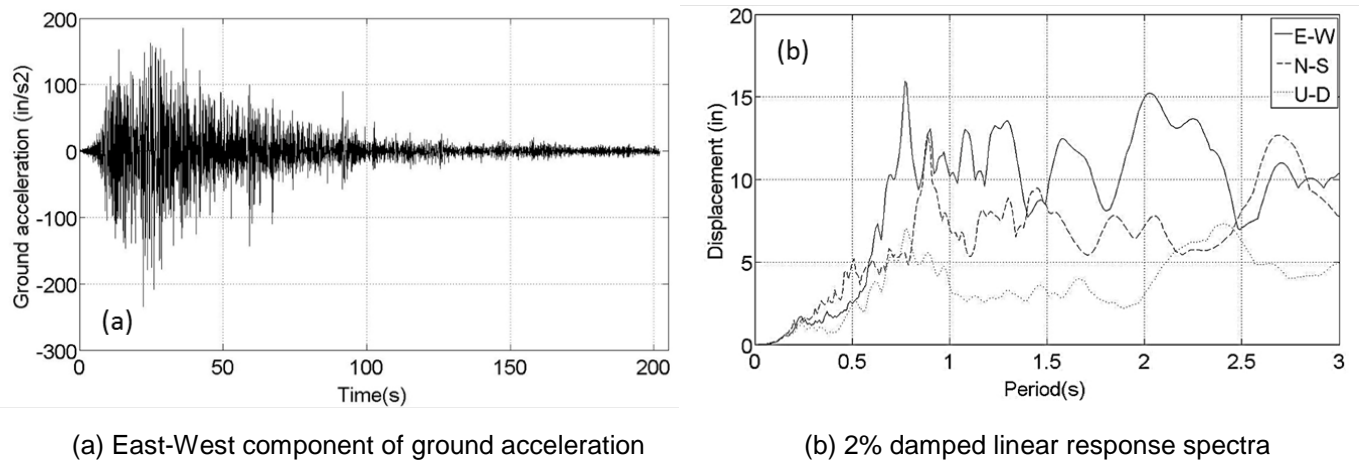


Figure 3-6 Ground acceleration and response spectra from the Concepción-San Pedro de la Paz recording station (data from GUC, 2010).

To estimate the response of the Alto Huerto building in the earthquake, a linear, fixed-based model was developed using ETABS, *Extended Three Dimensional Analysis of Building Systems* (CSI, 2013a). Effective stiffness values used for elements in the model were based on ASCE/SEI 41-06, *Seismic Rehabilitation of Existing Buildings* (ASCE, 2007), as follows:

- Walls: $0.5E_cI_g$ (flexural); $0.4E_cA_{cv}$ (shear)
- Columns: $0.3E_cI_g$ (flexural); $0.4E_cA_{cv}$ (shear)

- Slabs: $0.33E_cI_g$ (flexural)

where E_c is the elastic modulus of concrete, I_g is the gross moment of inertia, and A_{cv} is the shear area. Using this model, the fundamental translational periods were calculated to be 0.57 seconds in the transverse (East-West) direction and 0.47 seconds in the longitudinal (North-South) direction.

Using these periods and the response spectra in Figure 3-6, the spectral displacement in each direction was estimated to be approximately 5 inches, which corresponds to a roof displacement of approximately 6 inches, and a roof drift ratio of approximately 0.004. The spectra also show that at moderately longer periods, a peak spectral displacement of 16 inches can occur, corresponding to a roof drift ratio of 0.013. This corresponds to an effective “upper bound” on the potential displacements in the Alto Huerto building given the assumptions that the selected ground motion represents the motion at the site, and that the building translational periods lengthen in each direction as a result of damage.

The wall on Line Ñ exhibited the most obvious case of apparent lateral buckling in the building. This wall has a T-shaped cross-section with a 2 m (6 feet) setback in the first story above grade. Figure 3-7a shows the wall in elevation, and Figure 3-7b shows a plan section of the wall in the first story.

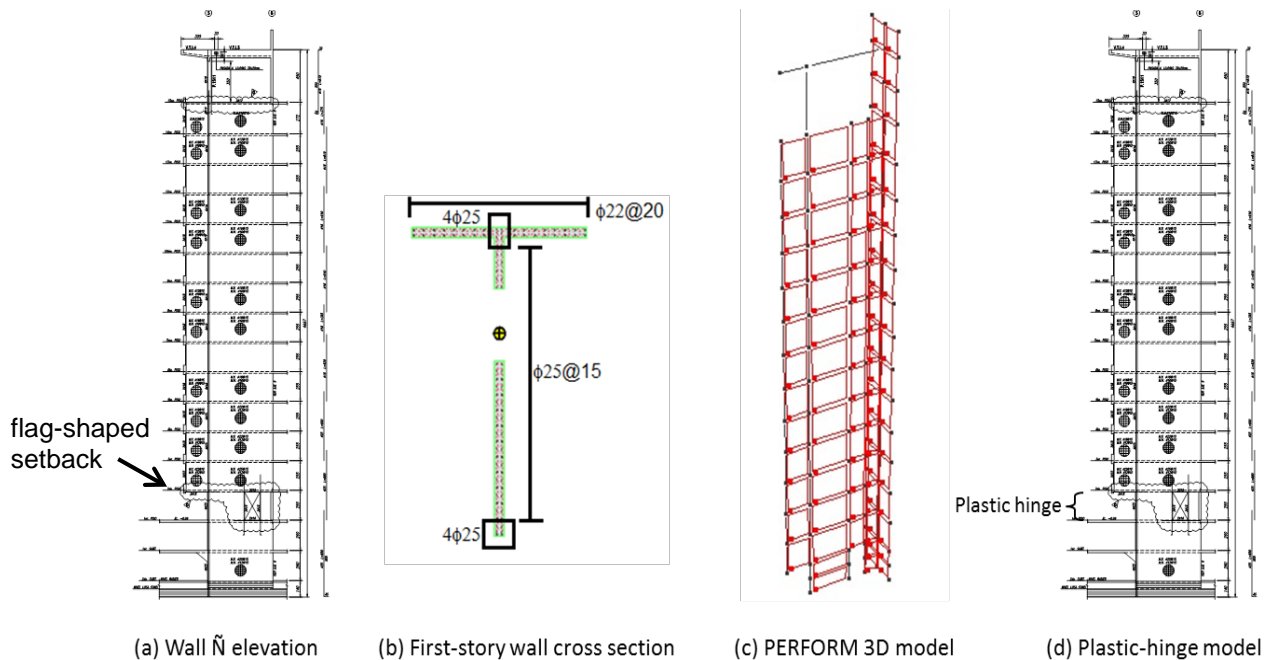


Figure 3-7 Alto Huerto building – wall Line Ñ elevation, cross-section, and nonlinear analysis models.

To investigate the potential cause of the observed damage, a nonlinear, fixed-base model of the wall on Line Ñ was developed using PERFORM-3D, *Nonlinear Analysis and Performance Assessment for 3D Structures* (CSI, 2013c). This model,

shown in Figure 3-7c, was studied using nonlinear static analysis and the Concepción-San Pedro de la Paz ground motion record. In addition, simplified models integrating curvature over height, including a plastic-hinge model, were also investigated (Figure 3-7d).

Results from all models were consistent. For lateral loading that puts the flange in tension and the stem in compression, the concrete in the boundary of the stem will crush at roof drift ratio of approximately 0.005.

Using Equation 3-1 to investigate wall buckling, a prior peak tensile strain of $e_{sm} \approx 0.03$ in the wall is necessary before out-of-plane buckling is likely to occur. This tensile strain would be reached at a roof drift ratio of approximately 0.014. Given the potential upper bound displacements calculated using the displacement response spectrum, this drift ratio is plausible, but it is also approximately three times the drift ratio that is expected to cause concrete crushing in the wall. Therefore, it seems more likely that the wall crushed first from loading with the stem in compression, and the damaged section then buckled out of plane. If it is assumed that spalling of the concrete cover leaves an intact core with a thickness of $b \approx 4.4$ inches, Equation 3-1 indicates that the reduced section would be prone to out-of-plane buckling at a roof drift ratio of 0.005.

The wall on Line K (Figure 3-8) is located immediately adjacent to the wall on Line Ñ. This wall also has a flag-shaped setback in the first story, but unlike the wall on Line Ñ, it has a rectangular cross-section. The wall on Line K experienced minor failure in the boundary, apparently due to compression. Because the wall lines are adjacent to each other, it is reasonable to infer that the walls were subjected to nearly identical displacement histories.

Using the same approach applied to the wall on Line Ñ, simplified models integrating curvature over height, including a plastic-hinge model, were used to study the likely strain demands in the first story of the wall on Line K. According to these models, crushing of the wall boundary is expected at a roof drift ratio of 0.006 (slightly larger than the drift ratio required for crushing at Line Ñ). At this drift ratio, the maximum tensile strain in the wall is approximately 0.008, which is much less than the value $e_{sm} \approx 0.03$ from Equation 3-1 that is likely to cause out-of-plane buckling to occur after spalling. This result indicates that concrete crushing would be expected to precede out-of-plane buckling, which matches the observed behavior of the wall on Line K.

Limited damage observed in the wall boundary on Line K suggests that the wall did not experience drifts that significantly exceeded the drift corresponding to the onset of concrete crushing (roof drift ratio ≈ 0.006). Therefore, it seems even less likely that the Alto Huerto building experienced roof drift ratios on the order of 0.014 that

would have been theoretically necessary to initiate out-of-plane buckling of the full cross-section of the wall on Line \tilde{N} , based on wall buckling relationships.

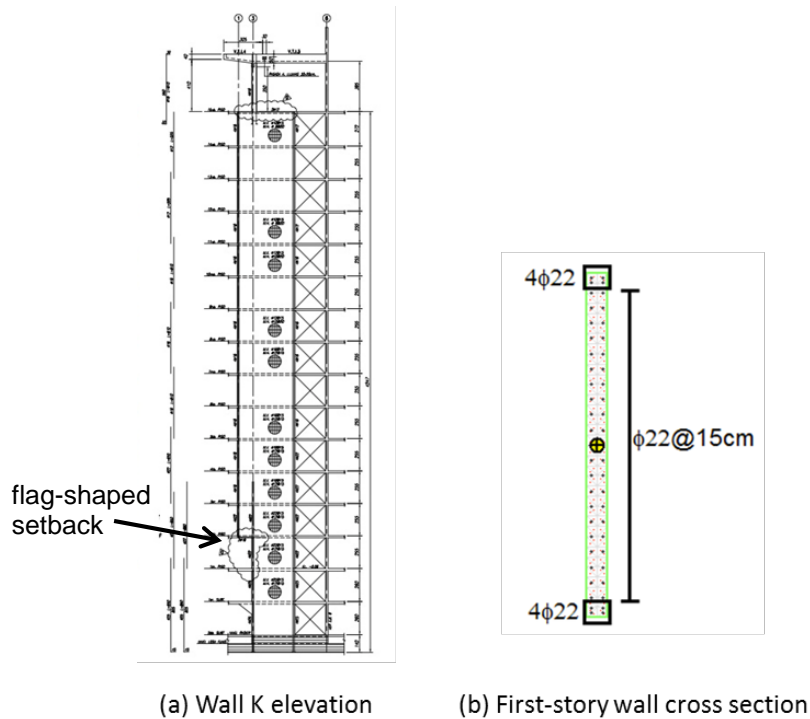


Figure 3-8 Alto Huerto building – wall Line K elevation and cross-section.

3.4.2 Undisclosed Building B

Undisclosed Building B is a 20-story structure with four basement levels located in Santiago (Figure 3-9a). The building sustained damage as a result of the 2010 Maule earthquake that was characterized by overall buckling in six walls in the transverse (East-West) direction, concentrated in the first subterranean level below-grade. Damage to the wall on Line O is shown in Figure 3-9b.

The building was designed in 2006 and constructed in 2009. The gravity and seismic force-resisting systems consist of reinforced concrete bearing walls with a typical thickness of 170 mm (6.7 inches). A typical floor plan is shown in Figure 3-10. The typical story height is 2.52 m (8 feet 3 inches). Transverse walls in subterranean levels have flag-shaped setbacks relative to the walls in upper stories (Figure 3-11).

Instruments recorded the ground acceleration at several locations in Santiago. The three stations closest to the building site are Santiago-Centro, Santiago-La Florida, and Santiago-Penalolen, owned by the Department of Civil Engineering at the University of Chile (RENADIC). The highest displacement demands were obtained from the Santiago-Centro ground station, which was selected for use in this study. It is also the station closest to the building site, and has a soil type (Soil Type II in

accordance with NCh433.Of96 (INN, 1996)), which is expected to be similar to the building site.



Figure 3-9 Undisclosed Building B: (a) exterior elevations; and (b) wall buckling in the first subterranean level along transverse Line O (DICTUC, 2010e).

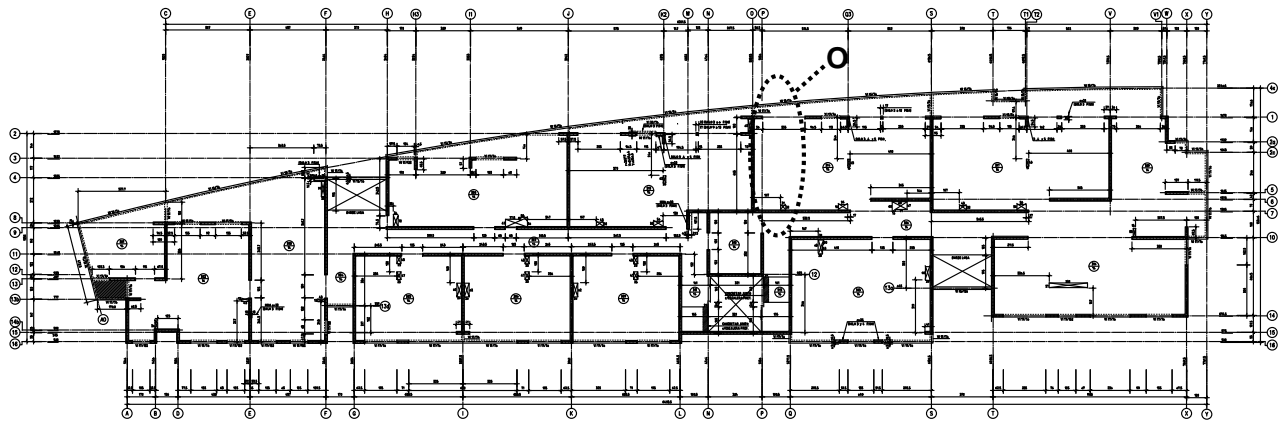


Figure 3-10 Undisclosed Building B – typical floor plan (DICTUC, 2010e).

Figure 3-12 presents the corrected ground acceleration record as a function of time (East-West component) and the 2% damped linear response spectra from the Santiago-Centro station. To estimate the response of the building in the earthquake, a linear, fixed-based model was developed using ETABS. Effective stiffness values used for elements in the model were based on ASCE/SEI 41-06. Using this model, the fundamental translational periods were calculated to be 1.56 seconds in the transverse (East-West) direction and 0.75 seconds in the longitudinal (North-South) direction.

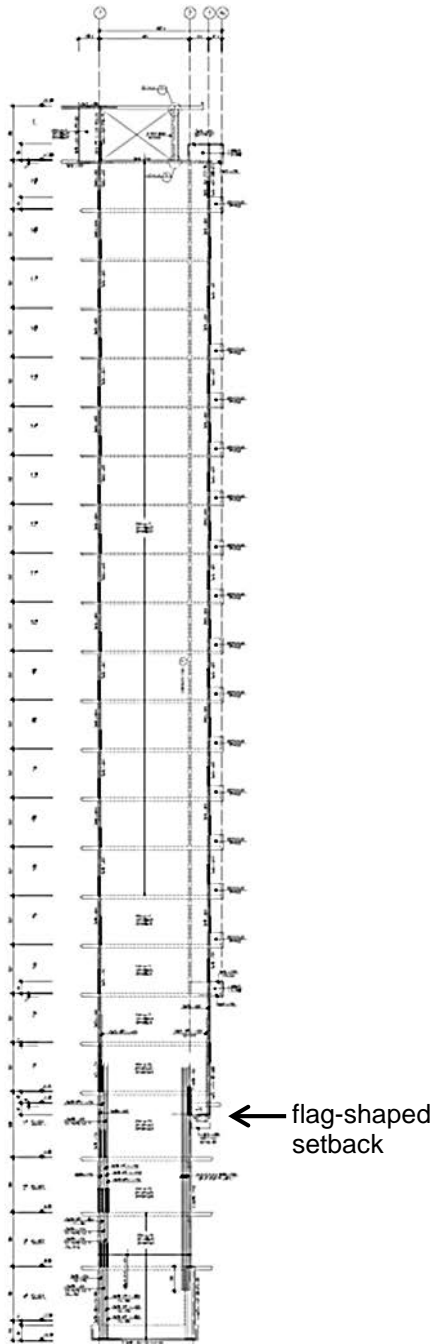
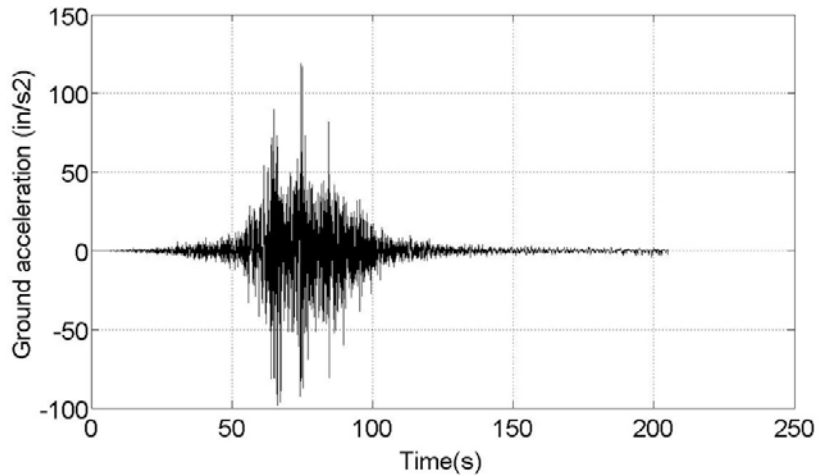
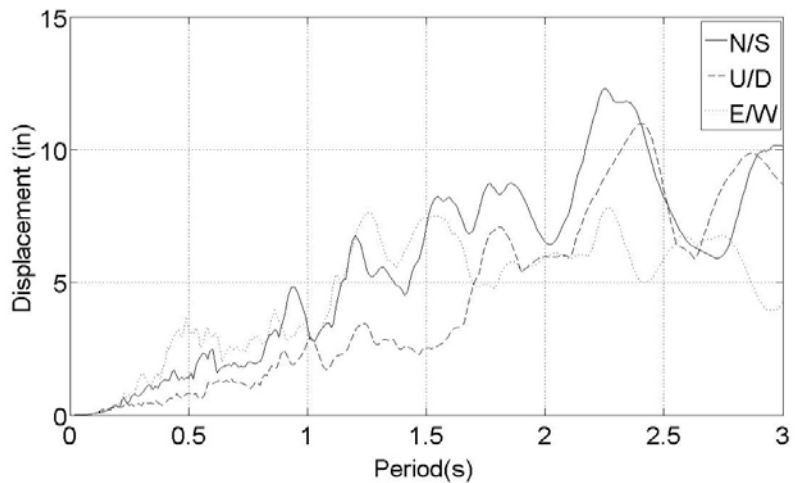


Figure 3-11 Undisclosed Building B – elevation of wall Line O.



(a) East-West component of ground acceleration



(b) 2% damped linear response spectra

Figure 3-12 Ground acceleration and response spectra from the Santiago-Centro recording station (data from University of Chile, 2012).

Using these periods and the response spectra in Figure 3-12, spectral displacement in the transverse (East-West) direction was estimated to be approximately 7.5 inches, which corresponds to a roof displacement of approximately 12 inches, and a roof drift ratio of approximately 0.006. Spectral displacement in the East-West direction is relatively insensitive to period elongation. In the North-South direction, however,

spectral displacement increases to more than 12 inches at periods longer than the elastic period.

To investigate the potential cause of the observed damage in the transverse walls, a simplified plastic-hinge model of the wall on Line O was studied. This wall has a T-shaped cross-section. For lateral loading that puts the flange in tension and the stem in compression, the concrete in the boundary of the stem will crush at roof drift ratio of approximately 0.003, which is about half of the drift ratio expected for the East-West ground motion (0.006).

Using Equation 3-1 to investigate wall buckling, a prior peak tensile strain of $e_{sm} \approx 0.02$ in the wall is necessary before out-of-plane buckling is likely to occur. Because the drift ratio associated with concrete crushing is smaller than the drift ratio associated with out-of-plane buckling, it seems much more likely that the failure mode associated with wall crushing will occur before wall buckling.

If it is assumed that wall crushing and spalling of the cover concrete leaves a core with a reduced thickness, Equation 3-1 indicates that the reduced wall section would be prone to out-of-plane buckling at a peak tensile strain of $e_{sm} \approx 0.008$. At a roof drift ratio of 0.003, at which crushing is expected to occur, the maximum tensile strain in the wall would be approximately 0.005 (close to e_{sm}), which indicates that it is possible that buckling could be triggered. Similar conclusions were obtained for the other damaged walls in the building. Thus, the likely sequence of damage observed in the transverse walls is crushing and spalling of concrete cover, followed by out-of-plane buckling of the reduced wall section.

3.5 Findings and Recommendations

In the 2010 Maule earthquake, wall boundaries were observed to have exhibited out-of-plane buckling behavior. Overall wall buckling has generally been associated with wall slenderness, but a theoretical model for wall instability considers the effect of maximum tensile strain on lateral instability. In this model, tensile strains followed by an unbalanced response under subsequent compression strains result in lateral deformation and curvature that can be related to the slenderness ratio of a wall.

Studies of buildings in which apparent out-of-plane buckling was observed showed that overall wall buckling can be predicted using the theoretical model for wall instability; however, the observed damage was likely initiated by concrete crushing at the extreme fibers due to flexural compression, rather than gross-section buckling. Although some walls exhibited a characteristically buckled shape following the earthquake, calculations showed that initial gross concrete sections were laterally stable, and failure modes associated with concrete crushing were likely to have initiated first. Once the initial concrete sections had degraded due to crushing and spalling of cover concrete, application of wall instability relationships on the residual

core sections suggested that out-of-plane buckling was the next likely mechanism to occur. As a result, observed instances of overall wall buckling resulting purely from wall slenderness and lateral instability are relatively few.

To address wall slenderness, and also to consider that concrete spalling can contribute to slenderness, the following potential changes to ACI 318 requirements are recommended for consideration:

- ACI 318 Chapter 21 currently permits a single curtain of reinforcement for thin walls with low average shear stress. Based on theoretical out-of-plane buckling considerations, flexure-controlled special structural walls should be required to have two curtains of reinforcement within the intended hinge zone, regardless of shear demand.
- ACI 318 Chapter 21 should have a slenderness ratio limit for the intended hinge zone of special structural walls. The 1997 UBC historic limit of $h_u/b \leq 16$ is recommended for walls that are expected to maintain their concrete cover, where h_u is the unsupported height of the wall, and b is the wall thickness. In the case of walls that are expected to lose their concrete cover due to spalling, the same limit could be applied, but b should refer to the thickness of the confined core. This thickness is denoted b_c in ACI 318. Such a limit could be specified as a simplified alternative to the use of Equations 3-1 to 3-3, which could be used in more detailed calculations when the maximum tensile strain demand is known.
- Application of a slenderness ratio limit to walls extending over multiple stories without lateral support from floor diaphragms (e.g., as might occur in an atrium) could be difficult, and might be overly restrictive. For such walls, Equations 3-1 to 3-3 can be used to determine wall thickness. In such an application, the result is likely to be conservative because these equations assume that tensile yielding extends over the full unsupported height of the wall. In a tall unsupported wall, however, tensile yielding is likely to be restricted to only a portion of the wall height. Alternative analysis methods not explored here (e.g., second-order analysis that models the likely variation in stiffness along the wall height; consideration of wall flanges and other stiffening elements) can be considered in such cases.

Investigation of Building Configuration Issues

This chapter presents the results of a series of studies investigating building configuration issues that were associated with observed damage, and provides recommendations for avoiding such issues or accounting for them in analysis and design. Investigation of building configuration issues in this chapter included studies on: (1) the behavior of discontinuity regions located above or below vertically aligned openings; (2) vertical discontinuities, strength and stiffness irregularities, and the extent to which currently available evaluation tools capture these effects; (3) wall coupling behavior; (4) local wall geometric discontinuities; and (5) pier-spandrel system behavior.

4.1 Description of Observed Damage due to Building Configuration Issues

Much of the observed damage in concrete wall buildings following the 2010 Maule earthquake could be attributed to building configuration issues. Patterns of damage highlighted aspects of building configuration that are known to affect component demands and overall building performance, such as vertical discontinuities, irregularities in strength and stiffness, and changes in the length, cross-sectional shape, or location of walls from one story to the next. In addition, coupling of walls through slabs, beams, spandrels, and nonstructural elements, such as stairs, was also attributed to damage in many cases. Figure 4-1 illustrates typical wall configuration issues associated with observed damage in Chile.

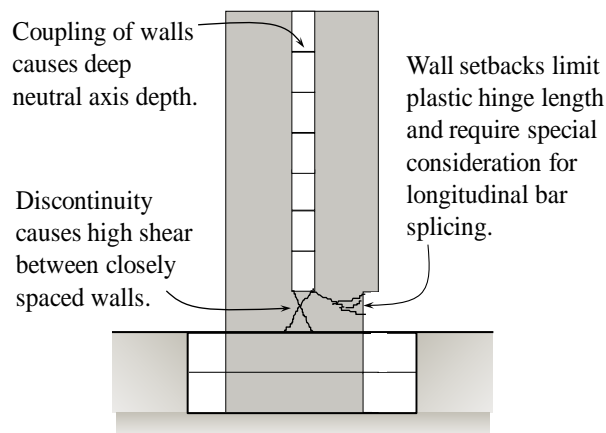
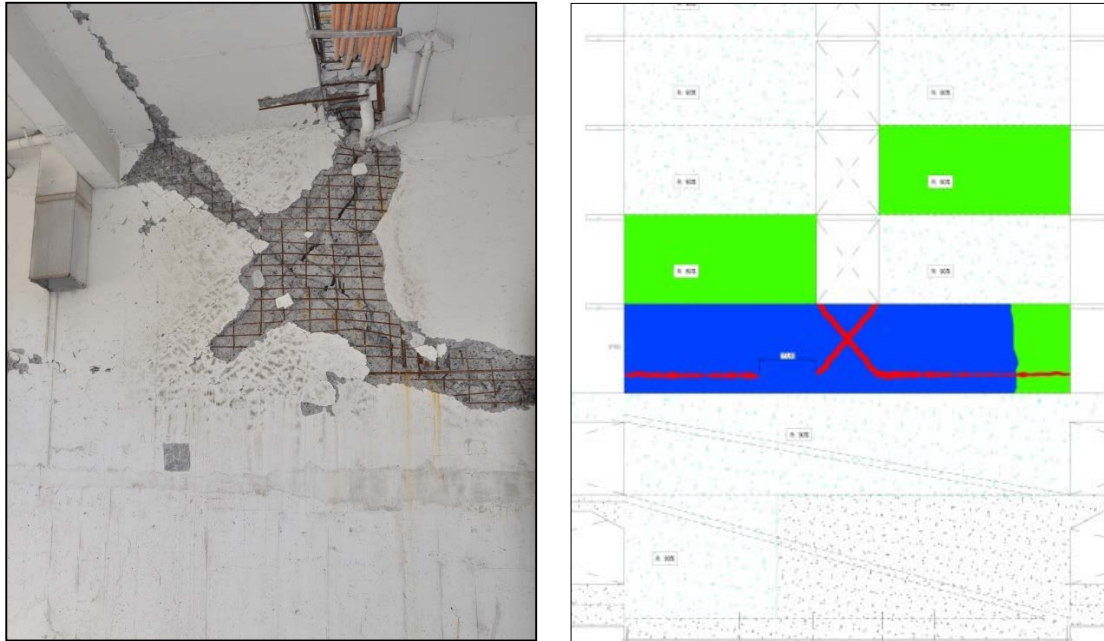


Figure 4-1 Wall configuration issues associated with observed damage in Chile.

Figure 4-2 shows damage to a solid wall located below a vertically aligned stack of openings. This configuration issue is investigated in Section 4.3.



(a) Photograph of damaged wall.

(b) Sketch of building section shown in (a). Green regions suffered minor damage; blue, moderate damage; red, severe damage.

Figure 4-2 Photograph and sketch of damage below stacked openings where coupled walls above frame into solid wall below at the Centro Mayor building, Concepción (photo courtesy of EERI).

Figures 4-3 through 4-12 show damage resulting from vertical discontinuity issues where the term vertical discontinuity is used to describe a significant change in the cross-sectional area or reinforcement layout of a wall from one story to the next. Typically, a change in cross-sectional area or reinforcement that results in a reduction in a lower story relative to an upper story is more critical because of increased force demands in the lower stories. For example, many damaged buildings in Chile include what have been called “flag-shaped” walls in which the wall in the lower story is set back from the wall in the upper story, as shown on the right side of Figure 4-1.

Three-dimensional sketches in Figures 4-7 and 4-8 depict wall configuration scenarios that have been identified for use in quantifying discontinuities in individual walls. Issues related to vertical discontinuities are investigated in Section 4.4.

Figure 4-13 shows observed damage at the O’Higgins building which is the subject of the pier-spandrel investigation summarized in Section 4.5.



Figure 4-3 Earthquake damage photographs illustrating a geometric wall discontinuity at the Centro Mayor building, Concepción (DICTUC, 2010a).



Figure 4-4 Earthquake damage photographs illustrating a geometric wall discontinuity at the Rio Petrohue building, Viña del Mar (photos courtesy of Joseph Maffei).



Figure 4-5 Earthquake damage photographs illustrating a geometric discontinuity and geometry change resulting in a wall partially supported on a column in the Centro Mayor building, Concepción (DICTUC, 2010a).

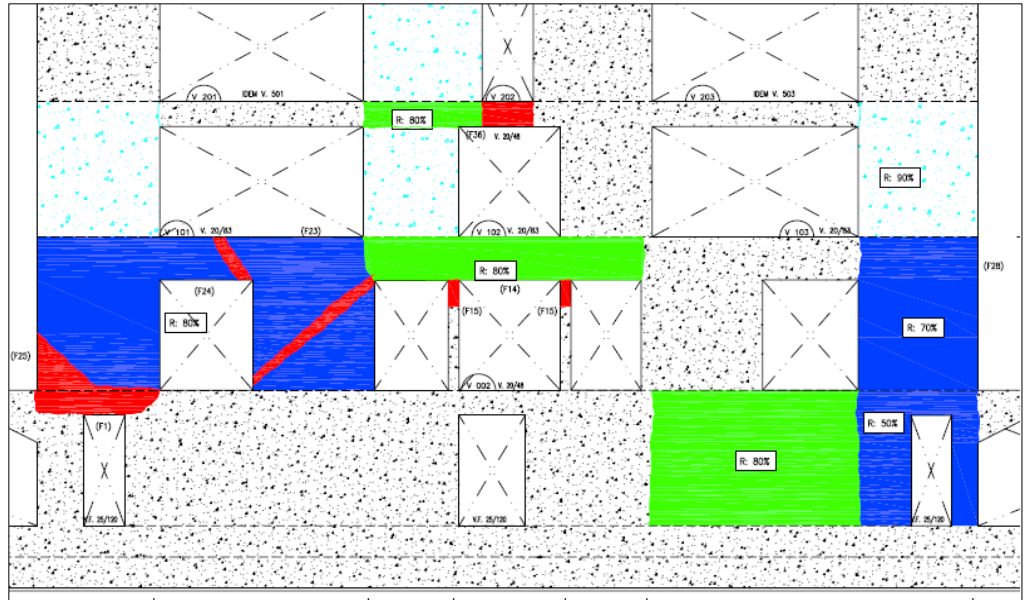


Figure 4-6 Sketch of building section, including the region shown in Figure 4-5, showing location and severity of damage (green indicates minor damage; blue indicates moderate damage; red indicates severe damage).

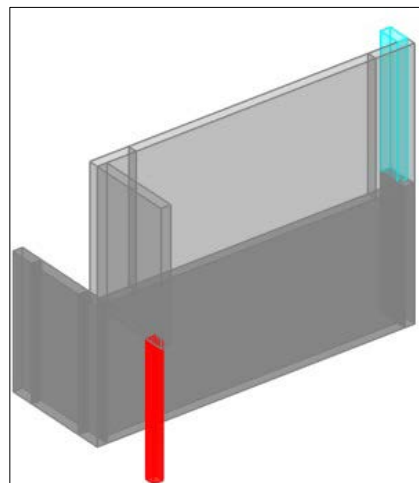


Figure 4-7 Three-dimensional sketch of a wall configuration illustrating geometry change resulting in a wall partially supported on a column at the location of damage shown in Figure 4-5.

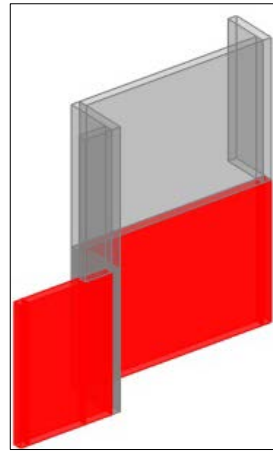


Figure 4-8 Photographs of damage at discontinuities in Z-shaped walls at the south end of Plaza del Rio Building A. Three-dimensional rendering illustrates wall configuration showing that a flange in the second story is not present in the first story. Red regions in the rendering indicate locations of damage (photos courtesy of Jack Moehle).

Figure 4-9 shows a sketch of a damaged region of Plaza del Rio Building A. The damage shown is associated with a complex wall configuration in which: (1) the centroid of the wall shifts significantly; (2) reduction of flange occurs from the second to first story; and (3) damage to the adjacent slab indicates significant out-of-plane demands at the top of the wall in the first story despite no portion of the wall existing immediately above. Figure 4-10 shows photographs of the damaged region.

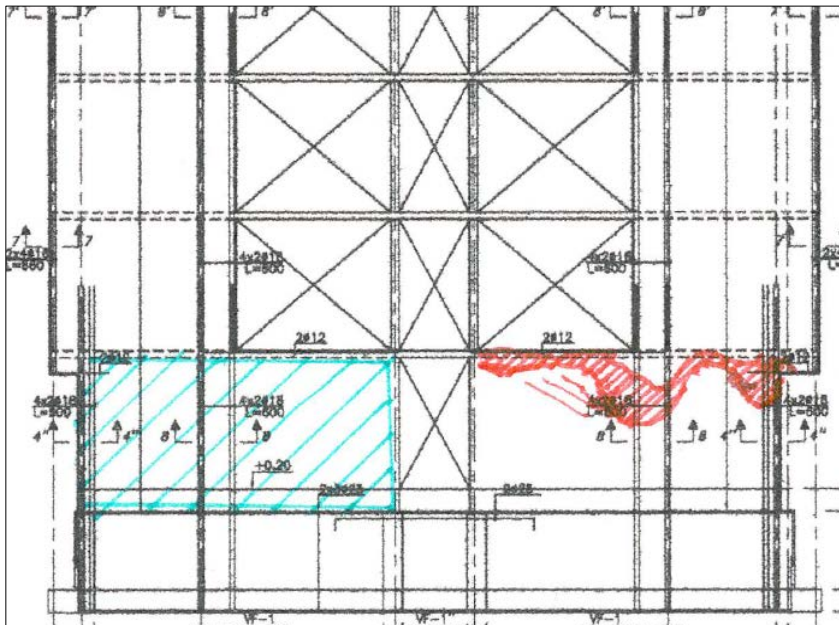
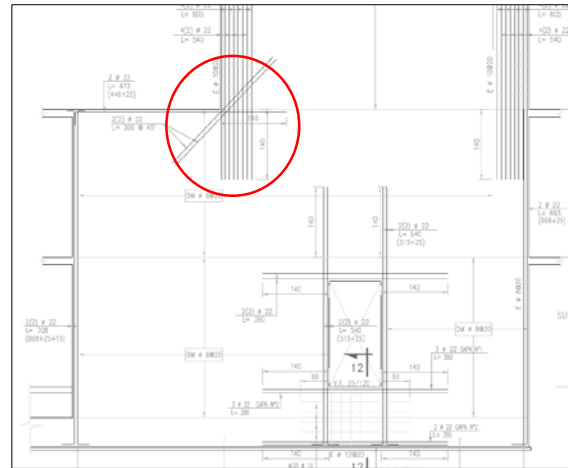


Figure 4-9 Sketch of damaged region in Plaza del Rio Building A; blue hatched region indicates moderate cracking and red hatched region indicates severe damage.



Figure 4-10 Photographs of the damaged section illustrated in Figure 4-9 at wall discontinuity in Plaza del Rio Building A (photos courtesy of Jack Moehle).



(a) Photo of bar termination (lap splice) in beam hinge region (photo courtesy of Jack Moehle)

(b) Illustration of abrupt termination of boundary element reinforcement in wall elevation

Figure 4-11 Two examples showing termination of reinforcement: (a) photograph of damage in a reinforced concrete beam at the face of a connection where lap splices were used in the plastic hinge region of the beam; and (b) wall elevation showing termination of boundary element reinforcement in the O'Higgins building in Concepción.



(a) Festival building, Viña del Mar (photo courtesy of ASCE)



(b) O'Higgins building, Concepción (photo courtesy of Jack Moehle)

Figure 4-12 Damage observed at non-seismic force-resisting components such as stairs (shown here), indicating the possibility of coupling of seismic force-resisting components by non-seismic force-resisting components.



Figure 4-13 Photograph of damage to the O'Higgins building, Concepción. Damage was attributed, in part, to vertical discontinuities in the building configuration. Significant damage, including partial collapse of upper floors, was observed (photo courtesy of Joseph Maffei).

4.2 Relevant U.S. Code Requirements and Design Practice

Section 12.3 of ASCE/SEI 7-10, *Minimum Design Loads for Buildings and other Structures* (ASCE, 2010), defines several structural irregularities that require special consideration in design. Depending on the seismic design category of the structure, these structural irregularities may require, for example, designing for amplified seismic forces, performing more detailed analysis, or in some cases the irregularities

are not permitted. Standard practice in the United States typically results in mid-rise to high-rise walled buildings with the following characteristics:

- There are relatively few structural walls that provide lateral load resistance, because gravity load is carried by a structural system, such as a reinforced concrete slab-column system or a pre-stressed or post-tensioned slab-column system that is separate from the lateral force-resisting system. Accordingly, the structural walls typically have axial load demands less than $0.1A_g f'_c$.
- The most common wall sections are rectangular, or flanged with C-, L-, T- or H-shaped configurations. In less common cases, alternative sections may be used, including those that resemble a Z-shape.
- The structural irregularity provisions of ASCE/SEI 7-10 discourage system-level discontinuities including stiffness and mass irregularities. However, walls may have discontinuities from one floor to another, such as reduced cross-sectional area and significant changes in the longitudinal reinforcement layout, and still meet the system-level continuity requirements.
- Walls are typically thicker than 8 inches with two curtains of longitudinal and horizontal reinforcing steel.
- Section 21.9.7 of ACI 318-11, *Building Code Requirements for Structural Concrete and Commentary* (ACI, 2011), provides detailing requirements for coupling beams connecting structural walls, including transverse reinforcement at close spacing and in some cases diagonal longitudinal reinforcement, particularly in beams with short shear spans.

In comparison, Chilean buildings considered as part of this study included the following characteristics:

- A large number of walls are used to provide both gravity and lateral load resistance; thus, most walls would be identified as bearing walls per ASCE/SEI 7-10. Despite the large number of walls, gravity loads in some cases are relatively high, ranging from $0.01A_g f'_c$ to $0.4A_g f'_c$ for the buildings studied in this chapter.
- Buildings have few nonstructural partitions because structural walls are used to divide rooms. Wall cross sections and configurations are designed to accommodate architectural demands.
- Walls may have severe discontinuities including reduction in cross-sectional area, significant changes in cross-section configuration, or significant changes in longitudinal reinforcement layout. In part, these discontinuities result from changes in architectural constraints from one floor to the next. Detailing to enable load transfer across discontinuities may or may not be provided.

- Walls are typically supported on thin mat foundations, on the order of 400 mm (16 inches) thick.
- Walls are typically thin (200 mm; 8 inches or less) with one or two curtains of steel, and boundary elements are lightly confined.
- Anchorage length for the vertical reinforcing bars is limited.
- Coupling beams are lightly reinforced without diagonal reinforcement or confinement ties.
- Foundations are generally smaller and lightly reinforced compared to typical U.S. practice.

4.3 Investigation of Wall Panels Above or Below Vertically Aligned Openings

A vertically aligned series of openings in a wall often extends over the full height of the building, although in some buildings, stacks of openings terminate in solid wall panels below or above the stack, as shown in Figure 4-14. The solid panel constitutes a discontinuity region that can be subjected to large shear stresses when the coupled walls are loaded laterally. This section summarizes an investigation of shear stresses in discontinuity regions above and below vertically aligned openings, and proposes a design approach. Appendix C provides additional detailed information.

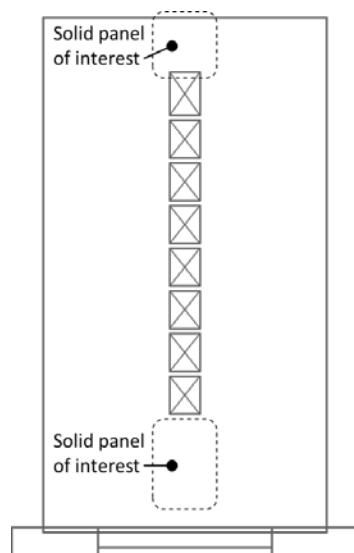


Figure 4-14 Coupled walls with a vertically aligned stack of openings terminating in a solid wall panel above and below.

4.3.1 Characteristic Design Practice and Observed Damage

Several examples of damage to discontinuity regions above or below vertically aligned openings were observed following the 2010 Maule earthquake (Figures 4-10 and 4-11), and following the 1989 Loma Prieta earthquake in California. Figure 4-15

shows an example of a typical reinforcement layout in the vicinity of discontinuities below stacks of openings. Boundary reinforcing bars are terminated 49 inches below the openings in Chile.

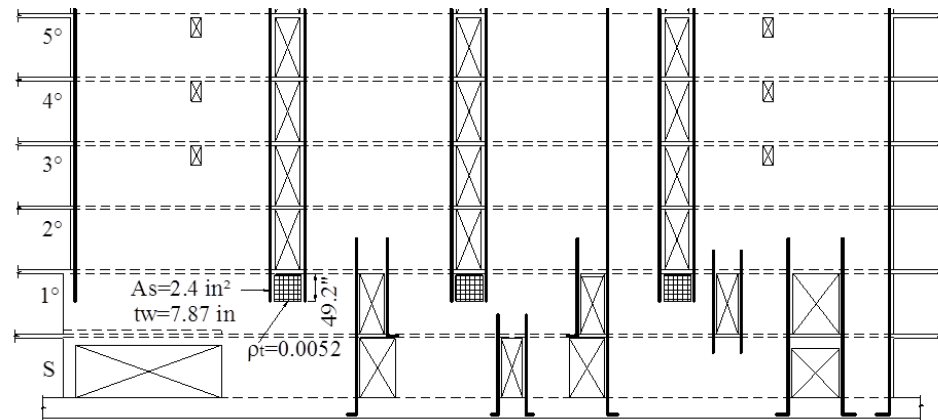


Figure 4-15 Typical reinforcement layout around stacks of openings terminating in a solid wall, Torre Mayor building, Chillán (A_s is the area of boundary reinforcement, t_w is the panel thickness, and ρ_t is the steel reinforcement ratio in the panel).

The Torre Mayor building, from which Figure 4-15 was taken, suffered damage in the solid wall panels above and below the openings. Figures 4-16 and 4-17 show damage to solid wall panels in the Torre Mayor building, which is consistent with damage patterns observed in other buildings with similar discontinuities following the 2010 Maule earthquake and the 1989 Loma Prieta earthquake.



Figure 4-16 Damage observed in a solid wall panel above a stack of openings in the Torre Mayor building, Chillán (photo courtesy of EERI).



Figure 4-17 Damage observed in a solid wall panel below a stack of openings in the Torre Mayor building, Chillán (photo courtesy of EERI).

4.3.2 Local Stress Distribution

Local stresses in solid wall panels below coupled walls have been investigated using numerical models by Naeim et al. (1990) and Tanyeri and Moehle (2014). Naeim et al. (1990) employed linear finite element analysis in which all components were modeled using elastic shell elements, and the steel reinforcement was not explicitly modeled. The Naeim et al. (1990) study concluded the following about stresses in a solid wall panel directly below a stack of openings: (1) the stresses are significantly larger than elsewhere in the walls; (2) the stresses are 2.5 to 5.0 times the average stress acting on a section cut across the entire solid wall panel; and (3) the stresses extend down into the solid wall panel a distance equal to 1.0 to 1.5 times the width of the opening.

Tanyeri and Moehle (2014) used PERFORM-3D, *Nonlinear Analysis and Performance Assessment for 3D Structures* (CSI, 2013c), to investigate stress distributions in the discontinuity regions of the Alto Rio building, which collapsed during the 2010 Maule earthquake. Four-node shear wall elements available in PERFORM-3D were used to model the coupled walls, along with an extended portion of the solid wall panel below the coupled walls. Flexure and shear responses in these elements are decoupled. To simulate flexural response, the shear wall element employs a fiber-type section model with user-defined, one-dimensional stress-strain models for concrete and steel fibers. The shear response is simulated by a user-defined, one-dimensional shear stress-strain model. Both linear and nonlinear shear response models were used.

The linear shear model predicted local shear stresses in the discontinuity regions that were approximately three times the average shear stress in the story level below the

openings. This is consistent with the results reported by Naeim et al. (1990). When the nonlinear shear model was used, shear failure of the solid wall panel in the discontinuity region was predicted.

Tanyeri and Moehle (2014) also investigated average shear stresses in the discontinuity region using a simplified model of load transfer in a solid wall panel. Figure 4-18 shows the assumed internal forces in the panel zone below stacked openings in a coupled wall. Resolving tension and compression forces, T_1 and C_1 , originating at the base of the coupled wall boundary regions, results in a shear stress, v_1 within panel zone **abcd**. Equilibrium requires stress v_1 to act along both the vertical and the horizontal faces of panel zone **abcd**, and the horizontal shear stress acting along segment **ab** requires reinforcement along (and anchored beyond) segment **ab**. The shear stress along segment **cd** can either be transferred to the panel below, or can be “dragged out” by reinforcement that is anchored beyond segment **cd**.

In this example, the coupled walls are assumed to be weightless, lightly coupled, and of equal length. Accordingly, the panel shear stress is calculated as:

$$v_1 = \frac{1}{1 + l_h / 2l_w} \left(\frac{T_1}{h_s b_w} \right) \quad (4-1)$$

where l_h is the length of the coupled wall openings (distance between **a** and **b** in Figure 4-18), l_w is the length of the coupled wall piers, T_1 is the tension force developed in the reinforcement in the coupled wall boundary element, h_s is the height of the story below the coupled walls (distance between **a** and **d** in Figure 4-18), and b_w is the thickness of the solid wall panel. If shear stress v_1 exceeds the available stress capacity, it is necessary to strengthen the discontinuity region or distribute the forces deeper within the solid wall panel.

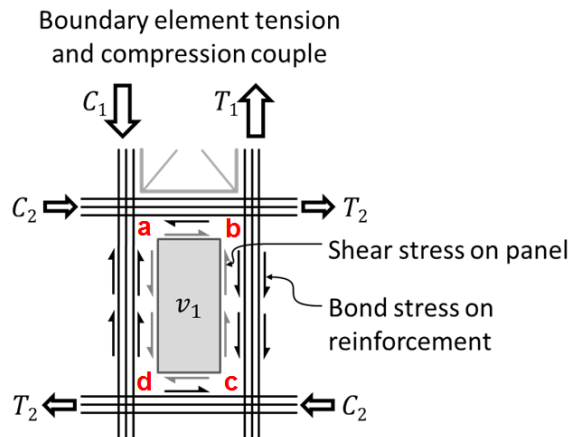


Figure 4-18 Assumed panel zone forces in walls below stacks of vertically aligned openings.

4.3.3 Case Study Buildings

Using this simplified model, panel zone shear stresses were calculated in selected discontinuity regions of four case study buildings. These buildings included:

- Alto Rio, which is a 15-story structure located in the city of Concepción. The building collapsed during the 2010 Maule earthquake, overturning onto its side. Extensive damage to the discontinuity regions immediately below stacks of openings was observed.
- Torre Mayor, which is a 17-story structure located in the city of Chillán. The building did not collapse during the 2010 Maule earthquake, but suffered damage in discontinuity regions above and below stacks of door openings.
- Centro Mayor, which is a 16-story structure located in the city of Concepción. The building did not collapse during the 2010 Maule earthquake, but suffered extensive damage in the first four stories, including damage to a wall below a stack of openings.
- Marina del Sol, which is a 20-story structure located in the city of Viña del Mar. The building did not collapse during the 2010 Maule earthquake, but suffered damage to a first floor wall below a stack of openings.

4.3.4 Findings and Recommendations

Calculated shear stresses were compared to cracking strength and nominal strength and the results were generally consistent with observed failures. Details of these calculations are documented in Appendix C.

Based on case study findings and available research, the following design approach is recommended. Two design zones should be established below (or above) a vertically aligned stack of openings, as illustrated in Figure 4-19:

- Zone 1 extends below the openings a distance equal to the greater of l_d (the anchorage length of the boundary reinforcement as required in ACI 318) and h_s (the story height below the stack of openings), but not less than the length required to transfer shear within acceptable limits on shear stress in the wall.
- Zone 2 is defined as the remaining portion from Zone 1 to the foundation (or roof, if considering the panel above of a stack of openings).

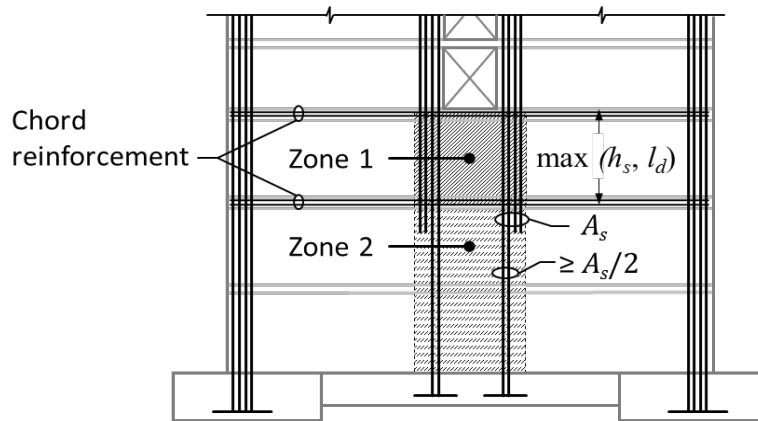


Figure 4-19 Recommended details for reinforcement in wall panels beneath stacks of vertically aligned openings in coupled walls.

All boundary reinforcement should extend through Zone 1, and at least half of the bars should extend all the way to the foundation (or roof). Zone 1 should be proportioned and reinforced for panel zone shear stresses equal to at least $1.25A_s f_y/2$, where A_s is the area of the boundary element reinforcement, f_y is the nominal yield strength, the factor 1.25 accounts for overstrength, and the factor 2 considers that half of the boundary reinforcement is extended into Zone 2.

Zone 2 should be designed for the remainder of the panel zone shear. It is acceptable to consider the force as being transferred to the foundation where adequate provision is made to develop the force at the foundation level. The amount of chord reinforcement above and below Zone 1 should resist the shear stresses assumed to be within Zone 1. Chord bars can be terminated progressively along the length.

Most building codes are not explicit about shear stress limits for wall panel zones described above. A reasonable upper bound shear stress in the panel zone is $10\phi\sqrt{f'_c}$ psi ($0.83\phi\sqrt{f'_c}$ MPa). Naeim et al. (1990) recommended that this stress can be as high as $15\phi\sqrt{f'_c}$ psi ($1.25\phi\sqrt{f'_c}$ MPa), provided special confinement is used wherever shear stress exceeds $10\phi\sqrt{f'_c}$ psi ($0.83\phi\sqrt{f'_c}$ MPa).

4.4 Investigation of Vertical Discontinuities

Many buildings damaged in the 2010 Maule earthquake were observed to have significant vertical discontinuities in walls that were considered to be primary elements of the lateral force-resisting system. This section summarizes investigations related to vertical discontinuities, which included comparisons of observed damage with available evaluation procedures. Appendix D provides additional detailed information on the investigation of vertical discontinuities.

Evaluation procedures set forth in ASCE/SEI 31-03, *Seismic Evaluation of Existing Buildings* (ASCE, 2003), and ASCE/SEI 41-06, *Seismic Rehabilitation of Existing*

Buildings (ASCE, 2007), were used to evaluate buildings that experienced the earthquake. Evaluation results were compared with observed damage to explore the extent to which these commonly used evaluation tools captured the observed discontinuities, and to develop recommendations for improved assessment of shear wall discontinuities that contributed to damage.

4.4.1 Case Study Buildings

Five mid-rise and high-rise buildings located in Concepción were selected for investigation of vertical discontinuities. Case study buildings included:

- Plaza del Rio Building A, which is the first of a pair of buildings located immediately adjacent to one another, but structurally separated. Plaza del Rio Building A is 12-story structure that experienced damage concentrated in the first two stories. This building was investigated using ASCE/SEI 31-03 procedures for Tier 1, Tier 2, and Tier 3 Evaluations.
- Plaza del Rio Building B, which is the second of a pair of buildings located immediately adjacent to one another, but structurally separated. Plaza del Rio Building B is 13-story structure that was relatively undamaged in the earthquake. This building was investigated using ASCE/SEI 31-03 procedures for Tier 1 and Tier 2 Evaluations.
- Centro Mayor, which is a 17-story structure that sustained localized damage at discontinuities and irregularities. This building was investigated using ASCE/SEI 31-03 procedures for Tier 1 and Tier 2 Evaluations.
- Alto Huerto, which is a 15-story structure that sustained localized damage at wall discontinuities. This building was investigated using ASCE/SEI 31-03 procedures for a Tier 1 Evaluation only.
- Concepto Urbano, which is a 22-story structure that was relatively undamaged in the earthquake. This building was investigated using ASCE/SEI 31-03 procedures for a Tier 1 Evaluation only.

Tier 1, Tier 2, and Tier 3 Evaluations were conducted on these buildings to varying levels of detail. Summary results from these evaluations are described in this section, and specific results are presented for one building (Plaza de Rio Building A), which was subjected to the most detailed evaluation.

4.4.2 Summary of Observed Damage

Three of the case study buildings were significantly damaged in the earthquake, and two were essentially undamaged. Plaza del Rio Building A was severely damaged, while the adjacent Plaza del Rio Building B was relatively undamaged. The condition of the five buildings following the earthquake led to the following general observations regarding damage:

- Some walls did not have a clearly defined location where a plastic hinge could form.
- In damaged buildings, wall confinement reinforcement was light, widely spaced, detailed with 90-degree rather than 135-degree hooks, and, in some cases, non-existent.
- Damage was observed at solid walls above or below stacks of aligned openings.
- Damage was observed at splice locations.
- Damage was observed at severe vertical discontinuities in walls where supplemental reinforcement was not provided to assist in transfer of forces.
- Several damaged buildings had walls that were 130 mm to 200 mm (5 inches to 8 inches) thick.
- Damage consistent with wall coupling (e.g., crushing of concrete in walls due to high compressive loads, and cracking and spalling of concrete in coupling beams and slabs) was observed.
- One building (Concepto Urbano), which was essentially undamaged, had a thick, well-reinforced mat foundation, while another building (Plaza del Rio Building A), which was severely damaged, had a thin, lightly reinforced mat foundation that showed evidence of soil heaving.

4.4.3 ASCE/SEI 31-03 Tier 1 Evaluations

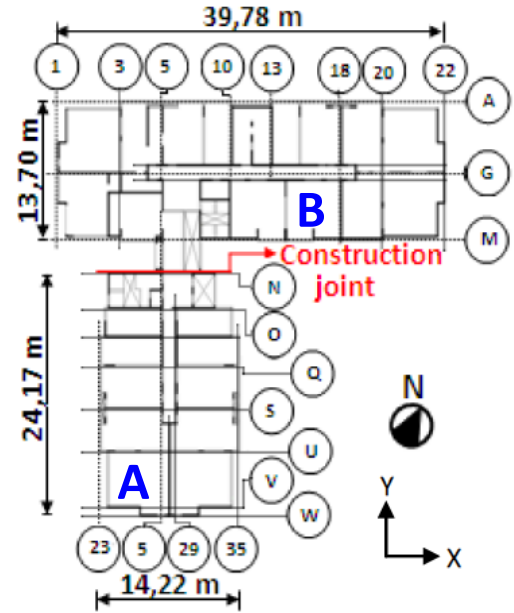
All five buildings were evaluated using ASCE/SEI 31-03 Tier 1 basic and supplemental checklists. Tier 1 Evaluation results for Plaza del Rio Building A are provided below. Results for other case study buildings are provided in Appendix D.

4.4.3.1 Plaza del Rio Building A – Tier 1 Evaluation Results and Correlation with Observed Damage

The typical floor plate of Plaza del Rio Building A measures approximately 24 meters (79 feet) by 14 meters (47 feet), with the longitudinal axis oriented approximately in the north-south direction. Figure 4-20 shows the exterior of the building (along with the adjacent Plaza del Rio Building B) and the typical floor plan.

Walls in Plaza del Rio Building A are typically 150 mm (6 inches) thick, and slabs are typically 130 mm (5 inches) thick. The foundation is a mat foundation approximately 400 mm (16 inches) thick, with a small basement under the elevator core. The soil at the site is on the boundary of Site Class D and E (per ASCE/SEI 7-10 designations). The design concrete strength is 25 MPa (3.6 ksi).

Tier 1 checklist evaluation results for Plaza del Rio Building A are summarized in Table 4-1. Figure 4-21 shows the layout of the walls in the first two stories, with the damage level indicated by the colors specified in the accompanying legend.



(a) Exterior view of both towers (Cerdea, 2011)

(b) Typical floor plan (Westenenk et al., 2012)

Figure 4-20 Exterior elevation and typical floor plan of Plaza del Rio Buildings A and B. The two buildings form an L-shape, and are separated by a construction joint.

Table 4-1 Summary of Tier 1 Checklist Items Identified as Non-Compliant for Plaza del Rio Building A

Checklist Items	Plaza del Rio Building A
Weak story	NC
Soft story	NC
Vertical discontinuities (discontinuous walls)	NC
Shear stress check (in concrete walls)	NC
Foundation dowels (not able to develop strength of walls or foundation)	..1
Overtuning (walls with aspect ratio greater than 4:1)	NC ²
Confinement reinforcing (lacking closely-spaced boundary ties)	NC ²
Reinforcing at openings (lacking trim bars)	NC ²
(Diaphragm) Openings at shear walls	NC
(Diaphragm) Plan irregularities (limited reinforcement at re-entrant corners)	NC ²

¹ Condition not known

² Non-compliance for Immediate Occupancy performance level only

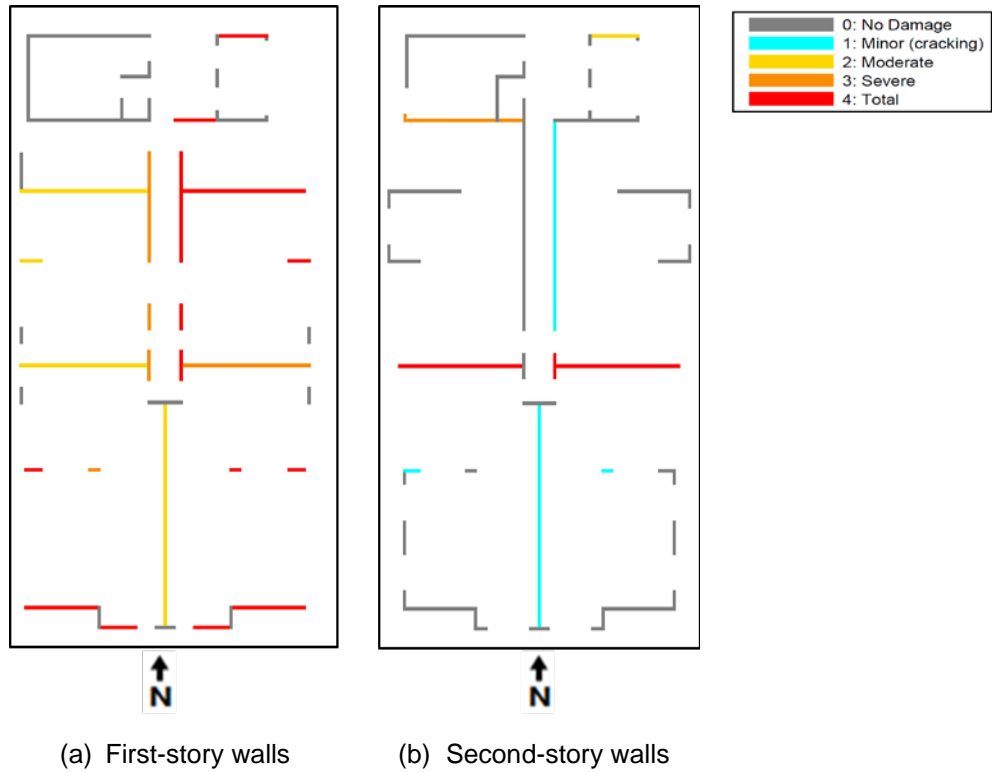


Figure 4-21 Layout of walls in the lower two stories of Plaza del Rio Building A (colors indicate level of observed damage).

Observed damage in Plaza del Rio Building A was concentrated in the first two stories and included the following: (1) damage to walls in the east-west (transverse) direction, including concrete cracking, concrete spalling, bar buckling, bar fracture, crushing of core concrete, and global buckling of wall piers; (2) heaved soil around the foundation; and (3) damage to elevator shaft walls and coupling beams.

Observed damage patterns were consistent with deficiencies identified in Table 4-1, which included a soft first story, weak first story, and the first story shear stress check. Additionally, the Tier 1 Evaluation identified non-compliant perimeter walls on the south end of the building that were discontinuous in the first story, and the most severe damage occurred in a pair of Z-shaped walls at this location, as well as a pair of T-shaped walls oriented in the east-west direction in the center of the building.

In the case of Plaza del Rio Building A, Tier 1 Evaluation results were consistent with observed damage, with the following exception: the checklists identified large diaphragm openings at the elevator and stair shafts (north end of building) as non-compliant, but significant slab damage was not observed in the vicinity of these openings.

4.4.4 Summary of Tier 1 Evaluation Results

All five buildings were evaluated using ASCE/SEI 31-03 Tier 1 basic and supplemental checklists. None of the buildings were found to be compliant with all Tier 1 checklist statements. Across all buildings, the list of Tier 1 deficiencies included:

- walls with vertical discontinuities (i.e., not continuous to the foundation) (observed in all buildings);
- one or more soft stories (observed in all buildings);
- weak stories (observed in all but one undamaged building);
- walls lacking confined boundary elements (observed in all but one undamaged building);
- slender walls with aspect ratios greater than 4:1 (observed in all but one undamaged building);
- diaphragm openings at shear walls (observed in all but one undamaged building);
- diaphragm plan irregularities (observed in three buildings);
- shear stress check in walls exceeds capacity (observed in three buildings);
- changes in the horizontal dimension of the lateral force-resisting system (observed in two buildings);
- lack of trim reinforcing at wall openings (observed in two buildings);
- insufficient dowels at foundation (observed in two buildings);
- insufficient horizontal wall reinforcement (observed in one building); and
- mass irregularity (observed in one building).

In comparing observed damage with Tier 1 Evaluation results across all buildings, the following general observations were made: (1) the shear-stress check did not correlate well with damage; (2) a significant change in stiffness or strength between two adjacent stories is more critical if the lower story is the one that is more flexible or weaker; and (3) the weak story check was a marginally better predictor of a higher likelihood of damage than the soft story check.

4.4.5 ASCE/SEI 31-03 Tier 2 Evaluations

In ASCE/SEI 31-03, non-compliant checklist statements receive further evaluation in Tier 2. Three of the five buildings were evaluated using the ASCE/SEI 31-03 Tier 2 Evaluation procedure, which includes computation of demand-capacity ratios (DCRs) on individual components using a linear analysis method. For these buildings, the Linear Dynamic Procedure (LDP) specified in ASCE/SEI 41-06 was used.

Linear response spectrum analyses were conducted using SAP2000, *Integrated Software for Structural Analysis and Design*, Version 15 (CSI, 2013b) with building models including walls, beams, and slabs. Effective stiffness values prescribed in Table 6-5 of *Supplement No.1 to ASCE 41-06* (ASCE, 2008) were used to model the elements, as summarized in Table 4-2. Foundation flexibility and soil-structure interaction were not included in the model.

Table 4-2 Effective Stiffness Values for Tier 2 Analysis Models

Component	Flexural Rigidity	Shear Rigidity
Beams	$0.30E_cI_g$	$0.40E_cA_w$
Walls	$0.50E_cI_g$	$0.40E_cA_w$
Slabs	$0.33E_cI_g$	$0.40E_cA_w$

Response spectra used in the analyses are shown in Figure 4-22. Demands were calculated using the spectra as shown in the figure to represent the design earthquake (DE) hazard level, and multiplied by 1.5 to represent the maximum considered earthquake (MCE) hazard level. The following spectra were considered:

- U.S. design spectra based ASCE/SEI 7-10, for Site Class D, in a region of high seismicity in the United States (designated “ASCE” in the figure).
- Chilean design spectra based on the code in effect at the time the building was designed (designated as “NCh” in the figure), and as proposed since the earthquake (designated “NCh Proposed”), for Chilean Soil Type III (equivalent to Site Class D per ASCE/SEI 7-10).
- Spectra generated from ground motion recordings at the Concepción station and the Concepción-San Pedro de la Paz station.

Linear dynamic analyses were conducted on Plaza del Rio Building A, Plaza del Rio Building B, and the Centro Mayor building as part of the Tier 2 Evaluation procedure. Tier 2 Evaluation results for Plaza del Rio Building A are provided below. Results for Plaza del Rio Building B and Centro Mayor are provided in Appendix D.

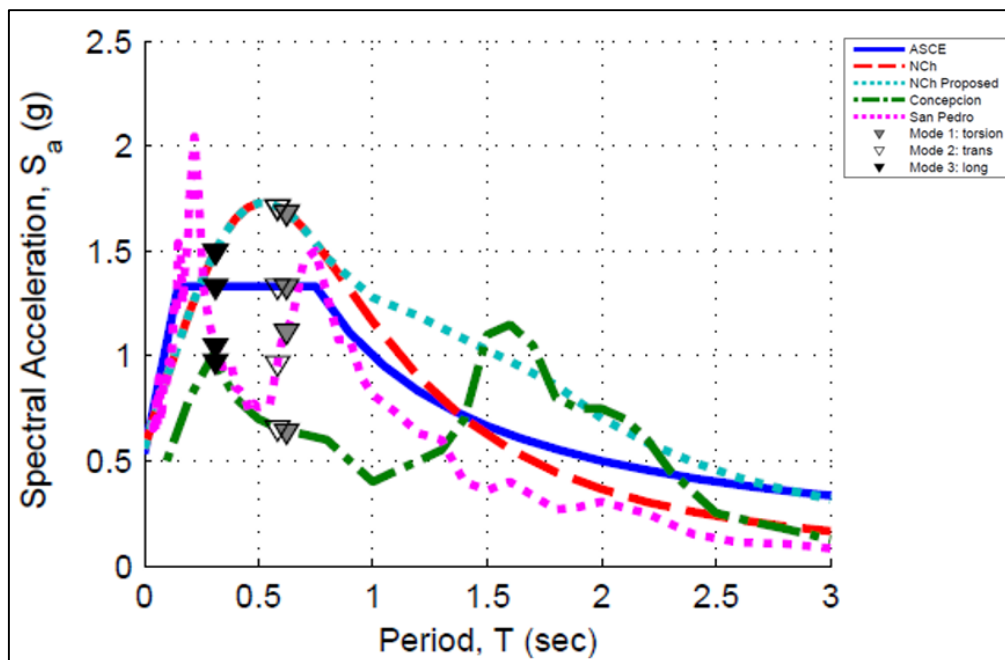


Figure 4-22 Response spectra used in Tier 2 analyses (triangles identify spectral acceleration values at calculated periods for Plaza del Rio Building A).

4.4.5.1 Plaza del Rio Building A – Tier 2 Evaluation Results for Demand-Capacity Ratios and Correlation with Controlling Mechanisms

Unfactored demand-capacity ratios (DCR_u) are used to evaluate component behaviors. The relative magnitude of DCR_u values for each component action (flexure, shear, or axial load) can be used to determine the controlling mechanism for the component. These results are compared to observed damage mechanisms to investigate correlation.

Maximum calculated DCR_u values for the walls in the first story of Plaza del Rio Building A are shown in Figure 4-23. In ASCE/SEI 41-06, DCR_u values in excess of 2.0 indicate that a linear analysis is not sufficient for evaluation, and a nonlinear analysis (Tier 3) should be performed. DCR_u values varied significantly at each wall, and were different for each spectrum used in the analysis. For the ASCE design spectrum, almost all DCR_u values exceeded 2.0, indicating that nonlinear analysis should be performed on this building at this hazard level. For the Concepción response spectrum, DCR_u values were approximately equal to 2.0.

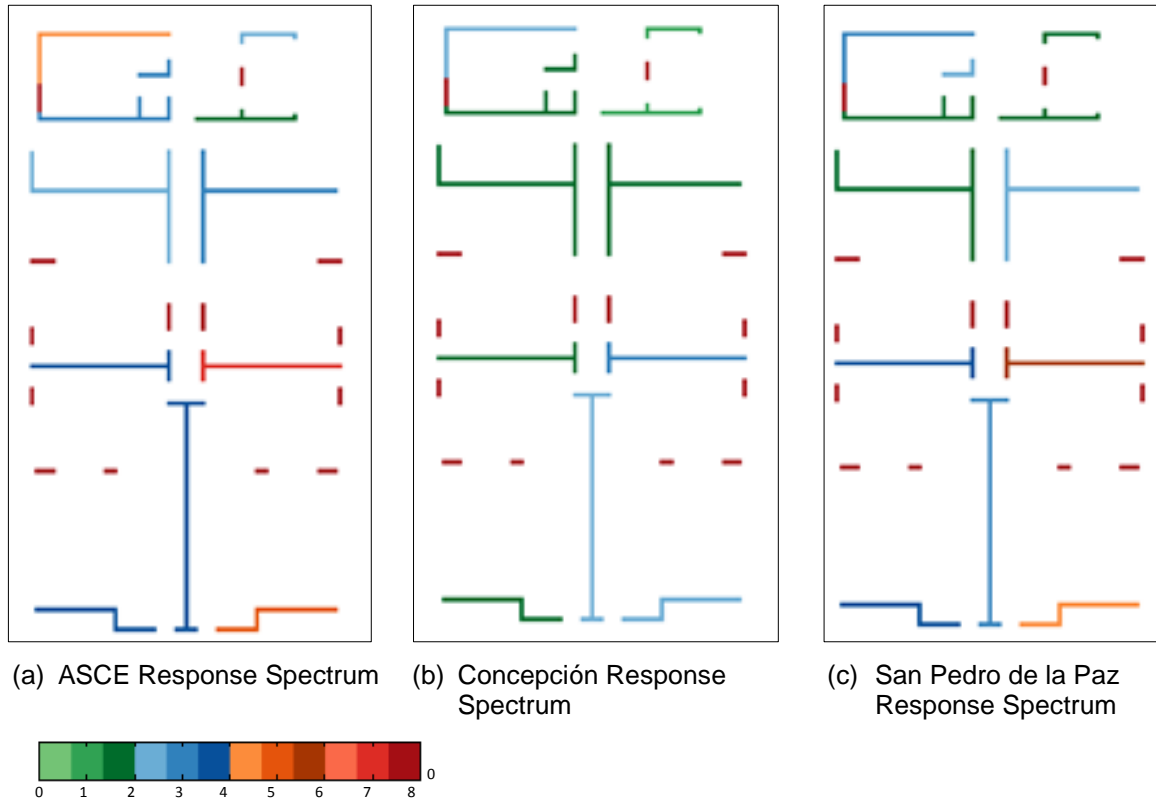


Figure 4-23 Maximum DCR_u values in first story walls of Plaza del Rio Building A (colors indicate values of DCR_u , ranging from 0 to 8).

Figure 4-24 shows the controlling mechanism for each wall in the first story of Plaza del Rio Building A, determined based on calculated values of DCR_u . For longitudinal walls, the calculated mechanism was shear; for transverse walls, the calculated mechanism was flexure; and for short wall piers, the calculated mechanism was shear. As expected, the controlling mechanism for each wall was essentially independent of the spectrum used in the analysis.

Actual response mechanisms for the walls of Plaza del Rio Building A were inferred from the reported earthquake damage. Diagonal cracking was considered to indicate a shear-controlled mechanism. Concrete crushing, bar buckling, and horizontal planes of failure were considered to indicate flexure-controlled or flexure-axial interaction mechanisms.

In general, calculated mechanisms were found to be consistent with observed mechanisms. For the primary longitudinal walls, shear was predicted to be the controlling mechanism, and significant, well-distributed diagonal cracking was observed following the earthquake. For the primary transverse walls, flexure was predicted to be the controlling mechanism, and most walls exhibited concrete crushing, particularly at the wall boundaries, or along an approximately horizontal plane of damage. Significant and well-distributed diagonal shear cracking was

observed in the interior pair of transverse T-shaped walls; however this damage was also accompanied by concrete crushing at the wall boundaries, which is indicative of both shear response and flexural response mechanisms.

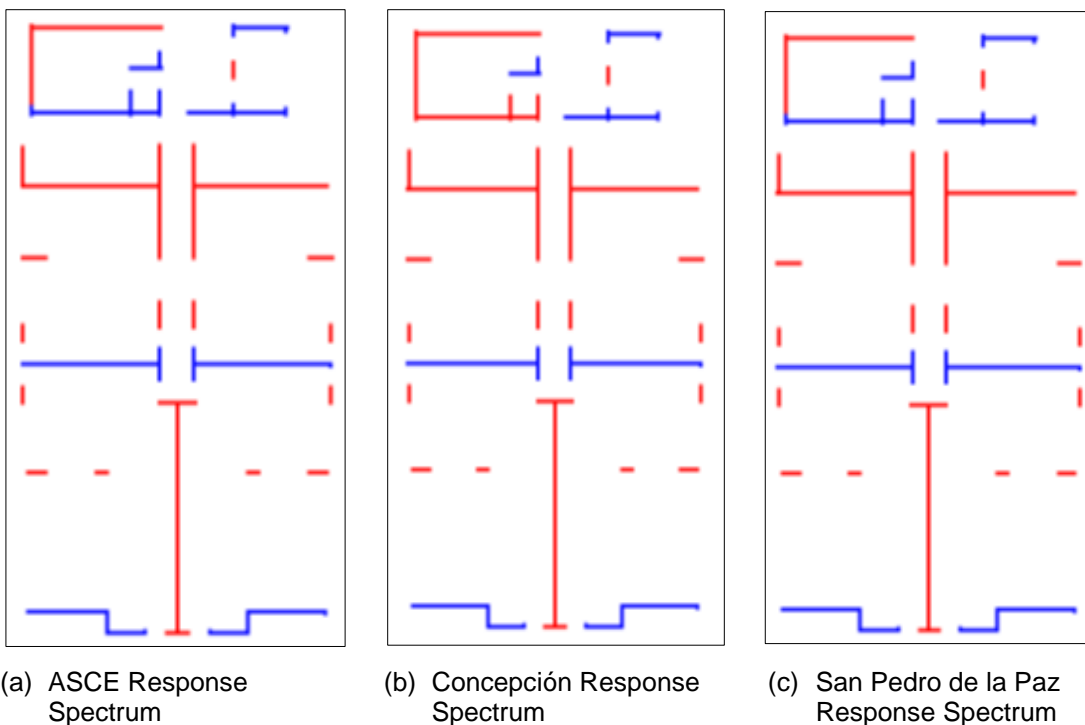


Figure 4-24 Controlling mechanisms in first story walls of Plaza del Rio Building A (blue indicates flexure mechanism; red indicates shear mechanism).

4.4.5.2 Plaza del Rio Building A – Tier 2 Evaluation Results and Correlation with Observed Severity of Damage

ASCE/SEI 31-03 Tier 2 Evaluation results were used to compare predicted performance with the severity of observed damaged. For deformation-controlled actions, factored demand-capacity ratios (DCR_f) on individual components are used to predict the performance of the structure (linear demands are acceptable for this purpose as long as DCR_u values are less than 2.0). Demands are adjusted by m -factors to account for ductility, depending on the response mechanism, design characteristics, and performance level. A DCR_f value that exceeds 1.0 indicates that a component is inadequate for the selected performance level (although adequacy may potentially be demonstrated by a more detailed (Tier 3) evaluation).

Although DCR_u values exceeding 2.0 indicate that nonlinear analysis should be performed, an evaluation using linear analysis results and DCR_f values was conducted to investigate the potential correlation between DCR_f values and damage. DCR_f values were computed for each of the spectra in Figure 4-22 using m -factors specified in ASCE/SEI 41-06.

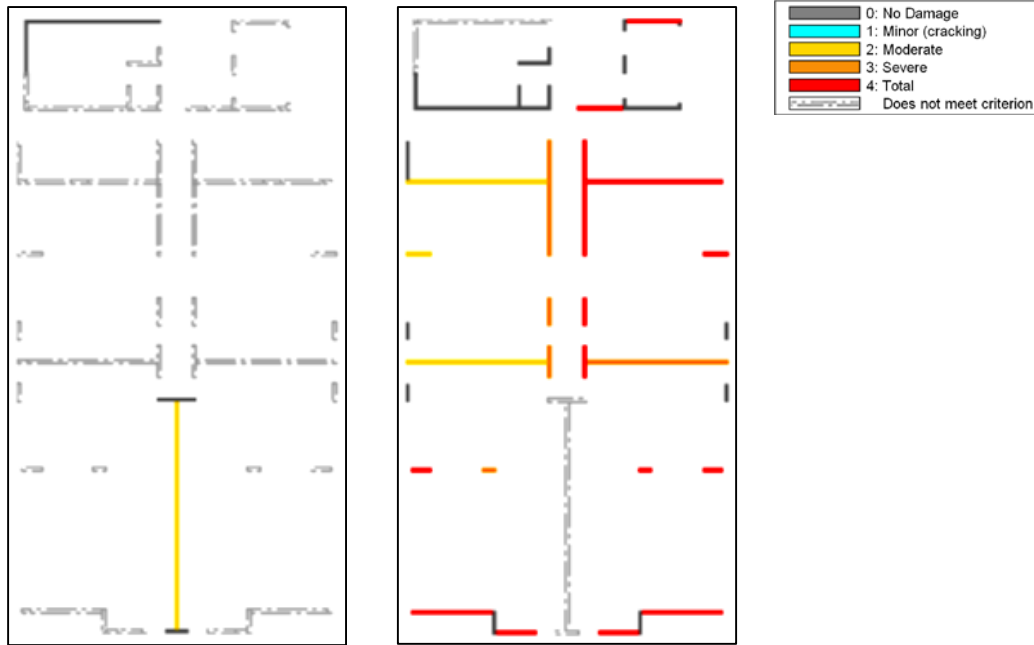
For each spectra, DCR_f values were computed for walls at the critical floor level, and the building was assessed for three performance objectives: (1) Collapse Prevention at the MCE hazard level (CP-MCE); (2) Life Safety at the DE hazard level (LS-DE); and (3) Immediate Occupancy at the DE hazard level (IO-DE). Similarly, for demands based on spectra from recorded motions, DCR_f values were computed for the unscaled ground motions (GM), and the three performance objectives were identified as CP-GM, LS-GM and IO-GM.

Per ASCE/SEI 41-06, minor damage (concrete cracking) is considered to be consistent with the Immediate Occupancy (IO) performance level, moderate damage (initial spalling of concrete cover) is considered to be consistent with the Life Safety (LS) performance level, and more severe levels of damage (short of collapse) are considered to be consistent with the Collapse Prevention (CP) performance level. Thus, a component with a DCR_f value less than 1.0 for the LS-DE performance objective would be expected to exhibit none, minor, or moderate damage, while a component with DCR_f greater than 1.0 would be expected to exhibit severe damage.

Figure 4-25 summarizes an evaluation of the first story walls in Plaza del Rio Building A based on calculated DCR_f values for the unscaled Concepción spectrum. In the panels of the figure, results for four cases are shown: (a) inadequate for all performance objectives; (b) adequate for Collapse Prevention; (c) adequate for Life Safety; and (d) adequate for Immediate Occupancy. Colored wall lines in each panel meet the criterion for that panel. For example, colored wall lines in panel (b) are adequate for CP-GM, meaning these walls have calculated DCR_f values that meet the Collapse Prevention performance level for the Concepción ground motion. Dashed gray lines indicate walls that do not meet the criterion for that panel.

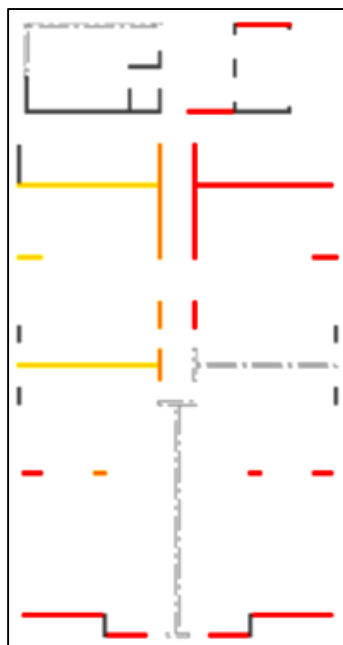
Based on the results shown in panel (b) of Figure 4-25, almost all of the primary longitudinal and transverse walls in Plaza del Rio Building A would be expected to meet the Collapse Prevention performance level for the Concepción ground motion. A significant exception is the longitudinal I-shaped wall at the south end of the building, which is inadequate for all performance objectives.

Each of the walls shown in Figure 4-25 is also assigned a fill color indicating the severity of the observed earthquake damage in the wall. The range of colors that appear in each panel is an indication of the level of correlation between the Tier 2 Evaluation criteria and the observed damage. If the correlation was perfect, the walls in each panel would have colors corresponding to levels of damage (i.e., none, minor, moderate, severe, or total) that are consistent with (or better than) the performance level associated with the objective. For example, all walls in panel (d) that are adequate for IO-GM should be colored blue or gray; all walls in panel (c) that are adequate for LS-GM should be colored blue, gray, or yellow; and no walls that appear in panels (b), (c), and (d) should be colored red.



(a) Inadequate for all performance objectives

(b) Adequate for CP-GM



(c) Adequate for LS-GM

(d) Adequate for IO-GM

Figure 4-25 Tier 2 evaluation results for first story walls in Plaza del Rio Building A subjected to the Concepción ground motion record (dashed gray walls in each panel do not meet the performance criterion for that panel, colored walls meet the performance criterion for that panel, and colors indicate the severity of the observed earthquake damage).

To assess how well the Tier 2 Evaluation criteria correlated with observed damage in Plaza del Rio Building A, the number of walls expected to meet the criteria (i.e.,

DCR_f < 1.0), the number of walls not expected to meet the criteria (i.e., DCR_f > 1.0), and the number of walls in each damage state (i.e., none, minor, moderate, severe, or total) were counted. Results are shown in Figure 4-26. In the figure, the height of the bars indicates the number of first and second story walls in Plaza del Rio Building A that are in each category, and the color indicates the portion of the walls that are in each state of observed earthquake damage.

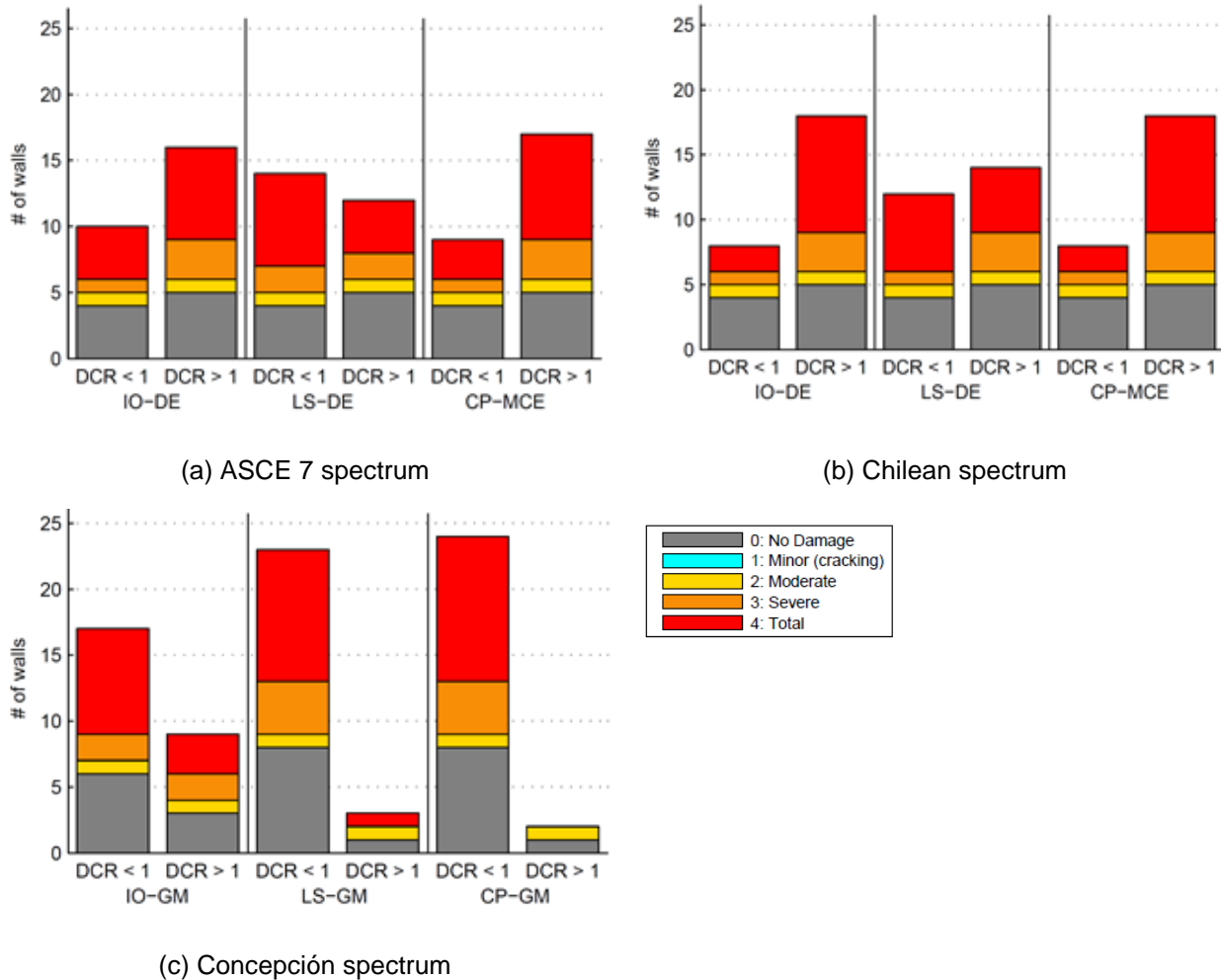


Figure 4-26 Number of walls in Plaza del Rio Building A that meet (or do not meet) various performance categories (colors indicate the severity of the observed earthquake damage for walls in each category).

The range of colors that appear in each bar is an indication of the level of correlation between the Tier 2 Evaluation criteria and the observed damage. If the criteria and the observed damage were correlated, each bar would have colors corresponding to levels of damage (i.e., none, minor, moderate, severe, or total) that are consistent with (or better than) the performance level identified. For example, none of the bars in these figures should be colored red.

It can be seen from Figure 4-26 that there is little correlation between Tier 2 Evaluation criteria and the observed damage in Plaza del Rio Building A. Regardless of the calculated DCR_f values, the distribution of the severity of damage for each performance objective shows a similar proportion of both damaged and undamaged walls. Figure 4-26 also highlights the sensitivity of these results to the spectrum used in the analysis, as can be seen by the changes in the height of the bars in each panel.

In spite of a lack of correlation at the individual component level, it is noted that evaluation of Plaza del Rio Building A using the Concepción spectrum indicates that the building would be expected to achieve the Collapse Prevention performance level, given the intensity of shaking at the site, which is consistent with the observed performance of the overall building in the earthquake.

4.4.6 Summary of Tier 2 Evaluation Results

Results from ASCE/SEI 31-03 Tier 2 Evaluations on Plaza del Rio Building A, Plaza del Rio Building B, and the Centro Mayor building can be summarized as follows:

- DCR_u values for the study buildings indicated that significant inelastic response could be expected and that nonlinear analysis should be performed.
- DCR_u values indicate that in lower stories primary lateral force-resisting walls were equally likely to be controlled by flexure or shear, with shear expected to control primary response in the longitudinal direction, and flexure expected to control primary response in the transverse direction.
- DCR_f values did not correlate well with observed earthquake damage at the component level.

4.4.7 ASCE/SEI 31-03 Tier 3 Evaluations

In ASCE/SEI 31-03, detailed evaluation is conducted under Tier 3. Only one of the five buildings (Plaza del Rio Building A) was evaluated using the ASCE/SEI 31-03 Tier 3 Evaluation procedure, which includes computation of maximum deformation demands and comparison with deformation capacities using nonlinear analysis. In this case, the Nonlinear Dynamic Procedure (NDP) specified in ASCE/SEI 41-06 was used. Tier 3 model development, loading, analyses, and results are presented in detail in Appendix D. Summary information for the Tier 3 Evaluation of Plaza del Rio Building A is presented this section.

Deformation demands were computed for a suite of seven ground motions in Chile, scaled to match the ASCE/SEI 7-10 target spectrum for Site Class D in a region of high seismicity in the United States. Demands were also computed for the unscaled Concepción and Concepción-San Pedro de la Paz ground motions, with the objective of comparing calculated results with observed damage.

4.4.7.1 Overview of Tier 3 Nonlinear Modeling

Nonlinear dynamic analyses were completed using the OpenSees analysis platform (OpenSees, 2013) and PERFORM-3D. Design and expected material strengths were determined in accordance with ASCE/SEI 41-06. In both analysis platforms, Rayleigh damping was employed, and a damping ratio of 2% was defined for the first and third elastic modes. In OpenSees, Rayleigh damping was computed using the current, committed stiffness matrix. In both analysis platforms, P-delta effects were included.

Details of the PERFORM-3D models are as follows:

- Analyses were conducted assuming a fixed base (referred to as the “Perform Basic” model), and also using elastic foundation springs that provided the same resistance in tension and compression (referred to as the “Perform SSI” model).
- The nonlinear fiber-shell element of PERFORM-3D was used to simulate wall response in flexure. A planar section of wall was typically discretized horizontally into several elements depending on the wall geometric configuration and discontinuities along the building height, and intersecting walls and beams. Each wall element was discretized horizontally into eight fibers of steel and concrete. Walls were discretized vertically into two elements per story with a single integration point at the mid-height of each wall segment.
- A nonlinear shear model was employed in conjunction with the fiber-shell element. This model uses the ASCE/SEI 41-06 backbone curve, and a degrading unloading-reloading stiffness calibrated to provide the same hysteretic energy dissipation as a perfect pinching model (i.e., no positive shear strength for negative shear strain and no negative shear strength for positive shear strain).
- Preliminary analyses indicated that coupling beams would respond in shear rather than flexure; thus, coupling beams were modeled using nonlinear shear hinges located at the mid-span of the beam and connected via elastic beam-column elements at each side.
- Analyses were conducted with a rigid diaphragm constraint imposed at each story.
- Analyses were conducted only for the unscaled Concepción and Concepción-San Pedro de la Paz ground motion records.

Details of the OpenSees model are as follows:

- Force-based beam-column elements with fiber-type section models were used to simulate the nonlinear flexural response of individual walls. Typically, one element with five integration points was used per floor level, and fiber dimensions were approximately 0.4 inches by 1.2 inches.

- A nonlinear shear response model was employed; the model included a trilinear envelope in which the final segment had a small positive stiffness, non-degrading unloading stiffness, and approximately perfect pinching response (i.e., no positive shear strength for negative shear strain and no negative shear strength for positive shear strain) under cyclic loading.
- In places where the centroid of the wall moved due to a change in wall geometry, an approximately rigid beam element was used to link line-element nodes and enable load transfer between the two segments of the wall.
- The concrete slab and coupling beams were not included in the model; instead walls were connected via a rigid diaphragm constraint imposed at each floor level.
- Analyses were conducted for the unscaled Concepción and Concepción-San Pedro de la Paz ground motion records, as well as for a suite of seven Chilean ground motions (including the Concepción and Concepción-San Pedro de la Paz records) scaled per ASCE/SEI 7-10 procedures to the minimum target spectra for Site Class D in a region of high seismicity in the United States.

Initial evaluation of the OpenSees and PERFORM-3D models included determination of fundamental periods and response modes for the undamaged structure. These were compared with periods and mode shapes computed using SAP2000 and an elastic effective-stiffness (cracked section) model of the structure. Periods and mode shapes for the OpenSees, Perform Basic, and SAP2000 effective-stiffness models were comparable; periods for the Perform SSI model were significantly longer.

4.4.7.2 Plaza del Rio Building A – Tier 3 Analysis Results for the Unscaled Concepción Ground Motion Record

Results from the OpenSees, Perform Basic, and Perform SSI models using the Concepción record are summarized in this section. Results for other analyses and other ground motions are provided in Appendix D.

Table 4-3 lists simulated maximum and residual drift results from the OpenSees, Perform Basic, and Perform SSI models. The data show that drifts determined using the OpenSees model were substantially smaller than those determined using the Perform models. This was attributed to the fact that the OpenSees model did not simulate strength loss due to shear failure of the walls while the Perform models did.

Drifts determined using the Perform SSI model were typically larger than those determined using the Perform Basic model, as expected. In addition, foundation flexibility elongated the fundamental period of the Perform SSI model into the long-period range of the Concepción response spectrum, which has unusually large spectral accelerations.

Both Perform models predicted extremely large (i.e., greater than 3.0%) first-story drifts in the longitudinal direction at approximately 30 seconds into the Concepción record following several large amplitude response cycles. These large drifts were the result of calculated shear failure of the primary lateral load-resisting walls in the longitudinal direction. According to Birely (2012), symmetrically flanged walls lose lateral load-carrying capacity at a median story drift of 3.0%. Thus, analysis results were considered to indicate failure of the building. Despite shear failure of the primary longitudinal walls, simulated flexural capacity of these walls (which was decoupled from shear capacity), and simulated flexure and shear capacity of secondary walls, enabled the structure to remain stable.

Table 4-3 Plaza del Rio Building A – Tier 3 Analysis Maximum and Residual Drifts Predicted for the Concepción Ground Motion

Model	E-W (Transverse) Direction						N-S (Longitudinal) Direction					
	Maximum Drift			Residual Drift			Maximum Drift			Residual Drift		
	Roof	1st Story	2nd Story	Roof	1st Story	2nd Story	Roof	1st Story	2nd Story	Roof	1st Story	2nd Story
OpenSees	0.82%	0.12%	0.51%	0.09%	0.01%	0.06%	0.60%	0.17%	0.35%	0.03%	0.01%	0.02%
Perform Basic	2.31%	0.50%	1.93%	0.50%	0.06%	0.52%	0.74%	>3.0%	0.68%	0.05%	0.35%	0.10%
Perform SSI	2.80%	1.48%	2.52%	1.48%	0.23%	0.63%	1.09%	>3.0%	1.08%	0.03%	0.30%	0.07%

Following the 2010 Maule earthquake, a residual roof drift of approximately 1.5% was observed in Plaza del Rio Building A in the transverse direction. In addition, pounding damage was observed between Plaza del Rio Buildings A and B, suggesting relatively large drifts for Plaza del Rio Building A in the longitudinal direction. These observations are most consistent with the results obtained using the Perform SSI model.

4.4.7.3 Plaza del Rio Building A – Tier 3 Evaluation Results and Correlation with Controlling Mechanisms

Figure 4-27 shows first- and second-story walls in Plaza del Rio Building A that were predicted to fail in shear based on the OpenSees and Perform models subjected to the Concepción ground motion record. These results were compared to the observed severity of damage to investigate potential correlation.

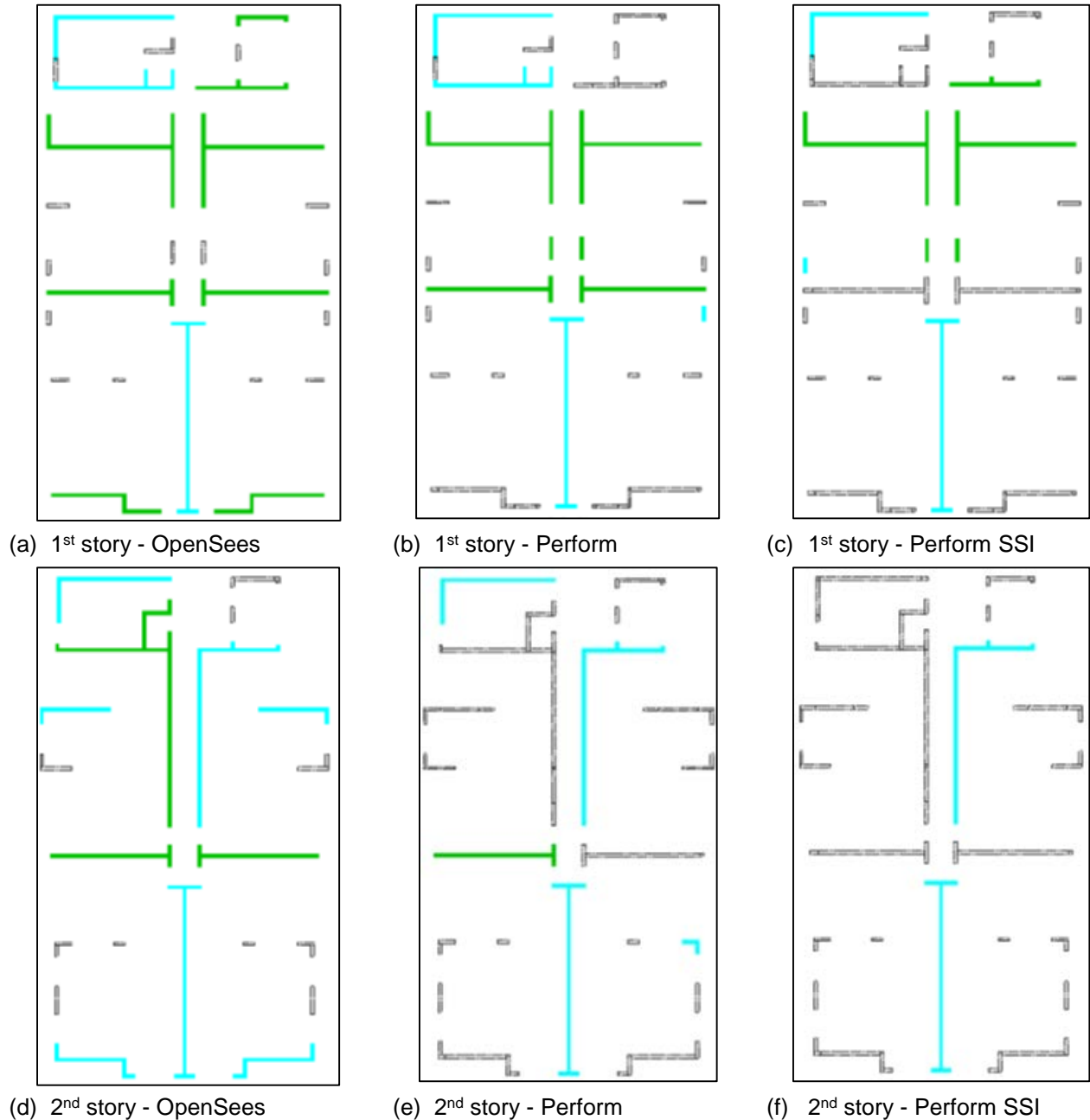


Figure 4-27 Shear failures in first and second story walls of Plaza del Rio Building A, as predicted using OpenSees, Perform Basic, and Perform SSI models. Colored wall lines indicate shear failures with $V_u > 1.1V_n$. Fill color indicates the severity of observed earthquake damage (green corresponds with severe or total damage; blue corresponds with none, minor, or moderate damage). Dashed gray walls indicate walls that are not predicted to fail in shear.

In the figure, colored wall lines indicate shear failures with $V_u > 1.1V_n$ (where V_u is the shear demand from nonlinear analysis, and V_n is the calculated shear capacity). The fill color indicates the severity of observed earthquake damage, where green corresponds with severe or total damage, and blue corresponds with none, minor, or moderate damage.

Based on the results shown in Figure 4-27, shear failure predictions were somewhat consistent with observed damage. In the longitudinal direction, shear failures were predicted, and diagonal cracking consistent with a shear response mechanism were observed in these walls. In the I-shaped wall at the south end of the building, however, the observed level of damage was less severe than would have been expected given a calculated shear failure.

In the transverse direction, shear failure predictions were different for the different models, and the results of the Perform SSI model appear to be the most consistent with observed damage. In the case of the transverse T-shaped walls located in the center of the building, diagonal shear cracking accompanied by concrete crushing at the wall boundaries was observed, which is indicative of both shear response and flexural response mechanisms. Depending on the model and the analysis, these walls are predicted to be controlled by shear or flexural mechanisms.

4.4.7.4 Plaza del Rio Building A – Tier 3 Evaluation Results and Correlation with Observed Severity of Damage

ASCE/SEI 31-03 Tier 3 Evaluation results were used to compare predicted performance with the severity of observed damaged. Three approaches were used to determine the deformation capacity of structural wall components and assess performance (or the predicted level of damage):

- Rotation limits for wall components responding in flexure and shear, as provided in ASCE/SEI 41-06. These deformation capacities are a function of axial load and shear force demands, as well as wall design characteristics, and are used to assess acceptance for the Immediate Occupancy (IO), Life Safety (LS), and Collapse Prevention (CP) performance levels.
- Deformation limits from empirical fragility functions for slender walls responding in flexure from Birely (2012). These limits were used to determine the predicted damage state of wall components.
- Usable strain limits for concrete and longitudinal reinforcement, steel yield strain, concrete spalling strain, and concrete crushing strain, as provided in ASCE/SEI 41-06. These limits were used to assess material damage.

Figure 4-28 summarizes the results of an evaluation of the first-story walls in Plaza del Rio Building A, subjected to the Concepción ground motion record. Colored walls lines in each panel meet ASCE/SEI 41-06 acceptance criteria for the identified performance level (e.g., no damage, IO, LS, CP, or shear failure) at the recorded level of motion. The fill color indicates correlation between observed and predicted levels of earthquake damage, where red indicates observed damage is greater than predicted, green indicates observed damage is equal to predicted, and blue indicates observed damage is less than predicted.

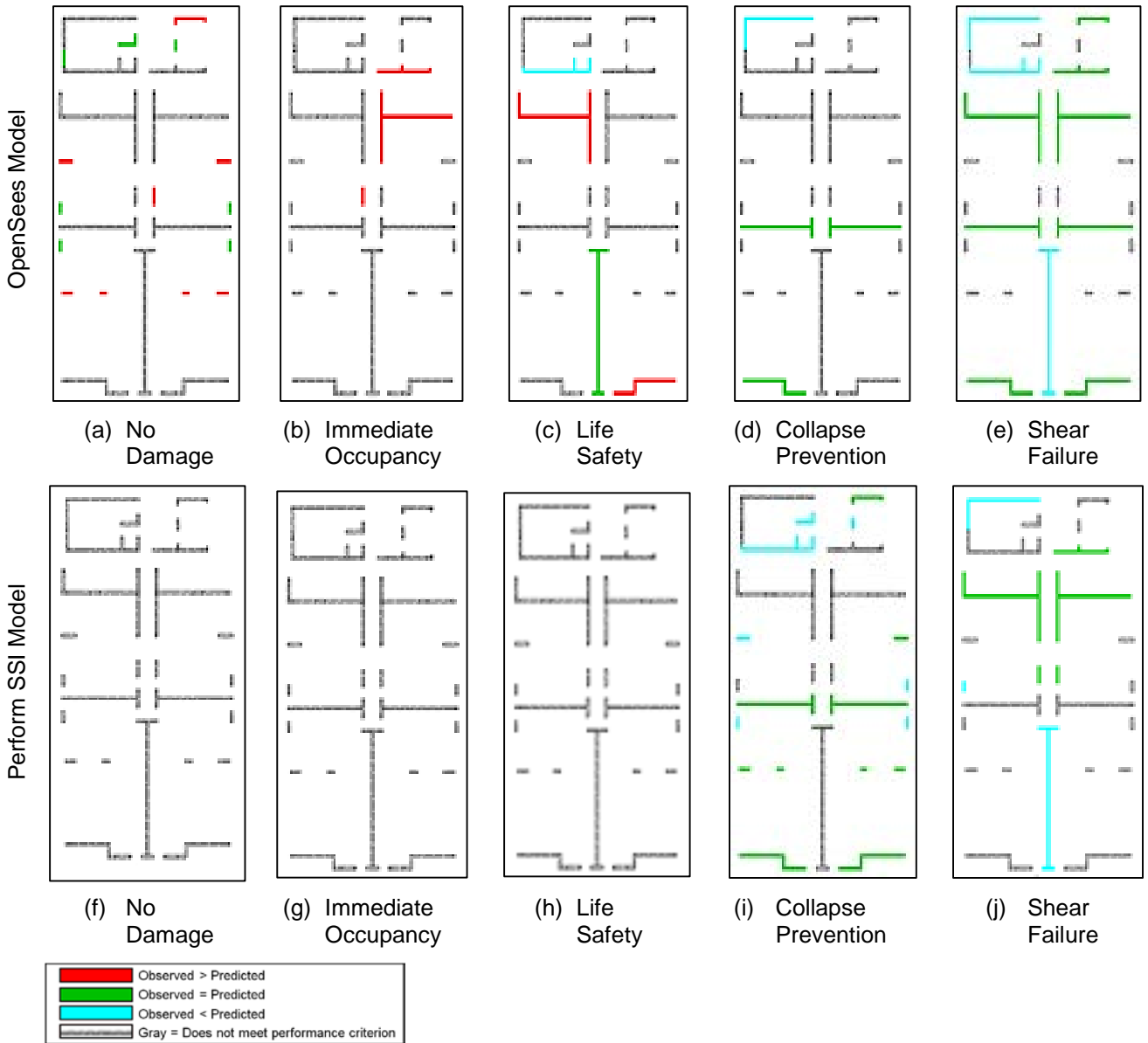


Figure 4-28 Tier 3 evaluation results for first story walls in Plaza del Rio Building A subjected to the Concepción ground motion record (colored walls in each panel meet the performance criterion for that panel, and colors indicate correlation with the observed earthquake damage). Dashed gray walls indicate walls that do not meet the performance criterion for that panel.

If Tier 3 Evaluation criteria were perfectly correlated with the observed earthquake damage, the wall lines in each panel of Figure 4-28 would be colored green. Wall lines that are colored blue indicate Tier 3 Evaluation results that were conservative relative to observed damage (i.e., observed damage was less than predicted). Wall lines colored red in any panel of Figure 4-28 indicate Tier 3 Evaluation results that were unconservative relative to observed damage (i.e., observed damage was greater than predicted).

Figure 4-28 shows that in the OpenSees model, several walls achieved the Immediate Occupancy and Life Safety performance levels, but many of these walls were observed to have experienced more damage than predicted by analysis. In the Perform SSI model, most walls achieved only the Collapse Prevention performance level, and in these cases, observed damage was generally consistent with the assessed performance. The data in Figure 4-28 were combined with similar data from other assessment criteria and models to produce the bar charts shown in Figure 4-29.

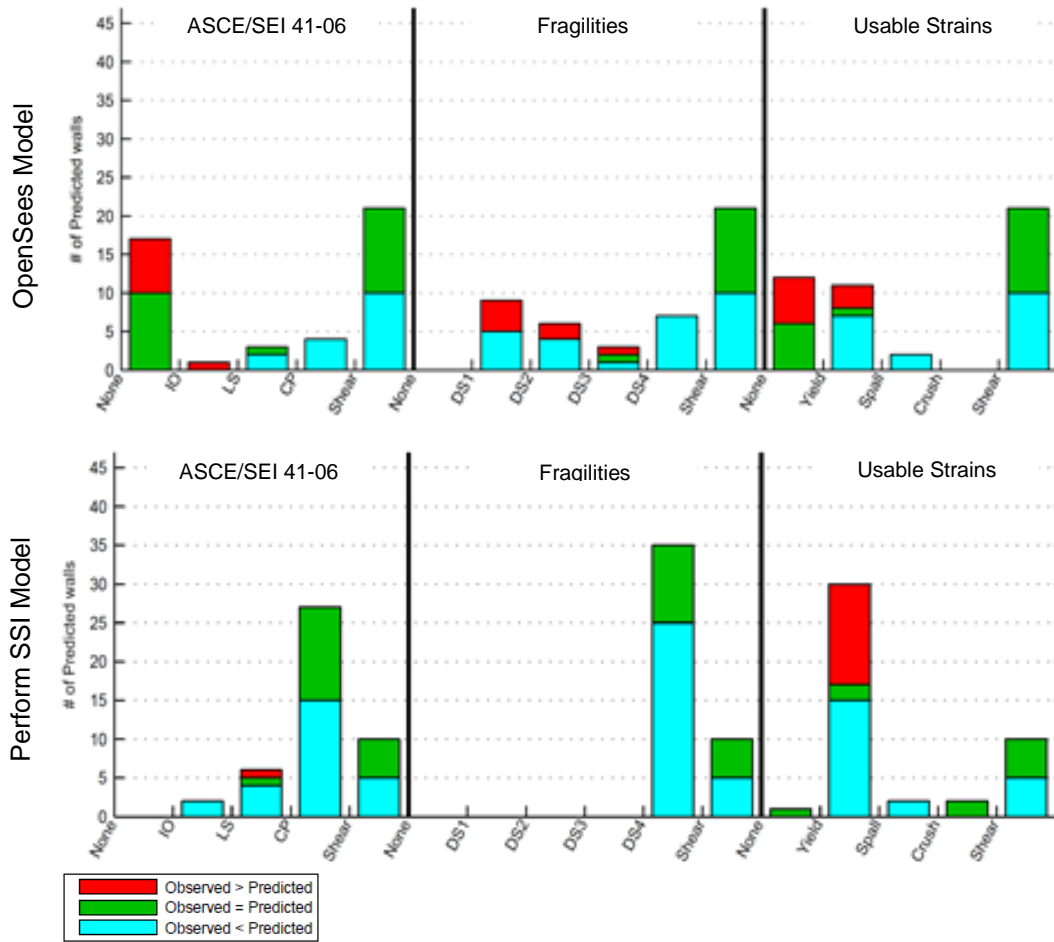


Figure 4-29 Number of walls in Plaza del Rio Building A meeting (or exceeding) acceptance criteria for different performance measures and different models (colors indicate correlation between predicted and observed earthquake damage).

In Figure 4-29, the height of the bars indicates the number of walls in Plaza del Rio Building A that are in each category of performance, and the color indicates the level of correlation between observed and predicted levels of damage. If the criteria and observed damage were perfectly correlated, the bars would be colored green. Portions of the bars in Figure 4-29 that are blue indicate criteria that are conservative relative to observed damage (i.e., observed damage was less than predicted), and

portions of the bars that are red indicate criteria that are conservative relative to observed damage (i.e., observed damage was more than predicted).

Based on the information shown in Figure 4-29, the range of colors in each bar indicate that current evaluation criteria (and response simulation techniques) do not result in a highly accurate prediction of observed damage, meaning that damage at the component level can be more or less than predicted. However, the relative proportion of the bars in the figure that are colored red (i.e., unconservative) is small, which means that the criteria are producing a generally conservative assessment (for this case study building).

4.4.8 Summary of Tier 3 Evaluation Results

Based on results from ASCE/SEI 31-03 Tier 3 Evaluations on Plaza del Rio Building A, the following observations can be made:

- ASCE/SEI 41-06 assessment criteria provided an acceptably accurate measure of overall building performance.
- Consideration of foundation flexibility (i.e., use of the Perform SSI model) resulted in the most consistency between predicted and observed damage.
- Predictions of the controlling mechanism, and shear failure, using ASCE/SEI 41-06 assessment criteria were somewhat consistent with observed damage.
- Prediction of observed damage at the component level, using various assessment criteria investigated in this study (e.g., ASCE/SEI 41-06 rotation limits, fragility functions, usable strain limits), was not accurate, meaning that component damage may be more or less than predicted using these criteria.
- Use of ASCE/SEI 41-06 assessment criteria generally resulted in a conservative assessment of performance at the component level.
- Use of fragility function assessment criteria developed for planar walls (Birely, 2012) generally resulted in a conservative assessment of performance for walls of variable configurations.
- Assessment criteria based on usable strain limits were generally unconservative, and were more sensitive to record-to-record variability.

4.4.9 Study of Coupled Wall Response

Coupled walls are defined by two or more solid walls interconnected by beams, slabs or spandrels aligned over the height of the building, creating a vertically aligned series of openings. A study was conducted to investigate the effect of coupling on wall response by comparing the estimated axial load from elastic analysis of the entire building to axial load under gravity loading.

4.4.9.1 Coupled Wall Behavior

Figure 4-30 shows an idealization of the load distribution in a coupled wall system subjected to lateral loading. When subjected to earthquake loading, a coupled system can develop more strength and stiffness than two independent walls of similar construction. Coupling beams typically undergo multiple inelastic deformation cycles; thus, damage to coupling elements may be substantial. If coupling elements are not designed and detailed to maintain strength under severe deformation demands, wall piers will become “uncoupled” as the strength of the coupling elements deteriorates. Figure 4-31 shows damage to a coupling beam observed following the 2010 Maule earthquake.

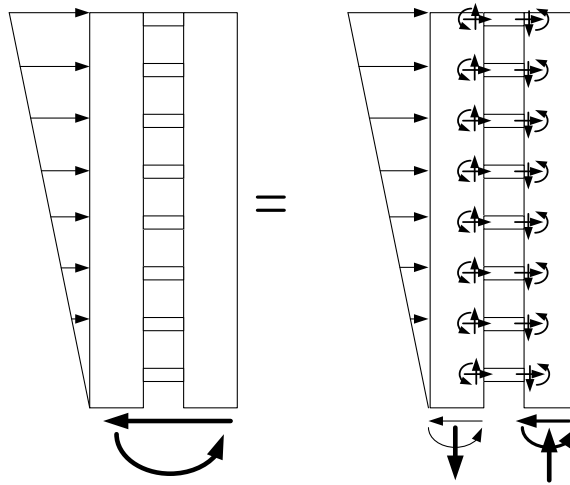


Figure 4-30 Idealized load distribution in a coupled wall system (arrows show loads acting on wall piers).



Figure 4-31 Damage to coupling beam in the Centro Mayor building, Concepción (DICTUC, 2010b).

Damage and reinforcement visible in Figure 4-31 indicate that the coupling beam was not designed to provide ductile, flexure-controlled behavior. Similar coupling-induced damage was also observed in floor slabs of other buildings (Birely, 2012).

Slabs (and other “accidental” coupling elements) are not typically expected (or designed) to act as coupling elements, and code requirements do not address detailing of these elements to maintain strength through multiple inelastic deformation cycles.

Research on the seismic response of concrete walls, including coupled walls, shows that walls can exhibit limited-ductility compression-controlled failure, and that the likelihood of this failure mode developing is related to the compression and shear forces in the wall pier (Turgeon, 2012). Research addressing coupled wall systems shows also that the “compression” pier in the coupled wall system has substantially greater lateral stiffness than the “tension” pier if the tension pier is carrying tension; this depends on the degree of coupling as well as other aspects of the system.

The idealized load distribution in Figure 4-30 shows how shear forces that develop in the coupling elements accumulate as added tension and compression forces in the wall piers. It also shows how axial loads in the coupling elements transfer horizontal shear between the wall piers resulting in the accumulation of more base shear in the stiffer compression wall pier relative to the more flexible tension wall pier.

Recent research by Lehman et al. (2013) has recommended that coupled walls be designed for the expected axial compression in wall piers, and that each wall pier in the coupled wall system be designed to carry a majority of the total shear, depending on the relative stiffness of the individual wall pier and the axial loads resulting from the coupled moment.

4.4.9.2 Elastic Investigation of Coupled Wall Response

Wall piers in Chilean buildings may have been subjected to increased axial and shear forces resulting from coupling via slabs, spandrels, and nonstructural elements. In general, shear and axial forces induced by slabs are small because typical slabs are relatively thin and flexible. In some buildings, however, coupling forces may be larger if slabs are thicker and beams and collector elements are engaged. Coupling forces induced by nonstructural elements, such as stairs, may be quite large depending on the construction of the nonstructural elements and how they are connected to the structural elements.

To investigate the effect of coupling on wall response, the axial load in the walls of Plaza del Rio Building A were computed considering gravity load alone, and gravity load plus induced seismic forces. It should be noted that forces were determined based on elastic analyses, and nonlinear behavior would be expected to reduce these forces somewhat. Additional supporting studies are provided in Birely (2012).

Figure 4-32 shows the ratio of maximum axial compression (gravity plus seismic) to gravity load in the first-story walls of Plaza del Rio Building A. Figure 4-33 shows maximum axial compression (gravity plus seismic) as a percentage of axial strength,

$A_g f'_c$. These figures indicate that elastic coupling response increased axial loads by a factor of 1.5 to 5.0, resulting in axial stress ratios as large as $0.5A_g f'_c$ in the walls of Plaza del Rio Building A.

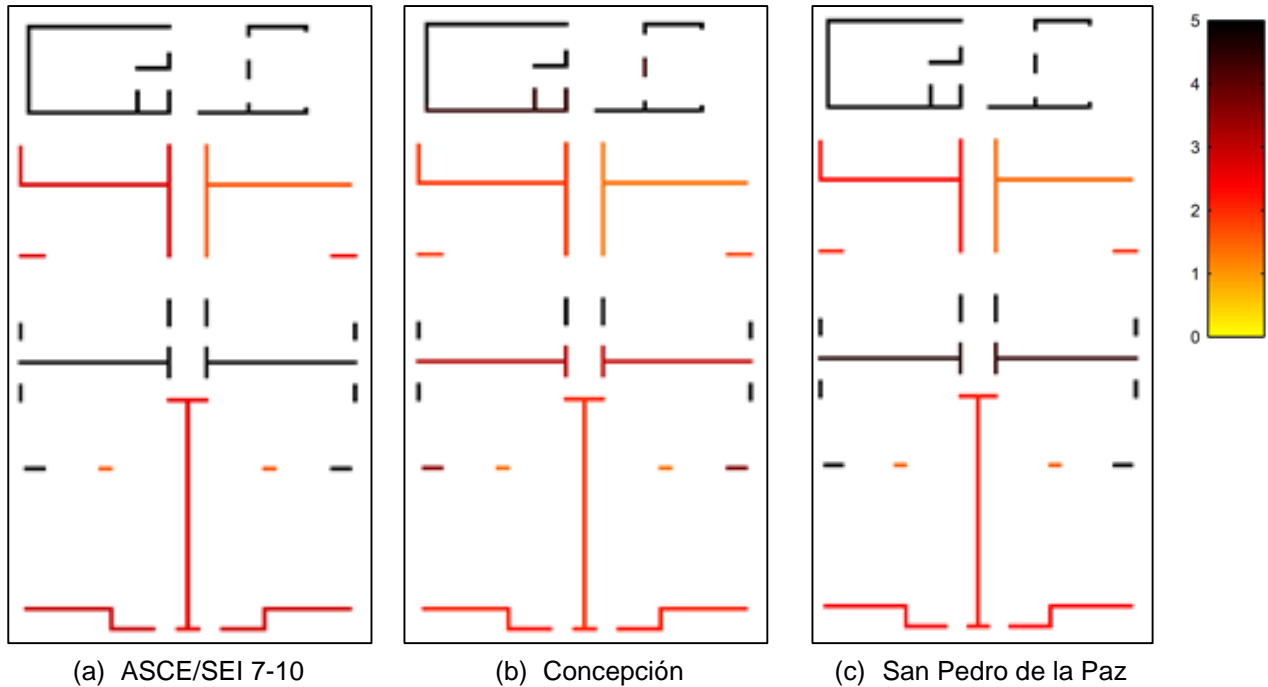


Figure 4-32 Ratio of maximum axial compression (gravity plus seismic) to gravity load in the walls of Plaza del Rio Building A, calculated using elastic analysis.

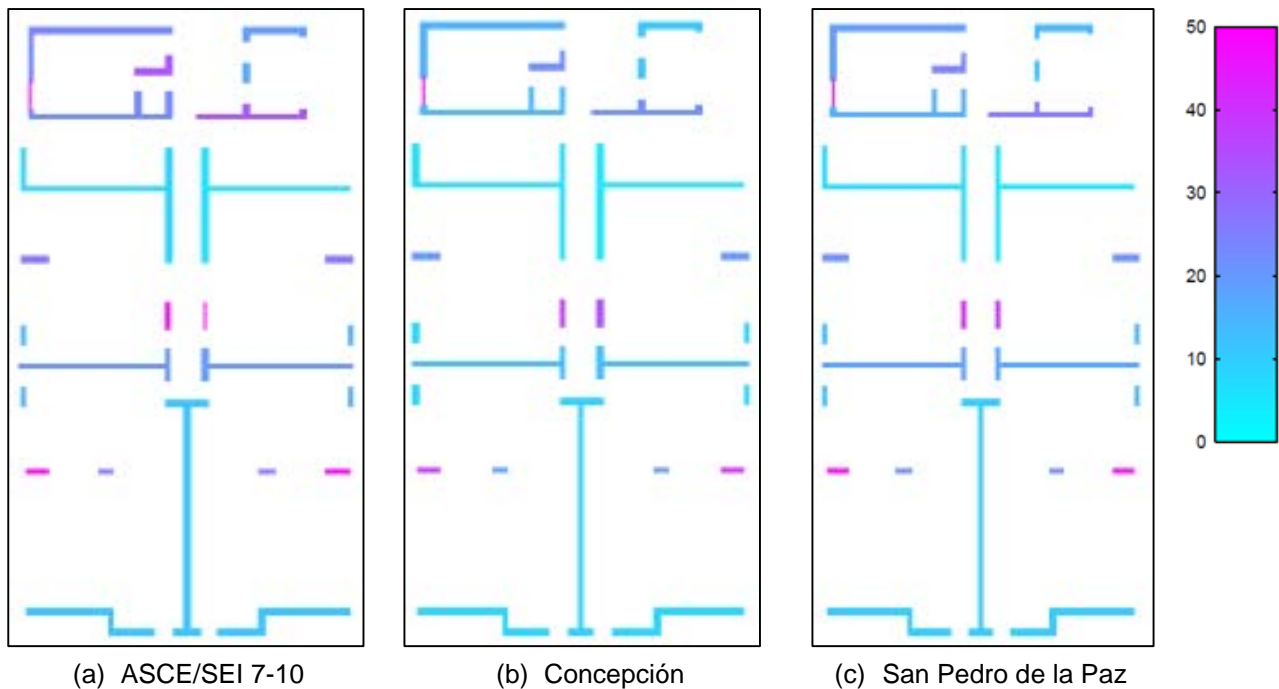


Figure 4-33 Maximum axial compression (gravity plus seismic) as a percentage of axial strength in the walls of Plaza del Rio Building A, calculated using elastic analysis.

4.4.9.3 Nonlinear Investigation of Coupled Wall Response

Nonlinear analysis results from the PERFORM-3D models subjected to the unscaled Concepción record were also used to investigate the impact of coupling response on wall axial loads. Figure 4-34 shows the maximum axial compression developed in the walls during the earthquake as a percentage of axial strength, $A_g f'_c$. In the figure, many walls are shown with compressive demands on the order of $0.1A_g f'_c$ or more (light blue or darker), with some as large as $0.5A_g f'_c$. These results are on the same order of magnitude as the elastic analysis results.

Research has shown that compressive demands in excess of $0.1A_g f'_c$ can result in reduced deformation capacity of walls (i.e., lower drift at onset of damage, and lower drift at onset of failure). As a result, many walls in Plaza de Rio Building A might have been expected to exhibit diminished performance due to induced coupling forces.

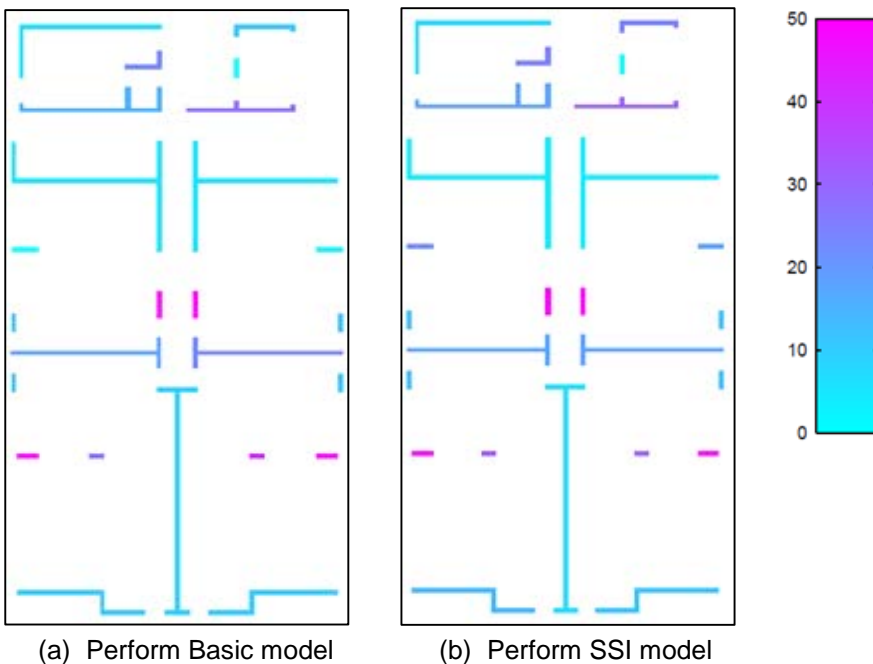


Figure 4-34 Maximum axial compression (gravity plus seismic) as a percentage of axial strength in the walls of Plaza del Rio Building A, calculated using nonlinear analysis for the unscaled Concepción record.

4.4.9.4 Findings and Recommendations on Coupled Wall Response

Based on elastic and nonlinear analysis of Plaza del Rio Building A, the following observations and recommendations on the response of coupled walls can be made:

- Axial load amplification on walls due to slab and beam coupling may be significant, especially on small wall piers.

- Provisions and commentary in ACI 318 (e.g., in Section 21.9.5) should be added to force consideration of the effects of coupling elements connected to walls, including, for example, the influence of coupling behavior on axial force.

4.4.10 Study of Local Wall Discontinuities

ASCE/SEI 31-03 Tier 1 checklists consider vertical discontinuities in buildings through an evaluation of load path, verification that lateral force-resisting elements are continuous to the foundation, and evaluation of the strength and stiffness of a story relative to the stories above and below. Investigation of building configuration issues related to discontinuities, however, suggests that local changes in the stiffness and strength of individual wall components may be correlated with damage, and that checks on overall story strength and stiffness do not necessarily capture these effects.

A study was undertaken to investigate local discontinuities observed in walls of Chilean case study buildings, and to determine if there was any significant correlation between observed damage and different measures of local discontinuities. The four buildings included in this study were Plaza del Rio Building A, Plaza del Rio Building B, Centro Mayor, and Concepto Urbano. In this study, a local wall discontinuity was considered to be any location where the cross-section of a wall in a given story changed relative to the story above or below. Four types of local discontinuity measures were investigated:

- Change in cross-sectional area, as illustrated in Figure 4-35 (a) and (c).
- Change in maximum dimension in the x- or y-direction, as illustrated in Figure 4-35 (a) and (c).
- Change in centerline length, measured along the centerline of the cross-section, as illustrated in Figure 4-35 (c).
- Change in centroid location, measured by the coordinates of the geometric centroid of the cross-section, as illustrated in Figure 4-35 (b) and (c).

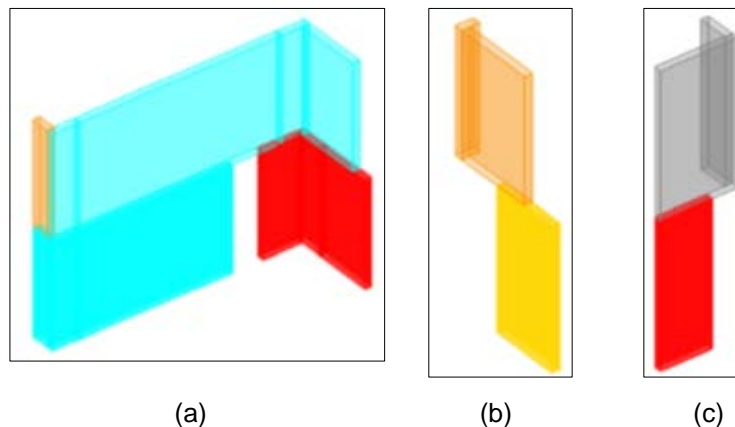


Figure 4-35 Illustration of local wall discontinuities.

Approximately 120 discontinuities were identified in the set of case study buildings. The magnitude of the discontinuity in terms of the percentage change in cross-sectional geometry was estimated, and correlations with the severity of observed damage were investigated. Results are provided in Appendix D and Birely (2012).

4.4.10.1 Recommendations on Local Wall Discontinuities

Based on the magnitude of the observed discontinuities and observed damage, this study concluded that damage was reasonably correlated with a change in local cross-sectional geometry that exceeded 30% in the centerline length or centroid location of a wall. From these results, it is recommended that the ASCE/SEI 31-03 Tier 1 Basic Structural Checklist be modified to include a check on local wall discontinuities related to centerline length and centroid location. Accordingly, the following new checklist statement should be considered:

LOCAL VERTICAL DISCONTINUITIES: In concrete shear walls that are continuous to the foundation, local discontinuities caused by changes in cross-sectional geometry from one story to the story below shall not exceed: (i) a reduction in centerline length greater than 30% (in either orthogonal direction); or (ii) a change in centroid location greater than 30% of the wall length measured in the direction of the change.

4.5 Investigation of Pier-Spandrel Systems

For pier-spandrel systems, ACI 318 includes provisions that require special moment frame requirements to be satisfied for transverse reinforcement in wall piers, depending on the dimensions of the wall pier. However, for wall piers with clear height less than twice the length, these requirements do not currently apply. Thus, it is necessary for designers to perform verification of the system response mechanism if strong-pier/weak-spandrel behavior is intended. Typical damage to pier-spandrel systems is observed in piers that are weaker than adjacent spandrels or in spandrels that are weaker than adjacent piers. The FEMA P-306 report, *Evaluation of Damaged Concrete and Masonry Walls Buildings* (FEMA, 1999), provides a method for determining component and system response mechanisms.

This section summarizes an evaluation of the expected mechanism of behavior for a pier-spandrel system, using hand calculations on the O'Higgins building as a case study example.

4.5.1 Approach

In FEMA P-306, the method for determining component and system response mechanisms identifies the controlling behavior for each component, and then employs joint equilibrium and the principles of virtual work to determine the

expected system response mechanism. Application of this approach to the O'Higgins building, located in Concepción, is described in Appendix E.

4.5.2 Findings and Recommendations

In this study, the FEMA P-306 method for evaluating pier-spandrel response mechanisms was shown to predict the expected behavior and observed damage that occurred in O'Higgins building during the earthquake. Although current U.S. seismic design provisions do not require designers to explicitly identify the overall mechanism of response for reinforced concrete wall buildings, employing such a process would be useful for verifying that the expected mechanism is consistent with the intended behavior. Also, it is recommended that the definition of wall piers in ACI 318 be expanded to include elements with a squat aspect ratio, such as 1:1.

Analytical Modeling of Concrete Wall Buildings

This chapter discusses approaches for modeling of concrete wall buildings, and presents a series of studies using analytical models in an attempt to simulate behavior observed in experimental tests of concrete wall specimens. A case study of the Alto Rio building in Concepción compares the behavior observed in the 2010 Maule earthquake to the simulated behavior predicted using several different modeling approaches. Comparison of modeling approaches with physical observations highlights key factors to consider in developing analytical models for concrete wall buildings.

5.1 Approaches for Analytical Modeling of Concrete Wall Buildings

5.1.1 *Shell Elements*

Models composed of nonlinear shell-type finite elements are likely to provide the best analytical representation for concrete wall buildings having interconnecting walls and significant irregularities. In principle, when using shell elements, all geometric irregularities can be accommodated explicitly, and accuracy is limited only by the capability of the element formulation and mesh density. Walls and floors can be modeled in the same way.

In a shell element representation, the axial, flexure, and shear responses of a wall are coupled because the model represents stress and strain fields rather than force-resultant and deformation-resultant fields. In addition, plane sections are not enforced to remain plane, allowing realistic strain and stress concentrations to develop at discontinuities. If the mesh density is sufficient between floor levels, and the large deflection formulation is used, overall wall buckling between floors can also be captured by the analysis.

In general, conventional plate and shell elements in finite element programs do not generate stiffness for the rotational degree of freedom normal to the reference surface of the element, and so coupling beams (modeled with beam elements) require special connection procedures to generate end fixity in shear walls modeled with shell elements. Typical buildings in Chile have relatively few instances of distinct beams, so this issue did not arise often.

As with any nonlinear analysis with strain-softening behaviors, the definition of stress-strain relationships for concrete and reinforcement at strains beyond peak strength requires correction to account for differences between test gauge length and the dimensions of the elements of the model.

5.1.2 Beam Elements

Conventionally, vertical beam-type elements are used for analysis of shear wall structures. Beams may be formulated as “lumped plasticity” models with finite plastic hinges or as “distributed plasticity” models with fiber elements. Plane sections are enforced to remain plane within each fiber section, and axial and flexure responses are typically uncoupled from shear behavior. In *PERFORM-3D, Nonlinear Analysis and Performance Assessment for 3D Structures* (CSI, 2013c), the wall elements are essentially of this fiber beam formulation.

Realistic representation of openings, discontinuities, and large joint zones presents difficulties with beam elements because the transition between each individual beam is effectively a rigid plane section that enforces planarity at the transition, and the non-planar strain distributions that actually occur are not represented. The degree to which this introduces significant divergence in modeled behavior from reality varies depending on the wall configuration and whether the failure modes are brittle or ductile. In general, the possibility of buckling of walls between floors will not be captured.

Modeling of coupling beams is more straightforward, although assuming that the end of the beam (at the face of the wall) is parallel to the centerline of the wall ignores the local deformation (beam strain penetration) at the joint between the beam and the wall.

5.1.3 Damping

The system damping specified in an analysis is required to model the energy dissipation that is not explicitly captured in nonlinear material hysteretic response. Therefore, the selection of the appropriate system damping level should depend upon the selected method of hysteretic modeling. In fiber element and nonlinear shell models, hysteretic response will generally include the energy dissipation from yielding of reinforcement at the extreme fibers of the wall section and from the different loading and unloading paths of the concrete due to cracking at demands well below the ultimate strength of the section. In lumped plasticity models, where there is no material hysteretic response in cycles and the demand is less than the specified strength of the section, it is appropriate that greater system damping be specified.

5.2 Calibration of Analysis Models Based on Experimental Tests

Complex physical phenomena affect stiffness, cracking, bar buckling, concrete crushing, overall wall buckling, and shear in concrete walls. Thus, it is important for an analyst to understand what behaviors can be reasonably captured and what assumptions and level of detail are appropriate for a given model. The following sections investigate the extent to which detailed, state-of-the-art analytical models are able to capture overall wall buckling and reinforcement buckling with concrete crushing observed in certain experimental tests of concrete walls. Additional details on the experimental tests and analysis results are provided in Appendix F.

The primary objective of these simulation studies was to explore possible explanations for differences between behaviors observed in cyclic tests on shear wall components versus behaviors intended by current U.S. design practice. A secondary objective was to identify the extent to which limitations in conventional fiber beam analysis theory and assumptions could be overcome using continuum methods with a nonlinear shell element formulation in software such as LS-DYNA (LSTC, 2010).

The models used in the examples are more complex than are generally used in current design practice; however, these studies indicate that the potential exists for analytical tools to capture the complex behavior of concrete walls, and they also offer insights related to the observations of concrete wall behavior presented in other chapters.

5.2.1 Simulation of Overall Wall Buckling

An analytical simulation was made of the performance of a rectangular reinforced concrete specimen tested and described in Acevedo and Moehle (2010). The specimen was designed to represent the boundary element in the end regions of a concrete wall, based on the requirements for non-special boundary elements in ACI 318-08, *Building Code Requirements for Structural Concrete and Commentary* (ACI, 2008). The specimen was first loaded in tension and then loaded in compression until failure.

The finite element simulation of the test was performed in LS-DYNA with the concrete modeled as shell elements and the reinforcing bars modeled with fiber integrated beam elements embedded into the concrete shells. LS-DYNA incorporates a large deformation formulation, which automatically incorporates P -delta effects, and an explicit solver which permits solution into the negative stiffness range.

The numerical model was loaded by displacement control replicating the displacement history in the test. The behavior, including displaced shapes and force-displacement curves from the experiment and simulation are compared in Figure 5-1c. The simulation captured the observed combined bar buckling and wall buckling behavior well. During the tension displacement phase, the concrete cracked

and its tensile resistance reduced to zero. During the subsequent compression phase, the wall started to buckle before concrete cracks fully closed. The effective section resisting buckling consisted of little more than the steel reinforcement.

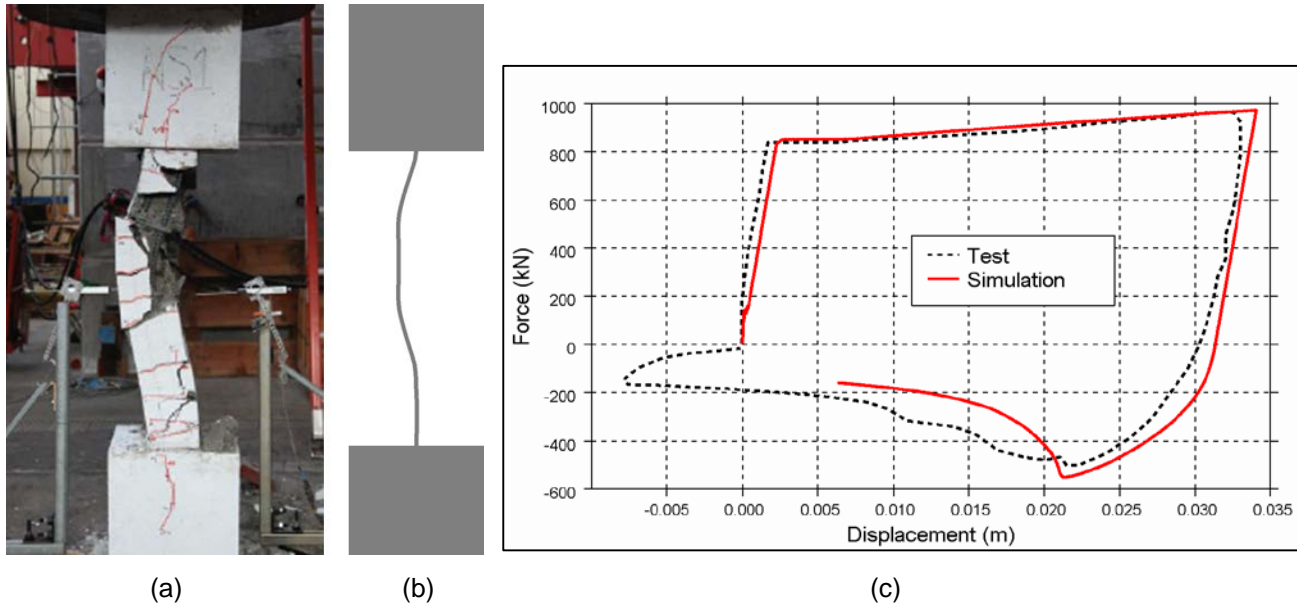


Figure 5-1 Displaced shape of wall: (a) at end of test; (b) in simulation; and (c) force deflection hysteresis.

This study numerically demonstrated the theory described in Chapter 3 in which overall wall buckling can be initiated by tension strain followed by compression, with one curtain of reinforcement yielding before the other. The study also indicated that modeling steel reinforcing bars using fiber integrated beam elements in LS-DYNA can give realistic predictions of overall wall buckling in tension-compression loading sequences.

5.2.2 Studies on Reinforcement Buckling

Numerical studies were undertaken with LS-DYNA to investigate the onset of buckling and post-buckling behavior (strength degradation) of steel reinforcing bars, including dependence on previous loading history, representing reinforcing bars with fiber beam elements. The analytical approach to modeling single reinforcing bars was first validated against available experimental data (Rodriguez et al., 1999) and then used to simulate the hysteretic behavior of reinforcing bars with a range of slenderness, s/d , ratios (where s is the spacing between restraints of the reinforcing bar and d is the diameter of the bar) subjected to a range of overall strain histories. The possible influence of reinforcing bar buckling on the overall compressive capacity of a typical reinforced concrete wall boundary zone was also studied.

5.2.2.1 Material Model

The cyclic stress-strain characteristic of the steel material model for the element fibers (in the absence of buckling) was compared with that measured by Rodriguez et al. (1999). The experimental and modeled steel stress-strain relationships are compared in Figure 5-2. The material model is therefore able to capture the cyclic stress-strain behavior of the steel reasonably well, displaying the Bauschinger effect on reversal of loading. While it tends to overestimate the reloading strength at lower strain levels, it is accurate at higher strain levels.

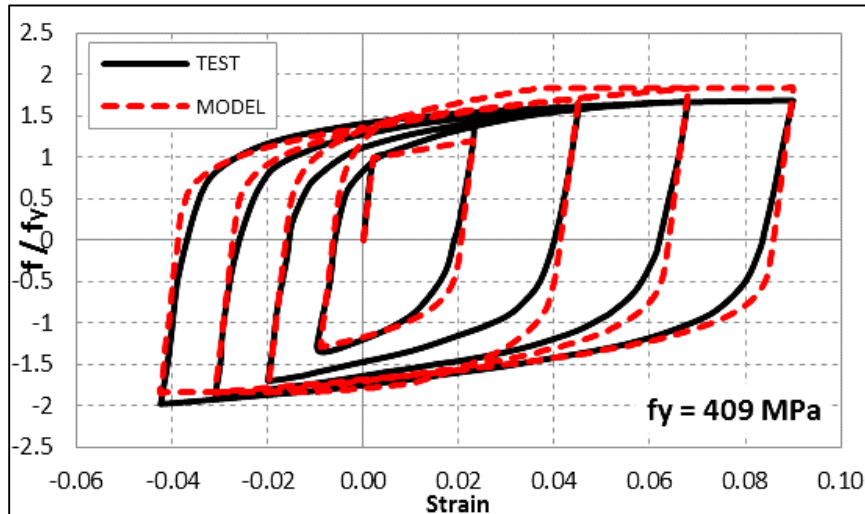


Figure 5-2 Comparison of predicted and experimental cyclic stress-strain in the absence of buckling.

5.2.2.2 Validation with Rodriguez et al. (1999) Test

A simulation of one of the buckling tests in Rodriguez et al. (1999), 16 mm (#5) bar with $s/d = 6$, was conducted to investigate if the onset of buckling under the experimental cyclic protocol could be replicated by analysis. The analysis model, shown in more detail in Appendix F, was discretized into ten fiber elements along the gauge length of the test specimen.

The analytical and experimental results were compared to verify that the model is capable of capturing the initiation of experimentally determined buckling by considering the difference in longitudinal strain ϵ_1 and ϵ_2 at opposite sides of the bar over the gauge length. The comparison shows that the analytical model captures the hysteretic stress-strain relationship at the two opposite sides of the test specimens well.

5.2.2.3 Effect of Loading History on Post-Buckling Response

The sensitivity of bar response to applied strain history was investigated by subjecting the analytical model to different loading protocols. Figure 5-3 shows the effect of seven different loading protocols on bars with two different slenderness

ratios. It was observed that the influence of loading sequence on response is more pronounced as slenderness increases. For $s/d = 8$, it can be seen that, depending on the previous cyclic history, as a bar reenters the compression zone (negative strain) the average stress it develops may be close to f_y or lower than $0.5f_y$. In almost all cases, the stiffness of the bars in the compression phase is negative. Generally, the higher the compressive stress the bar is developing as it enters net compression, the more negative is its stiffness. For $s/d = 2.5$, the average stress in the bar is generally between f_y and $1.7f_y$ and stiffness generally remains positive.

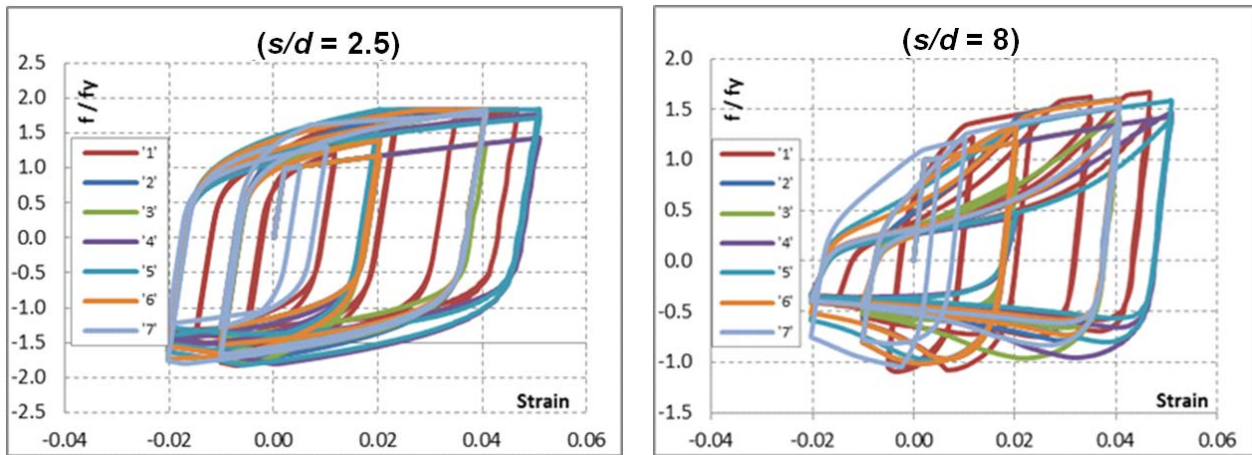


Figure 5-3 Simulated effect of loading history for bars with s/d ratios of 2.5 and 8.

5.2.2.4 Influence of Reinforcing Bar Buckling on Concrete Capacity

The results described above were used to investigate the possible influence of reinforcing bar buckling on the capacity of the concrete wall boundary element of the planar wall specimen PW4 tested and documented in Lowes et al. (2011). The main reinforcing bars are restrained with crossies such that the s/d ratio is 4.

Figure 5-4 shows predicted axial force versus compressive strain characteristics of the components of the whole boundary element (under uniform compressive strain) for the following assumptions:

- Reinforcing bars in compression follow monotonic steel stress-strain.
- Reinforcing bars are previously cycled in tension and reenter compression with minimum resistance.
- Reinforcing bars are previously cycled in tension and reenter compression with maximum resistance.

Reinforcing bars reentering compression with maximum resistance show significant negative stiffness beyond a strain of about 0.007.

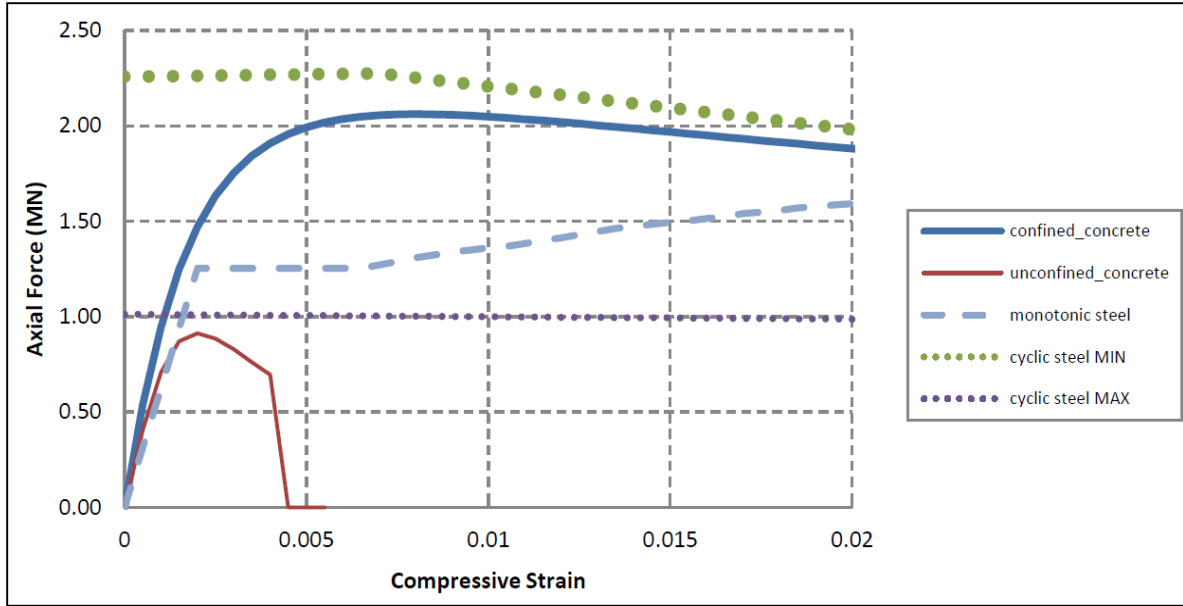


Figure 5-4 Axial force versus compressive strain in the boundary element components of specimen PW4.

Figure 5-5 shows the total resistance of the boundary element associated with the three different assumptions for the behavior of reinforcing bars. In all cases, there is net reduction in resistance as the unconfined cover concrete fails. Beyond that point, the resistance in all three cases remains fairly constant. It is observed that while the tangent stiffness remains positive when monotonic behavior of reinforcing bars is assumed, stiffness becomes negative when the cyclic behavior envelopes are adopted for compressive strains exceeding about 0.007.

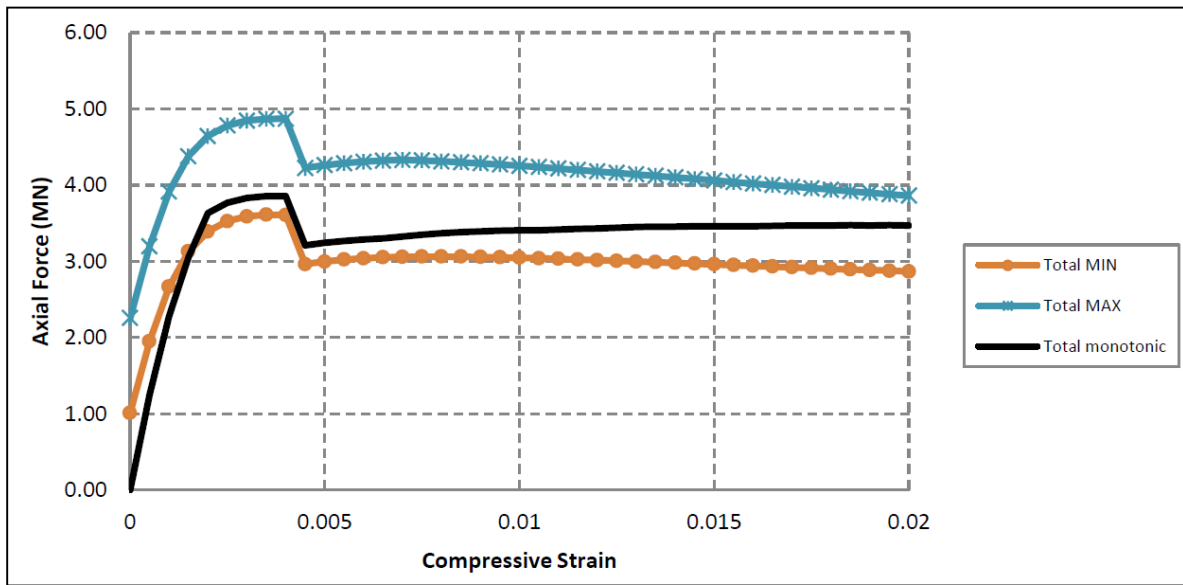


Figure 5-5 Total axial force versus compressive strain in the boundary element components of specimen PW4.

This simple study assuming uniform applied strain over the boundary element is not exhaustive, but it shows that the resistance of a boundary element can be significantly affected by previous cyclic loading of the reinforcement. The resisting force may be greater or lower than that assessed by normal (monotonic) design assumptions. It is also important to note that in this case, the maximum compressive strength is likely to occur prior to spalling of the cover concrete, and negative stiffness may continue after spalling. This may lead to rapid progression of damage and loss of stability of the concrete element.

5.2.3 Simulation of Walls with Boundary Elements

This study investigated the extent to which assumptions and limitations in conventional analysis theory in predicting the behavior of planar wall specimen PW4 described by Lowes et al. (2011) could be overcome by using continuum methods with a nonlinear shell element formulation

The LS-DYNA model of wall specimen PW4 is described in more detail in Appendix F. It is composed of a mesh of nonlinear multi-layer sandwich reinforced concrete shell elements. Layers can be defined through the thickness of the shell to represent unconfined or confined concrete and reinforcing bars oriented in any direction in the plane of the element, as illustrated in Figure 5-5.

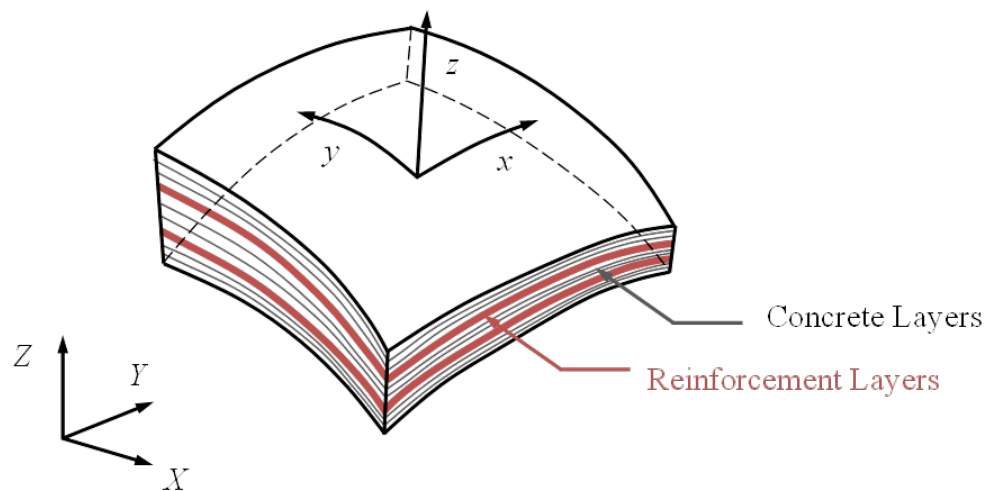


Figure 5-6 Schematic representation of a multi-layer shell element.

The large-deflection explicit dynamic solver in LS-DYNA enables softening, buckling, and incipient collapse behavior to be captured without numerical convergence problems. The smeared reinforcement model stores the strain history of the in-plane reinforcement and represents Bauschinger reloading effects. There is a simple reinforcement buckling algorithm, which had not been previously calibrated for low s/d ratios.

The cyclic test on axially loaded wall specimen PW4 described by Lowes et al. (2011) was intended to represent (at approximately 1/3 scale) the lower three stories of a 10-story full scale wall. The test wall incorporated design and detailing provisions that satisfy current U.S. code requirements. The specimens were subjected to constant vertical applied load and cyclically applied moment and shear demands of increasing amplitude (applied through a sophisticated hybrid control system). The axial stress ratio, $N/(A_g f'_c)$ was about 0.1. The wall failed by concrete compression and reinforcing bar buckling at the toe of the wall at a drift level that was well below the expected monotonic deflection capacity.

Material properties for the reinforcement and concrete (confined and unconfined) were based upon the test results associated with wall specimen PW4, and are detailed in Appendix F.

5.2.3.1 Results of Initial Simulation without Bar Buckling

An initial simulation was performed where the potential buckling of reinforcing bars was suppressed. Figure 5-7 compares the base moment versus drift hysteresis of the simulation with that of the test.

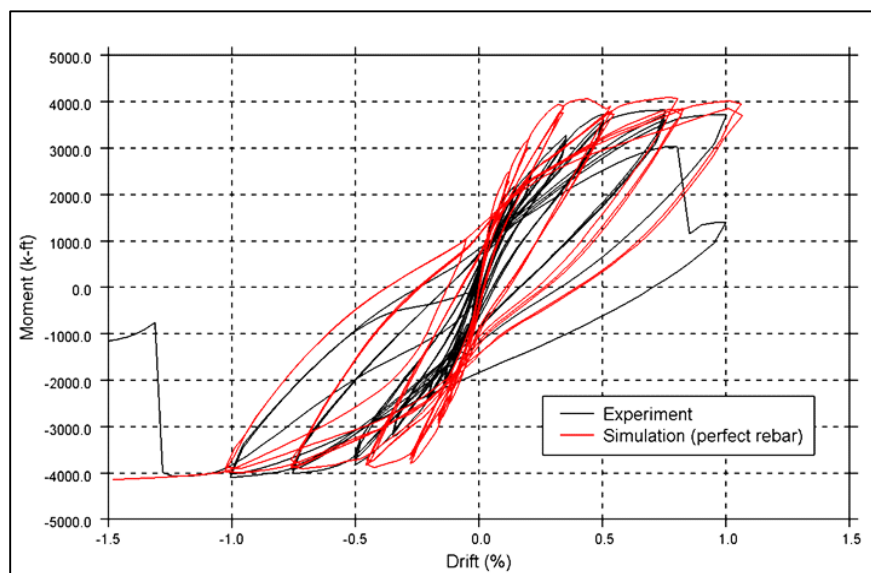


Figure 5-7 Comparison of specimen PW4 cyclic test and simulation results without bar buckling.

While the maximum flexural strength of the wall and the cyclic stiffness degradation are fairly well represented, the onset of gross strength reduction is not predicted. In the test, crushing of concrete and bar buckling occurred at the toe of one boundary at a drift ratio of 0.75%, followed by similar failure at the other boundary toe in the first cycle to 1% drift. Figure 5-8 shows the observed damage. The simulation predicted that drifts in excess of 2.0% could be achieved without loss of resistance.



Figure 5-8 Failed toe of specimen PW4 at 0.75% drift (Lowes et al., 2011).

5.2.3.2 Calibration of Reinforcing Bar Buckling Behavior

A detailed study was performed to investigate bar buckling in the confined boundary region of shear wall specimen PW4. The reinforcement cage was modeled using fiber beam elements (as for the Rodriguez et al. (1999) single bar tests), but because the middle bar on the end face of the wall was not restrained by a hook, the entire cage at the end of the wall was modeled. The reinforcement cage was restrained such that the bars could not deflect into the core of the wall, but could deflect outwards, as would be the case if the cover concrete had spalled. The modeled reinforcement cage was subjected to the vertical strain history predicted for the toe of the wall in Section 5.2.3.1, above. Figure 5-9 shows the shape of the reinforcement cage after buckling. The middle (untied) bar buckles first, followed by the corner bars.

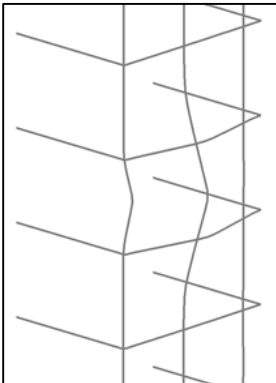


Figure 5-9 Simulation of reinforcement cage buckling in specimen PW4.

In order to incorporate this bar buckling performance into the shell model of wall specimen PW4, the parameters input to the bar buckling algorithm of the shell were adjusted, as well as possible, to represent the hysteresis of the detailed reinforcement cage model. This is described in Appendix F.

5.2.3.3 Results of Simulation with Bar Buckling

The LS-DYNA simulation of wall specimen PW4 was re-run with the effect of bar buckling represented within the shell element. Figure 5-10 compares the base moment versus drift hysteresis obtained from this simulation to that of the experiment. It can be seen that in this improved model, which includes bar buckling in the shell element, deterioration of strength is predicted once the wall is cycled beyond 0.75% drift. This is directly attributable to the representation of bar buckling because no other changes were made to the model. The simulations predict the cyclic response well (the boundary fails at 1% drift in the simulation, and in the test, one boundary fails at 1% drift and the other at 1.25% drift).

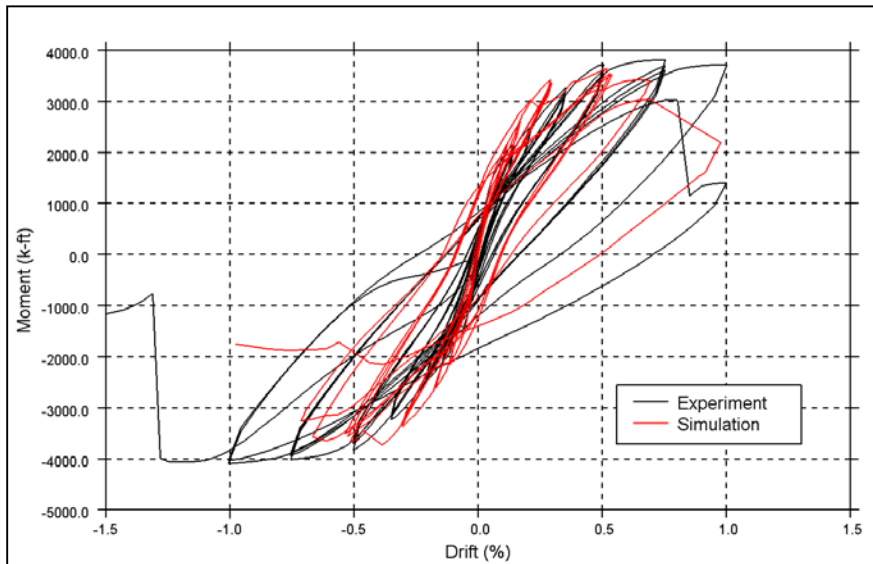


Figure 5-10 Comparison of specimen PW4 cyclic test and simulation results with bar buckling.

The predicted monotonic response of wall specimen PW4 is compared to the predicted cyclic response in Figure 5-11. It can be seen that under monotonic loading the predicted drift capacity is approximately twice that predicted under the cyclic loading protocol adopted in the test.

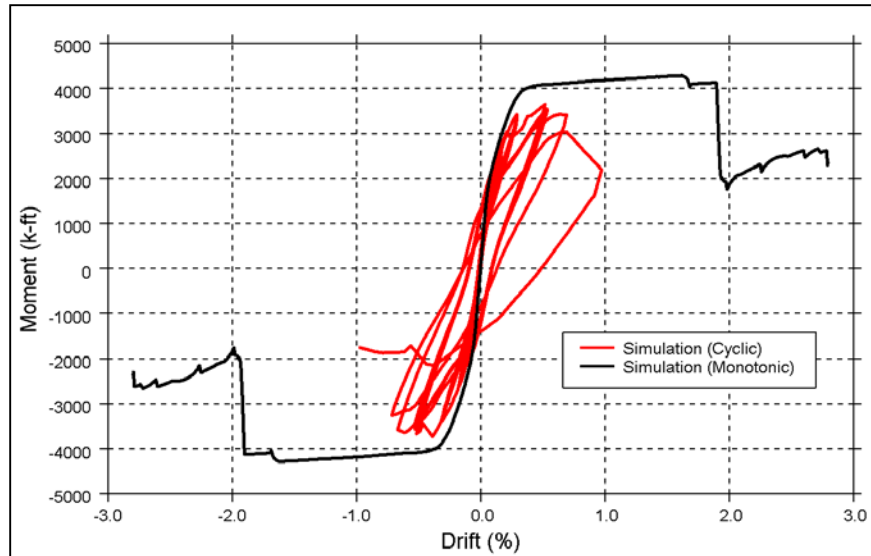


Figure 5-11 Comparison of cyclic and monotonic simulation results.

This set of simulations shows that the phenomenon of bar buckling has a major effect on the cyclic response of the wall, and that it is possible, in principle, to include bar buckling effects in predictive models.

5.3 Modeling Case Study of the Alto Rio Building

Located in Concepción, the Alto Rio building was designed in 2007, completed in 2009, and collapsed in the 2010 Maule earthquake. Studies conducted by engineers and researchers have led to a range of conclusions regarding the potential cause of collapse. The building was 15 stories tall with two basement levels supported by a mat foundation on alluvial soil. Photographs of the building before and after the earthquake are shown in Figure 5-12. Sections of the building are shown in Figure 5-13.

The construction of Alto Rio was typical of modern high-rise residential buildings in Chile comprising interconnected, lightly reinforced, thin concrete shear walls supporting reinforced concrete floor slabs without beams. Models of these buildings are likely to include three-dimensional assemblies of interconnected thin walls, with many openings, discontinuities, irregularities, and consideration of coupling via floor slabs. As a result, seismic response analysis of reinforced concrete wall buildings of this type presents several analytical challenges.

Using the findings from the preceding sections, a case study continuum model of the Alto Rio building was developed to simulate the observed damage and collapse behavior of the building. Material property information was collected from available design drawings and testing of samples from the building following the earthquake.

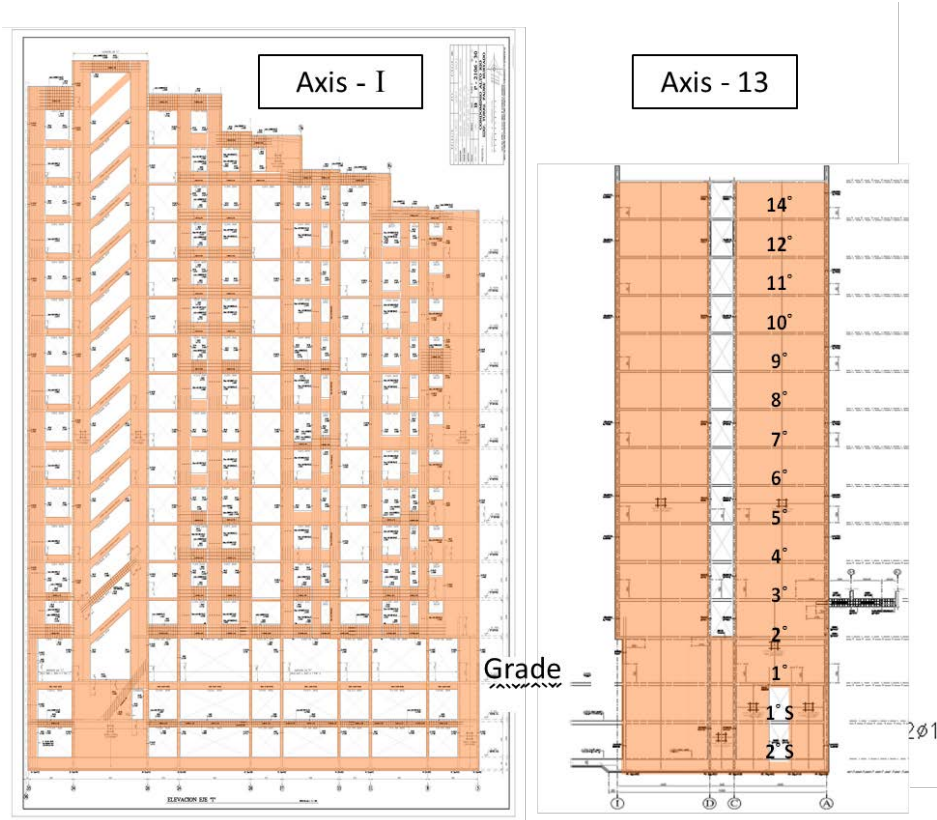


(a)



(b)

Figure 5-12 Alto Rio Building: (a) before the earthquake; and (b) after the earthquake (Tuna and Wallace, 2014).



(a)

(b)

Figure 5-13 Alto Rio Building: (a) longitudinal section; and (b) transverse section.

5.3.1 LS-DYNA Model Using Shell Elements

A three-dimensional finite element model of a representative slice of the Alto Rio building was modeled in LS-DYNA. The modeled zone incorporated Grids 13 to 17, as shown in plan in Figure 5-14. This zone has two basement levels and 12 floors above grade. The walls and floors of the building were modeled using a mesh of nonlinear shell elements. The model was built directly from the geometry and reinforcement details indicated on the construction drawings. No pre-calculation of section strength or stiffness was necessary because all walls, floors, reinforcement, openings, and discontinuities were represented explicitly. Almost all of the concrete was considered unconfined because the reinforcement had few cross-ties and bar spacing in the vertical direction was large.

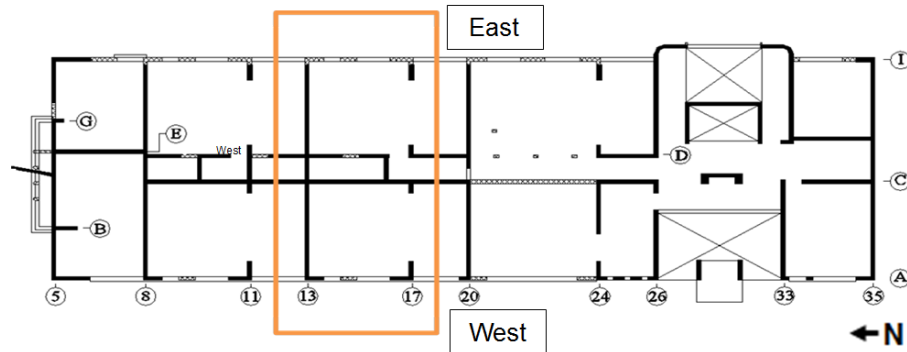


Figure 5-14 Plan view of LS-DYNA model slice for the Alto Rio building.

Figure 5-15 shows elevations of the principal walls modeled in the longitudinal and transverse directions to illustrate the irregularities and discontinuities. Figure 5-16 shows the plan for the first and second floors. The typical shell element used in the walls was 10 inches (250 mm) high by 8 inches (200 mm) wide.

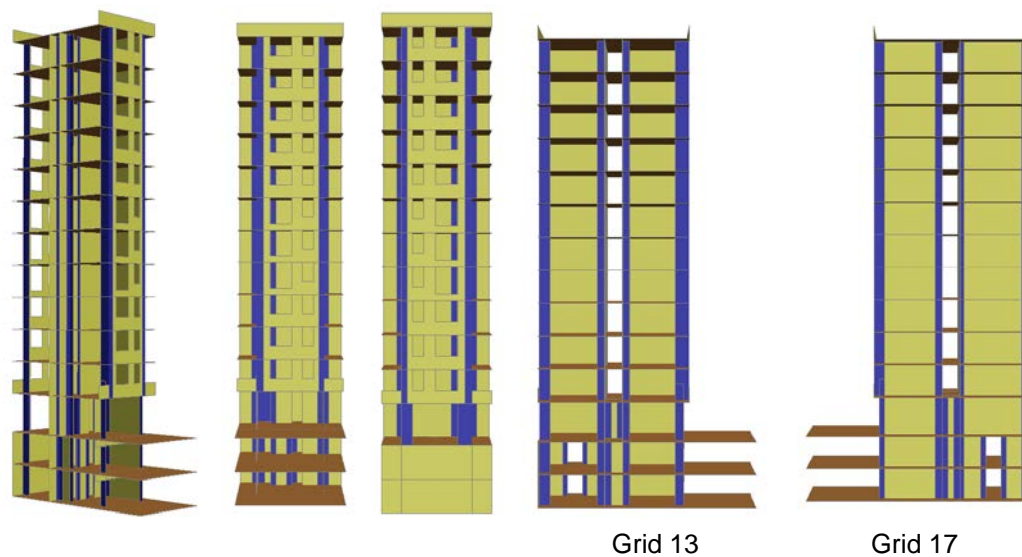


Figure 5-15 LS-DYNA model showing elevations. Dark blue color indicates corner elements that are lightly confined, light colors are unconfined.

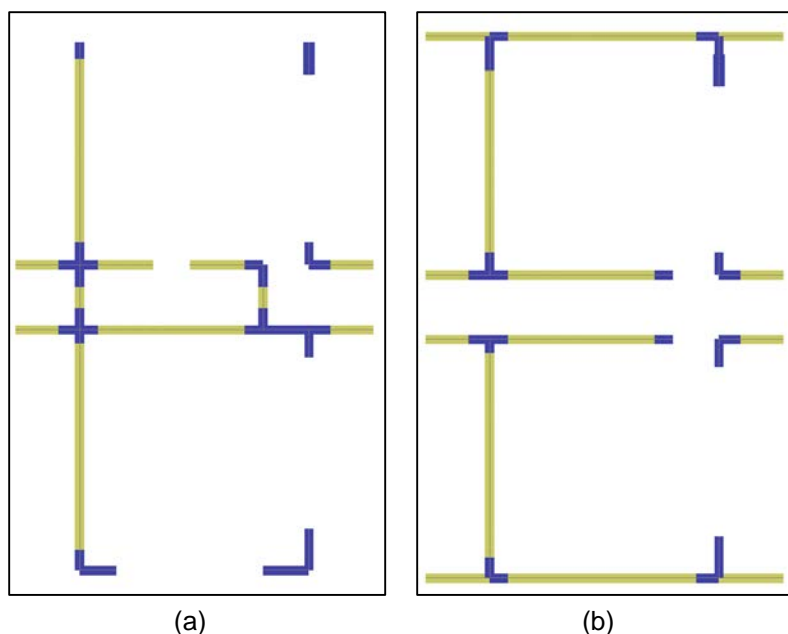


Figure 5-16 LS-DYNA shell element model showing: (a) first floor plan; and (b) second floor plan. Dark blue color indicates corner elements that are lightly confined, light colors are unconfined.

The natural period of the modeled slice depends on a number of assumptions, including: (1) the effective Young's modulus (cracked or uncracked sections); (2) conditions assumed at the base (rigid or flexible basement); and (3) effectiveness of coupling (slabs with uncracked stiffness properties or with zero stiffness). Some comparisons are documented in Appendix F.

Intrinsic small-strain energy dissipation not captured by nonlinear material hysteretic behavior was represented by incorporating a material damping ratio of 1% of critical in LS-DYNA.

5.3.2 Nonlinear Seismic Response Analyses

Nonlinear seismic response analyses were performed to explore the sensitivity of the response to assumptions regarding the following:

- Material properties
- Inclusion of the vertical component of ground motion (in addition to the biaxial horizontal components)
- Effect of the basement structure
- Level of intrinsic damping

The following assumptions were common to all simulations:

- Cyclic boundary constraints were applied on the two longitudinal cut faces
- The vertical reinforcing bars were permitted to buckle

5.3.2.1 Simulation Results with Expected Properties

The specified concrete grades for the building correspond to cylinder strengths f'_c of 2.9 ksi (20 MPa) and 3.6 ksi (25 MPa). Initial simulations assumed a single concrete material strength for the entire building of 4.4 ksi (30 MPa), allowing for an overstrength factor, Ω , of 1.25 to 1.50 on the nominal strengths. The external faces of the basement box were assumed to be effectively rigid.

Simulations were performed in which the exterior of the basement box was subjected to either the triaxial Concepción ground motion time histories or to the biaxial horizontal components only. In both cases, the simulation predicted concrete crushing failure, which was initiated where the concentration of compression strain occurs in the extreme fiber of the walls at ground level. The compression failure zone does not spread vertically, but propagates across the width of the wall in successive cycles, during which the sway period of the building elongates from 0.6 seconds to 2.2 seconds. The crushing is driven by both the effect of the weight of the building acting on whatever area of concrete is in compression, and the lateral seismic demand in axial, flexural, and shear response.

Figure 5-17 illustrates vertical strain and stress distributions in the wall on Grid 13 before and after concrete crushing during the response cycle approximately 11 seconds into the motion record for the triaxial simulation. Tensile stresses and strains are positive. In this cycle, a horizontal band of (essentially unconfined) concrete is predicted to crush (i.e., compression resistance becomes zero at strain greater than 0.005) on the east side of the wall at Grid 13 at ground level. The stress distribution after crushing shows that the highest compression stress has moved from the extreme edge of the wall to a point 3.7 m (12 feet) inwards of this; the entire zone outwards of this has fully unloaded. Figure 5-18 illustrates shear stress distribution in the wall on Grid 13 before and after concrete crushing.

The shear stress distribution in Figure 5-18 just prior to crushing shows that, above the first story, more shear is taken in the east wall than the west wall. This is consistent with the fact that this wall carries a higher vertical stress at this time (about 0.9 ksi, 6 MPa) than the west wall (approximately zero). The peak shear stress in the east wall of less than 0.6 ksi (4 MPa) implies a principal compressive stress of 1.2 ksi (8 MPa) and principal tensile stress of 0.3 ksi (2 MPa), which is close to the tensile strength of the concrete. With the stiff basement assumption, there is clear evidence that the shear is transferring to the grade level slab for reaction into the soil.

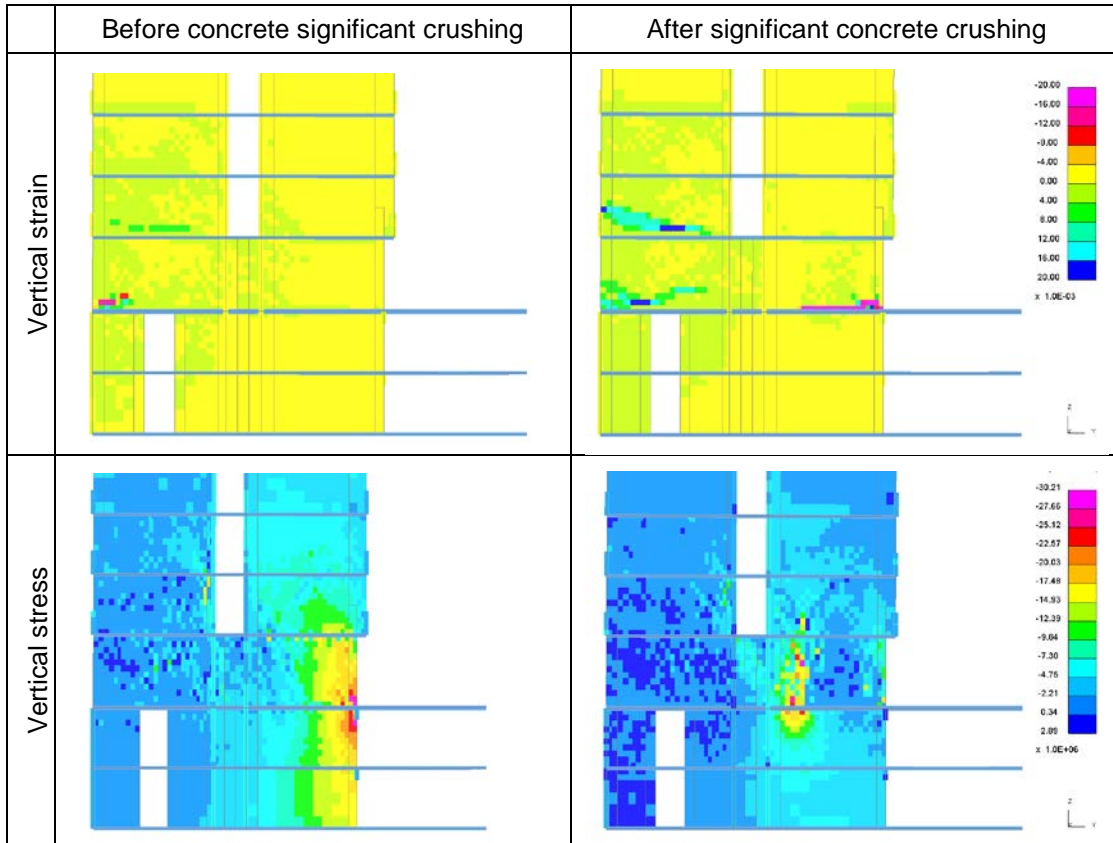


Figure 5-17 Vertical strain and stress distributions in the wall on Grid 13 before and after concrete crushing.

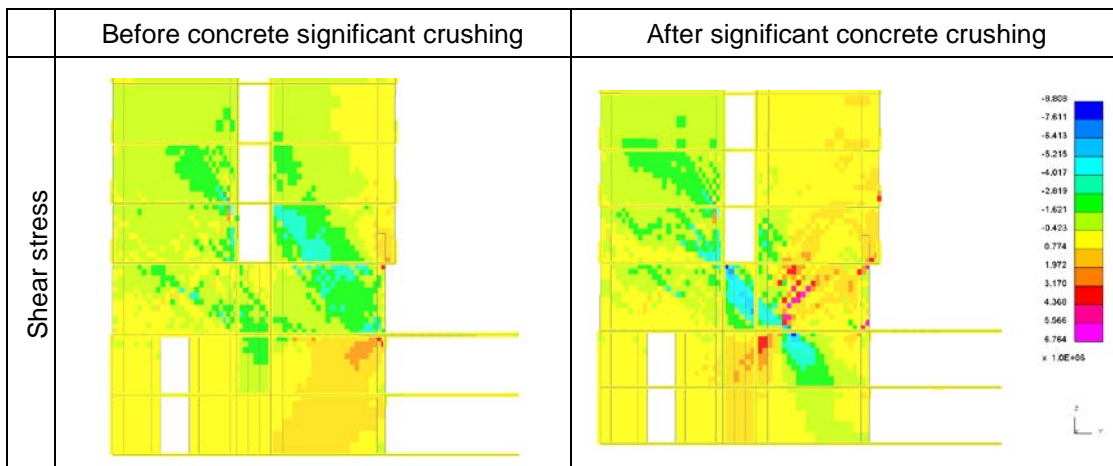


Figure 5-18 Shear stress distribution in the wall on Grid 13 before and after concrete crushing.

After the ground level concrete band on the east side of the wall on Grid 13 has crushed, the highest shear stress occurs in the region of solid wall in the first story below a series of stacked openings where the two upper walls connect, which is a

configuration investigated in Chapter 4 of this report. High shear stresses in the opposite direction are seen in the upper part of the first story east wall to enable the vertical gravity compression in the wall above to transition towards the center of the wall to circumvent the failed zone at grade level. As more of the concrete in the wall on Grid 13 crushes at grade level in successive loading cycles, more of the gravity load on this wall transfers to the longitudinal corridor walls. Eventually, the vertical load path at the base of the first story is reduced to the wall around the corridor.

Figure 5-19 shows the total axial force in the wall on Grid 13 under uniaxial, biaxial (no vertical component), and tri-axial simulation cases. Except in the uniaxial excitation case, a major reduction in load in this wall occurs between 11 and 15 seconds into the shaking due to the crushing effect described above, occurring first at the east, and then at the west end of the wall in the first story (with the vertical load transferring to the longitudinal corridor walls). The observation of compression damage over only a short height of the wall is predictable for the strain softening failure associated with largely unconfined concrete and low reinforcement ratio. It is also consistent with the observed damage on many of the buildings that remained standing after the event.

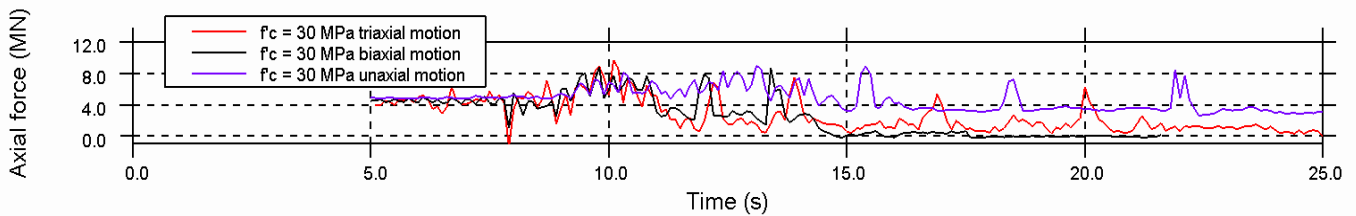


Figure 5-19 Total axial force in the wall on Grid 13 under uniaxial, biaxial (no vertical component), and tri-axial simulation cases.

For the uniaxial excitation case, there is concrete crushing at the top of the wall in the first story at the location where a reduction of wall area occurs; the crushing propagated to some degree, but did not cause collapse. Crushing in the biaxial and triaxial excitation cases contributes to a gross degradation of the overall lateral stiffness of the structure, and the elongation of fundamental period.

Figure 5-20 shows the response history of the transverse roof deflection ratio, indicating that the period increases from about 0.6 seconds to 2.2 seconds just prior to collapse. The elongation of the period beyond 1.3 seconds makes the building susceptible to the sharp peak in the horizontal pseudo-acceleration spectra in the 1.5 to 2 second period range. This makes the building substantially more vulnerable to damage, and ultimately leads to the rocking-induced collapse of the structure.

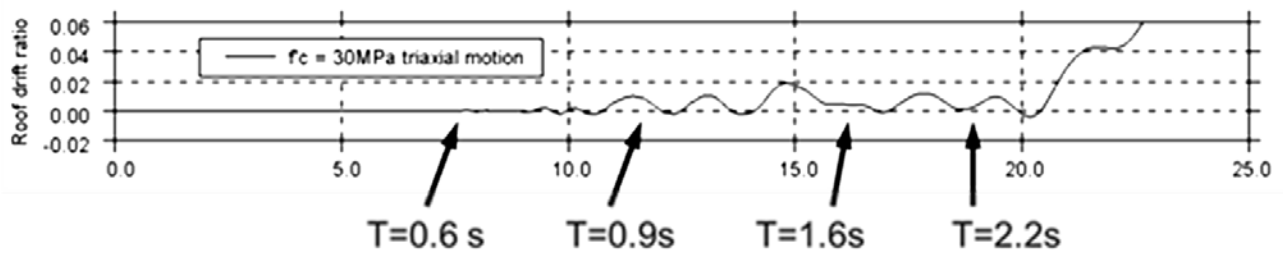


Figure 5-20 Roof deflection relative to ground and corresponding roof drift ratio showing period elongation prior to collapse.

The degradation of the strength of the structure is reflected in the moment and shear force histories in the wall on Grid 13, as illustrated in Figure 5-21 and Figure 5-22. It can be seen that the effective period of the building increases slightly more under triaxial excitation, perhaps reflecting slightly greater extent of concrete crushing.

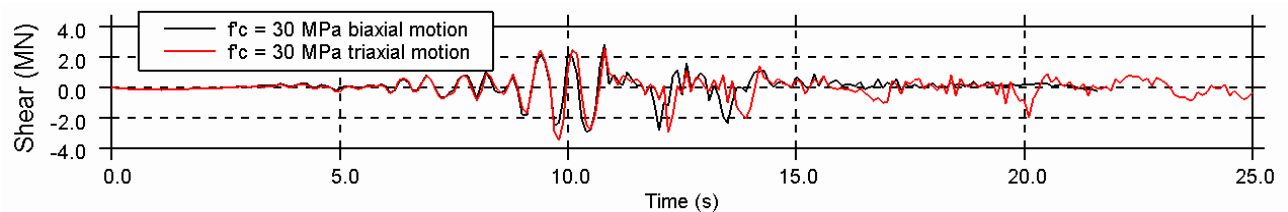


Figure 5-21 Shear force time-history of the wall on Grid 13.

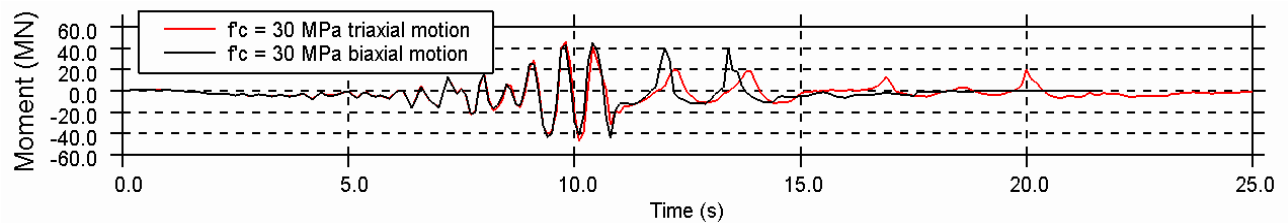


Figure 5-22 Moment time-history of the wall on Grid 13.

Figure 5-23 shows the time history of the predicted total base shear ratio at grade level. The maximum base shear ratio is 0.38, and is dominated by the first mode component, the period of which increases during the event.

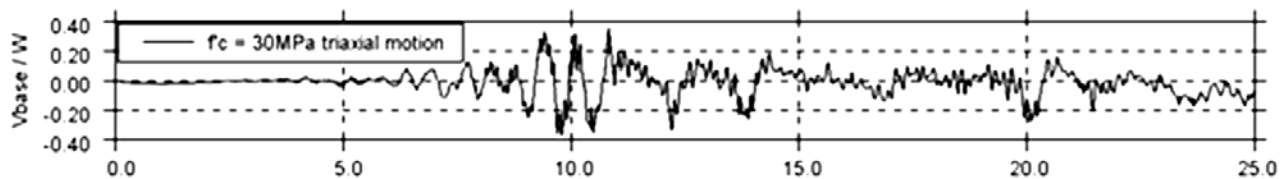


Figure 5-23 Total base shear ratio history at grade level of the wall on Grid 13.

Eventually, as vertical load-carrying capacity is lost at both ends of the wall at Grid 13, the building topples under gravity. Figure 5-24 shows a close-up of the damage

pattern in the lower stories of the wall as collapse approaches, with a concentration of vertical compression strain occurring at the first floor level.

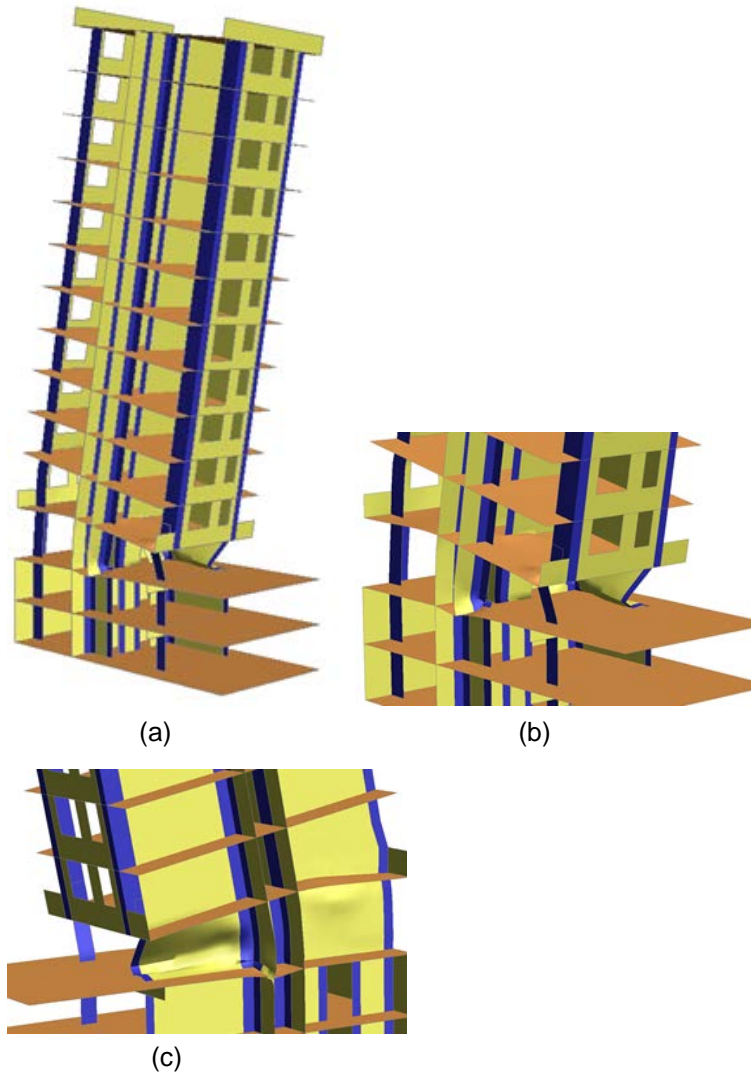


Figure 5-24 Predicted damage: (a) overall view; (b) close-up of damage pattern; and (c) alternate view of damage pattern.

5.3.2.2 Simulation Results with Measured Properties

Using test results on material samples taken from the structure after collapse, a further set of simulations was performed assuming concrete with $f'_c = 5.2$ ksi (43 MPa) and reinforcing bars with $f_y = 70$ ksi (480 MPa) and $f_u = 100$ ksi (720 MPa).

The performance under triaxial excitation using measured properties was almost identical to the performance of the simulations using expected properties (with $f'_c = 4.4$ ksi; 30 MPa), up to 11 seconds into the record. After the eleventh second, the increase in concrete strength substantially reduced the degree of crushing that

occurred, as compared to the simulations using the lower expected concrete properties.

5.3.2.3 Effect of Basement

The sensitivity of the predicted outcome to the assumption regarding the basement was explored under triaxial excitation, assuming that the basement box provided no lateral support. In this analysis, the motions were applied to the bottom of the basement only. No attempt was made to study soil-structure interaction.

Analysis with measured properties resulted in no significant zones of failure and the slice model did not collapse.

The analysis was repeated with expected properties. As shown in Figure 5-25, significant concrete crushing occurred in the walls at the bottom basement level, but the slice model did not collapse.

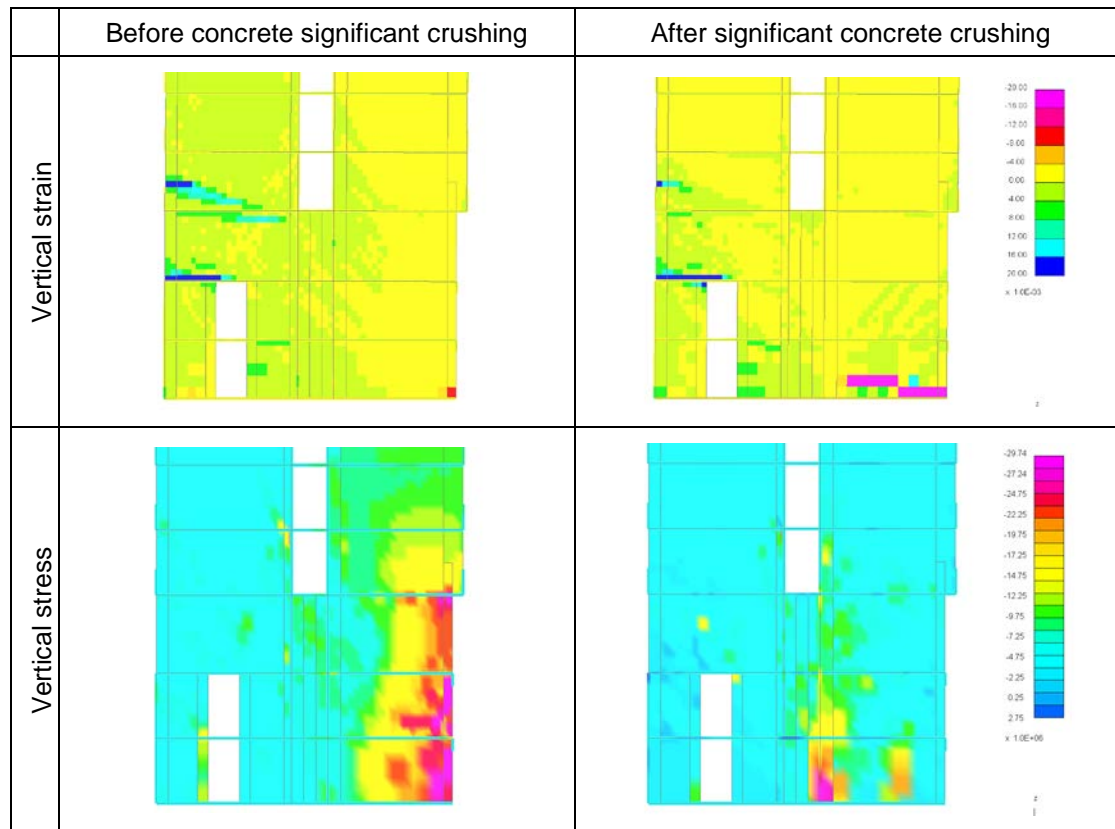


Figure 5-25 Vertical strain and stress distributions in the wall on Grid 13 before and after concrete crushing.

These simulations indicate that the assumption of a stiff basement is probably more realistic since the following were observed: (1) a greater susceptibility to collapse; (2) a collapse mode consistent with the observed damage; and (3) negligible damage predicted below ground level, consistent with observed damage.

5.4 Other Analyses of the Alto Rio Building

5.4.1 Tuna and Wallace (2014)

Nonlinear response history analysis of a slightly different slice of the Alto Rio building was undertaken by Tuna and Wallace (2014) using the PERFORM-3D software. This model represents the region centered around Grids 11 and 13. The walls cantilevered from the lowest basement level, thus no restraint from the basement was considered. Figure 5-26 illustrates the model.

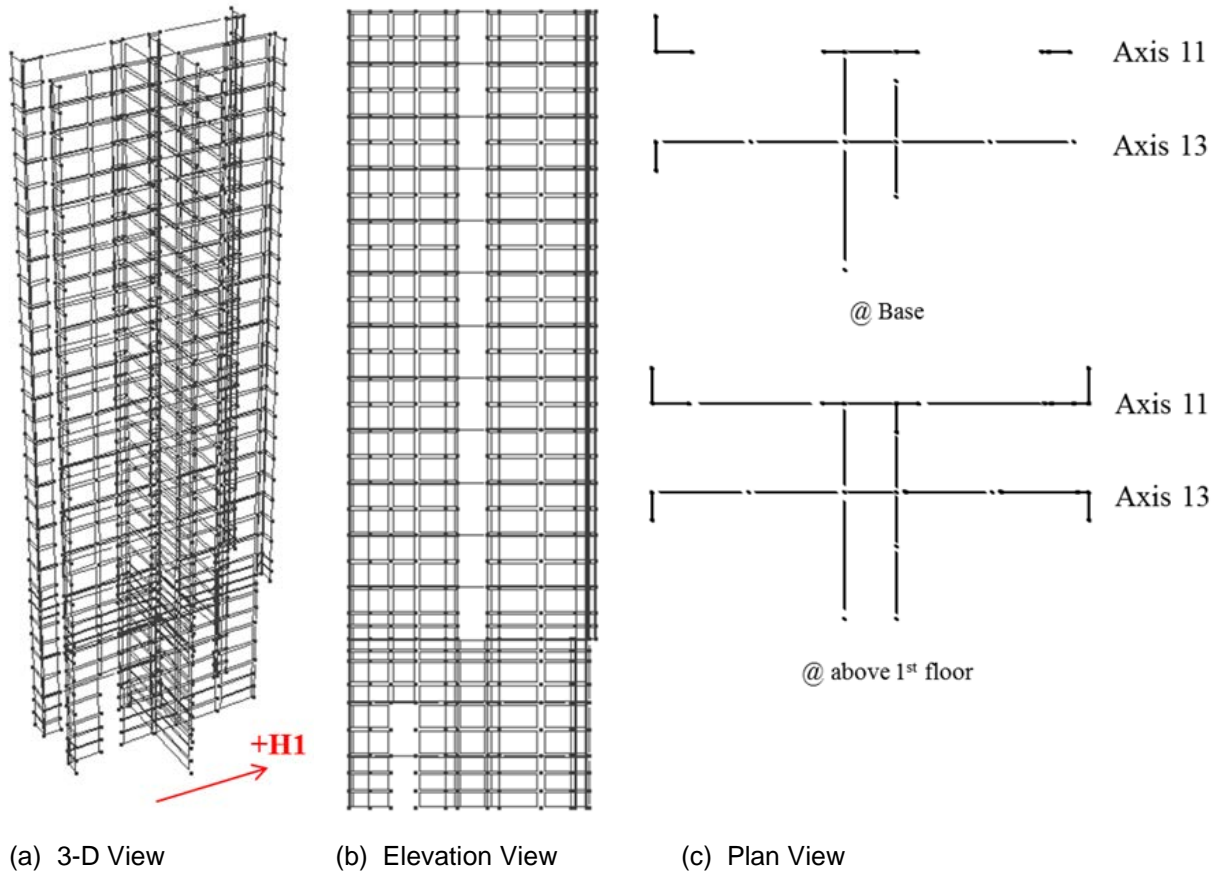


Figure 5-26 PERFORM-3D slice model used by Tuna and Wallace (2014).

Fiber beam cross sections assumed uniaxial stress versus strain relations for concrete and steel having expected material strengths of $f'_c = 4.7$ ksi (32.5 MPa) and $f_y = 70$ ksi (491 MPa). These values were 1.3 and 1.17 times the design strengths, respectively. Models were developed both with and without slab coupling, which affects the natural period of the model. More details of this study are provided in Appendix F.

Figure 5-27 shows the predicted roof drift ratio history, and Figure 5-28 shows the base shear ratio history. It was observed that significant reduction in strength commenced at 20 seconds (1.3% roof drift) and convergence failed at 25 seconds.

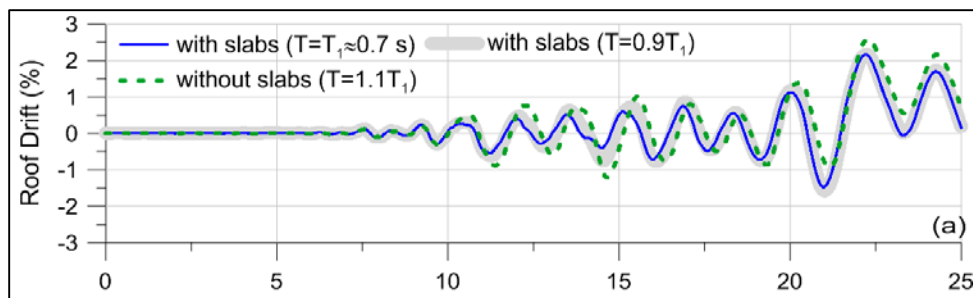


Figure 5-27 Roof drift ratio time-history with slabs (blue) and without slabs (green) (Tuna and Wallace, 2014).

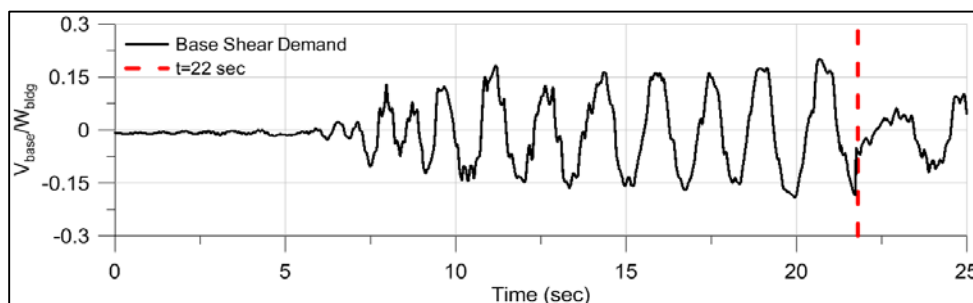


Figure 5-28 Base shear ratio time-history (Tuna and Wallace, 2014).

Although the models do not represent exactly the same slice of the building, broad comparisons can be made to the LS-DYNA analysis results for the flexible basement case. The following observations were made:

- Peak shear demands in the PERFORM-3D model are lower. This may be due in part to the higher damping in the PERFORM-3D model. The intended Rayleigh damping was 2.5% (between $0.2T$ and $1.0T$) compared to 1% (frequency independent) in the LS-DYNA model. However, significantly higher damping will have been generated in PERFORM-3D because the effective response period is about 1.6 seconds, which is more than twice the basic first mode period, and well outside the intended Rayleigh damping range.
- Degradation of strength starts at 11 seconds in the LS-DYNA model and at 20 seconds in the PERFORM-3D model. This may be due to the difference in damping, but may also be due to the plane-sections-remain-plane constraints on the walls in PERFORM-3D, which suppress strain concentrations that might lead to the initiation of crushing. Peak drifts in LS-DYNA are slightly higher (2.8% compared to 2.4%).
- It is not clear what the failure mechanism is in the PERFORM-3D model because the analysis terminated due to convergence difficulties.

5.5 Findings and Recommendations

Based on the results of wall simulation studies herein, the following observations are made regarding considerations for analytical modeling of reinforced concrete wall buildings:

- The lateral response of gravity loaded reinforced concrete walls is significantly different under cyclic loading conditions than monotonic loading. Brittle concrete crushing failure is possible even in walls that would be considered ductile under monotonic loading.
- Reinforcing bar buckling is observed in cyclic wall tests, even with ACI 318 conforming details, and can be a decisive factor in the seismic response. Reinforcing bar buckling can occur as the unconfined concrete cover spalls (i.e., when compressive strains exceed about 0.004). The initiation of buckling and post buckling resistance of a reinforcing bar cage is affected by s/d ratio and previous (tensile) loading history (such as described in Chapter 2 of this report).
- In relatively thin walls, the maximum compression resistance of the boundary zone is likely to occur as soon as the cover concrete spalls, irrespective of how well confined the core is. This can lead to major instantaneous loss of strength if the wall is supporting force-controlled gravity load.
- Overall wall buckling can be caused by concrete crushing, or by application of compression to a wall that has been subjected to significant tensile strain, such that the ensuing compression is resisted primarily by the previously stretched reinforcing bars (such as described in Chapter 3 of this report).
- All of the above effects can be analytically replicated using a large-deflection finite element solver with reinforcing bars modeled using a refined mesh of fiber beams and advanced (e.g., layered sandwich type) nonlinear shell elements to model the concrete. The steel material model must include Bauschinger type hysteresis.
- For practical purposes, it is not feasible to model every reinforcing bar with multiple fiber beam elements between restraining ties to simulate buckling explicitly. The possibility of a phenomenological algorithm for the reinforcing bar, including buckling (calibrated against tests and detailed fiber beam models) for use within a multi-layer reinforced concrete shell element was demonstrated. Further work is required to develop a generalized algorithm.
- The initiation of concrete spalling is a function of the local peak compression strain. Spalling permits bar buckling, and will often trigger significant loss of strength and negative stiffness. These studies and test measurements show that the plane-sections-remain-plane assumption will significantly underestimate peak compressive strain in the critical regions of planar shear walls, and the same is

true at any geometric discontinuity. If beam-type elements are used, spalling must be assumed to occur at a strain lower than the conventional spalling strain for concrete to account for this. The use of an adequately refined shell element model enables the nonlinear strain distributions that arise in walls approaching failure, and additional strain concentrations at discontinuities and irregularities, to be represented explicitly.

Based on the case study simulation of damage observed at the Alto Rio building, and results obtained from studies by other researchers, the following observations are made:

- LS-DYNA analyses using shell elements with expected material properties simulate overall building behavior that is consistent with the observed collapse of the Alto Rio building, and these analyses indicate that the collapse was governed by flexure-induced (and gravity driven) concrete crushing. However, because concrete crushing is a brittle behavior, the extent of concrete crushing observed in analysis is sensitive to modeling assumptions, such as the concrete strength at critical locations and ground motions at different times and in different directions.
- Once crushing initiates, it propagates extensively in a single load cycle. This is an example of in-cycle strength degradation. The gravity load being supported by the concrete at the point of crushing (in combination with flexure) is a force-controlled action, which is a particularly effective driver for propagation.
- LS-DYNA simulations and the assessments of others predict severe damage and reduction of lateral resistance at roof drifts of 1% to 1.3%, but collapse does not occur until drifts exceed 4%. The building has a redundant gravity-load carrying system with many walls, which the simulations indicate continue to carry load. These results are consistent with the observation that many heavily damaged buildings did not collapse.
- There is evidence of high shear stress beneath vertically aligned series of wall openings (such as described in Chapter 4 of this report) but the LS-DYNA simulation indicates that this was not the main factor leading to collapse in this case. One of the reasons may be that almost all of the flexure above the first story is taken in just one of the two walls, which is the one with the higher compression. This is consistent with the concern of Kohrangi et al. (2012) that the shear transferred by coupling could fully yield the small amount of tensile reinforcement in the tensile side wall.
- The effective period of the building nearing collapse is much longer than the nominal natural period. For such cases, the usual period range over which Rayleigh damping is to be targeted needs to be reconsidered, otherwise the

longer period responses will be over-damped, and the possibility of collapse may be suppressed in the analysis.

Summary of Findings and Recommendations

The February 27, 2010, magnitude 8.8 earthquake, which occurred off the coast near the Maule region of central Chile, was among the largest in recorded history. It caused widespread ground shaking that was felt in cities including Santiago, Valparaíso, Viña del Mar, Talca, Concepción, Temuco, and Valdivia, and deformations in the ocean floor generated a tsunami that was severe in the cities of Constitución and Talcahuano near the fault-rupture zone.

This chapter summarizes the findings and recommendations resulting from a series of studies investigating the effects of the earthquake on selected buildings and potential causes of the observed damage.

6.1 Overview

Since 1985, Chilean seismic design and construction practice has been largely modeled after U.S. practice, and Chilean design standards are comparable to U.S. codes and standards that were in effect during the mid-1990s. Although requirements are similar overall, certain specific enhancements to U.S. seismic design requirements have occurred since the 1990s and have not been reflected in Chilean standards:

- Requirements for confinement in shear wall boundary zones and plastic hinge regions.
- Requirements for ductile detailing of coupling beams.
- Limitations on the use of certain irregular structural configurations.

Although the collective performance of buildings in the earthquake was generally considered to be very good, a number of mid-rise and high-rise buildings experienced heavy damage, and a few collapsed, as a result of the earthquake. Similarities between U.S. and Chilean codes and practices presented a unique opportunity to investigate the observed performance of buildings subjected to strong ground shaking, and to extract lessons for improving design and construction of reinforced concrete buildings in U.S. practice.

In response, several U.S. organizations sent reconnaissance teams to Chile to gather information that could be used to study implications for U.S. design and construction

practice. These teams observed many instances of structural damage in reinforced concrete walls that appeared to warrant further investigation. Observed damage included concrete crushing and buckling of longitudinal reinforcement at wall boundaries, out-of-plane buckling of walls, damage from coupling of walls through slabs and other elements, and damage concentrated at wall discontinuities.

Studies were organized around the recurring patterns of damage and grouped into the following areas for detailed investigation:

- Study Area 1: Investigation of concrete crushing and longitudinal bar buckling in wall boundary elements.
- Study Area 2: Investigation of overall wall buckling behavior.
- Study Area 3: Investigation of building configuration issues related to discontinuities, irregularities, and coupling.
- Study Area 4: Analysis and advanced simulation of reinforced concrete wall behavior.

The following sections synthesize findings and recommendations based on the studies presented in Chapters 2 through 5.

6.2 Wall Boundary Element Studies

Damage to wall boundary elements in the earthquake typically consisted of buckling of longitudinal (vertical) reinforcing bars and crushing of concrete near the base of the walls. This type of failure was most severe at wall boundaries, but damage also tended to propagate over much of the length of the wall, and in some cases over the entire wall length.

6.2.1 Findings

In most cases, the observed damage was generally consistent with what would be expected based on a lack of confinement at wall boundaries and relatively large spacing of horizontal reinforcement as compared to current U.S. requirements. Investigation of ACI 318 boundary element triggers, study of plastic hinge length, and study of concrete crushing and bar buckling behaviors concluded the following:

- Application of ACI 318 boundary element triggers to walls in Chilean buildings indicated that most walls would have required special boundary element detailing in accordance with ACI 318. In general, observed damage correlated well with the need for special boundary elements. Results supported the need for special boundary element detailing in walls with: (1) asymmetric flanged cross-sections (e.g., L-shaped and T-shaped); (2) high axial load ratios; and (3) large displacement demands.

- Investigation of plastic hinge length revealed that ACI 318 triggers for special boundary elements are sensitive to the assumed plastic hinge length, and that observed wall damage in Chile occurred over much shorter heights (e.g., one to three times the wall thickness) than traditional assumptions on the order of half the wall length (e.g., $l_p = 0.5l_w$), especially in compression-controlled walls.
- Investigation of potential concrete crushing and bar buckling behaviors at the boundaries of Chilean structural walls revealed that some walls would have been expected to exhibit bar buckling behavior, while other walls would have been expected to exhibit concrete crushing prior to bar buckling. There was some correlation between observed damage and the expected onset of bar buckling, but correlation was better in tension-controlled walls, and worse in compression-controlled walls.

6.2.2 Recommendations

ACI 318 requirements for boundary elements in reinforced concrete walls have evolved over many code cycles, and ACI committees have recently considered several changes that have not yet been implemented. In some cases, requirements that were removed in prior code cycles should be considered for reinstatement. Based on the findings from wall boundary element investigations conducted herein, the following impacts to ACI 318 requirements for design of reinforced concrete walls can be considered (or reconsidered):

- The limiting neutral axis depth trigger for special boundary elements can be adjusted to provide improved performance at MCE-level ground shaking hazards. One approach would be to adjust ACI 318 Equation 21-8 to include a factor of about two in the denominator, as shown in Equation 2-4.
- The assumed plastic hinge length of $l_p = 0.5l_w$ can be maintained in the case of tension-controlled walls.
- Current provisions, which essentially require special boundary elements in walls that are not tension-controlled (i.e., compression-controlled walls), should be maintained.
- Increased minimum wall thickness should be considered for improved lateral stability under large compressive loads and potential spalling of concrete cover. One approach would be to prescribe a minimum wall thickness that is 10 times the cover, including an allowance for cover tolerance, which has demonstrated improved ductility in tests of concrete wall specimens.
- The use of ACI 318 Equation 21-4 (in addition to ACI 318 Equation 21-5) to determine the amount of transverse reinforcement at wall boundaries should be considered.

- The current maximum horizontal spacing of hoops or crossties in wall boundary elements is inconsistent with requirement for vertical spacing, which is limited to one-third the wall thickness. An additional limit should be considered for special boundary elements such that the horizontal distance between legs of hoops or crossties is limited to a factor (e.g., two-thirds or one) times the wall thickness. In addition, intermediate, unsupported bars at the wall edge should not be permitted.
- The buckling strain indicator, ε_p^* , proposed by Rodriguez et al. (1999) can be considered for use as a tool to evaluate the susceptibility of longitudinal bars to buckling in concrete walls subjected to flexure.

6.3 Overall Wall Buckling Studies

Overall wall buckling refers to the lateral instability of the entire wall section over a portion of the wall length and height. Prior to the earthquake, overall wall buckling had been observed in experimental tests, but had not been reported in an actual earthquake. Since the 2010 Maule earthquake, overall wall buckling behavior was also observed in the 2011 Christchurch earthquake in New Zealand. Relative to other types of wall damage, however, cases of documented overall wall buckling behavior are relatively few.

Overall wall buckling is differentiated from individual bar buckling, but overall wall buckling damage was most apparent in the end regions of walls where vertical tension and compression strains from in-plane wall flexure were the greatest. As a result, it was difficult to differentiate between damage that was initiated by bar buckling or concrete crushing, versus overall wall buckling.

6.3.1 Findings

The basic phenomenon of overall wall buckling can be explained by theoretical wall instability relationships. Although global wall buckling occurs when the wall boundary is in compression, buckling is influenced by residual tensile strain in the wall due to prior loading in the opposite direction. The critical slenderness ratio of a wall, kh_w/b , can be related to the maximum prior tensile strain, ε_{sm} , using equations presented in Chapter 3.

Investigation of two case study buildings that exhibited apparent out-of-plane buckling behavior in the 2010 Maule earthquake showed that:

- Drift ratios associated with concrete crushing in thin wall sections were much smaller than drift ratios associated with theoretical out-of-plane buckling considering gross concrete wall sections. It is therefore more likely that damage was initiated by concrete crushing at the extreme fibers due to flexural compression, rather than gross-section buckling.

- If it is assumed that concrete crushing and spalling of cover concrete leaves a core with a reduced thickness, theoretical instability relationships indicated a potential for out-of-plane buckling to occur in the reduced wall sections.
- The likely sequence of damage related to the observed behavior of the case study buildings was concrete crushing and spalling of concrete cover, followed by out-of-plane buckling of the reduced wall section.

6.3.2 Recommendations

To address potential wall slenderness issues, and also to consider that spalling of concrete cover can contribute to slenderness, the following potential changes to ACI 318 requirements are recommended for consideration:

- ACI 318 Chapter 21 currently permits a single curtain of reinforcement for thin walls with low average shear stress. Based on theoretical out-of-plane buckling considerations, flexure-controlled special structural walls should be required to have two curtains of reinforcement within the intended hinge zone, regardless of shear demand.
- ACI 318 Chapter 21 should have a slenderness ratio limit for the intended hinge zone of special structural walls. The 1997 UBC historic limit of $h_u/b \leq 16$ is recommended for walls that are expected to maintain their concrete cover, where h_u is the unsupported height of the wall, and b is the wall thickness. In the case of walls that are expected to lose their concrete cover due to spalling, the same limit could be applied, but b should refer to the thickness of the confined core. This thickness is denoted b_c in ACI 318. Such a limit could be specified as a simplified alternative to the use of Equations 3-1 to 3-3, which could be used in more detailed calculations when the maximum tensile strain demand is known.
- Application of a slenderness ratio limit to walls extending over multiple stories without lateral support from floor diaphragms (e.g., as might occur in an atrium) could be difficult, and might be overly restrictive. For such walls, Equations 3-1 to 3-3 can be used to determine wall thickness. In such an application, the result is likely to be conservative because these equations assume that tensile yielding extends over the full unsupported height of the wall. In a tall unsupported wall, however, tensile yielding is likely to be restricted to only a portion of the wall height.

6.4 Building Configuration Studies

Much of the observed damage in concrete wall buildings following the 2010 Maule earthquake could be attributed to building configuration issues. Patterns of damage highlighted aspects of building configuration that are known to affect component demands and overall building performance, such as vertical discontinuities, irregularities in strength and stiffness, and changes in the length, cross-sectional

shape, or location of walls from one story to the next. In addition, coupling of walls through slabs, beams, spandrels, and nonstructural elements, such as stairs, was also attributed to damage in many cases.

6.4.1 Findings

Investigation of building configuration issues included studies on: (1) the behavior of discontinuity regions located above or below vertically aligned openings; (2) vertical discontinuities, strength and stiffness irregularities, and the extent to which currently available evaluation tools capture these effects; (3) wall coupling behavior; (4) local wall geometric discontinuities; and (5) pier-spandrel system behavior.

6.4.1.1 Vertically Aligned Openings

Studies on solid wall panels directly above or below a vertically aligned stack of openings concluded that: (1) stresses are significantly larger than elsewhere in the walls; (2) stresses are many times the average shear stresses acting on entire wall; and (3) stresses extend into the solid wall panel a distance equal to 1.0 to 1.5 times the width of the openings.

6.4.1.2 Vertical Discontinuities

Based on results from ASCE/SEI 31-03 Tier 1 Evaluations across all buildings, the following observations were made: (1) the shear-stress check did not correlate well with damage; (2) a significant change in stiffness or strength between two adjacent stories is more critical if the lower story is the one that is more flexible or weaker; and (3) the weak story check was a marginally better predictor of a higher likelihood of damage than the soft story check.

Based on results from ASCE/SEI 31-03 Tier 2 Evaluations on selected buildings, the following observations were made:

- Unfactored demand-capacity ratios larger than two were a good indication that significant inelastic response could be expected and that nonlinear analysis should be performed.
- Factored demand-capacity ratios based on demands calculated from an elastic analysis did not correlate well with observed earthquake damage at the component level.

Based on results from detailed ASCE/SEI 31-03 Tier 3 Evaluations on a representative building, the following observations were made:

- ASCE/SEI 41-06 assessment criteria provided an acceptably accurate measure of overall building performance.
- Models that considered foundation flexibility resulted in the most consistency between predicted and observed damage.

- Predictions of the controlling mechanism, and shear failure, using ASCE/SEI 41-06 assessment criteria were somewhat consistent with observed damage.
- Prediction of observed damage at the component level, using various assessment criteria investigated in this study (e.g., ASCE/SEI 41-06 rotation limits, fragility functions, usable strain limits), was not accurate, meaning that component damage may be more or less than predicted using these criteria.
- Use of ASCE/SEI 41-06 assessment criteria generally resulted in a conservative assessment of performance at the component level.
- Use of fragility function assessment criteria developed for planar walls (Birely, 2012) generally resulted in a conservative assessment of performance for walls of variable configurations.
- Assessment criteria based on usable strain limits was generally unconservative, and was more sensitive to record-to-record variability.

6.4.1.3 Wall Coupling Behavior

Based on elastic and nonlinear analyses of a representative building, it was concluded that axial load amplification on walls due to slab and beam coupling can be significant, especially on small wall piers.

6.4.1.4 Local Wall Geometric Discontinuities

Investigation of wall discontinuities suggested that local changes in the stiffness and strength of individual wall components may be correlated with damage, and that checks on overall story strength and stiffness do not necessarily capture these effects. Based on a study of the magnitude of the measured local discontinuities and observed damage, it was concluded that damage was reasonably well correlated with a change in local geometry that exceeded 30% in the centerline length or 30% in the centroid location of a wall cross-section.

6.4.1.5 Pier-Spandrel System Behavior

In a study of pier-spandrel system behavior, the FEMA P-306 method for evaluating pier-spandrel response mechanisms was shown to predict the expected behavior and observed damage that occurred in a representative building.

6.4.2 Recommendations

Findings from building configuration studies conducted in each area resulted in the recommendations identified in the following sections.

6.4.2.1 Vertically Aligned Openings

To account for stress concentrations and force transfer in wall panels above or below a vertically aligned stack of openings, two new design zones should be established:

- Zone 1, extending below the openings a distance equal to the greater of l_d (the anchorage length of the boundary reinforcement as required in ACI 318) and h_s (the story height below the stack of openings), but not less than the length required to transfer shear within acceptable limits on shear stress in the wall.
- Zone 2, defined as the remaining portion from Zone 1 to the foundation (or roof, if considering a panel above of a stack of openings).

All boundary reinforcement should extend through Zone 1, and at least half of the bars should extend all the way to the foundation (or roof). Zone 1 should be proportioned and reinforced for panel zone shear stresses equal to at least $1.25A_s f_y / 2$, where A_s is the area of the boundary element reinforcement, f_y is the nominal yield strength, the factor 1.25 accounts for overstrength, and the factor 2 considers that half of the boundary reinforcement is extended into Zone 2.

Zone 2 should be designed for the remainder of the panel zone shear. It is acceptable to consider the force as being transferred to the foundation where adequate provision is made to develop the force at the foundation level. The amount of chord reinforcement above and below Zone 1 should resist the shear stresses assumed to be within Zone 1. Chord bars can be terminated progressively along the length.

Most building codes are not explicit about shear stress limits for wall panel zones above or below a vertically aligned stack of openings. A reasonable upper bound shear stress in the panel zone is $10\phi\sqrt{f'_c}$ psi.

6.4.2.2 Vertical Discontinuities

Based on application of ASCE/SEI 31-03 evaluation procedures to buildings in Chile, the following recommendations are made:

- Use of nonlinear analysis is recommended as a better predictor of demands, especially in cases that include complex geometries.
- Consideration of foundation flexibility and soil-structure-interaction effects is recommended to improve overall building response simulation and prediction of demands.

6.4.2.3 Wall Coupling Behavior

To account for observed effects due to coupled wall response, it is recommended that provisions and commentary be added in ACI 318 (e.g., in Section 21.9.5) to enforce consideration of the effects of coupling elements that are connected to structural walls, including the influence of coupling behavior on axial and shear force demands.

6.4.2.4 Local Wall Geometric Discontinuities

It is recommended that the ASCE/SEI 31-03 Tier 1 Basic Structural Checklist be modified to include a check on local wall discontinuities related to centerline length and centroid location. Accordingly, the following new checklist statement should be considered:

LOCAL VERTICAL DISCONTINUITIES: In concrete shear walls that are continuous to the foundation, local discontinuities caused by changes in cross-sectional geometry from one story to the story below shall not exceed: (i) a reduction in centerline length greater than 30% (in either orthogonal direction); or (ii) a change in centroid location greater than 30% of the wall length measured in the direction of the change.

6.4.2.5 Pier-Spandrel System Behavior

Although current U.S. seismic design provisions do not require designers to explicitly identify the overall mechanism in pier-spandrel systems, employing the method identified in FEMA P-306 to determine the response mechanism is recommended for verifying that the likely mechanism is consistent with the intended behavior.

For pier-spandrel systems, ACI 318 includes provisions that require special moment frame requirements to be satisfied for transverse reinforcement in wall piers, depending on the dimensions of the wall pier. For wall piers with clear height less than twice the length, however, these requirements do not currently apply. It is recommended that ACI code committees consider expanding the definition of “wall pier” to include elements with a squat aspect ratio, such as 1:1 so that adequate transverse reinforcement is provided.

6.5 Analytical Modeling Studies

Typical, modern, high-rise buildings in Chile comprise interconnected, lightly reinforced, thin concrete shear walls supporting reinforced concrete floor slabs without beams. Models of these buildings are likely to include three-dimensional assemblies of interconnected thin walls, with many openings, discontinuities, irregularities, and consideration of coupling via floor slabs.

Analytical modeling of the seismic behavior of complex concrete wall systems is difficult because:

- The stiffness of concrete elements depends on a number of variables including section shape, reinforcement ratio, axial load, prior strain, and others.
- Walls can exhibit unstable strength-degrading behaviors that are not well-understood, such as shear failure, bar buckling, concrete crushing, and overall wall buckling.

As a result, seismic response analysis of reinforced concrete wall buildings of the type prevalent in Chile presents several analytical challenges, and the applicability and capabilities of existing analytical tools were evaluated.

6.5.1 Findings and Recommendations

Based on the results of wall simulation studies, complex reinforced concrete wall behaviors can be successfully simulated in an analysis. The following observations and recommendations were made regarding analytical modeling of reinforced concrete wall buildings and components:

- Reinforcing bar buckling can occur as the unconfined concrete cover spalls (such as described in Chapter 2 of this report). The initiation of buckling and post buckling resistance of a reinforcing bar cage is affected by spacing, bar diameter, and previous (tensile) loading history.
- Overall wall buckling can be caused by concrete crushing, or by application of compression to a wall that has been subjected to significant tensile strain, such that the ensuing compression is resisted primarily by the previously stretched reinforcing bar (such as described in Chapter 3 of this report).
- There is analytical evidence of high shear stress beneath vertically aligned series of wall openings (such as described in Chapter 4 of this report).
- The lateral response of gravity loaded reinforced concrete walls is significantly different under cyclic loading conditions than monotonic loading. Brittle concrete crushing failure is possible even in walls that would be considered ductile under monotonic loading.
- Because concrete crushing is a brittle behavior, the extent of concrete crushing observed in analysis is very sensitive to modeling assumptions, such as the concrete strength at critical locations and ground motions at different times and in different directions. Once crushing initiates, it propagates extensively in a single load cycle.
- In relatively thin walls, the maximum compression resistance of the boundary zone is likely to occur as soon as the cover concrete spalls, irrespective of how well confined the core is. This can lead to major instantaneous loss of strength if the wall is supporting force-controlled gravity load.
- Initiation of concrete spalling is a function of the local peak compression strain. Spalling permits bar buckling, and will often trigger significant loss of strength and negative stiffness. These studies and test measurements show that the plane-sections-remain-plane assumption will significantly underestimate peak compressive strain in the critical regions of planar shear walls, and the same is true at any geometric discontinuity. If beam-type elements are used, spalling must be assumed to occur at a strain lower than the conventional spalling strain

for concrete to account for this. The use of an adequately refined shell element model enables the nonlinear strain distributions that arise in walls approaching failure, and additional strain concentrations at discontinuities and irregularities, to be represented explicitly.

- The effective period of a building nearing collapse is much longer than the nominal natural period. For such cases, the usual period range over which Rayleigh damping is to be targeted needs to be reconsidered, otherwise the longer period responses will be over-damped, and the possibility of collapse may be suppressed in the analysis.
- All of the above effects can be analytically replicated using a large-deflection finite element solver with reinforcing bars modeled using a refined mesh of fiber beams and advanced (e.g., layered sandwich type) nonlinear shell elements to model the concrete. The steel material model must include Bauschinger type hysteresis.
- For practical purposes, it is not feasible to model every reinforcing bar with multiple fiber beam elements between restraining ties to simulate buckling explicitly. It is possible, however, to use a phenomenological algorithm for the reinforcing bar, including buckling (calibrated against tests and detailed fiber beam models), within a multi-layer reinforced concrete shell element.

6.6 Recommendations for Further Study

Based on findings and recommendations from a series of studies investigating the effects of the 2010 Maule earthquake on Chilean buildings presented herein, the following additional studies are recommended:

- **Investigation of confined wall boundaries.** Observed damage in Chile correlated well with the need for special boundary elements, however, the lack of special boundary element confinement in Chilean walls did not provide information that directly confirms or refutes the adequacy of current ACI 318 requirements for the amount and spacing of transverse reinforcement in special boundary elements. Chilean engineers reported that some designs included some level of boundary element confinement, but data on these buildings is not immediately available, presumably because these buildings were not significantly damaged in the earthquake. Further investigation to identify buildings in Chile that included boundary confinement and studies correlating demands with observed damage (or lack of damage) are recommended.
- **Bar buckling versus concrete crushing mechanism.** The relationship between bar buckling behavior, confinement, and concrete crushing is complex, and two somewhat different explanations for observed damage to flexure-governed walls in Chile have been offered:

- i. *Failure initiated by concrete spalling*, primarily because of compressive strain demands. When concrete spalls, the area of concrete is reduced, and crushing behavior concentrates at that section causing bars to buckle. This explanation implies that the cause of damage in Chile was a lack of adequate transverse ties for confinement, and that a moderate amount of well-detailed ties would not have improved performance in Chile because the wall sections were too thin.
- ii. *Failure initiated by buckling of longitudinal reinforcing bars*, primarily because of cyclic tensile and compressive strains. Bar buckling helps spall cover concrete, and also reduces the effective confinement of the concrete core. This explanation implies that the main cause of damage in Chile is a lack of adequate transverse ties to restrain bar buckling, and that a moderate amount of well-detailed ties in the compression zone of walls would have improved performance.

Additional investigation into the controlling mechanisms of bar buckling versus concrete crushing, and experimental tests on reinforced concrete wall sections with varying details of transverse reinforcement are recommended.

- **Calibration of bar buckling criteria.** The buckling indicator, ε_p^* , proposed by Rodriguez et al. (1999) merits further investigation as a tool for evaluating the susceptibility of longitudinal bars to buckling in concrete walls subjected to flexure. Calibration of this approach with a larger set of test data is recommended.
- **Refinement of wall slenderness limits.** Recommendations for wall slenderness ratio limits applied to tall, unsupported walls are likely to be overconservative and difficult to implement. Investigation of alternative analysis methods (e.g., second-order analyses that model the likely variation in stiffness along the wall height, and consideration of wall flanges and other stiffening elements) are recommended to refine slenderness limits for special cases.

Wall Boundary Element Studies

This appendix presents detailed information on the approaches and assumptions used in modeling reinforced concrete shear walls and assessing boundary element behavior in Chapter 2. Studies investigated ACI 318-11, *Building Code Requirements for Structural Concrete and Commentary* (ACI, 2011), provisions for special boundary elements, plastic hinge length, and longitudinal bar buckling in buildings that experienced the 2010 Maule earthquake and in wall specimens from experimental tests in the literature.

A total of seven Chilean buildings were selected to investigate the performance of boundary elements during the earthquake. Additional information was obtained from tests on wall specimens conducted by Thomsen and Wallace (1995) to investigate and calibrate the potential effects of bar buckling in the boundary zones of thin structural walls. Details of case study building design, construction, material properties, seismic demands, and response quantities are described for each building and experiment considered in the investigations.

A.1 Building Descriptions

Walls from seven mid-rise and high-rise buildings in Santiago, Viña del Mar, and Concepción were selected for investigating special boundary element requirements. Case study buildings included:

- Alto Rio, a 15-story building located in Concepción that collapsed in the earthquake (designated Building No. 1 in this study).
- Plaza del Rio Building B, one part of a two-building complex located in Concepción. Immediately adjacent to, but structurally separated from, Plaza del Rio Building A (which was damaged in the earthquake), Building B is a 13-story structure that was relatively undamaged in the earthquake (designated Building No. 2 in this study).
- Concepto Urbano, a 22-story building located in Concepción that was also relatively undamaged in the earthquake (designated Building No. 3 in this study).
- Toledo, a 10-story building located in Viña del Mar that experienced major damage in the form of concrete crushing and bar buckling at wall boundaries (designated Building No. 4 in this study).

- Undisclosed Building A, a 12-story building located in Santiago that experienced some damage at wall boundaries and overall wall buckling in the first subterranean level (designated Building No. 5 in this study).
- Undisclosed Building B, a 20-story building located in Santiago that also experienced overall wall buckling in the first subterranean level (designated Building No. 6 in this study).
- Mongolio, a 10-story building located in Santiago that experienced some shear failure and localized wall damage, but relatively little boundary zone damage, as a result of the earthquake (designated Building No. 7 in this study).

Building loads, roof heights, tributary areas, and modeled wall geometries for each structure were based on available construction documents and damage reports, and are reported in the following sections on a building-by-building basis. Buildings have been numbered for the purpose of tracking, tabulating, and cross-referencing results for individual walls in each building.

A.1.1 Alto Rio (Building No. 1)

The Alto Rio building (Building No. 1) is a 15-story structure above grade, with a podium level at grade and two levels of parking below grade, designed in 2007. The gravity and seismic force-resisting systems consist of reinforced concrete bearing walls.

A typical floor plan is shown in Figure A-1. The typical floor plate is rectangular in plan, measuring approximately 40 m (131 feet) long by 12 m (39 feet) wide. The overall building height is approximately 38 m (126 feet) above grade. The top three stories of the building taper off in plan, as shown in Figure A-2.

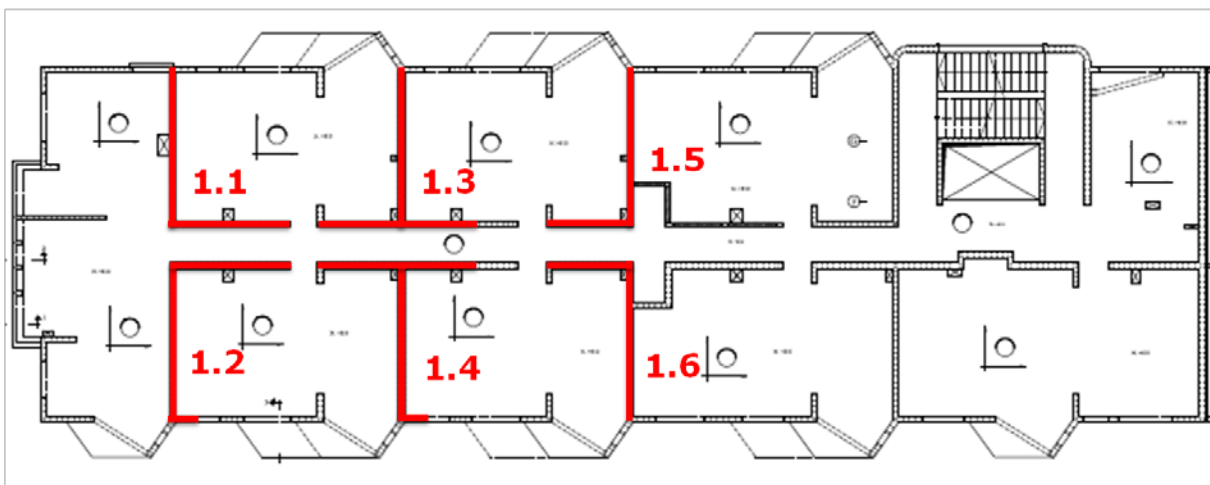


Figure A-1 Alto Rio (Building No. 1) – typical floor plan with case study walls highlighted.

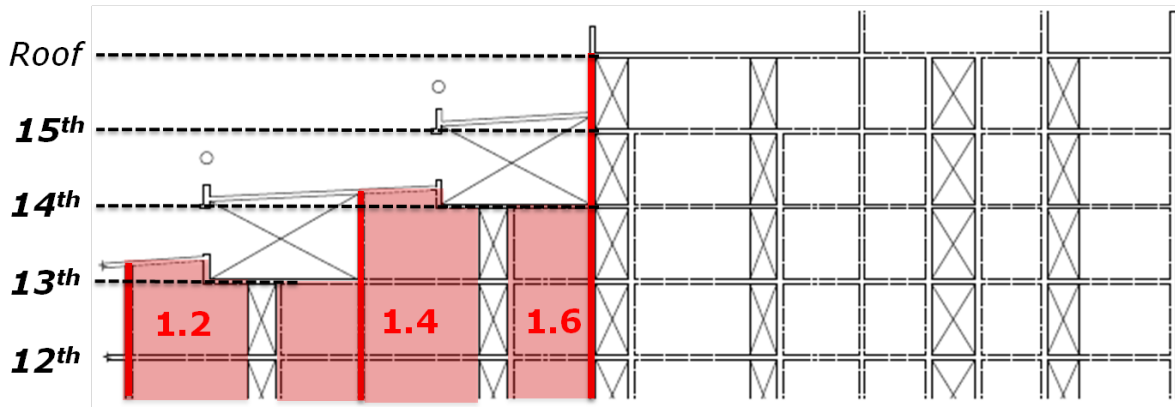


Figure A-2 Alto Rio (Building No. 1) – longitudinal section showing floor plate reductions in the upper three stories.

Typical concrete shear walls are 200 mm (8 inches) thick, with flanges on one end. Longitudinal reinforcement at wall boundaries ranges in diameter from 18 mm to 25 mm (#6 to #8). Web reinforcement consists of two curtains of either 8 mm or 10 mm diameter bars, typically spaced at 200 mm (8 inches) on center. No hoops or crossies were provided at wall boundaries. The floor plan shown in Figure A-1 identifies the walls investigated as part of this study.

Many of the transverse walls on the northern half of the building have setbacks in the first story. This configuration has been referred to as “flag-shaped,” and was a characteristic of many buildings in Chile. Also, the returns (i.e., flanges) in the upper stories are discontinued in the first story, resulting in localized vertical discontinuities in the walls. An elevation of a typical “flag-shaped” wall configuration, along with discontinuous flanges, is shown in Figure A-3.

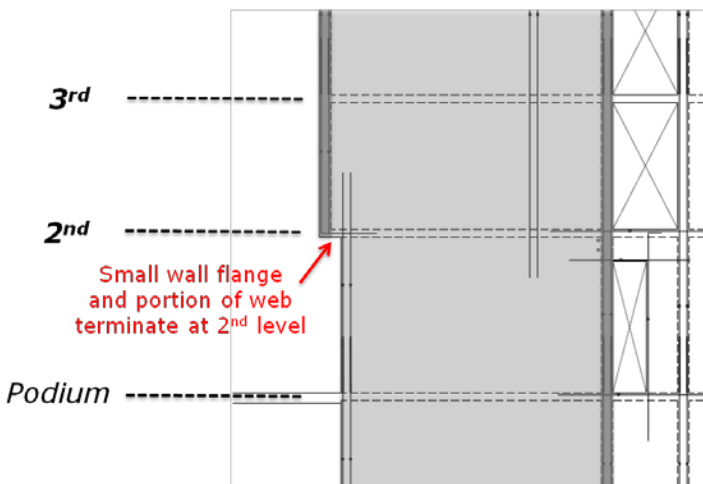


Figure A-3 Alto Rio (Building No. 1) – typical wall setback and discontinuous flanges in the first story.

The building collapsed as a result of the earthquake. The podium level was the critical level, and damage to the flag-shaped walls with discontinuous flanges in the first story was identified as the likely cause of collapse.

Table A-1 summarizes the geometric configuration of the six walls considered in the Alto Rio building (Building No. 1). Critical section web lengths and thicknesses, flange widths and thicknesses, aspect ratios, and total wall areas are tabulated. As shown in Figure A-2, the walls under investigation stop short of the roof, and were taken to have a height of approximately 36 m (117.5 feet).

Table A-1 Alto Rio (Building No. 1) – Geometry of Critical Wall Sections

Wall ID	Shape	Description	Vertical Discontinuity	Web Length (ft)	Web Thickness (in)	Wall Height (ft)	Aspect Ratio	Web Area (in ²)	North Flange Width (ft)	North Flange Thickness (in)	South Flange Width (ft)	South Flange Thickness (in)	Total Wall Area (in ²)
1.1	L	North Web Stem, South Flange	Yes; Flag	16'-5"	7.9"	117'-6"	7.2	1550	0'-0"	0.0"	5'-11"	7.9"	2170
1.2	L	North Flange, South Barbell	No	17'-9"	7.9"	117'-6"	6.6	1674	13'-3"	7.9"	2'-11"	7.9"	3209
1.3	T	North Web Stem, South Flange	Yes; Flag	16'-5"	7.9"	117'-6"	7.2	1550	0'-0"	0.0"	11'-8"	7.9"	2713
1.4	T	North Flange, South Barbell	No	17'-9"	7.9"	117'-6"	6.6	1674	22'-4"	7.9"	2'-11"	7.9"	4061
1.5	L	North Web Stem, South Flange	Yes; Flag	16'-5"	7.9"	117'-6"	7.2	1550	0'-0"	0.0"	9'-8"	7.9"	2527
1.6	L	North Flange, South Barbell	No	17'-9"	7.9"	117'-6"	6.6	1674	9'-8"	7.9"	1'-12"	7.9"	2775

A.1.2 Plaza del Rio Building B (Building No. 2)

Plaza del Rio consists of two buildings (Building A and Building B) that are located immediately adjacent to one another, but are structurally separated. Plaza del Rio Building B (Building No. 2) is a 13-story structure with no basement designed in 2004. The gravity and seismic force-resisting systems consist of reinforced concrete bearing walls. Plaza del Rio Building A was damaged in the earthquake, but Plaza del Rio Building B, oriented 90 degrees to Building A, experienced little damage.

A typical floor plan is shown in Figure A-4. The typical floor plate is rectangular in plan, measuring approximately 40 m (131 feet) long by 14 m (45 feet) wide. The overall building height is approximately 32 m (105 feet) above grade.

Typical concrete shear walls are 150 mm (6 inches) thick, with flanges on one end. Longitudinal reinforcement at wall boundaries is 18mm in diameter (#7). Web reinforcement consists of two curtains of 8 mm diameter bars, typically spaced at 200 mm (8 inches) on center. Drawings specify 8 mm diameter hoops with 135-degree hooks that encompass the longitudinal reinforcement at the wall boundaries (Figure A-5). Hoop spacing is 200 mm (8 inches). Crossties are not used if the hoops extend a modest distance into the wall web. The floor plan shown in Figure A-4 identifies the walls investigated as part of this study.



Figure A-4 Plaza del Rio Building B (Building No. 2) – typical floor plan with case study walls highlighted.

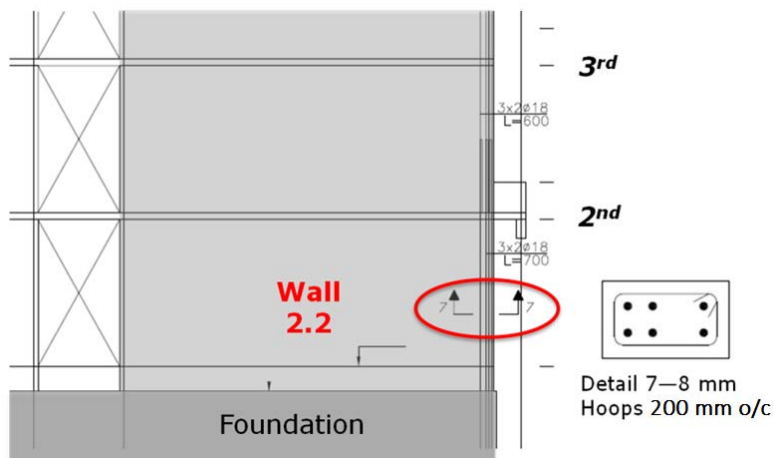


Figure A-5 Plaza del Rio Building B (Building No. 2) – hoop reinforcement at wall boundaries.

The walls selected for study include a few discontinuities. Wall 2.1 has flanges at each end in the first story, but these flanges are discontinued in the second story and above. Also, a small portion of the web that exists in upper stories is discontinued at the ground level. Similarly, Wall 2.3 has flange discontinuities between the first and

second stories, but no web discontinuity. As a result, models for these walls only consider the continuous portions of the flanges and webs. Table A-2 summarizes the geometric properties of the critical wall sections considered in Plaza del Rio Building B (Building No. 2).

Table A-2 Plaza del Rio Building B (Building No. 2) – Geometry of Critical Wall Sections

Wall ID	Shape	Description	Vertical Discontinuity	Web Length (ft)	Web Thickness (in)	Wall Height (ft)	Aspect Ratio	Web Area (in ²)	North Flange Width (ft)	North Flange Thickness (in)	South Flange Width (ft)	South Flange Thickness (in)	Total Wall Area (in ²)
2.1	R	Rectangular	Yes: Flange and Web Reduction	9'-10"	5.9"	105'-4"	10.7	698	0'-0"	0.0"	0'-0"	0.0"	698
2.2	T	North Web Stem, South Flange	No	19'-8"	5.9"	105'-4"	5.4	1395	0'-0"	0.0"	4'-2"	5.9"	1725
2.3	L	North and South Flanges	Yes: Flange Reduction	20'-4"	5.9"	105'-4"	5.2	1442	2'-0"	5.9"	1'-10"	5.9"	1711

A.1.3 Concepto Urbano (Building No. 3)

The Concepto Urbano building (Building No. 3) is a 22-story structure above grade, with a podium level at grade and two levels of parking below grade, designed in 2007. The gravity and seismic force-resisting systems consist of reinforced concrete bearing walls. This building was relatively undamaged as a result of the earthquake.

Typical floor plans are shown in Figure A-6. From the podium through the tenth floor, the floor plate is L-shaped in plan, with overall dimensions of approximately 49 m (159 feet) long by 23 m (75 feet) wide. From the eleventh floor through the roof, the floor plate is rectangular in plan, measuring approximately 29 m (96 feet) long by 17 m (57 feet) wide. The overall building height is approximately 56 m (183 feet) above grade.

Typical concrete shear walls are 300 mm (12 inches) thick, with both flanged and rectangular configurations. Longitudinal reinforcement at wall boundaries ranges in diameter from 22 mm to 25 mm (#7 to #8). Web reinforcement consists of two curtains of 16 mm diameter bars (#5), spaced at less than 200 mm (8 inches) on center. No hoops or crossies were provided at wall boundaries, but horizontal reinforcement was intended to wrap around longitudinal reinforcement and terminate at the far side of the wall with 135-degree hooks (Figure A-7).

The floor plan shown in Figure A-6 identifies the walls investigated as part of this study. Both walls extend from the base of the structure to the tower roof. One is rectangular (Wall 3.1), and the other is L-shaped (Wall 3.2) with a large flange along

the corridor wall. Table A-3 summarizes the geometric properties of the critical wall sections considered in the Concepto Urbano building (Building No. 3).



Figure A-6 Concepto Urbano (Building No. 3) – typical floor plans with case study walls highlighted: (a) ground through the tenth floor; and (b) eleventh floor through the roof.

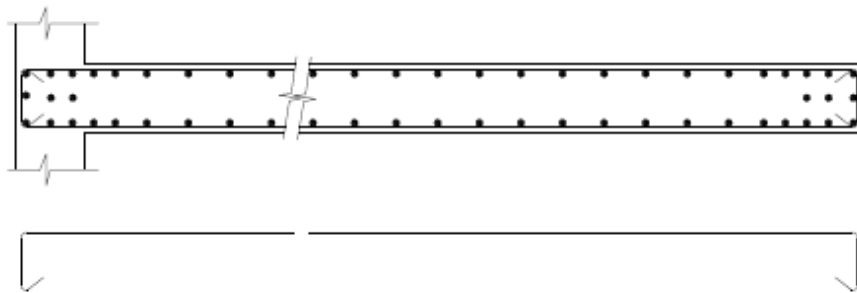


Figure A-7 Concepto Urbano (Building No. 3) – plan section of Wall 3.2, showing horizontal wall reinforcement detailing.

Table A-3 Concepto Urbano (Building No. 3) – Geometry of Critical Wall Sections

Wall ID	Shape	Description	Vertical Discontinuity	Web Length (ft)	Web Thickness (in)	Wall Height (ft)	Aspect Ratio	Web Area (in ²)	North Flange Width (ft)	North Flange Thickness (in)	South Flange Width (ft)	South Flange Thickness (in)	Total Wall Area (in ²)
3.1	R	Rectangular	Yes; Web Reduction	12'-10"	11.8"	182'-9"	14.3	1814	0'-0"	0.0"	0'-0"	0.0"	1814
3.2	L	North Web Stem, South Flange	Yes; Flag	22'-8"	11.8"	182'-9"	8.1	3209	0'-0"	0.0"	9'-5"	11.8"	4683

A.1.4 Toledo (Building No. 4)

The Toledo building (Building No. 4) is a 10-story structure with one level of parking below grade designed in 1996. The gravity and seismic force-resisting systems consist of reinforced concrete bearing walls. Extensive damage occurred in most transverse walls of the building at the ground level.

A typical floor plan is shown in Figure A-8. The floor plate is approximately rectangular in plan, measuring about 37 m (122 feet) long by 15 m (48 feet) wide. The overall building height is approximately 26 m (86 feet) above grade.

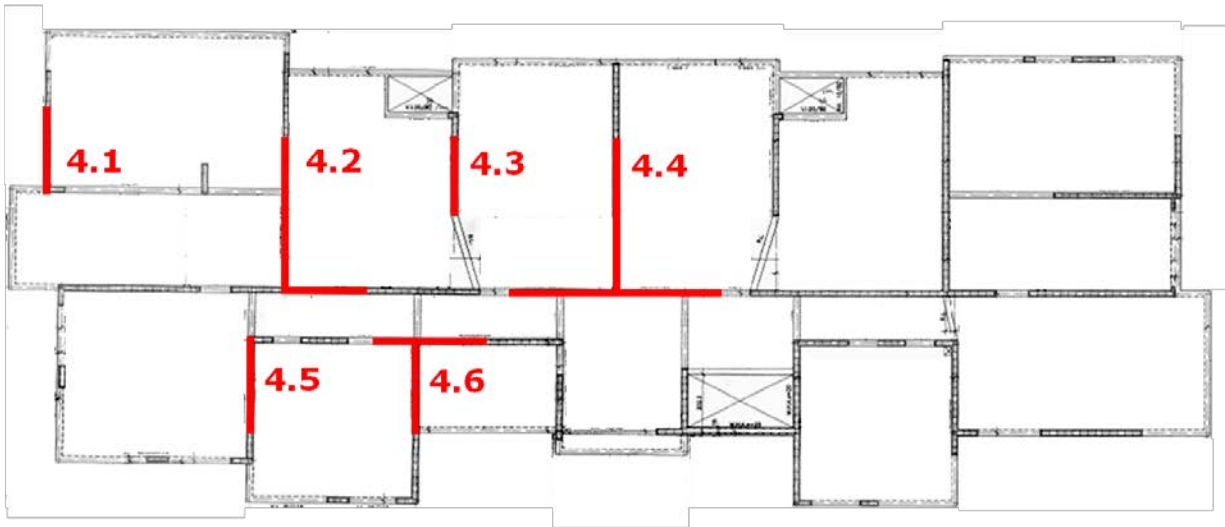


Figure A-8 Toledo (Building No. 4) – typical floor plan with case study walls highlighted.

Many of the transverse walls have setbacks in the first story, characteristic of a flag-shaped configuration. The floor plan shown in Figure A-8 identifies the walls investigated as part of this study. Figure A-9 illustrates a typical wall setback and reduction in the length of the web in the first story of the building.

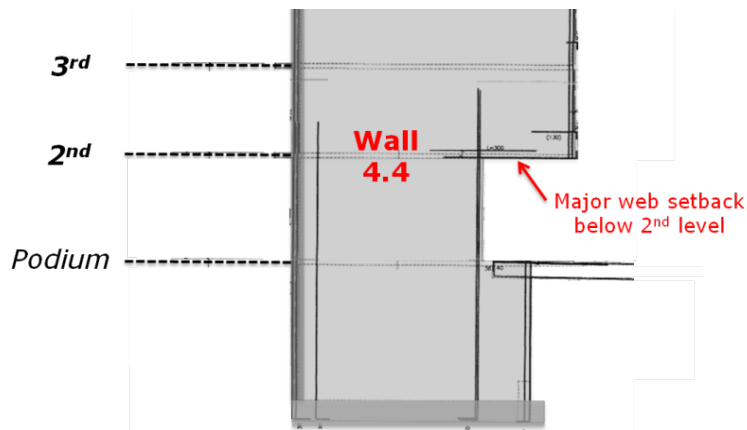


Figure A-9 Toledo (Building No. 4) – typical setback and reduced web in the first story walls.

Typical concrete shear walls are 200 mm (8 inches) thick, with both flanged and rectangular configurations. Longitudinal reinforcement at wall boundaries ranges in diameter from 18 mm to 32 mm (#6 to #10). Vertical web reinforcement consists of two curtains of 8 mm diameter bars, spaced at 250 mm (10 inches) on center. Horizontal web reinforcement consists of 8 mm or 10 mm diameter bars, spaced at 200 mm to 250 mm (8 inches to 10 inches) on center. No hoops or crossies were

provided at wall boundaries. Table A-4 summarizes the geometric properties of the critical wall sections considered in the Toledo building (Building No. 4).

Table A-4 Toledo (Building No. 4) – Geometry of Critical Wall Sections

Wall ID	Shape	Description	Vertical Discontinuity	Web Length (ft)	Web Thickness (in)	Wall Height (ft)	Aspect Ratio	Web Area (in ²)	North Flange Width (ft)	North Flange Thickness (in)	South Flange Width (ft)	South Flange Thickness (in)	Total Wall Area (in ²)
4.1	R	Rectangular	Yes; Flag and Web Loss	9'-8"	7.9"	85'-10"	8.9	915	0'-0"	0.0"	0'-0"	0.0"	915
4.2	L	North Web Stem, South Flange	Yes; Web Loss	17'-9"	7.9"	85'-10"	4.8	1674	0'-0"	0.0"	9'-5"	7.9"	2626
4.3	R	Rectangular	Yes; Flag	8'-8"	7.9"	85'-10"	9.9	822	0'-0"	0.0"	0'-0"	0.0"	822
4.4	T	North Web Stem, South Flange	Yes; Web Loss	17'-9"	7.9"	85'-10"	4.8	1674	0'-0"	0.0"	17'-3"	7.9"	3364
4.5	L	North Flange, South Web Stem	Yes; Flag	10'-8"	7.9"	85'-10"	8.0	1008	2'-7"	7.9"	0'-0"	0.0"	1194
4.6	T	North Flange, South Web Stem	Yes; Flag	10'-8"	7.9"	85'-10"	8.0	1008	11'-10"	7.9"	0'-0"	0.0"	2062

A.1.5 Undisclosed Building A (Building No. 5)

Undisclosed Building A (Building No. 5) is a 12-story building with two levels of underground parking designed in 2005. The gravity and seismic force-resisting systems consist of reinforced concrete bearing walls.

A typical floor plan is shown in Figure A-10. The floor plate is rectangular in plan, measuring approximately 35 m (115 feet) long by 21 m (69 feet) wide. The overall building height is approximately 30 m (100 feet) above grade.

Typical concrete shear walls are 150 mm (6 inches) thick, with both flanged and rectangular configurations. Longitudinal reinforcement at wall boundaries was highly variable, ranging in diameter from 12 mm to 28 mm (#4 to #9). Web reinforcement consists of 8 mm or 10 mm diameter bars, spaced at 150 mm or 200 mm (6 inches or 8 inches) on center. Hoops were provided at some wall boundaries, typically located at stems of flanged walls or rectangular wall ends, and staggered between web reinforcing bar bends. Where provided, hoops were spaced at the same interval as the horizontal web reinforcement.

Significant damage to walls was observed in the first subterranean level of parking. Many of the walls in the parking levels have significant setbacks and reduced web sections relative to the residential levels above. The floor plan in Figure A-10 identifies the walls that were damaged and investigated as part of this study.

Figure A-11 shows reinforcing details and exposed reinforcement in the boundary of a damaged wall. Table A-5 summarizes the geometric properties of the critical wall sections considered in Undisclosed Building A (Building No. 5).

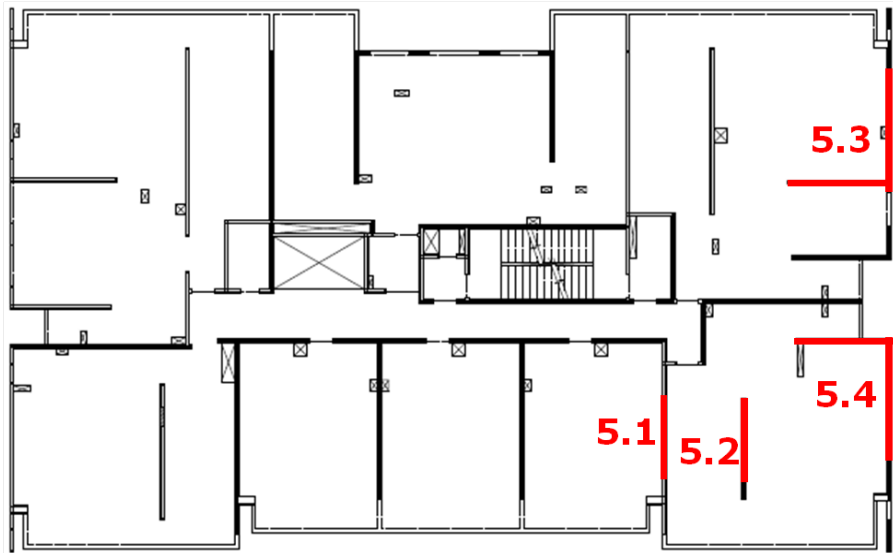


Figure A-10 Undisclosed Building A (Building No. 5) – typical floor plan with case study walls highlighted.

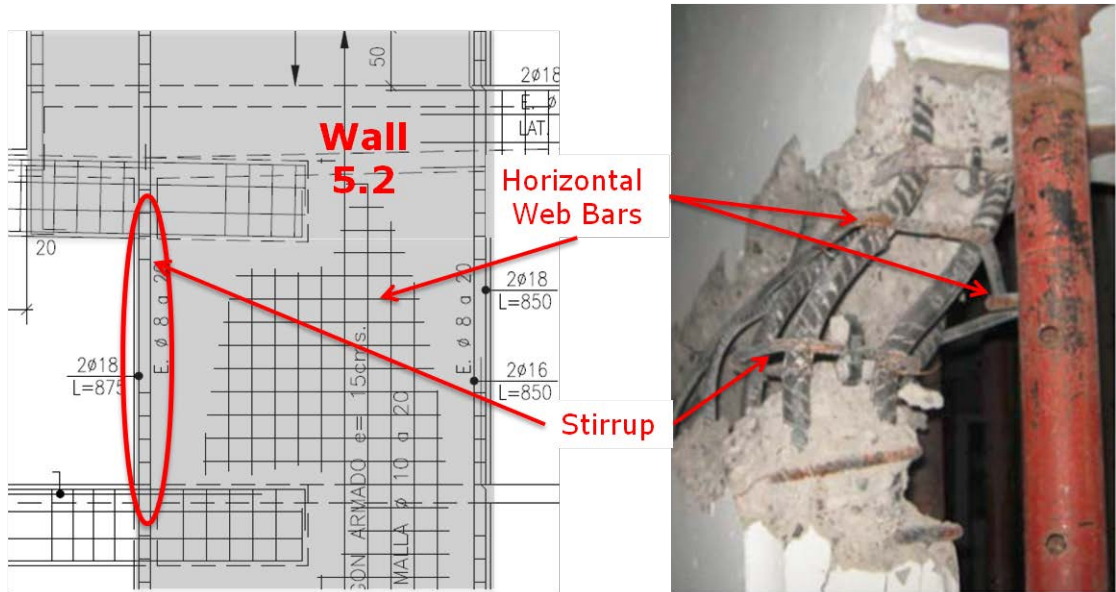


Figure A-11 Undisclosed Building A (Building No. 5) – wall reinforcing details and observed damage at the wall boundary (photo courtesy of Carl Luders).

Table A-5 Undisclosed Building A (Building No. 5) – Geometry of Critical Wall Sections

Wall ID	Shape	Description	Vertical Discontinuity	Web Length (ft)	Web Thickness (in)	Wall Height (ft)	Aspect Ratio	Web Area (in ²)	North Flange Width (ft)	North Flange Thickness (in)	South Flange Width (ft)	South Flange Thickness (in)	Total Wall Area (in ²)
5.1	R	Rectangular	Yes, Web Reduction	11'-3"	5.9"	99'-7"	8.9	795	0'-0"	0.0"	0'-0"	0.0"	795
5.2	R	Rectangular	Yes, Web Reduction	10'-1"	5.9"	99'-7"	9.9	716	0'-0"	0.0"	0'-0"	0.0"	716
5.3	L	North Web Stem, South Flange	Yes, Flag	13'-9"	5.9"	99'-7"	7.2	977	0'-0"	0.0"	7'-6"	5.9"	1541
5.4	L	South Web Stem, North Flange	Yes, Flag	17'-7"	5.9"	99'-7"	5.7	1249	8'-2"	5.9"	0'-0"	0.0"	1793

A.1.6 Undisclosed Building B (Building No. 6)

Undisclosed Building B (Building No. 6) is a 20-story structure with 4 levels of underground parking designed in 2006. The gravity and seismic force-resisting systems consist of reinforced concrete bearing walls. Damage was observed in the transverse walls of the first subterranean level of parking. Damage included concrete crushing and spalling of concrete cover, bar buckling and fracture, and apparent out-of-plane wall buckling.

A typical floor plan is shown in Figure A-12. The floor plate is approximately rectangular in plan with a curved facade. The overall building height is approximately 50 m (166 feet) above grade.

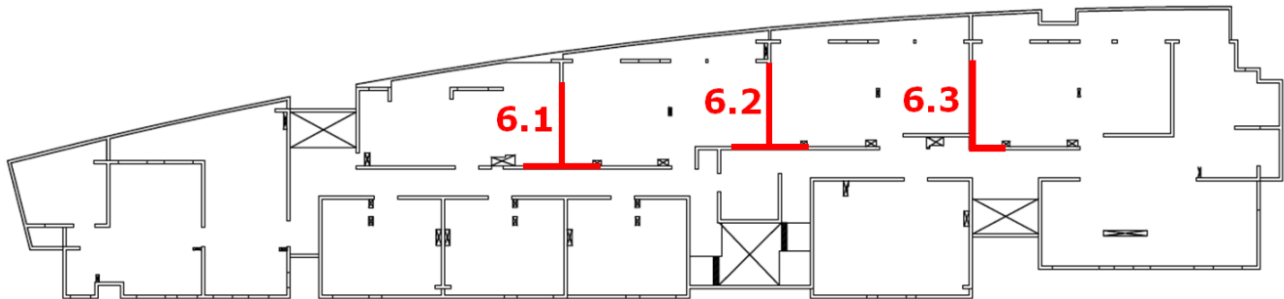


Figure A-12 Undisclosed Building B (Building No. 6) – typical floor plan with case study walls highlighted.

Typical concrete shear wall thickness varies, ranging from 170 mm (7 inches) at the narrowest, to 250 mm (10 inches) at the thickest. Two curtains of reinforcement are provided. No hoops were provided at wall boundaries, but horizontal web reinforcement wraps around longitudinal reinforcing bars and terminates with a 90-degree hook. Figure A-13 illustrates the typical wall boundary detail along with exposed reinforcement in the boundary of a damaged wall. Although cross-ties are shown at alternating sets of vertical web reinforcing bars, photos of observed damaged do not suggest the presence of these ties.

The floor plan in Figure A-12 identifies the walls that were damaged and investigated as part of this study. These walls all had setbacks in the first subterranean level and reduced web sections relative to the levels above. A typical wall setback is shown in Figure A-14.

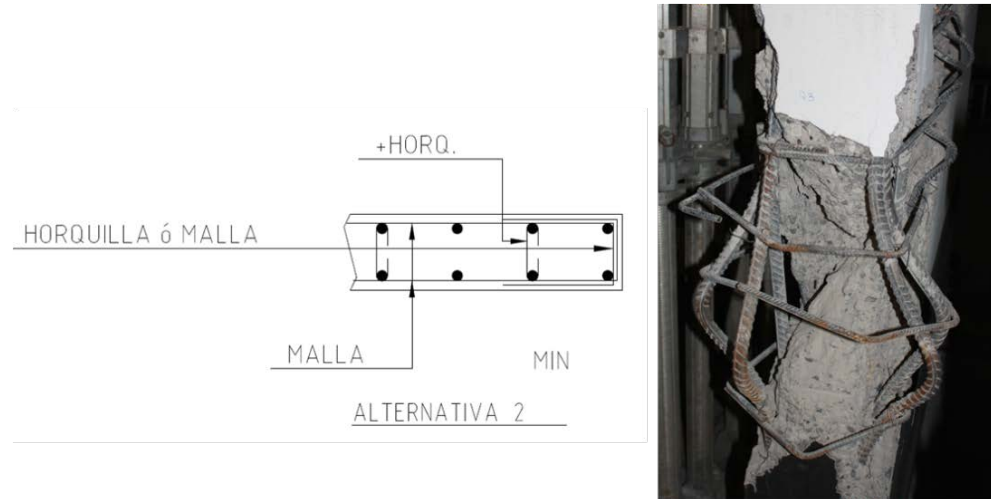


Figure A-13 Undisclosed Building B (Building No. 6) – typical wall boundary detail and photo of exposed reinforcement in the boundary of a damaged wall (photo courtesy of Jack Moehle).

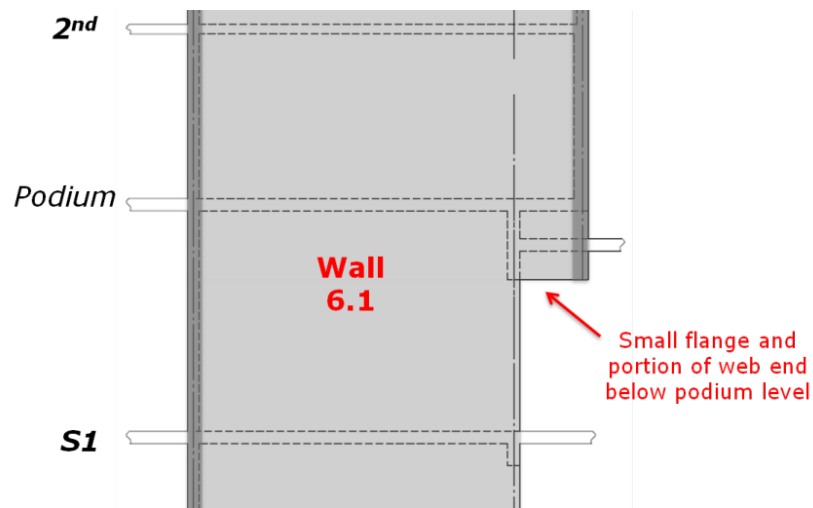


Figure A-14 Undisclosed Building B (Building No. 6) – typical setback and reduced web in the first subterranean level.

Table A-6 summarizes the geometric properties of the critical wall sections considered in Undisclosed Building B (Building No. 6).

Table A-6 Undisclosed Building B (Building No. 6) – Geometry of Critical Wall Sections

Wall ID	Shape	Description	Vertical Discontinuity	Web Length (ft)	Web Thickness (in)	Wall Height (ft)	Aspect Ratio	Web Area (in ²)	North Flange Width (ft)	North Flange Thickness (in)	South Flange Width (ft)	South Flange Thickness (in)	Total Wall Area (in ²)
6.1	T	North Web Stem, South Flange	Yes; Flag	19'-2"	9.8"	166'-3"	8.7	2259	0'-0"	0.0"	16'-9"	6.7"	3669
6.2	T	North Web Stem, South Flange	Yes; Flag	15'-10"	7.9"	166'-3"	10.5	1494	0'-0"	0.0"	11'-6"	6.7"	2469
6.3	L	North Web Stem, South Flange	Yes; Flag	15'-10"	6.7"	166'-3"	10.5	1270	0'-0"	0.0"	7'-4"	6.7"	1905

A.1.7 Mongolio (Building No. 7)

The Mongolio building (Building No. 7) is a 10-story structure with one level of parking below grade designed in 2007. The gravity and seismic force-resisting systems consist of reinforced concrete bearing walls. An independent report (Lemnitzer et al., 2012) documented shear wall and column damage in the first story; however, no damage to wall boundaries was reported.

A typical floor plan is shown in Figure A-15. The floor plate is approximately rectangular in plan. The overall building height is approximately 28 m (92 feet) above grade.

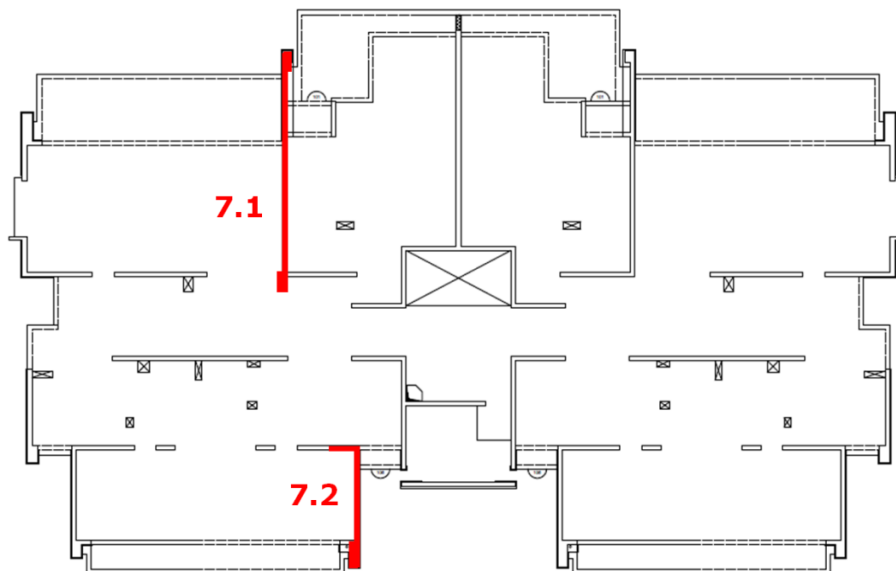


Figure A-15 Mongolio (Building No. 7) – typical floor plan with case study walls highlighted.

Typical concrete shear wall thickness varies, ranging from 170 mm (7 inches) to 250 mm (10 inches). Two curtains of reinforcement are provided. General notes specify that all stirrups terminate with 135-degree hooks.

The floor plan in Figure A-15 identifies the walls that were investigated as part of this study. Wall 7.1 has some vertical discontinuity in the flange at one end, but at the critical level, it has a barbell-shaped cross-section. Wall 7.2 is a flanged wall with a barbell-shaped stem. The barbell sections at each end have hoops around the longitudinal reinforcing bars, providing a more stable critical section than in other buildings investigated. Figure A-16 shows an elevation of Wall 7.1 along with the details of the barbell sections at each end.

Although wall damage was documented in several walls, little to no damage was noted in the boundaries of these walls. Table A-7 summarizes the geometric properties of the critical wall sections considered in the Mongolio building (Building No. 7).

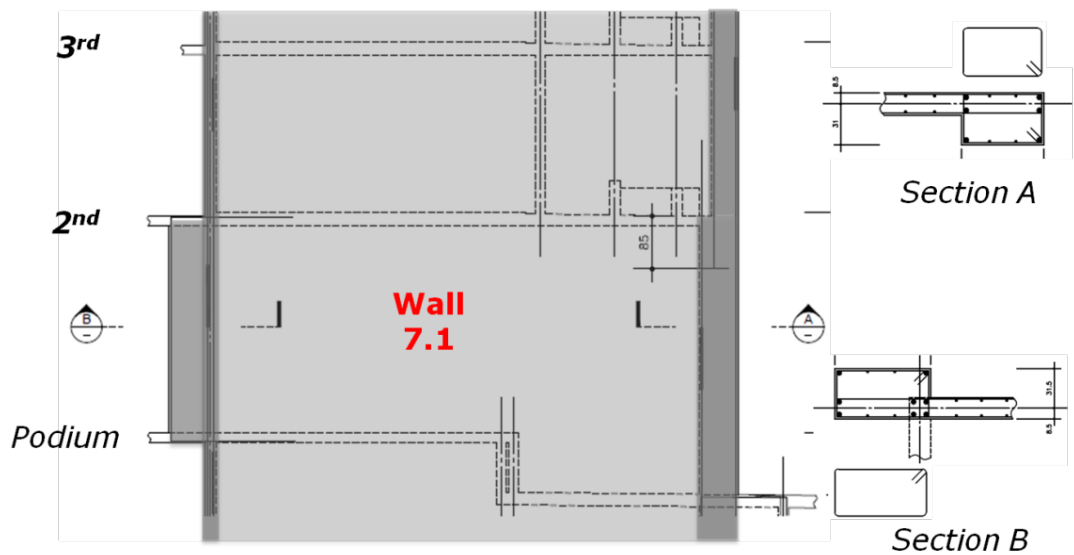


Figure A-16 Mongolio (Building No. 7) – elevation of Wall 7.1 and details of barbell sections at each end.

Table A-7 Mongolio (Building No. 7) – Geometry of Critical Wall Sections

Wall ID	Shape	Description	Vertical Discontinuity	Web Length (ft)	Web Thickness (in)	Wall Height (ft)	Aspect Ratio	Web Area (in ²)	North Flange Width (ft)	North Flange Thickness (in)	South Flange Width (ft)	South Flange Thickness (in)	Total Wall Area (in ²)
7.1	B	Barbell	Yes, Flange Reduction	30'-1"	6.7"	92'-4"	3.1	2419	1'-4"	24.6"	1'-4"	29.9"	3313
7.2	L	South Barbell, North Flange	Yes, Flange Reduction	15'-3"	9.8"	92'-4"	6.1	1798	4'-11"	6.7"	1'-3"	52.4"	3434

A.1.8 Gravity Load Calculations

Dead loads for floor slabs and roofs were estimated based on information available from structural drawings, architectural features, and building occupancy. A set of architectural, mechanical, and electrical assumptions were consistently applied for the buildings analyzed, unless weight information was specifically provided in

building documents. Weights for structural elements including walls, slabs, and beams were calculated based on structural drawings specific to the building being analyzed. Weights were distributed evenly across the floor plate for simple weight tabulation.

A residential live load of 40 psf was assumed on floor slabs, and a 20 psf live load was used on roof slabs. Because structural walls in Chilean buildings serve as partitions, additional partition loading was not considered. A sample tabulation of assumed gravity loading for a typical floor slab is provided in Table A-8.

Table A-8 Typical Gravity Load Assumptions (Alto Rio – Building No. 1)

Item	Value (psf)	Total (psf)	Value (kPa)
TYPICAL FLOOR DEAD LOAD			
Concrete slab (150 mm; 6 inches)	73.8		
Concrete Beams (200 mm × 93 mm; 515 m ²)	5.8		
Flooring (carpet and pad)	3.0		
Ceiling (plaster)	1.0		
HVAC	1.0		
Plumbing/Electrical	1.0		
Miscellaneous	5.0		
SUBTOTAL – FLOOR DEAD LOAD		90.6	4.34
ADDED DEAD LOAD			
Concrete walls (162.8 m × 2.4 m × 200 mm; 515 m ²) w/ plaster finish	88.5		
Columns (none)	0.0		
Other miscellaneous (none)	0.0		
SUBTOTAL – ADDED DEAD LOAD		88.5	4.23
TOTAL – FLOOR DEAD LOAD (rounded)		180.0	8.62
TYPICAL FLOOR LIVE LOAD			
Residential (private rooms; reducible)	40.0		
Partitions (negligible)	0.0		
TOTAL – FLOOR LIVE LOAD		40	1.92

Estimated unit weights for the floors in each building varied between 150 psf and 200 psf (7.2 kPa and 9.6 kPa), based on differences in slab thickness and distribution of structural elements (e.g., beams and walls). Unit weights between 150 psf and 200 psf are consistent with values for Chilean buildings reported in the literature (e.g., Massone et al., 2012).

Assumed dead and live loads were used to calculate axial loads at critical wall sections. Most often, critical wall sections were located in the first story or the first subterranean level. In analyses checking special boundary element triggers, factored axial loads were computed based on tributary area in a manner consistent with U.S. practice, using load combination $P_u = 1.2D + 0.5L + 1.0E_v$ from the *International Building Code* (ICC, 2009). Vertical earthquake load, E_v , was estimated to be approximately $0.2D$. In analyses studying the onset of bar buckling, the expected axial load $P_e = D + 0.25L$ was used.

A.1.9 Material Properties

Material properties were taken from construction documents, or assumed if unavailable. In Chile, strength of concrete, f'_c , is established through concrete cube tests. For example, concrete designated H30 must demonstrate a cube strength of at least 30 MPa, according to NCh170.Of 1985, *Concrete – General Requirements* (INN, 1985). Since design strength in ACI 318 is based on cylinder tests, adjustments are made in Section 5.1.2 of NCh430.Of2008, *Reinforced Concrete Design and Analysis Requirements* (INN, 2008), to translate cube strength into cylinder strength (and thus f'_c) as follows:

Table A-9 Design Strengths Corresponding to Cube Test Strengths (NCh430)

f'_c (MPa)	Concrete grade (NCh170 with 10% deficient fraction)
16	H20
20	H25
25	H30
30	H35
35	H40
40	H45
	>45 ¹

¹ For concrete compressive strength greater than H45 the value of f'_c shall be determined using standard cylindrical samples.

In the case study buildings, the most commonly specified concrete type was H30, with a few instances of H25. For concrete type H30, the design strength is 25 MPa (3625 psi); and for H25, the design strength is 20 MPa (2900 psi). Based on thin wall sections, with large vertical spacing between bars, and prevalent use of 90-degree hooks, the concrete was considered to be unconfined in all cases. Design documents specified H30 quality concrete for the walls in Building No. 1, 2, 3, and 7, and specified H25 quality concrete for the walls in Building No. 5 and 6. The stress-strain relationship for unconfined concrete is shown in Figure A-17a.

Reinforcing steel in all structures was specified as A63-42. According to NCh204.Of2006, *Reinforcing Steel – Hot-Rolled Rebar for Reinforced Concrete* (INN, 2006), A63-42 steel must have a minimum yield strength of 420 MPa (60.9 ksi), and an ultimate strength of 630 MPa (91.4 ksi). For analyses checking special boundary element triggers, an elasto-plastic model was used for the reinforcing steel to remain consistent with design assumptions prescribed in ACI 318. Analyses studying the onset of bar buckling in boundary elements used a nonlinear stress-strain relationship that included strain hardening and post-ultimate-strength softening before rupture. The elasto-plastic and nonlinear relationships for reinforcing steel are shown in Figure A-17b.

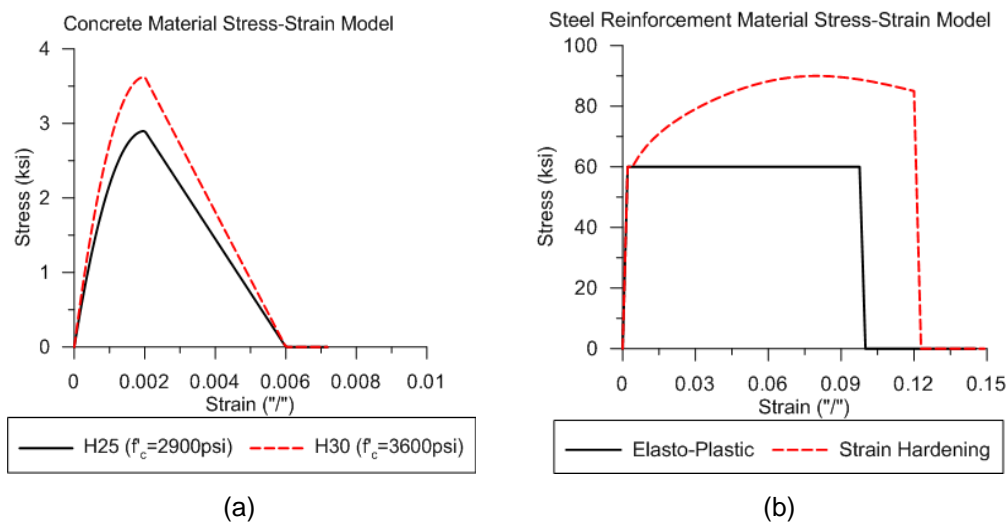


Figure A-17 BIAx program material models for: (a) H25 and H30 unconfined concrete; and (b) elasto-plastic and strain hardening reinforcing steel (Wallace and Ibrahim, 1996).

A.3 Estimation of Building Displacements

Expected roof drifts were estimated using a simplified approach consistent with the target displacement method in ASCE/SEI 41-06, *Seismic Rehabilitation of Existing Buildings* (ASCE, 2007), and the recommendations of Shimazaki and Sozen (1985):

- Ground motion records closest to a given building site were identified, and 2% damped linear displacement response spectra were computed for the two horizontal components of recorded ground motions.
- Building fundamental periods were estimated using a variety of methods, including consideration of the influence of concrete cracking. Uncracked periods (or periods at low-amplitude shaking) for each structure were initially estimated as $T = N/20$, where N is the number of stories above grade (Massone et al., 2012). Uncracked periods were amplified by $\sqrt{2}$ to account for wall section cracking.

- Estimated periods were used to determine the spectral displacement of a single-degree-of-freedom oscillator $\delta_{s dof}$, which was then translated to roof displacement assuming $\delta_{roof} = 1.5 \times \delta_{s dof}$.

A.3.1 Nearby Recording Stations

Recording station locations and orientations were reported by Boroschek et al. (2010). Four stations were selected based on their proximity to the seven case study buildings. These included the: (1) Concepción; (2) Viña del Mar-Centro; (3) Santiago-Centro; and (4) Santiago-Penalolen stations. A summary of building orientations (primary axis of building), nearest stations, and station orientations is provided in Figure A-18.

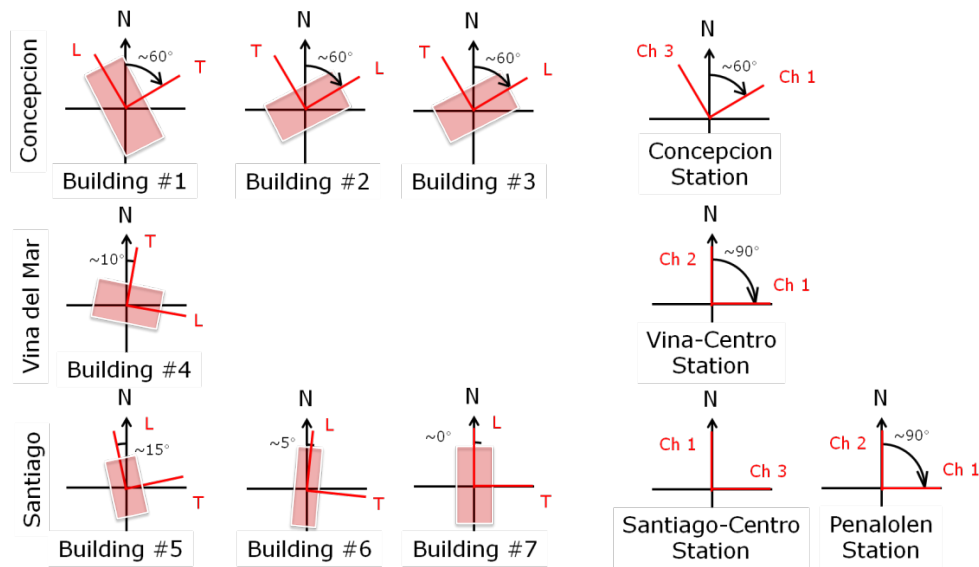


Figure A-18 Summary of building orientations, nearest recording stations, and station orientations.

Linear displacement response spectra for the four recording stations are shown in Figures A-19 through A-21. The channels used for determining response spectra correspond to the direction that most closely matches the wall orientations in the buildings. In each case, critical walls were oriented in the transverse direction of the building.

Spectra from both Santiago recording stations were considered for determining displacement demands on buildings in Santiago, and the larger of the spectral displacements determined for each period was used in the drift calculations.

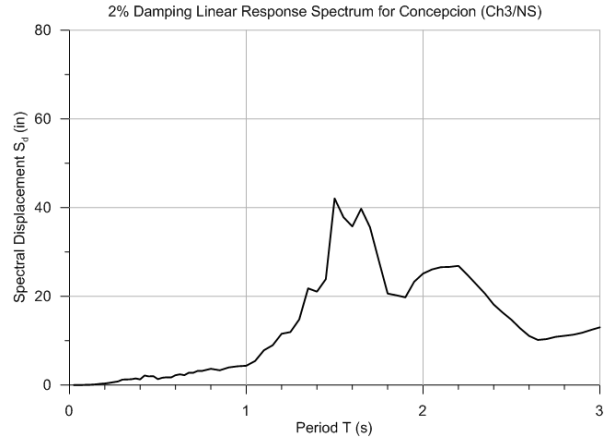
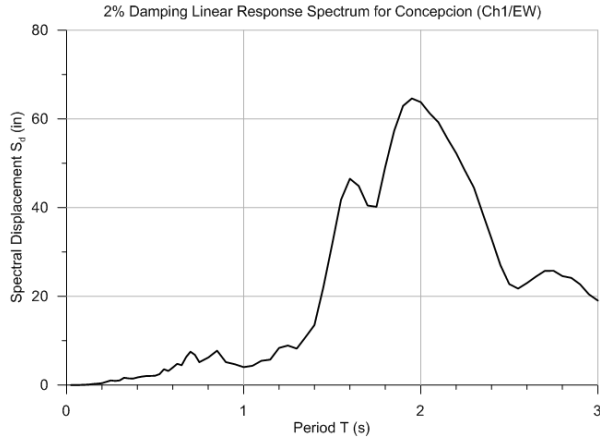


Figure A-19 Linear displacement response spectra for the Concepción station (data from University of Chile, 2012).

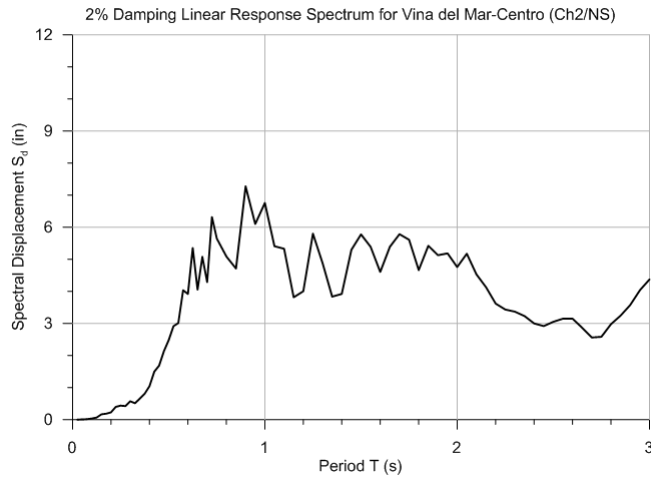


Figure A-20 Linear displacement response spectra for Viña del Mar-Centro station (data from University of Chile, 2012).

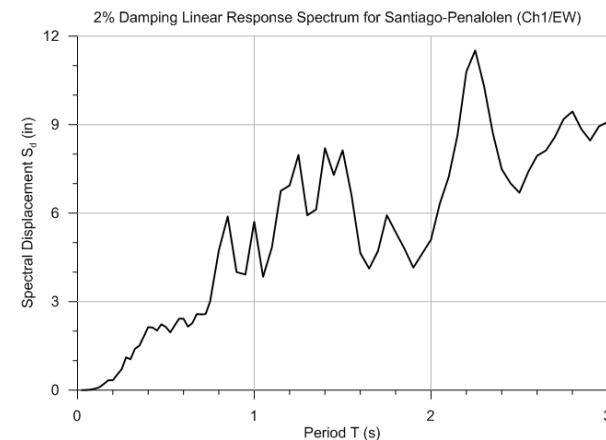
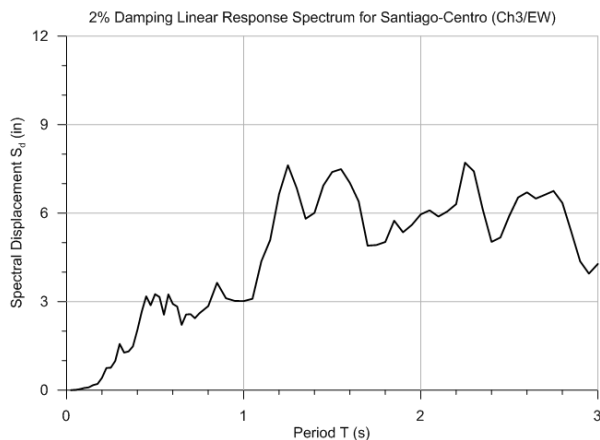


Figure A-21 Linear displacement response spectra for the Santiago-Centro station (left) and Santiago-Penalolen station (right) (data from University of Chile, 2012).

A.3.2 Building Period Estimates and Spectral Displacement Results

Uncracked building periods were approximated as $T = N/20$, where N is the number of stories above grade. Uncracked periods were amplified by $\sqrt{2}$ to account for wall section cracking. Where possible, results from other analysis methods were obtained for comparison. For example, results from two- and three-dimensional analyses were available for Alto Rio (Building No. 1) and Toledo (Building No. 4), and Mongolio (Building No. 7) was instrumented:

- For Alto Rio (Building No. 1), a two-dimensional nonlinear response history analysis was conducted on a “slice” of the building in the collapse direction to assess the potential impact of spectral shape on the roof displacement estimate (Tuna, 2012). A modal analysis in PERFORM 3D (CSI, 2013c) using material properties based on core tests and cracked section properties yielded a period of 0.69 seconds in the transverse direction. This value is similar to $N/20 = 0.75$ seconds obtained for this structure. Nonlinear time history plots of roof displacement using the Concepción record showed a forced frequency of roughly 3 cycles every 5 seconds as damage accrued, suggesting a period much higher than 0.69 seconds as shaking progressed. This likely would have pushed roof displacements much higher than estimated using the simplified models employed in this study.
- For Toledo (Building No. 4), a three-dimensional ETABS (CSI, 2013a) model prepared under a prior investigation (NIST, 2012) was used. Using uncracked section properties, the period calculated for translation in the transverse direction using the ETABS model was approximately 0.66 seconds. This value is significantly longer than $N/20 = 0.5$ seconds, and is much closer to $N/15 = 0.66$ seconds.
- Mongolio (Building No. 7) was instrumented with several accelerometers on various floor levels and the roof after the 2010 Maule earthquake. As reported by Lemnizter et al. (2012), more than twenty aftershocks were recorded in a one month period. Amplitudes of transfer functions of relative displacements on multiple floor levels indicate that the main frequency of building motion in the transverse direction was approximately 1.2 Hz, corresponding to a period of about 0.83 seconds. This value falls in between period estimates of $N/20 = 0.71$ seconds and $N/15 = 0.94$ seconds for a 10-story structure. The recorded frequency was obtained from relatively small aftershocks, so this value might represent the period of a wall that is not quite fully cracked, but is also not uncracked.

A comparison of periods determined using $N/20$ and other methods is provided in Table A-10.

Figures A-22 through A-25 show spectral displacement values obtained from uncracked periods ($N/20$) and cracked wall periods ($\sqrt{2} \times N/20$). In general, longer periods were usually associated with larger displacements, but if the estimated cracked section period fell in a trough in the associated displacement response spectrum, the largest spectral displacement value bounded by periods $N/20$ and $\sqrt{2} \times N/20$ periods was used in the analysis.

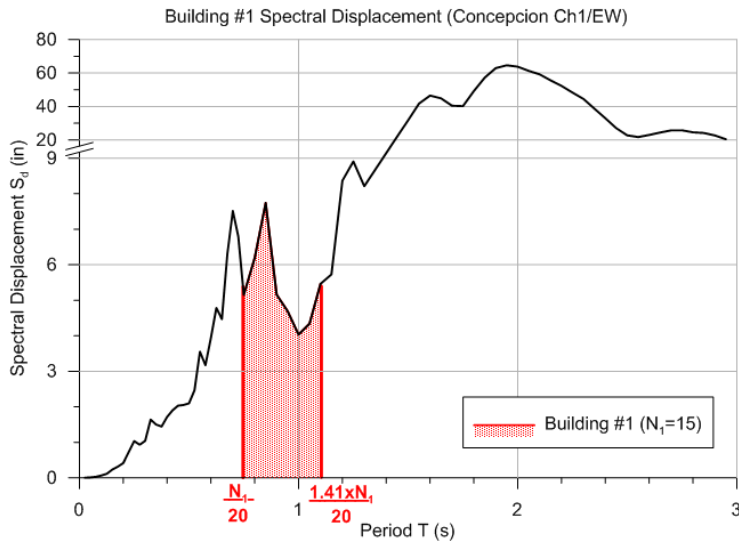


Figure A-22 Spectral displacements for Alto Rio (Building No. 1).

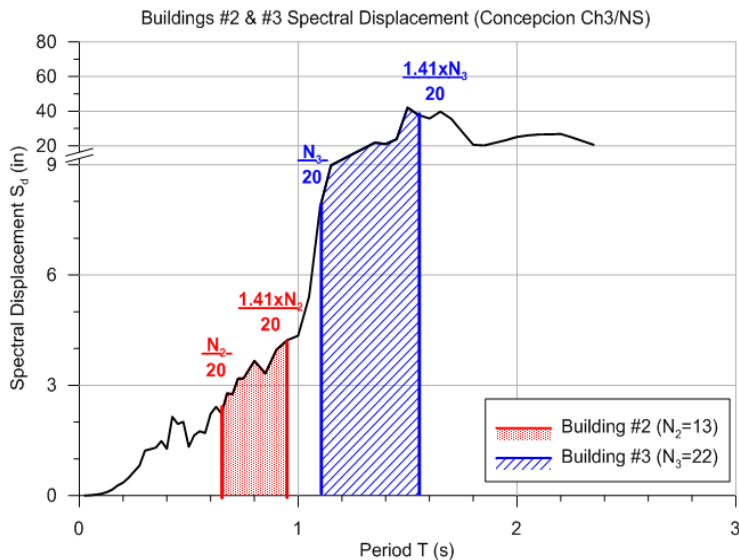


Figure A-23 Spectral displacements for Plaza del Rio Building B (Building No. 2) and Concepto Urbano (Building No. 3).

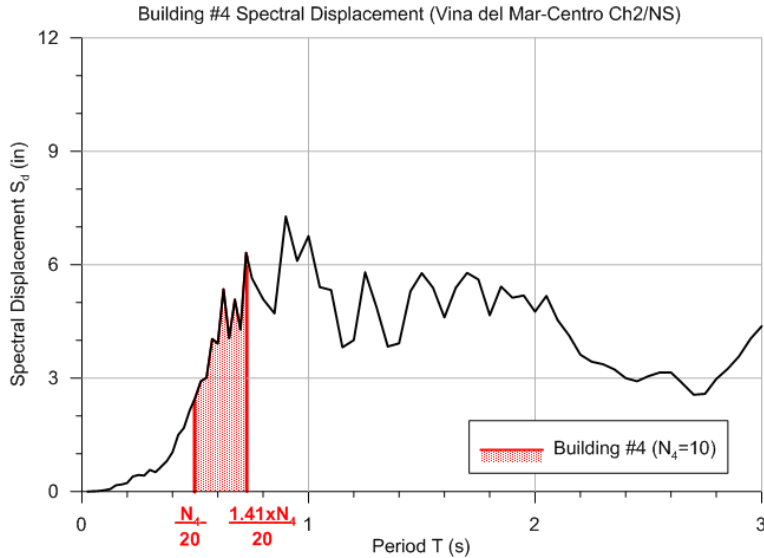


Figure A-24 Spectral displacements for Toledo (Building No. 4).

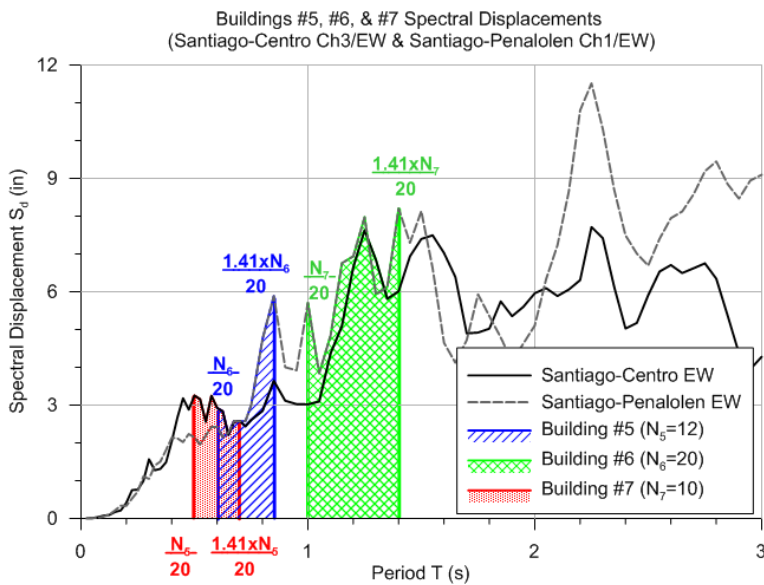


Figure A-25 Spectral displacements for Undisclosed Building A (Building No. 5), Undisclosed Building B (Building No. 6), and Mongolio (Building No. 7).

Period estimates for Alto Rio (Building No. 1) bound a peak spectral displacement value of about 8 inches (Figure A-22). The cracked period estimate is located just before spectral displacements begin to climb dramatically to approximately 40 inches at 1.5 seconds and more than 60 inches at 2.0 seconds. It is possible that the effective period of the structure increased beyond 1.1 seconds during the event, which may have drastically increased roof drift demands beyond simplified estimates.

Oriented perpendicular to Alto Rio (Building No. 1), the spectral displacement for Plaza del Rio Building B (Building No. 2) was about 4.5 inches for the cracked period estimate, and spectral displacements for Concepto Urbano (Building No. 3) were about 8 inches for the uncracked period and about 42 inches for the cracked period estimates. When transformed into roof displacement, drift demands are almost 3% for Concepto Urbano (Building No. 3) with cracked sections.

Spectral displacement for Toledo (Building No. 4) was about 6 inches for the cracked section period estimate of approximately 0.7 seconds. When transformed into roof displacement, drift demands are approximately 0.9%.

Displacement response spectra for the two stations adjacent to Undisclosed Building A (Building No. 5), Undisclosed Building B (Building No. 6), and Mongolio (Building No. 7) yielded similar spectral displacement values in the period ranges considered. Where they differed, higher values were used in the analyses.

Table A-10 summarizes estimated periods, spectral displacements, and roof drift ratios for the case study buildings. Calculated roof drift ratios typically fell between 0.4% and 1.0%, with the exception of Concepto Urbano (Building No. 3), which had the highest drift ratio at almost 3%.

Table A-10 Summary of Estimated Periods, Spectral Displacements, and Roof Drift Ratios

Building	Study Bldg. No.	Location	No. Stories	$N/20$ Period Estimate (s)	Roof Height (ft)	ASCE 7 Approx. Period ¹ (s)	$\sqrt{2} \times N/20$ Period Estimate (s)	Spectral Disp. (in)	Roof Drift Ratio
Alto Rio	1	Concepción	15	0.75	125.8	0.75	1.06	8	0.0082
Plaza del Rio (B)	2	Concepción	13	0.66	105.4	0.66	0.92	6	0.0053
Concepto Urbano	3	Concepción	22	1.10	182.8	0.99	1.56	42	0.0290
Toledo	4	Viña del Mar	10	0.50	85.8	0.56	0.71	7	0.0090
Undisclosed Building (A)	5	Santiago	12	0.60	99.6	0.63	0.85	6	0.0075
Undisclosed Building (B)	6	Santiago	20	1.00	166.3	0.93	1.41	8	0.0062
Mongolio	7	Santiago	10	0.50	92.3	0.60	0.71	3.2	0.0044

¹ Approximate period calculated using Equation 12.8-7 in ASCE/SEI 7-10 (ASCE, 2010). Used for comparison with values of $N/20$.

A.4 ACI 318 Special Boundary Element Trigger Checks

To evaluate ACI 318 triggers for special boundary elements, moment-curvature analyses using BIAX (Wallace and Ibrahim, 1996) were performed. An elasto-plastic material model was used for longitudinal steel reinforcement, and all concrete was assumed to be unconfined. Factored axial loads based on $P_u = 1.2D + 0.5L + 1.0E_v$ were applied to the critical wall section, along with roof drift demands estimated using the displacement response spectra. Moment-curvature analysis results were used to compare with special boundary element requirements in Section 21.9.6.2 of ACI 318 at each end of the selected walls.

In Section 21.9.6.2, the roof drift ratio shall not be taken less than 0.007 when checking the need for special boundary elements. Where calculated roof drift ratio demands did not exceed 0.007 in a building, two checks were made: (1) whether or not the calculated neutral axis from the BIAX analysis exceeded the trigger neutral axis depth (c_{trig}) using the ACI-specified minimum drift ratio of 0.007; and (2) whether or not the calculated neutral axis exceeded the trigger neutral axis depth using the estimated drift ratio, regardless of the code minimum value (designated c_{trig}^*). Three buildings had roof drift estimates that were less than 0.007: Plaza del Rio Building B (Building No. 2), Undisclosed Building B (Building No. 6), and Mongolio (Building No. 7).

A.4.1 Moment-Curvature Neutral Axis Depth Results

In the following sections, Tables A-11 through A-17 report the results of ACI 318 special boundary element trigger checks on concrete shear walls in Chilean case study buildings. Neutral axis depths are normalized by web length for easier comparison among different walls and buildings. Additionally, neutral axis analysis results are compared to trigger neutral axis depths as a ratio. Entries in bold text indicate where special boundary element requirements were triggered, and highlighted entries indicate correlation between the need for special boundary elements and the observed damage.

A.4.1.1 Alto Rio (Building No. 1)

Six transverse T-shaped or L-shaped walls were examined in Alto Rio (Building No. 1). As shown in Table A-11, the stems of all walls would have required ACI 318 special boundary elements for the estimated roof drift ratio. Walls 1.1, 1.3, and 1.5 exceeded ACI neutral axis depth triggers by at least 80%. These three walls were located on the north side of the building, with their stems oriented toward the exterior, and the building collapsed in this direction (Figure A-26).

Table A-11 Alto Rio (Building No. 1) Special Boundary Element Trigger Evaluation

Wall ID	Design Load $1.2D+0.5L+E_v$ (% $A_g f'_c$)	Roof Drift Ratio	Trigger Depth C_{trig}/I_{web}	North End c/C_{trig}	North End Damage	South End c/C_{trig}	South End Damage
1.1	11.8	0.0085	0.196	1.94	Collapse	0.21	Collapse
1.2	10.1	0.0085	0.196	0.17	Collapse	1.01	Collapse
1.3	14.0	0.0085	0.196	2.40	Collapse	0.12	Collapse
1.4	9.3	0.0085	0.196	0.06	Collapse	1.59	Collapse
1.5	10.1	0.0085	0.196	1.86	Collapse	0.11	Collapse
1.6	9.2	0.0085	0.196	0.11	Collapse	1.33	Collapse

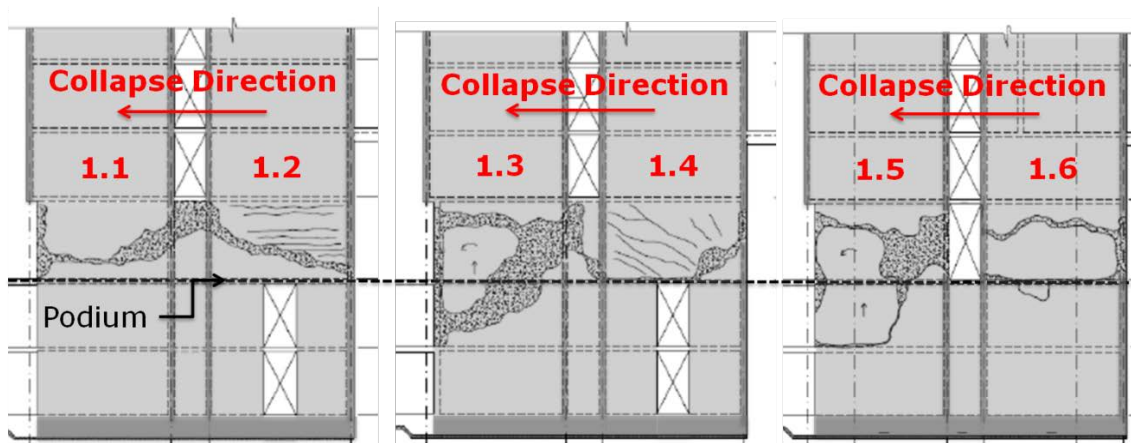


Figure A-26 Illustration of damage reported in walls of Alto Rio (Building No. 1) (IDIEM, 2010).

A.4.1.2 Plaza del Rio Building B (Building No. 2)

Three transverse walls were examined in Plaza del Rio Building B (Building No. 2), which was relatively undamaged in the earthquake. Because the roof drift ratio did not exceed 0.007 for this structure, two trigger evaluations were performed. As shown in Table A-12, the stem of the flanged wall (Wall 2.2) would have required ACI 318 special boundary elements at either drift ratio. The stem of the other flanged wall (Wall 2.3) and one end of the rectangular wall (Wall 2.1) were just under the limit for triggering special boundary element requirements based on the minimum drift ratio.

Table A-12 Plaza del Rio Building B (Building No. 2) Special Boundary Element Trigger Evaluation

Wall ID	Design Load $1.2D+0.5L+E_v$ (% $A_g f'_c$)	Roof Drift Ratio	Trigger Depth C_{trig}/I_{web}	Trigger Depth C_{trig^*}/I_{web}	North End c/C_{trig}	North End c/C_{trig^*}	North End Damage	South End c/C_{trig}	South End c/C_{trig^*}	South End Damage
2.1	10.5	0.0053	0.24	0.31	0.83	0.63	No	0.96	0.73	No
2.2	12.3	0.0053	0.24	0.31	1.44	1.09	No	0.18	0.14	No
2.3	10.7	0.0053	0.24	0.31	0.94	0.71	No	0.53	0.40	No

A.4.1.3 Concepto Urbano (Building No. 3)

Two transverse walls were examined in Concepto Urbano (Building No. 3), which was also relatively undamaged in the earthquake. As shown in Table A-13, both ends of rectangular Wall 3.1, and the stem of flanged Wall 3.2, significantly exceeded ACI neutral axis depth triggers, and would have required ACI 318 special boundary elements for the estimated roof drift ratio. Walls in this building were significantly larger than typical walls in other buildings investigated. Also, 135-degree hooks were specified for the termination of web horizontal bars. It is noted that the displacement response spectrum from which the roof drift was estimated is very steep in the period range of interest, and this building had the highest estimated drift ratio across all buildings. It is possible that the apparent discrepancy between the trigger evaluation and lack of observed damage could have been caused by overestimation of the roof drift ratio.

Table A-13 Concepto Urbano (Building No. 3) Special Boundary Element Trigger Evaluation

Wall ID	Design Load $1.2D+0.5L+E_v$ (% $A_g f'_c$)	Roof Drift Ratio	Trigger Depth c_{trig}/l_{web}	North End c/c_{trig}	North End Damage	South End c/c_{trig}	South End Damage
3.1	26.8	0.0285	0.058	6.3	No	6.3	No
3.2	14.4	0.0285	0.058	2.71	No	0.37	No

A.4.1.4 Toledo (Building No. 4)

Six transverse walls were examined in Toledo (Building No. 4), which was severely damaged in the earthquake. As shown in Table A-14, the stems of all flanged walls, and the ends of all rectangular walls, significantly exceeded ACI neutral axis depth triggers, and would have required ACI 318 special boundary elements for the estimated roof drift ratio. Walls in this building exhibited concrete crushing and bar buckling. Photos of observed damage revealed that there were no hoops or ties provided at the wall boundaries.

Table A-14 Toledo (Building No. 4) Special Boundary Element Trigger Evaluation

Wall ID	Design Load $1.2D+0.5L+E_v$ (% $A_g f'_c$)	Roof Drift Ratio	Trigger Depth c_{trig}/l_{web}	North End c/c_{trig}	North End Damage	South End c/c_{trig}	South End Damage
4.1	15.5	0.009	0.185	1.59	Yes	1.59	Yes
4.2	10.7	0.009	0.185	1.39	Yes	0.19	No
4.3	28.4	0.009	0.185	2.57	Yes	2.57	Yes
4.4	10.4	0.009	0.185	2.80	Yes	0.07	No
4.5	12.6	0.009	0.185	0.44	No	1.73	No
4.6	6.5	0.009	0.185	0.1	No	1.90	No

A.4.1.5 Undisclosed Building A (Building No. 5)

Four transverse walls in Undisclosed Building A (Building No. 5) were examined. Selected walls were identified in an independent damage report as exhibiting some level of damage in the first subterranean level. As shown in Table A-15, rectangular walls (Walls 5.1 and 5.2) had high axial load demands (about 40% $A_g f'_c$) and would have required ACI 318 special boundary elements at each end. These walls suffered crushing and bar buckling over the majority of the wall length. The flanged walls (Walls 5.3 and 5.4) had somewhat lower axial load demands (about 25% $A_g f'_c$), but triggered ACI 318 special boundary elements at the stems. Wall 5.3 experienced some spalling at the stem. Wall 5.4 exhibited significant crushing and bar buckling over the majority of the wall length.

Table A-15 Undisclosed Building A (Building No. 5) Special Boundary Element Trigger Evaluation

Wall ID	Design Load $1.2D+0.5L+E_v$ (% $A_g f'_c$)	Roof Drift Ratio	Trigger Depth C_{trig}/l_{web}	North End c/C_{trig}	North End Damage	South End c/C_{trig}	South End Damage
5.1	39.0	0.0075	0.22	2.05	Yes	2.05	Yes
5.2	43.3	0.0075	0.22	2.29	Yes	2.29	Yes
5.3	24.1	0.0075	0.22	2.67	Slight	0.46	No
5.4	20.2	0.0075	0.22	0.08	No	2.98	Yes

A.4.1.6 Undisclosed Building B (Building No. 6)

Three transverse walls were examined in Undisclosed Building B (Building No. 6), all of which were damaged in the earthquake. Because the roof drift ratio did not exceed 0.007 for this structure, two trigger evaluations were performed. All walls had flanges, high axial load demands (up to 45% $A_g f'_c$), and would have required ACI 318 special boundary elements in the stems at either roof drift ratio. As shown in Table A-16, Walls 6.2 and 6.3 had crushed boundary elements and buckled longitudinal bars in the stem, extending through the web and into the flange.

Table A-16 Undisclosed Building B (Building No. 6) Special Boundary Element Trigger Evaluation

Wall ID	Design Load $1.2D+0.5L+E_v$ (% $A_g f'_c$)	Roof Drift Ratio	Trigger Depth C_{trig}/l_{web}	Trigger Depth C_{trig}^*/l_{web}	North End c/C_{trig}	North End c/C_{trig}^*	North End Damage	South End c/C_{trig}	South End c/C_{trig}^*	South End Damage
6.1	22.7	0.0062	0.24	0.27	2.32	2.06	Slight	0.15	0.13	No
6.2	28.1	0.0062	0.24	0.27	2.59	2.30	Yes	0.43	0.38	Yes
6.3	45.1	0.0062	0.24	0.27	3.34	2.96	Yes	1.79	1.58	Yes

Observed damage in the flanged end of these walls was probably not due to boundary element crushing at that end, but probably due to an “unzipping” of the wall after the

boundary in the stem crushed. Wall 6.1 exhibited minor spalling near the roof interface.

A.4.1.7 Mongolio (Building No. 7)

Two transverse walls were examined in Mongolio (Building No. 7). Neither wall was damaged in the earthquake. Because the roof drift ratio did not exceed 0.007 for this structure, two trigger evaluations were performed. As shown in Table A-17, neither wall exceeds ACI 318 special boundary elements triggers at either the estimated drift ratio or the specified minimum drift ratio. No boundary element damage was reported in these walls.

Table A-17 Mongolio (Building No. 7) Special Boundary Element Trigger Evaluation

Wall ID	Design Load $1.2D+0.5L+E_v$ (% $A_g f'_c$)	Roof Drift Ratio	Trigger Depth C_{trig}/l_{we} b	Trigger Depth C_{trig}^*/l_{we} b	North End c/C_{trig}	North End c/C_{trig}^*	North End Damage	South End c/C_{trig}	South End c/C_{trig}^*	South End Damage
7.1	9.4	0.004 3	0.24	0.38	0.49	0.31	No	0.57	0.36	No
7.2	5.6	0.004 3	0.24	0.38	0.11	0.07	No	0.76	0.48	No

A.4.1.8 Summary

In general, correlation between ACI 318 special boundary element triggers and observed damage in the case study buildings was good. This can be seen by the highlighted entries in Tables A-11 through A-17. In most cases, the need for special boundary elements corresponded with damage at the wall boundary. Similarly, wall sections that did not exceed special boundary element triggers were undamaged at the wall boundary. Notable exceptions include Concepto Urbano (Building No. 3) in which the wall sections significantly exceeded special boundary element triggers at the estimated roof drift ratio, but were relatively undamaged in the earthquake. A possible explanation for this discrepancy is that the building drift ratio was overestimated in the case of this building. Other exceptions occur in Alto Rio (Building No. 1) in which wall flanges did not exceed special boundary element triggers, yet were noted as damaged. It is possible that the impending collapse of the degrading building resulted in extensive damage across all walls, masking individual cases where wall boundaries might have otherwise not been damaged.

A.5 Review of Plastic Hinge Lengths

Wall damage observed in Chile tended to concentrate over a relatively short height (e.g., 2 to 3 wall thicknesses). A study of plastic hinge length was undertaken to reassess the assumption of $l_p = 0.5l_w$.

A.5.1 Literature Review

Section 21.9.6.2 of ACI 318 is based on an assumed plastic hinge length equal to half the length of the wall (i.e., $l_p = 0.5l_w$). ASCE/SEI 41-06 also uses a plastic hinge length equal to half the length of the wall, as did its predecessor document, FEMA 356, *Prestandard and Commentary for the Seismic Rehabilitation of Buildings* (FEMA, 2000). ASCE 41-06 and FEMA 356 limit the plastic hinge length to less than one story height, but this limitation is not included in ACI 318.

Kabeyasawa et al. (1983) assumed uniform axial strains at wall boundaries over one story height, h_w , which is a practical limit given that walls in Japanese buildings tend to be long and have low aspect ratios, h_w/l_w . Other lengths also have been suggested, including $h_w/8$ (Orakcal and Wallace, 2006), and $0.3l_w$ (Tabata et al., 2003). A value of $2.5t_w$ (Takahashi et al., 2011) is intended to be used for walls with light transverse reinforcement at wall boundaries, as in the case of special structural walls detailed in accordance with Section 21.9.6.5, or ordinary structural walls.

More complex relationships for plastic hinge lengths have been recommended, such as Baker and Amarakone (1965) derived from beam and column tests, which considers both member length and member depth (i.e., $l_p = C \times z^{0.25} \times d^{0.75}$). Paulay and Priestley (1993) recommended a simpler plastic hinge length model that scales depending on both wall length and aspect ratio (i.e., $l_p = (0.2 + 0.044A_r) \times l_w$).

Other relationships, most of them derived from beam and column tests, include: $l_p = 0.25d + 0.075z$ (Sawyer, 1964); $l_p = 0.5d + 0.05z$ (Mattock, 1967); $l_p = 0.12z + 0.014d_b f_y$ (Panagiotakis and Fardis, 2001); and $l_p = 0.5l_w + 0.022d_b f_y$ (Hines et al., 2004). Some of these latter relations include a component based on the strength of steel reinforcement, which is related to “yield penetration.” Bae and Bayrak (2008) compare several of these relationships for various shear span-depth ratios (i.e., aspect ratios). Results presented in Figure 2-4 (Chapter 2) are similar to a figure provided in Bae and Bayrak, and indicate a wide-range of recommended values for plastic hinge length.

A.6 Longitudinal Bar Buckling Assessments

Typical vertical spacing of transverse reinforcement in the boundary zones of structural walls in Chile resulted in ratios of hoop (or tie) spacing to longitudinal bar diameter, s/d_b , between 8 and 11. For comparison, ACI 318 requirements for spacing of transverse reinforcement include a ratio of $s/d_b = 6$ as one of a series of limits. Large s/d_b ratios reduce confinement of concrete, and leave longitudinal reinforcement more susceptible to buckling. The following study was undertaken to investigate the relationship between concrete crushing and bar buckling, and to estimate the likelihood of the occurrence of longitudinal bar buckling at the boundaries of structural walls in Chilean case study buildings.

A.6.1 Criterion for Bar Buckling Assessment

The criterion used to assess bar buckling behavior is based on monotonic and cyclic tests on isolated reinforcing bar coupons for various s/d_b ratios in an experiment by Rodriguez et al. (1999). In this experiment, the onset of buckling was defined as when the difference in strain readings on opposite sides of the rebar coupon exceeded 20% of the total of the minimum and maximum strain in the cycle. Tests indicated that bars subjected to cyclic loading were more prone to buckling failures than bars subjected to monotonic loading. Rodriguez et al. (1999) introduces the parameter ϵ_p^* , which measures the amount of bar strain from the point of reloading bars in compression to the point when bars begin to buckle (Figure A-27). For cyclic loading, Rodriguez et al. (1999) proposed the use of parameter ϵ_p^* as an indicator of the onset of bar buckling. The variation of ϵ_p^* versus ratios of unbraced length to bar diameter, S_h/D (i.e., s/d_b) is presented in Figure A-28.

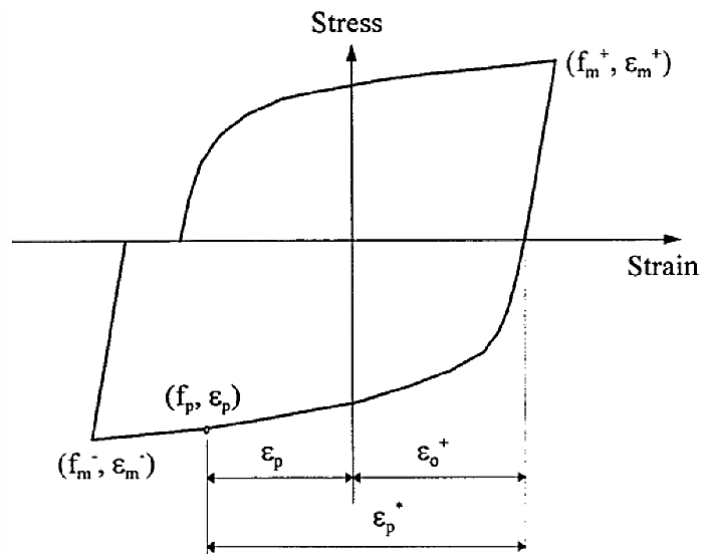


Figure A-27 Definition of parameter ϵ_p^* , which measures the amount of bar strain from the point of reloading bars in compression to the point when the bars begin to buckle (Rodriguez et al., 1999).

In Figure A-28, the trend of earlier onset of bar buckling for larger unbraced lengths can be seen in that the value of the parameter ϵ_p^* drops substantially for large S_h/D (i.e., s/d_b) ratios. This suggests that very low ϵ_p^* values would be obtained for typical s/d_b ratios (e.g., 8 to 11) in wall boundaries of typical Chilean buildings.

Use of this criterion for assessing observed behavior in concrete walls in Chile is limited in that it is based on tests of isolated bars (i.e., tested bars were not embedded in concrete). In concrete walls with large s/d_b ratios, the presence of cover concrete could provide some resistance to buckling. Also, transverse hoops (or ties) may not provide the same level of fixity for longitudinal reinforcement as was provided in the boundary conditions for the tested bars.

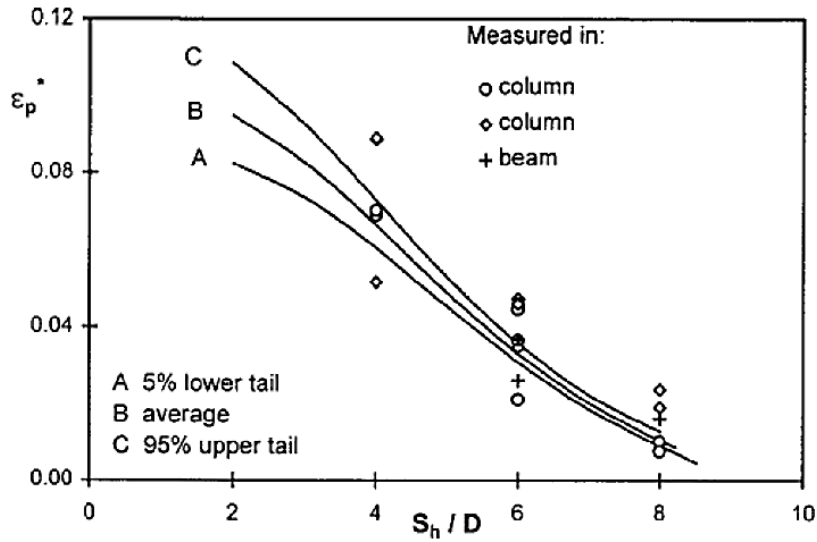


Figure A-28 Parameter ϵ_p^* versus ratios of unbraced length to bar diameter (S_n/D) (Rodriguez et al., 1999).

It should be noted that buckling of an individual bar (or pair of bars) at a wall boundary may not lead to significant (or observed) strength loss in the wall, especially if there is a large number of longitudinal bars distributed along the length of the boundary region. Wall sections have demonstrated this behavior in tests. For example, in test specimen RW1 (Thomsen and Wallace, 1995 and 2004), bar buckling was observed to initiate at 1.0% to 1.5% drift, yet the specimen was able to sustain several cycles of 2.0% drift prior to significant strength loss in the first cycle at 2.5% drift.

A.6.2 Assessment of Bar Buckling at Wall Boundaries in Chilean Buildings

In this investigation, approximate analyses were used to estimate ϵ_p^* for each wall, and then the likelihood of longitudinal bar buckling at wall boundaries in Chilean case study buildings was assessed using the criterion based on Rodriguez et al. (1999).

First, a set of moment-curvature analyses using BIAX were performed at the critical section for each wall. Critical sections were typically located at wall setbacks at grade, or one level below grade. Nonlinear material stress-strain relations and best estimates for the quantity and distribution of vertical (boundary and web) and boundary transverse reinforcement were used for the analyses. The expected axial load was based on the load combination $P_e = D + 0.25L$.

The parameter ϵ_p^* (referred to as the “buckling strain indicator”) was determined for the outermost layer of boundary reinforcement. Since response-history analyses were

not performed, strain histories in the reinforcement were not available. Instead the parameter ϵ_p^* was estimated using the following process:

- It was assumed that buildings would experience approximately equal roof displacements for positive and negative cycles of loading parallel to the wall web.
- The drift-curvature Equation 2-5 (Chapter 2) was used to relate moment-curvature results to drift demands. Use of Equation 2-5 requires assumptions on the yield curvature (i.e., the curvature associated with first yield of outermost longitudinal reinforcement), the seismic loading pattern experienced by the structure (e.g., inverted triangular distribution, representative of 1st mode behavior), and plastic hinge length (e.g., l_p equal to the smaller of $0.5l_w$ or the story height, consistent with other investigations on the walls in these buildings).
- The buckling strain indicator, ϵ_p^* , was estimated as described below, for an asymmetric flanged wall, and illustrated in Figure A-29):
 - Moment-curvature analyses were used to calculate the web boundary compression strain associated with an arbitrary level of drift causing flange tension.
 - Moment-curvature analyses were used to calculate the maximum tensile strain in web boundary reinforcement associated with an equal (but in the opposite direction) level of drift causing flange compression.
 - Tensile and compressive strains in the web were added, and then adjusted for elastic strain recovery and compressive strain gradient to determine ϵ_p^* .

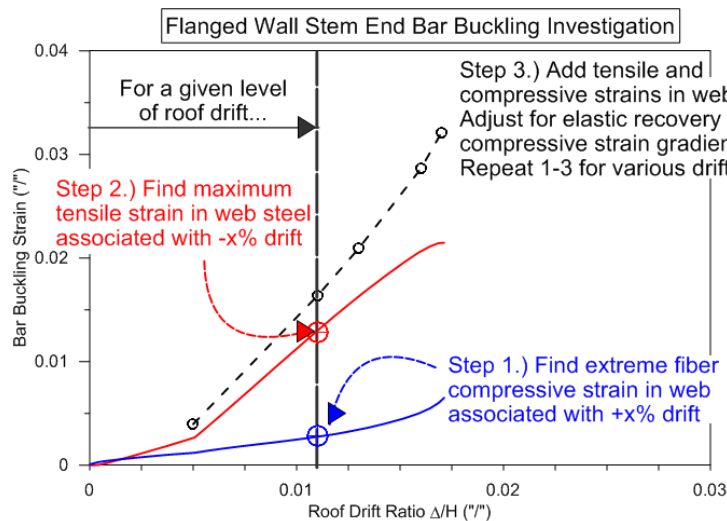


Figure A-29 Illustration of process for estimating ϵ_p^* in the web of a flanged wall.

Repeating this process for a range of drift levels generates a relation for ϵ_p^* , which can easily be repeated for the opposite wall boundary. Once ϵ_p^* values are evaluated

for a set of drift ratios, the relationship suggested by Rodriguez et al. (1999) is used to determine the drift ratio associated with concrete crushing and rebar buckling. This process is depicted in Figure A-30.

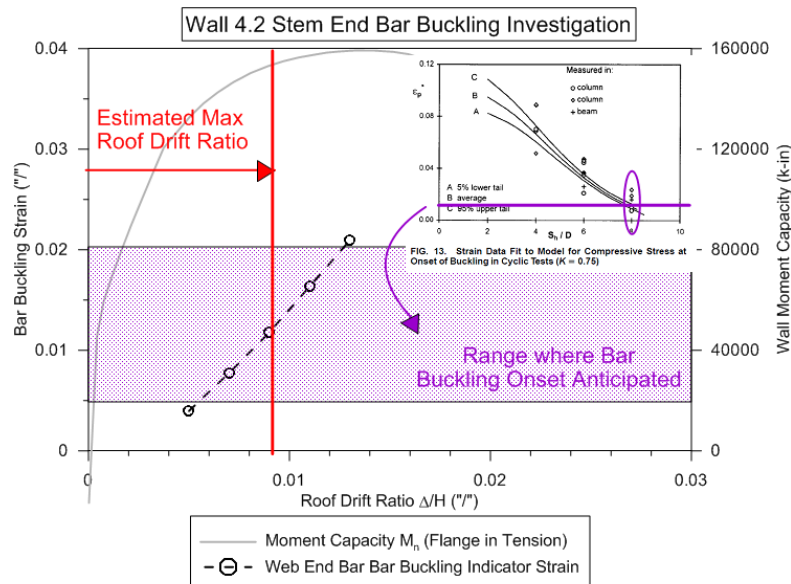


Figure A-30 Illustration of the use of Rodriguez et al. (1999) to determine the drift ratio associated with concrete crushing and bar buckling.

Figure A-30 includes a moment capacity versus drift curve along with a curve showing values of the buckling strain indicator, ϵ_p^* , calculated at various drift ratios. The shaded region identifies the range over which isolated bar buckling would be expected to initiate based on Rodriguez et al. (1999). The moment capacity versus drift curve is plotted considering concrete failure (i.e., crushing) in compression or reinforcement failure (i.e., rupture) in tension, but no buckling limit state is considered. By comparing the moment capacity curve to buckling indicator curve, it is possible to assess the drift ratios at which bar buckling and concrete crushing would be anticipated, and which is more likely to occur first.

In Figure A-30, bar buckling is expected at bar strains in the range between 0.005 and 0.02. From the buckling indicator curve, onset of buckling might occur at roof drift ratios as low as 0.005 (0.5% drift), and is likely to occur at roof drift ratios between 0.01 and 0.012 (1% and 1.2% drift). From the moment capacity curve, crushing of the concrete would not be expected until the roof drift ratio reaches approximately 0.016 (1.6% drift). The buckling indicator strain at the expected maximum roof drift ratio is approximately 0.011 (1.1%), which is well beyond the threshold minimum buckling strain of 0.005 from Rodriguez et al. (1999). As a result, longitudinal bars in the boundary of this example would be expected to buckle before the concrete crushes in compression.

A.6.3 Building-Specific Results

Building-specific results for bar buckling assessments are summarized in the sections that follow. Transverse hoop (or tie) spacing is provided for each wall, based upon construction documents and field reconnaissance. In some walls, hoops (or ties) were not provided. In these cases the reported s/d_b value represents the spacing of the horizontal web reinforcement used to confine boundary zone longitudinal bars, and is indicated as such in the tables.

Upper and lower bound estimates for the onset of bar buckling for a particular wall s/d_b value are given in the figures and tables. These are based on the confidence curves that bound the trend established in Rodriguez et al. (1999). Calculated strains at the estimated maximum roof drift ratio, ϵ_p^{*calc} , are read from the buckling indicator curves at the maximum estimated roof drift ratio, which is based on the assumption of equal roof displacements for positive and negative cycles of loading parallel to the wall web.

Each figure includes a plot of moment capacity versus drift for each wall, represented by a solid line. Moment capacity values are listed on the right vertical axis. Bar buckling indicator strains are illustrated by a dotted line, and buckling indicator strain values are listed on the left vertical axis. The shaded region corresponds to the range over which bar buckling is expected for the wall s/d_b ratio. The Rodriguez et al. (1999) relation for bar buckling versus s/d_b ratio is inset into each figure, for reference.

For walls with s/d_b ratio greater than 8 (the maximum ratio investigated by Rodriguez et al.), the lower estimate for the strain at which bar buckling initiates is set as 0.005 (0.5%) and the upper estimate is 0.015 (1.5%). As the calculated reloading strain, ϵ_p^{*calc} , in the longitudinal bars increases from the lower bound estimate to the upper bound estimate for initiation of bar buckling, it is considered more likely that the bars will buckle.

In the tables that follow, entries in bold text identify where strains indicate that bar buckling would be initiated, and highlighted entries identify correlation between bar buckling strains and observed bar buckling damage.

A.6.3.1 Alto Rio (Building No. 1)

As shown in Table A-18, ratios of spacing of horizontal web reinforcement relative to longitudinal bar diameters (s/d_b) are large in Alto Rio (Building No. 1).

Table A-18 Alto Rio (Building No. 1) Bar Buckling Assessment

Wall ID	Expected Load $D+0.25L$ ($\%A_g f_c$)	Web s/d_b Ratio ¹	ϵ_p^* Lower Estimate	ϵ_p^* Upper Estimate	Calc. Strain $\epsilon_p^*_{calc}$	Bar Buckling Expected?	Bar Buckling Observed?
1.1	8.8	9.1	0.005	0.015	0.009	Yes	Collapse ²
1.2	7.6	8.0	0.005	0.020	0.009	Yes	Collapse ²
1.3	10.5	9.1	0.005	0.015	0.009	Yes	Collapse ²
1.4	7.0	9.1	0.005	0.015	0.011	Yes	Collapse ²
1.5	7.5	11.1	0.005	0.015	0.008	Yes	Collapse ²
1.6	6.9	11.1	0.005	0.015	0.009	Yes	Collapse ²

¹ Based on horizontal web reinforcement. No hoops (or ties) provided.

² Bar buckling is presumed to have occurred as part of the collapse.

Buckling strain indicators and moment capacity curves associated with wall webs in compression are shown in Figures A-31 through A-36. In even-numbered walls, web compression corresponds with building drift in the direction of reference North. In odd-numbered walls, web compression corresponds to drift to the opposite direction (reference South).

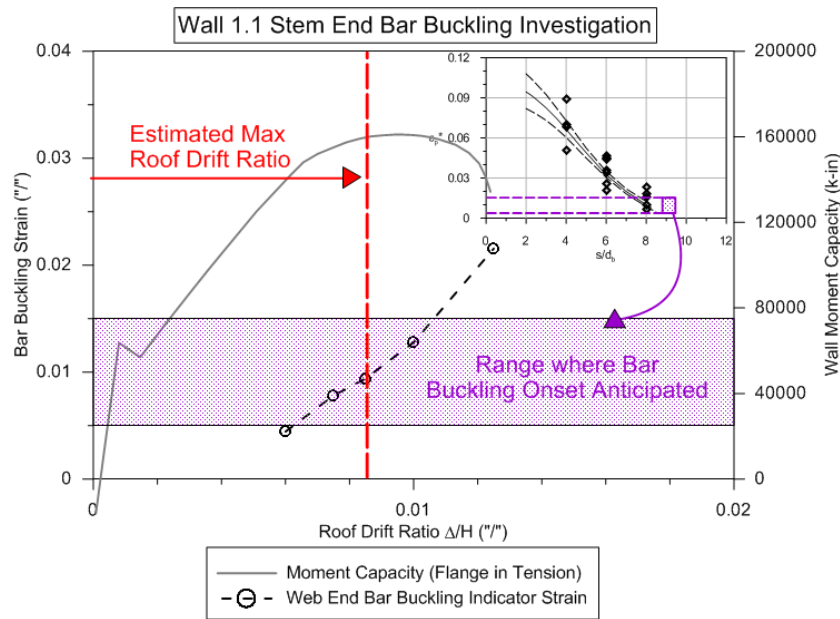


Figure A-31 Moment capacity and buckling strain indicator relations versus roof drift ratio for Wall 1.1.

At the estimated drift demand calculated for Alto Rio (Building No. 1), all walls are approaching their peak moment capacity, and each wall experiences strain levels that are in the range where onset of buckling might be expected. If drift levels exceeded calculated demands, both concrete crushing and bar buckling would be expected to occur.

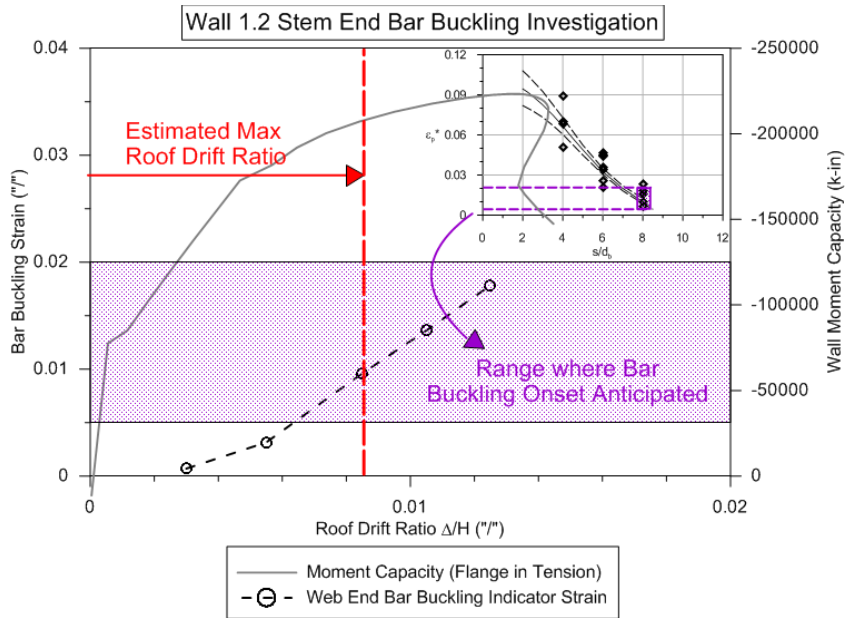


Figure A-32 Moment capacity and buckling strain indicator relations versus roof drift ratio for Wall 1.2.

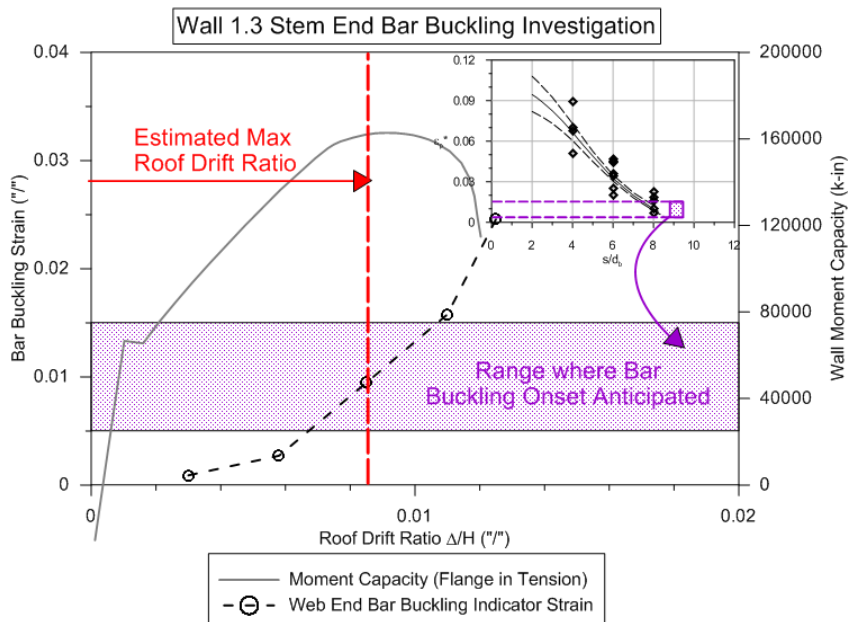


Figure A-33 Moment capacity and buckling strain indicator relations versus roof drift ratio for Wall 1.3.

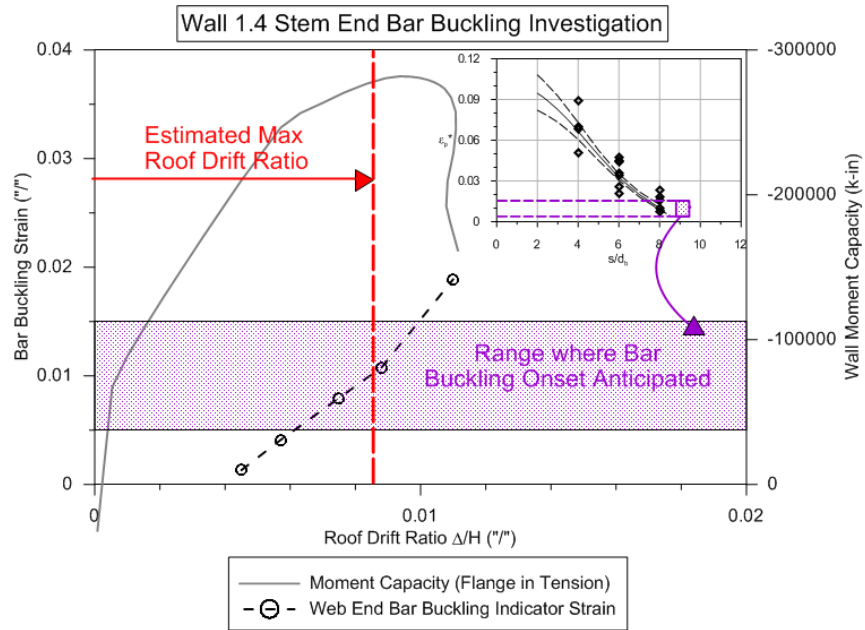


Figure A-34 Moment capacity and buckling strain indicator relations versus roof drift ratio for Wall 1.4.

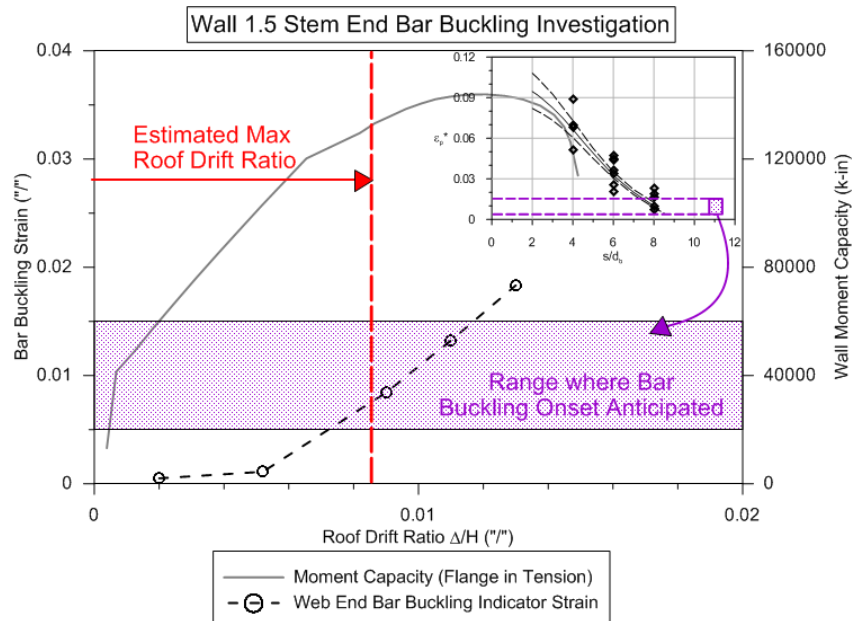


Figure A-35 Moment capacity and buckling strain indicator relations versus roof drift ratio for Wall 1.5.

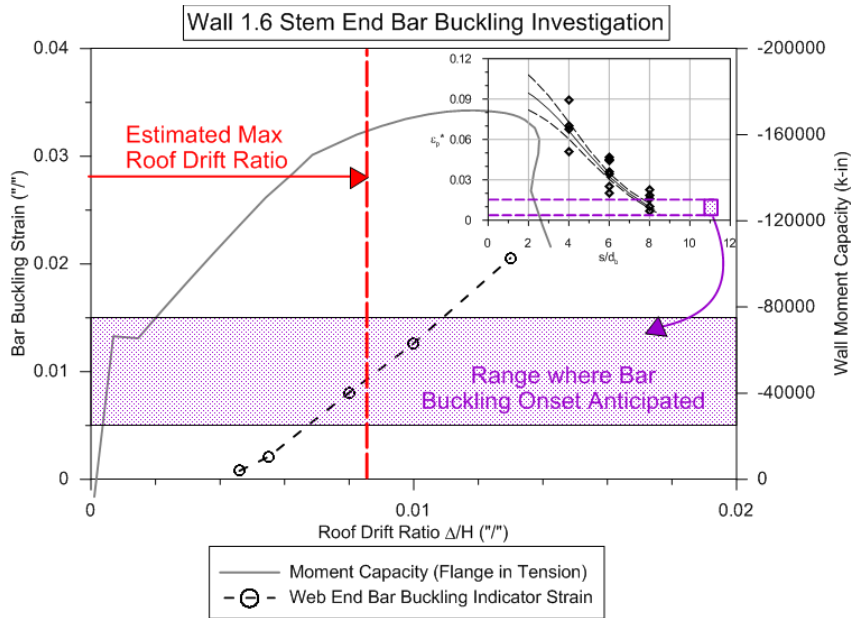


Figure A-36 Moment capacity and buckling strain indicator relations versus roof drift ratio for Wall 1.6.

A.6.3.2 Plaza del Rio Building B (Building No. 2)

Plaza del Rio Building B (Building No. 2) did not suffer the severe damage experienced by the adjacent Plaza del Rio Building A. As shown in Table A-19, despite having large spacing to longitudinal bar diameter ratios (e.g., above 11 for all walls considered), bar buckling indicator strains did not reach the levels where onset of bar buckling would be expected.

Table A-19 Plaza del Rio Building B (Building No. 2) Bar Buckling Assessment

Wall ID	Expected Load	Web s/d_b Ratio	ϵ_p^* Lower Estimate	ϵ_p^* Upper Estimate	Calc. Strain $\epsilon_p^*_{calc}$	Bar Buckling Expected?	Bar Buckling Observed?
	$D+0.25L$ ($\%A_g f'_c$)						
2.1	7.7	11.1	0.005	0.015	0.0006	No	No
2.2	9.0	11.1	0.005	0.015	0.003	No	No
2.3	7.8	11.1	0.005	0.015	0.001	No	No

Buckling strain indicators and moment capacity curves associated with Walls 2.1 to 2.3 are shown in Figures A-37 through A-39.

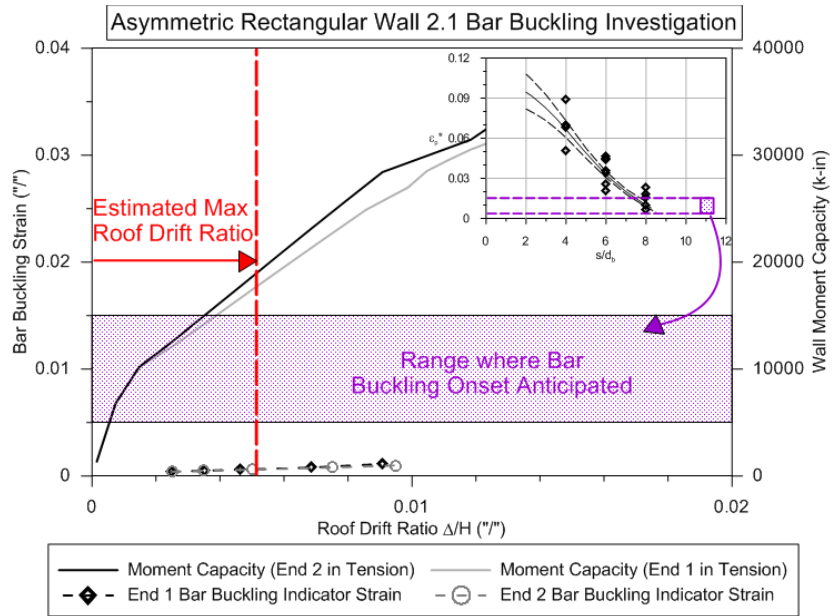


Figure A-37 Moment capacity and buckling strain indicator relations versus roof drift ratio for Wall 2.1.

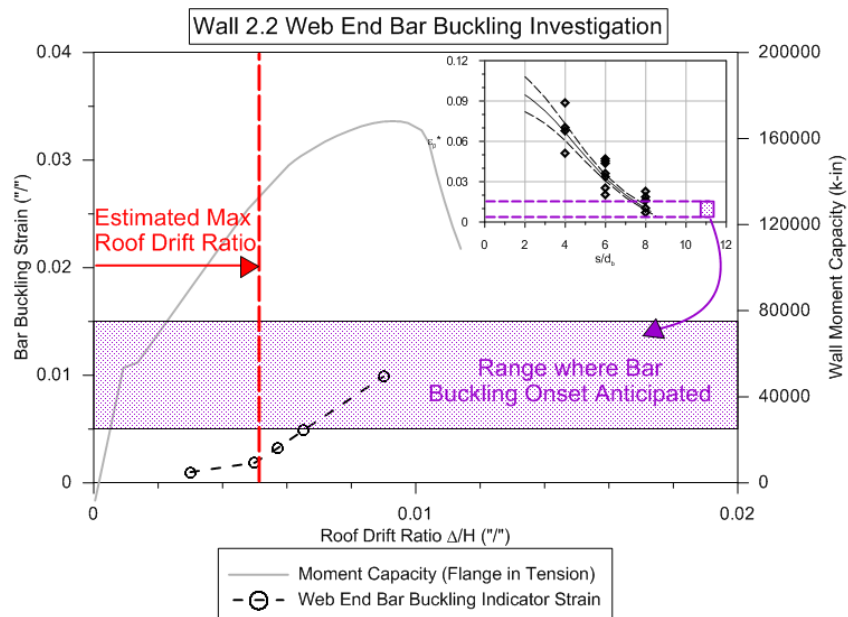


Figure A-38 Moment capacity and buckling strain indicator relations versus roof drift ratio for Wall 2.2.

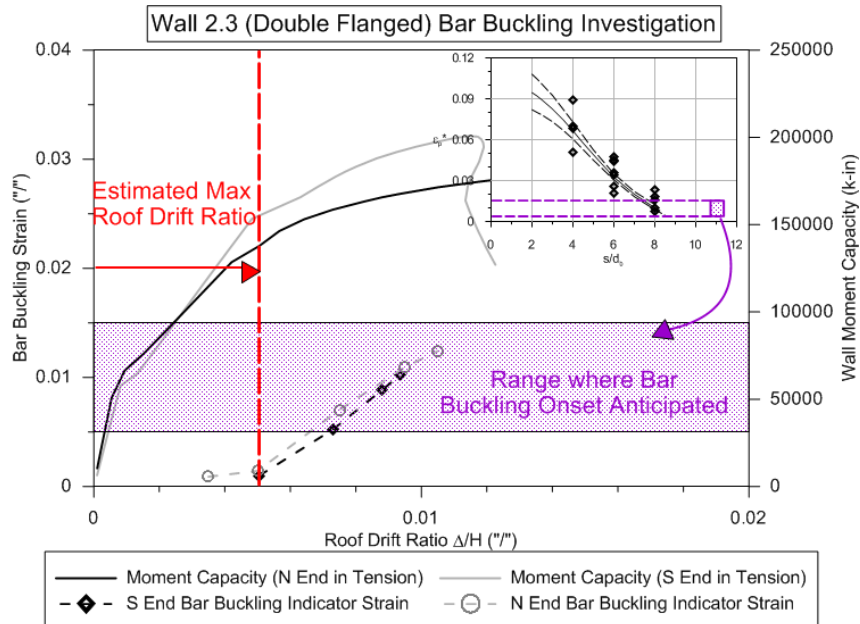


Figure A-39 Moment capacity and buckling strain indicator relations versus roof drift ratio for Wall 2.3.

A.6.3.3 Concepto Urbano (Building No. 3)

Results for Concepto Urbano (Building No. 3) are not consistent with the observed behavior of the building. Based on the simplified displacement demand approach for determining expected roof drifts, the drift ratio for this building was nearly 3%, as shown in Table A-20. As noted previously, the displacement response spectrum from which the roof drift was estimated is very steep in the period range of interest, and it is possible that the apparent discrepancy is due to overestimation of the roof drift ratio.

Table A-20 Concepto Urbano (Building No. 3) Bar Buckling Assessment

Wall ID	Expected Load	Web s/d_b Ratio ¹	ϵ_p^*		Calc. Strain $\epsilon_p^*_{calc}$	Bar Buckling Expected?	Bar Buckling Observed?
	$D+0.25L$ ($\%A_g f'_c$)		Lower Estimate	Upper Estimate			
3.1	19.6	6.8	0.02	0.03	>0.015	No ²	No
3.2	10.5	6.8	0.02	0.03	>0.025	No ²	No

¹ Based on horizontal web reinforcement. No hoops (or ties) provided.

² Concrete crushing likely to occur prior to estimated roof drift ratio.

Drawings called for horizontal web reinforcement to wrap around longitudinal boundary reinforcement and terminate at the far side of the wall with 135-degree hooks. With a relatively small vertical spacing, and correspondingly smaller s/d_b ratios, the walls evaluated in Concepto Urbano (Building No. 3) would not be expected to exhibit bar buckling until after the concrete crushed (as long as the

horizontal reinforcement remained engaged with the confined core of the wall boundary). Buckling strain indicators and moment capacity curves associated with Walls 3.1 and 3.2 are shown in Figures A-40 and A-41.

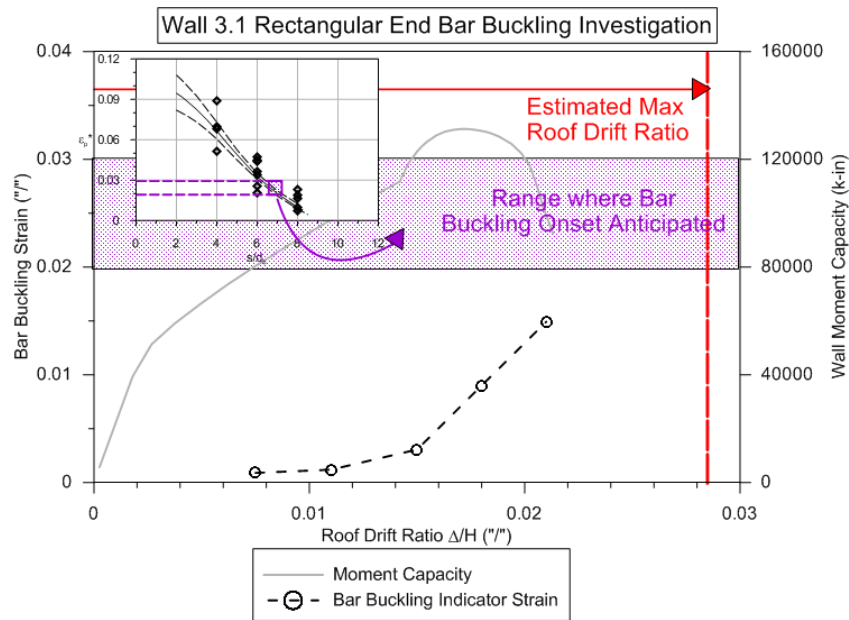


Figure A-40 Moment capacity and buckling strain indicator relations versus roof drift ratio for Wall 3.1.

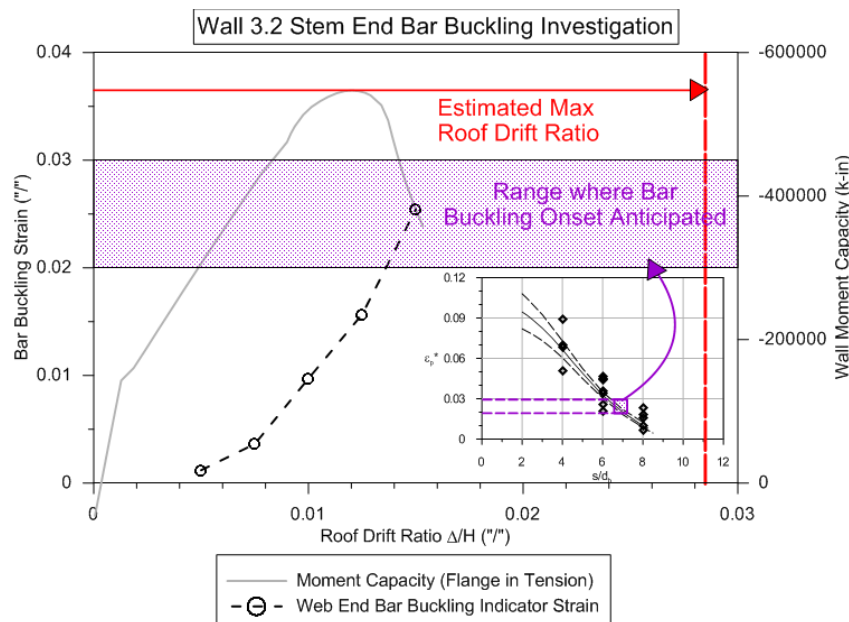


Figure A-41 Moment capacity and buckling strain indicator relations versus roof drift ratio for Wall 3.2.

A.6.3.4 Toledo (Building No. 4)

With differing longitudinal bar diameters and spacing of horizontal web reinforcement, the walls in Toledo (Building No. 4) had different s/d_b ratios. Hoops or ties were not provided at the boundaries of these walls. As shown in Table A-21, some walls (e.g., Walls 4.1 and 4.3), would not be expected to exhibit bar buckling at the expected roof drift ratio. Other walls (e.g., Walls 4.5 and 4.6) would be expected to exhibit bar buckling prior to concrete crushing. It appears that Wall 4.4 was especially susceptible to concrete crushing at the expected roof drift level.

Table A-21 Toledo (Building No. 4) Bar Buckling Assessment

Wall ID	Expected Load $D+0.25L$ ($\%A_g f'_c$)	Web s/d_b Ratio ¹	ϵ_p^* Lower Estimate	ϵ_p^* Upper Estimate	Calc. Strain $\epsilon_p^*_{calc}$	Bar Buckling Expected?	Bar Buckling Observed?
4.1	11.8	6.4	0.02	0.035	0.002	No	Yes
4.2	8.1	8.0	0.005	0.02	0.011	Yes	Yes
4.3	21.9	11.1	0.005	0.015	0.001	No	Yes
4.4	7.8	6.3	0.02	0.035	0.018	No ²	Yes
4.5	9.5	11.4	0.005	0.015	0.007	Yes	No
4.6	5.1	10.0	0.005	0.015	0.008	Yes	No

¹ Based on horizontal web reinforcement. No hoops (or ties) provided.

² Concrete crushing likely to occur.

Buckling strain indicators and moment capacity curves associated with Walls 4.1 to 4.6 are shown in Figures A-42 through A-47. The building was severely damaged in the earthquake. In Walls 4.1, 4.3, and 4.4, calculated strains do not suggest that bar buckling would be initiated, but in the absence of hoops or ties at the wall boundaries, it is likely that effective s/d_b ratios were larger than reported.

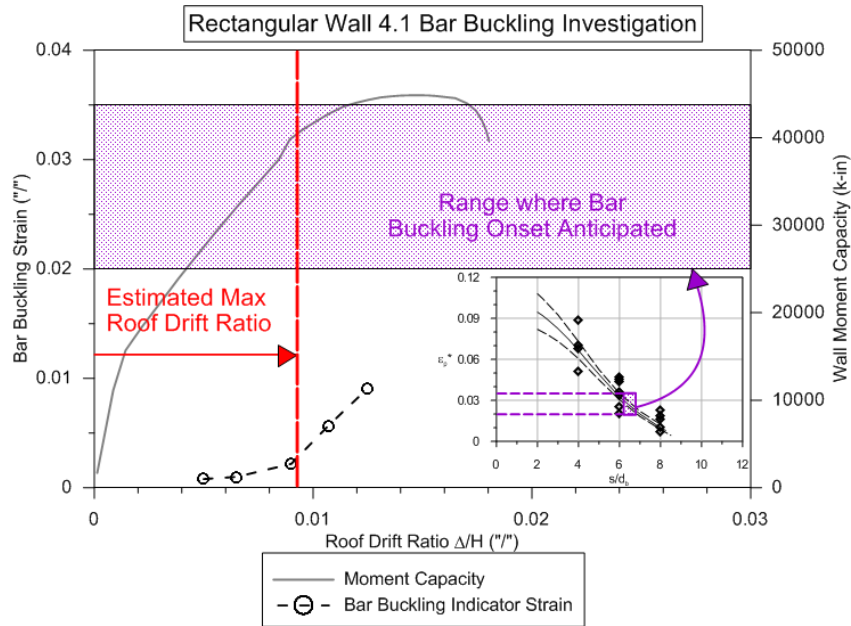


Figure A-42 Moment capacity and buckling strain indicator relations versus roof drift ratio for Wall 4.1.

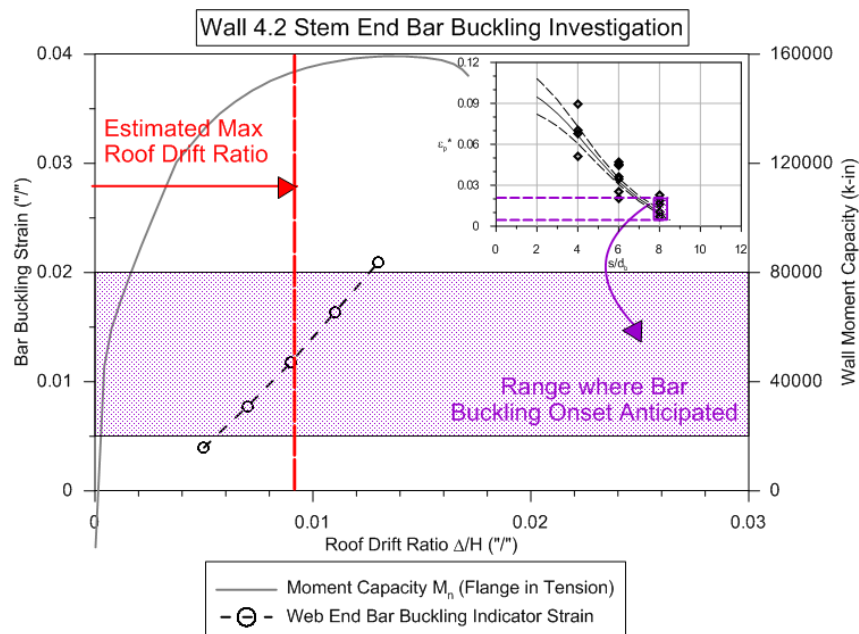


Figure A-43 Moment capacity and buckling strain indicator relations versus roof drift ratio for Wall 4.2.

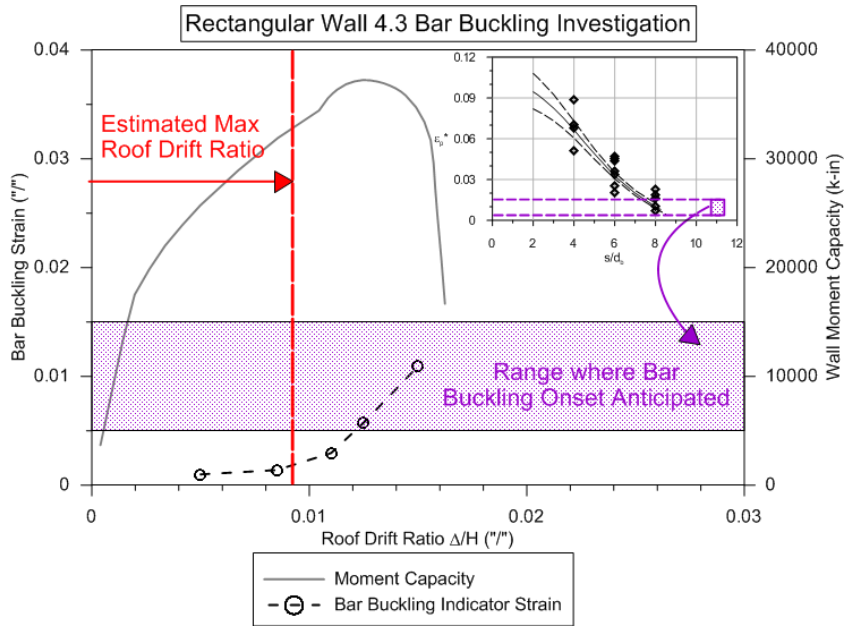


Figure A-44 Moment capacity and buckling strain indicator relations versus roof drift ratio for Wall 4.3.

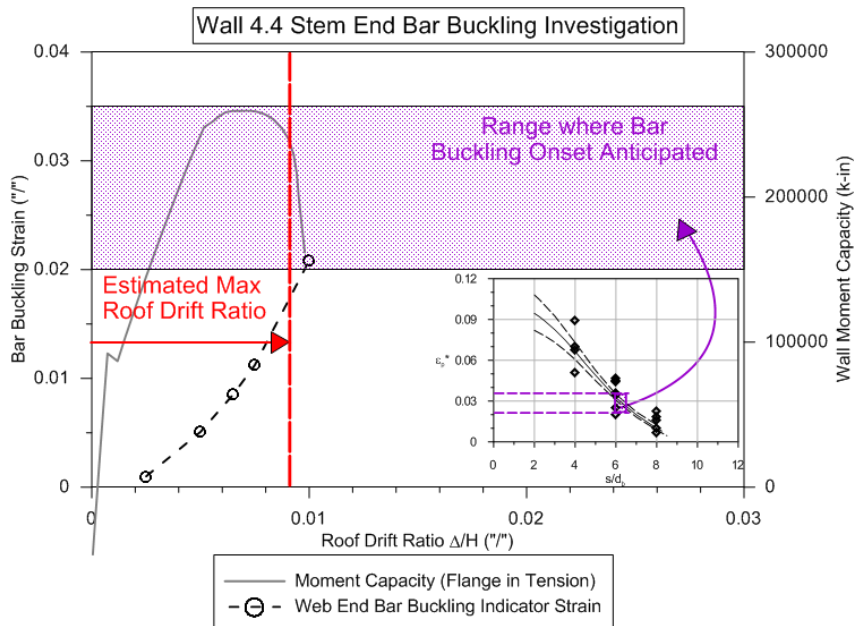


Figure A-45 Moment capacity and buckling strain indicator relations versus roof drift ratio for Wall 4.4.

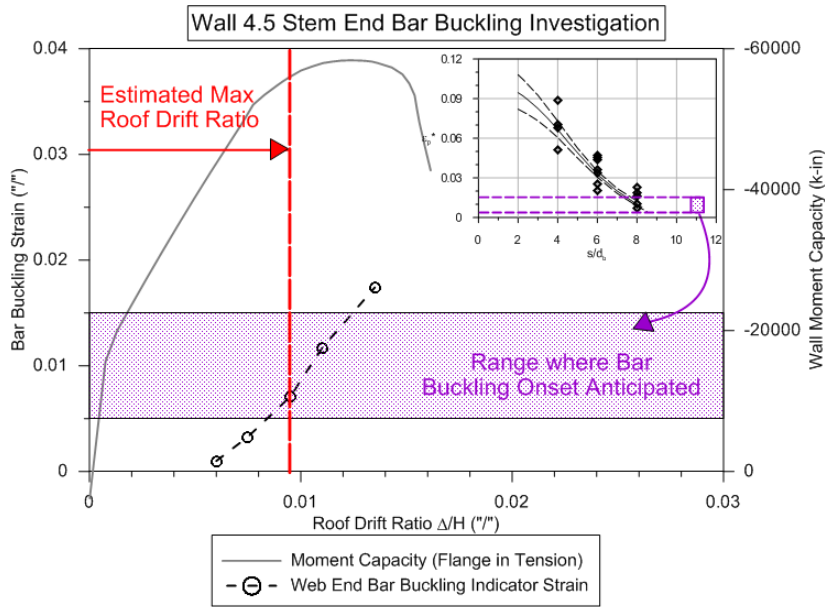


Figure A-46 Moment capacity and buckling strain indicator relations versus roof drift ratio for Wall 4.5.

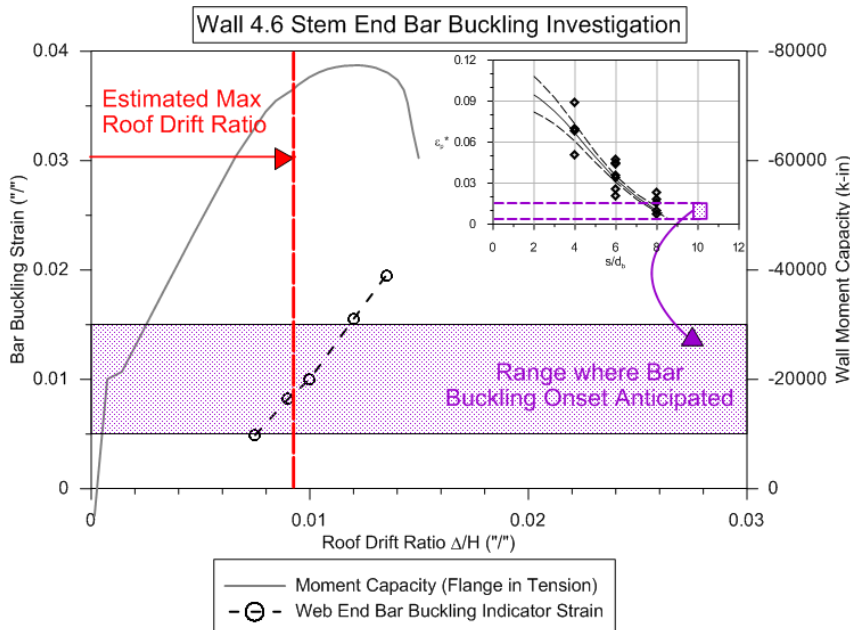


Figure A-47 Moment capacity and buckling strain indicator relations versus roof drift ratio for Wall 4.6.

A.6.3.5 Undisclosed Building A (Building No. 5)

All of the walls in Undisclosed Building A (Building No. 5) exhibited some level of bar buckling in the first subterranean level. Walls 5.1, 5.2, and 5.4 exhibited crushed boundary elements and buckled bars, and were damaged along the entire length of

the web. Wall 5.3 showed some spalling with slightly buckled bars, but was far less damaged than the other three walls.

Most of these walls were compression controlled, and the resulting moment capacity curves may overestimate the drift capacity (and therefore underestimate buckling indicator strains). As shown in Table A-22, Walls 5.1 and 5.2 both had fairly large axial load ratios (about 30% $A_g f'_c$) and likely experienced web crushing prior to bar buckling. Wall 5.4 had an extremely large amount of longitudinal reinforcement in the flange, which never yielded (according to BIAX moment-curvature analyses). Buckling strain indicators and moment capacity curves associated with Walls 5.1 to 5.4 are shown in Figures A-48 through A-51.

Table A-22 Undisclosed Building A (Building No. 5) Bar Buckling Assessment

Wall ID	Expected Load $D+0.25L$ ($\%A_g f'_c$)	Web s/d_b Ratio ¹	ϵ_p^* Lower Estimate	ϵ_p^* Upper Estimate	Calc. Strain $\epsilon_p^*_{calc}$	Bar Buckling Expected?	Bar Buckling Observed?
5.1	28.5	6.0	0.03	0.04	0.0015	No	Yes
5.2	31.7	11.1	0.005	0.015	0.0014	No	Yes
5.3	17.6	16.7	0.005	0.010	0.0065	Yes	Yes
5.4	14.8	16.7	0.005	0.010	0.010	Yes ²	Yes

¹ Based on horizontal web reinforcement. No hoops (or ties) provided.

² Concrete crushing also possible.

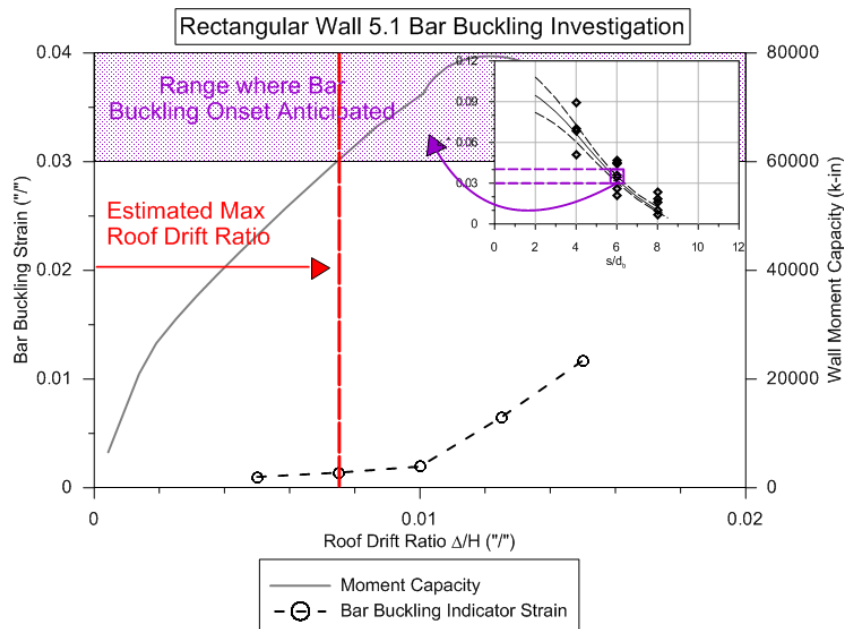


Figure A-48 Moment capacity and buckling strain indicator relations versus roof drift ratio for Wall 5.1.

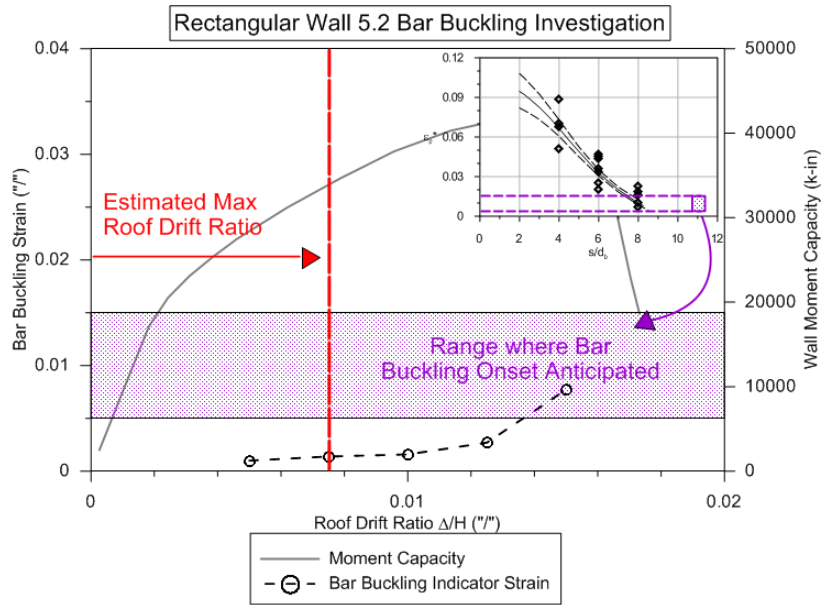


Figure A-49 Moment capacity and buckling strain indicator relations versus roof drift ratio for Wall 5.2.

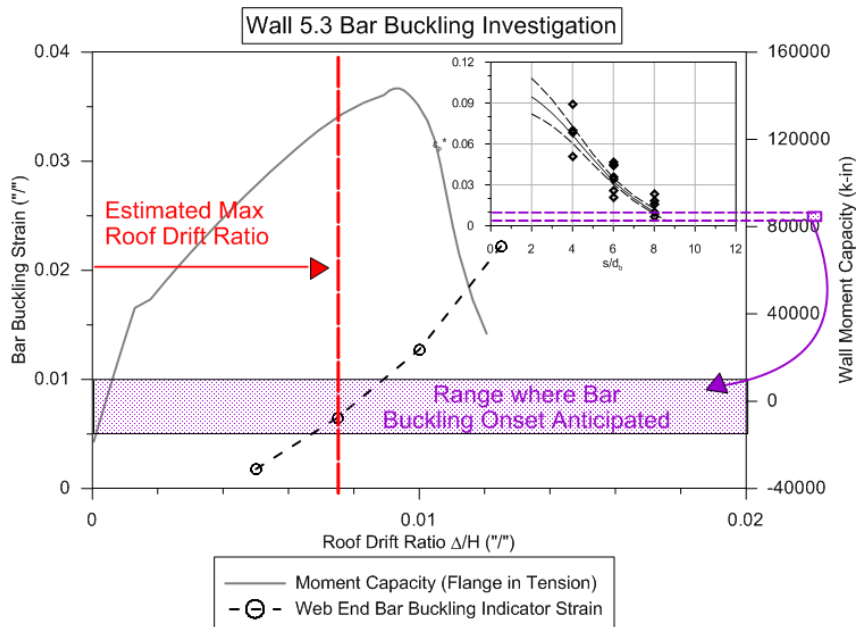


Figure A-50 Moment capacity and buckling strain indicator relations versus roof drift ratio for Wall 5.3.

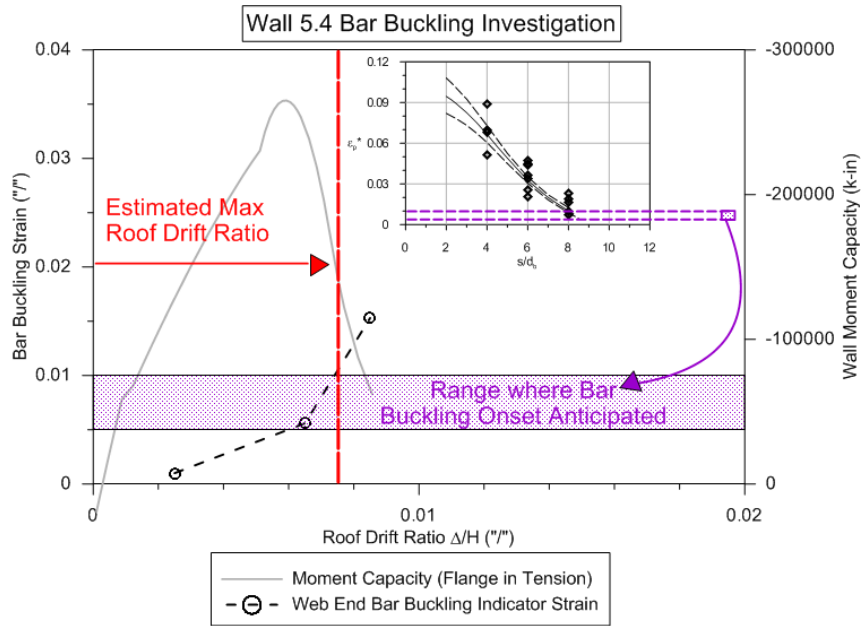


Figure A-51 Moment capacity and buckling strain indicator relations versus roof drift ratio for Wall 5.4.

A.6.3.6 Undisclosed Building B (Building No. 6)

In Undisclosed Building B (Building No. 6), damage was concentrated in the first subterranean level. Photos of observed damage revealed that no hoops (or ties) were provided to confine the longitudinal boundary reinforcement, so s/d_b ratios reflect the spacing of horizontal web reinforcement. Because these bars terminated with 90-degree hooks, it is unlikely that they provided much restraint against longitudinal bar buckling, especially after spalling of the concrete cover. As such, calculated buckling indicator strains probably overestimate the strain history that the longitudinal bars could withstand before buckling.

As shown in Table A-23, expected axial loads in the walls were quite large, and all of the walls were compression-controlled when loaded with the webs in compression.

Table A-23 Undisclosed Building B (Building No. 6) Bar Buckling Assessment

Wall ID	Expected Load $D+0.25L$ ($\%A_g f'_c$)	Web s/d_b Ratio ¹	ϵ_p^* Lower Estimate	ϵ_p^* Upper Estimate	Calc. Strain $\epsilon_p^*_{calc}$	Bar Buckling Expected?	Bar Buckling Observed?
6.1	16.6	5.2	0.04	0.05	0.04	No	No
6.2	20.6	7.1	0.015	0.025	0.015	No	Yes
6.3	33.0	4.8	0.04	0.05	0.04	No	Yes

¹ Based on horizontal web reinforcement. No hoops (or ties) provided.

In Walls 6.2 and 6.3, calculated bar strains barely surpassed the yield strain (Wall 6.2) or never yielded (Wall 6.3), and the curvature associated with a concrete

compressive strain of 0.003 was taken as the yield curvature of the wall. The resulting moment capacity curves probably overestimate the ductility possible in these walls since they are derived assuming a plastic hinge length equal to half the length of the walls, which unlikely in compression controlled walls without special boundary element detailing

Buckling strain indicators and moment capacity curves associated with Walls 6.1 to 6.3 are shown in Figures A-52 through A-54. Calculated strains do not suggest that bar buckling would be initiated at the expected roof drift ratio. However, it is likely that, with 90-degree hooks on the horizontal web reinforcement, effective s/d_b ratios were larger than reported. Due to the large axial loads present, it is likely that concrete crushing initiated failure in the walls, followed by bar buckling once the concrete cover was lost.

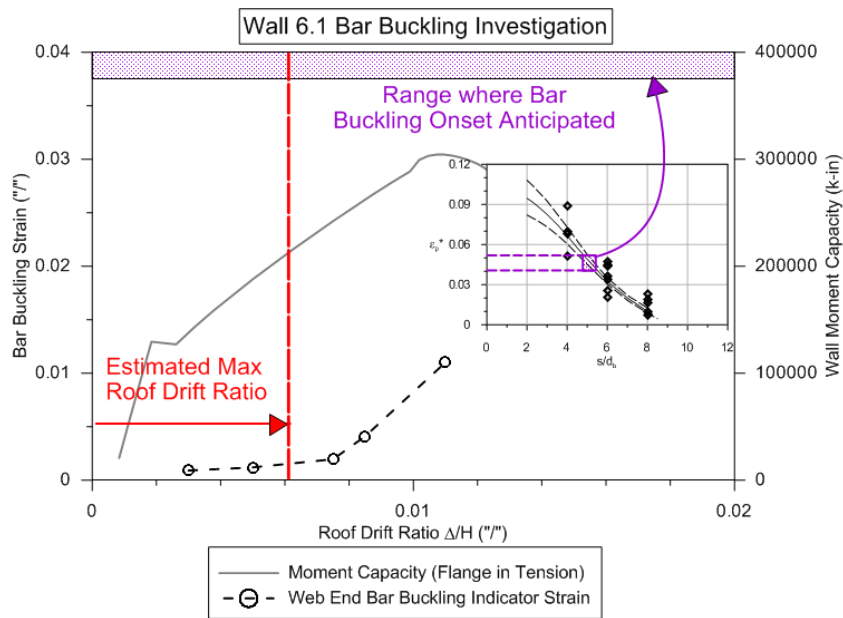


Figure A-52 Moment capacity and buckling strain indicator relations versus roof drift ratio for Wall 6.1.

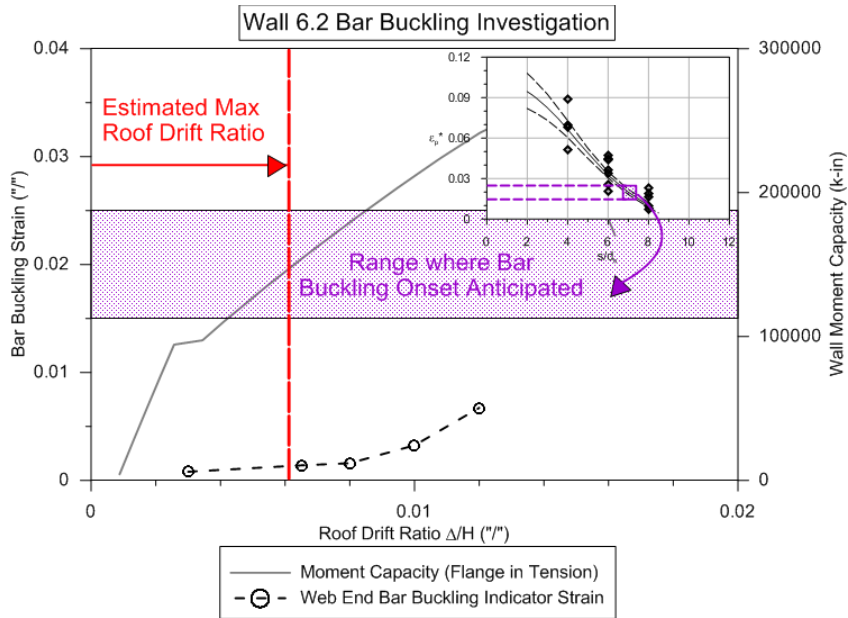


Figure A-53 Moment capacity and buckling strain indicator relations versus roof drift ratio for Wall 6.2.

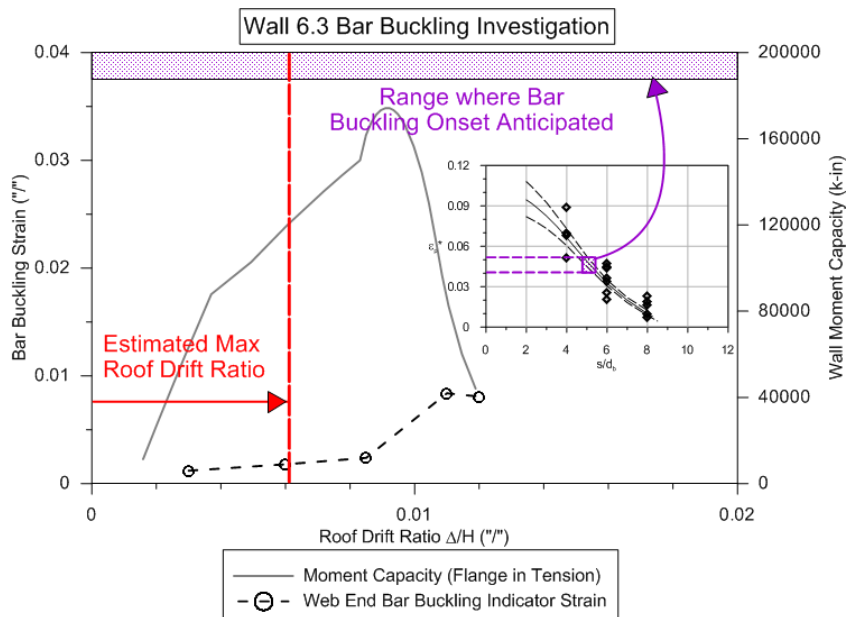


Figure A-54 Moment capacity and buckling strain indicator relations versus roof drift ratio for Wall 6.3.

A.6.3.1 Mongolio (Building No. 7)

The walls considered in Mongolio (Building No. 7) had either barbell or flanges at each end, and hoops were specified at the barbell. No significant damage was reported in either wall. As shown in Table A-24, neither concrete crushing nor bar buckling would be expected to occur at the estimated roof drift ratio.

Table A-24 Mongolio (Building No. 7) Bar Buckling Assessment

Wall ID	Expected Load $D+0.25L$ ($\%A_g f'_c$)	Web s/d_b Ratio	ϵ_p^* Lower Estimate	ϵ_p^* Upper Estimate	Calc. Strain $\epsilon_p^*_{calc}$	Bar Buckling Expected?	Bar Buckling Observed?
7.1	6.9	8.3	0.005	0.02	0.0044	Yes	No
7.2	4.1	8.3	0.005	0.02	0.0008	No	No

Buckling strain indicators and moment capacity curves associated with Walls 7.1 and 7.2 are shown in Figures A-55 and A-56. Expected axial loads in the walls were relatively low. At $l_p = 0.5l_w$, the assumed plastic hinge length of Wall 7.1 would be larger than the height of one story, so the curvature-drift relation was altered by limiting the plastic hinge length to the story height.

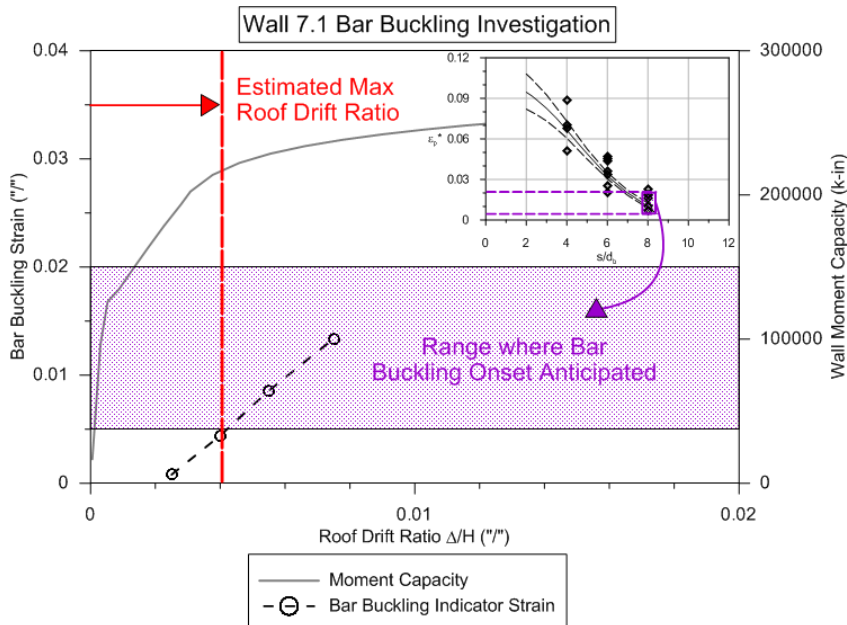


Figure A-55 Moment capacity and buckling strain indicator relations versus roof drift ratio for Wall 7.1.

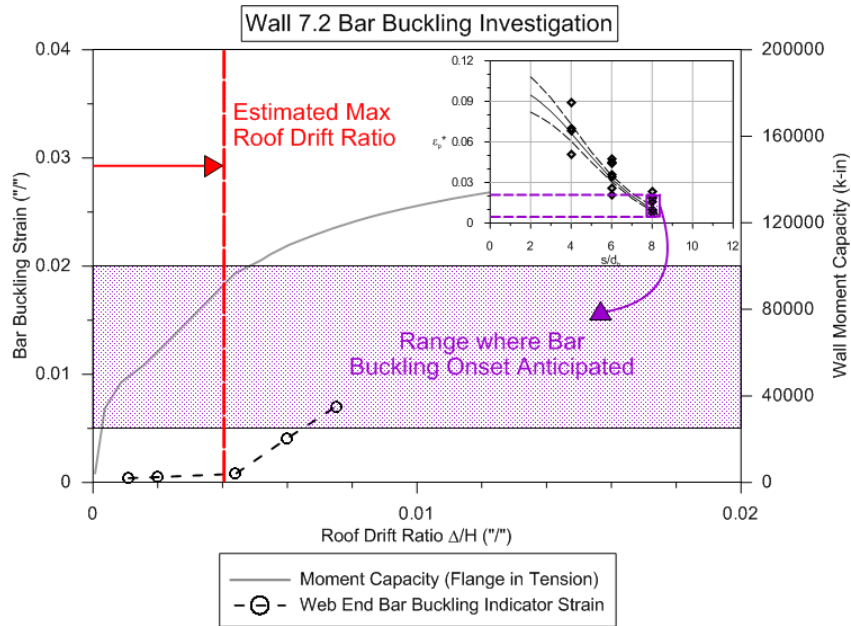


Figure A-56 Moment capacity and buckling strain indicator relations versus roof drift ratio for Wall 7.2.

A.6.4 Calibration of Bar Buckling Approach with Past Experimental Test Results

The procedure used to assess the onset of bar buckling for structural walls based on Rodriguez et al. (1999) was calibrated by comparing with test results for cantilever walls with both rectangular and T-shaped cross-sections.

Comparison with test results indicated that, for the range of strain values expected at the onset of bar buckling: (1) onset of buckling (i.e., minor out-of-plane displacement of vertical bar) with no observed loss in lateral strength was typically associated with the lower-bound of the range; (2) bar buckling with noticeable out-of-plane displacements and significant spalling of concrete cover was associated with the mid-to upper-levels of the range; and (3) significant loss in lateral strength was generally associated with the upper-bound of the range (or values slightly above the upper-bound). Calibration of this approach with a larger test data set is recommended.

A.6.4.1 Walls Tested by Thomsen and Wallace (1995, 2004)

The consistency of the approach applied to analyze Chilean walls for bar buckling was assessed by comparing analytical results to test results for the walls tested by Thomsen and Wallace (1995, 2004). These tests included drift and strain data for walls with both rectangular and T-shaped cross sections, making it possible to verify calculated strains with recorded data. In the following paragraphs, results for wall specimens TW1, RW1, TW2, and RW2 are presented. Specimens TW1 and RW1 are particularly relevant to the walls investigated in Chile because the detailing at the

wall boundaries most closely resembles that used in Chilean buildings (i.e., s/d_b on the order of 8).

Material test data for concrete cylinders and rebar coupons reported by Orakcal and Wallace (2006) were used to develop monotonic stress-strain relations for concrete in compression and reinforcement in tension and compression. The load versus lateral displacement relation at the top of the wall was derived by integrating elastic curvatures, and then rotations, and by using a plastic hinge model approach for inelastic deformations (a plastic hinge length equal to $0.5l_w$ was assumed). The resulting force-displacement plot matched the experimentally obtained relation, so bar buckling assessment advanced to the next stage of evaluating ϵ_p^* .

Figures A-57 and Figure A-58 show the indicator strain values calculated for specimens TW1 and RW1, respectively, for each half-cycle beyond 0.5% drift, taking into account the bar strains associated the drift at the previous half cycle. The hatched region in each figure indicates the range where the onset of bar buckling would be expected according to the data fit presented by Rodriguez et al. (1999). The dashed and solid lines track the respective strain histories of the longitudinal bars in the compression zone from cycle to cycle.

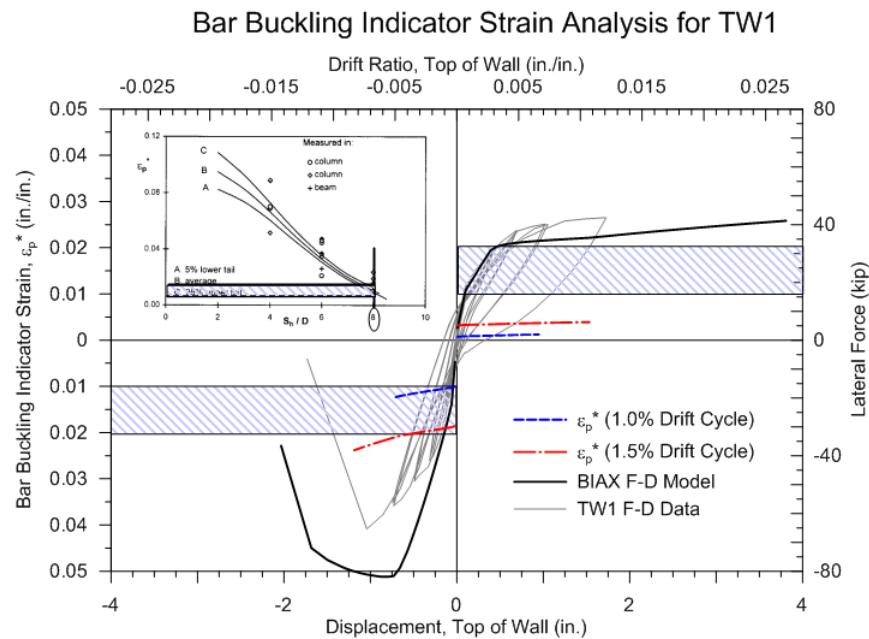


Figure A-57 Bar buckling analysis of wall specimen TW1 (Thomsen and Wallace (1995, 2004).

The drift cycle history used in the test program was well documented, eliminating the need for the equal displacement assumption; however, it is noted that the test specimens were subjected to equal drift levels for positive and negative loading under displacement control. Knowing the maximum drift in the previous half cycle

permitted calculation of indicator strains for each drift level cycle, rather than assuming values for the prior drift cycle and bar strain history.

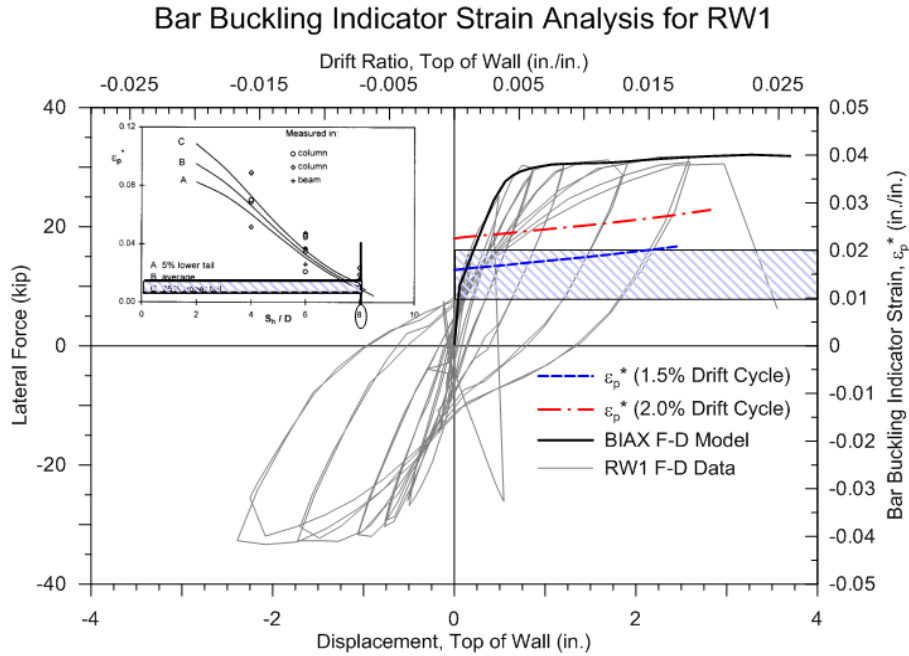


Figure A-58 Bar buckling analysis of wall specimen RW1 (Thomsen and Wallace (1995, 2004).

For example, the plot shows that for the 1% drift cycle longitudinal bar strains entered the lower bound range of when onset of buckling might be expected. By the time the experiment reached the 1.5% drift cycle, bar strains were beyond the upper bound of when buckling would initiate. Analyses also indicated that when the flange was in compression, bar strain history never exceeded 0.5%. This was much lower than the anticipated level where buckling might initiate, and no damage associated with bar buckling was observed at the flanged end of the wall.

TW1 experienced sudden loss of lateral strength during the first (negative) cycle to 1.5% drift, which loaded the web boundary (opposite the flange) in compression. At approximately -1.0% drift, based on video data, minor concrete spalling occurred, corner bars appeared to grow unstable, and then a brittle, explosive failure occurred where all eight vertical boundary bars and several pairs of web vertical bars buckled, thrusting off the concrete cover. The calculated ϵ_p^* at a drift level of -1.0%, after considering the web longitudinal bars had already experienced tensile strains associated with the +1.5% drift cycle, was about 0.023. Longitudinal bar strain history plots (Thomsen and Wallace, 1995) revealed that maximum tensile strain for boundary vertical bars was about 0.025, and the extreme fiber concrete compression strain at the wall web boundary opposite the flange at the 1.5% drift level was about 0.005, producing an ϵ_p^* value of 0.03 from the test, suggesting that the calculated ϵ_p^* of 0.023 from moment-curvature analysis was fairly conservative (i.e., predicted

onset of buckling for lower strains than measured). One possible reason for this discrepancy is the role of concrete cover, which might provide some lateral support and delay the onset of bar buckling. Another possible reason for the discrepancy is that the onset of bar buckling occurred prior to observed strength loss.

The results for RW1 indicate that the onset of bar buckling would be possible at a drift ratio as low as 1.0%, would be quite likely at a drift ratio of 1.5%, and would be expected at a drift ratio of 2.0%. These results are consistent with test observations, where initial (onset) of buckling was noted between 1.0% and 1.5% drift, visible and significant buckling of boundary edge bars was observed for 1.5% and 2.0% drift cycles, and significant strength loss was noted for the first cycle to 2.5% drift.

Two additional walls with tighter hoop spacing (wall specimens RW2 and TW2) were also analyzed using this same approach and results suggested that initiation of bar buckling was unlikely. Investigation of bar strain data and testing observations confirmed these results. Wall specimen RW2 had a s/d_b ratio of 5.3. Rodriguez et al. (1999) suggests that bar buckling would initiate around 4% strain. The hoop spacing in wall specimen TW2 was even smaller than in specimen RW2, with an s/d_b ratio of 3.3. Bar buckling would be expected to initiate in the range of 7%-9% strain. As exhibited in Figures A-59 and A-60, bar buckling indicator strain values, ϵ_p^* , did not reach the range where onset of bar buckling would be expected in either case, and no bar buckling was observed in either experiment.

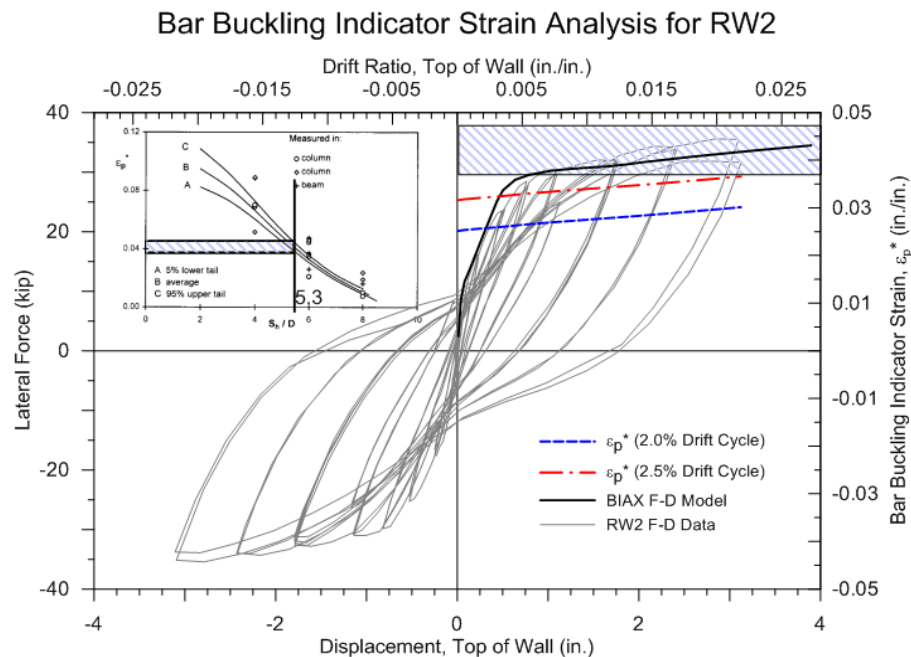


Figure A-59 Bar buckling analysis of wall specimen RW2 (Thomsen and Wallace (1995, 2004).

Bar Buckling Indicator Strain Analysis for TW2

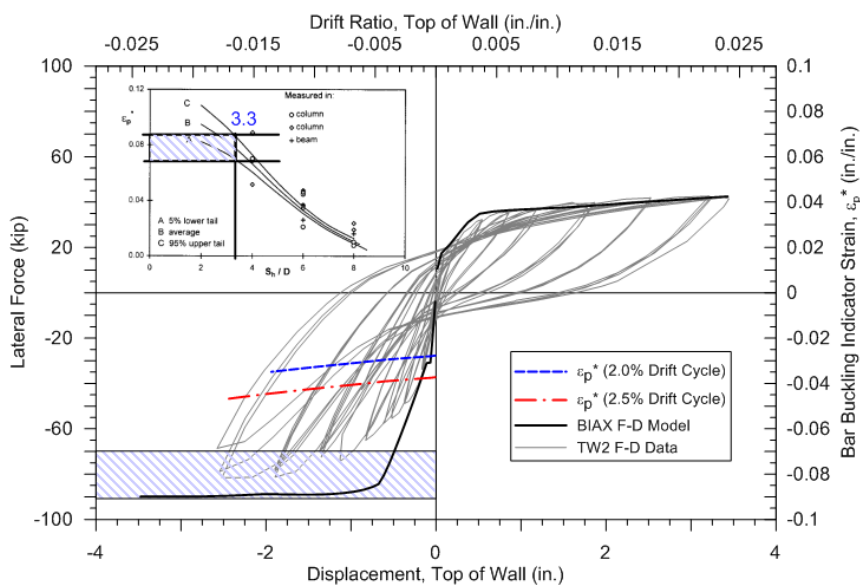


Figure A-60 Bar buckling analysis of wall specimen TW2 (Thomsen and Wallace (1995, 2004).

Table A-25 provides a summary of bar buckling analysis results for the four wall specimen tests (RW1, RW2, TW1, and TW2).

Table A-25 Summary of Bar Buckling Analysis Results for Wall Specimen Tests

Wall ID	Applied Axial Load (% $A_g f_c$)	Web s/d_b Ratio	ϵ_p^* Lower Estimate	ϵ_p^* Upper Estimate	Calc. Strain $\epsilon_p^*_{calc}$	Bar Buckling Expected?	Bar Buckling Observed?
RW1	10.0	8.0	0.01	0.02	0.03	Yes	Yes
RW2	7.0	3.3	0.07	0.09	0.05	No	No
TW1	9.0	8.0	0.01	0.02	0.025	Yes	Yes
TW2	7.5	5.3	0.035	0.045	0.035	No	No

Appendix B

Derivation of Overall Wall Buckling Relationships

This appendix presents the derivation of wall instability relationships provided in Equations 3-1 to 3-3 of Chapter 3. Design practices prior to the 1990s favored rectangular walls with enlarged boundary elements, contributing to stability of the flexural compression zone. More recently, however, prevailing practices in many countries have favored rectangular sections without enlarged boundaries. More slender flexural compression zones can be susceptible to inelastic lateral buckling, as reported in EERI (2010) and EERI (2011), and shown in Figure B-1.



Figure B-1 Examples of wall lateral buckling: (a) 2010 Maule earthquake (DICTUC, 2010d); and (b) 2011 Christchurch earthquake (photo courtesy of Ken Elwood).

B.1 Derivation of Theoretical Model for Wall Instability

Although overall wall buckling occurs when the wall boundary is in compression, buckling may be influenced by tensile strain in the wall from prior loading in the opposite direction (Corley et al., 1981; Paulay and Priestley, 1993; Chai and Elayer, 1999). Some of the derivations below follow the general approach of Paulay and Priestley (1993).

Consider a wall with two curtains of longitudinal reinforcement, as shown in Figure B-2. Wall lateral buckling is constrained at each end of the story clear height (Figure B-2a). The wall is assumed to have been previously loaded in flexure, such that the boundary yields in tension (Figure B-2b). A unit length of the boundary element develops a tension force, T , maximum tensile stress, f_{sm} , and tensile strain, ϵ_{sm} .

Upon deformation reversal, just before the boundary elements yields in compression, the longitudinal reinforcement will have unloaded by a strain of $\epsilon_s = f_{sm} / E_s$, and reloaded in compression to a strain of $-\epsilon_y$ (ignoring the Bauschinger effect), such that the residual tensile strain is approximately $\epsilon_{res} = \epsilon_{sm} - f_{sm} / E_s - \epsilon_y \approx \epsilon_{sm} - 0.005$ (Figure B-2d). Invariably, one curtain of reinforcement will yield before the other, producing curvature, and out-of-plane displacement as illustrated in Figures B-2a and B-2c. Whether or not the boundary remains stable depends on magnitude of the lateral displacement, δ , relative to the wall thickness, b , which relates to the maximum previous tensile strain, ϵ_{sm} , and the resulting curvature, as illustrated in Figure B-2c.

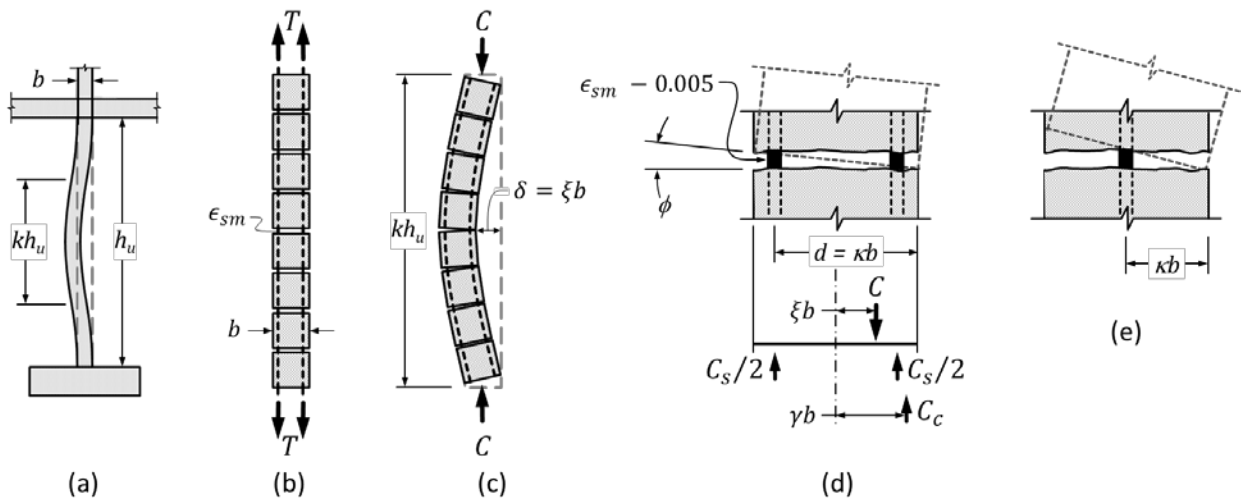


Figure B-2 Lateral instability of a wall boundary that is previously yielded in tension.

To estimate conditions for stability, the effective length (height) must be approximated. For a multistory wall with height, h_w , not less than the first-story clear height, h_u , it is reasonable to assume that the flexural plastic hinge extends over the height of the first story. Assuming fixity top and bottom, with a simple harmonic buckled shape, the effective length in Figure B-2a can be taken as $kh_u = 0.5h_u$. The maximum deflection can be expressed as a fraction of wall thickness ($\delta = \xi b$), as shown in Figure B-2c. The relation between maximum deflection and maximum curvature, ϕ_{max} , is:

$$\delta = \xi b = \phi_{max} \left(\frac{kh_u}{\pi} \right)^2 \quad (B-1)$$

As a first approximation, the maximum curvature from Figure B-2d can be written as:

$$\phi_{max} = \frac{\varepsilon_{sm} - 0.005}{d} \quad (B-2)$$

where d is the effective depth for out-of-plane bending of the wall. Equilibrium of forces and moments on the free-body diagram of Figure B-2d results in the following two expressions:

$$\Sigma F = 0 \rightarrow C = C_s + C_c \quad (B-3)$$

$$\Sigma M = 0 \rightarrow C \xi b = C_c \gamma b \quad (B-4)$$

In Equation B-4, moments are taken about the centerline, such that moments of longitudinal reinforcement compressive force resultants (assumed to be equal) cancel. Assuming that longitudinal reinforcement is stressed to f_y , and assuming the concrete compressive force, C_c , is represented by the usual rectangular stress block with depth $\beta_1 c$ and average stress $0.85 f'_c$:

$$C_s = \rho b f_y \quad (B-5)$$

$$C_c = 0.85 f'_c \beta_1 c = 0.85 f'_c (1 - 2\gamma) b \quad (B-6)$$

where ρ is the reinforcement ratio, and γ is a fraction of wall thickness, as defined in Figure B-2d. Substituting Equations B-3, B-5, and B-6 into Equation B-4, and manipulating the results:

$$(1 - 2\gamma) \left(\frac{\gamma}{\xi} - 1 \right) = \frac{\rho f_y}{0.85 f'_c} = \frac{m}{0.85} \quad (B-7)$$

in which $m = \rho f_y / f'_c$ is the mechanical reinforcement ratio. This expression has real roots only if the following is satisfied:

$$\xi \leq 0.5 \left(1 + \frac{2m}{0.85} - \sqrt{\left(\frac{2m}{0.85} \right)^2 + \frac{4m}{0.85}} \right) \quad (B-8)$$

Substituting ξ from Equation B-8 into Equation B-1, solving for b/h_u , and defining width b as the critical width, b_{cr} , results in

$$\frac{b_{cr}}{kh_u} = \frac{1}{\pi} \sqrt{\frac{\varepsilon_{sm} - 0.005}{\kappa \xi}} \quad (B-9)$$

Key terms in Equation B-9 are the critical slenderness ratio, kh_n/b_{cr} , the maximum tensile strain in the longitudinal reinforcement, ε_{sm} , the effective depth parameter for

longitudinal reinforcement, κ , and ξ . Typical values of κ are 0.8 for walls with two curtains of reinforcement and 0.5 for walls with one curtain of reinforcement, and it is clear that walls with two curtains of longitudinal reinforcement are inherently more stable than walls with a single curtain of reinforcement. The parameter ξ is related to the mechanical reinforcement ratio in Equation B-8, but this an inconvenient parameter for preliminary design. For practical construction, $0.4 \leq \sqrt{\xi} \leq 0.6$.

For walls with two curtains of reinforcement, substituting values of $\kappa = 0.8$ and $\sqrt{\xi} = 0.5$ into Equation B-9, and inverting, gives:

$$\frac{kh_u}{b_{cr}} = \frac{1}{0.7\sqrt{\varepsilon_{sm}} - 0.005} \quad (\text{B-10})$$

For typical slender wall geometries, the wall can be approximated as having fixed-end boundary conditions (i.e., $k = 0.5$), and Equation B-10 becomes:

$$\frac{b_{cr}}{h_u} = 0.35\sqrt{\varepsilon_{sm}} - 0.005 \quad (\text{B-11})$$

The preceding derivations, and available test data, are based on idealized wall boundaries of limited length, subjected to uniform compressive strain. Actual wall boundaries will have a strain gradient along the length of the wall, which would tend to brace the edge of the wall. This suggests that the preceding results will be conservative for actual wall boundaries.

B.2 Comparison of Theoretical Model and Laboratory Tests

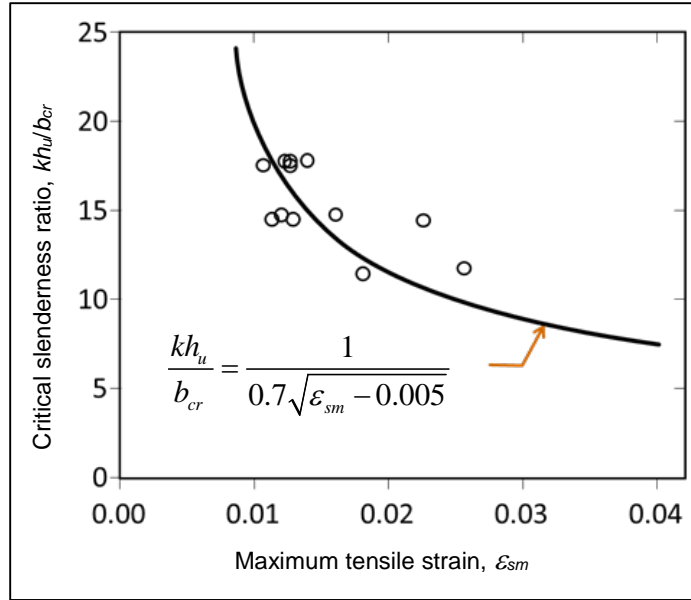
Equation B-10 expresses a relation between the critical slenderness ratio for a wall boundary and the maximum previous tensile strain. It is of interest to compare the results of Equation B-10 with results obtained from laboratory tests. This section presents highlights of the comparison. Additional details are provided in Parra and Moehle (2013).

Chai and Elayer (1999) reports data from cyclic tension-compression tests of rectangular prisms reinforced in a manner similar to rectangular wall boundaries. The prisms were subjected to alternating tension and compression cycles to increasing strain amplitude until failure occurred due to out-of-plane instability. All test specimens in this case had pin-ended boundary conditions (i.e., $k = 1.0$).

In Figure B-3, the results of Equation B-10 are plotted with test data from prismatic sections that buckled following tensile strain excursions to ε_{sm} . The equation matches the trend in the data fairly well. Although the data could also have been represented by a linear relation, a quadratic relation was chosen to avoid unnecessarily penalizing walls with $\varepsilon_{sm} > 0.04$.



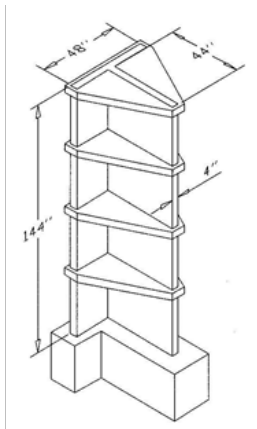
(a)



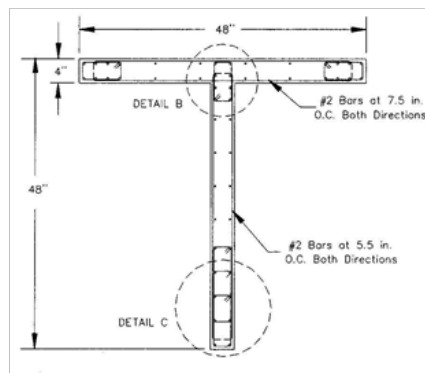
(b)

Figure B-3 Comparison between the theoretical relation for wall instability and test results for buckling of prismatic sections reinforced as rectangular wall boundaries: (a) test specimen; and (b) plot of data (Chai and Elayer, 1999).

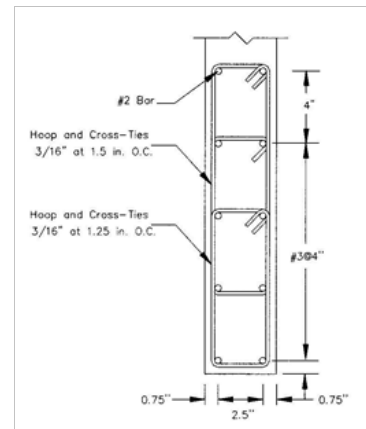
Thomsen and Wallace (2004) presents results of tests on wall specimens subjected to lateral deformation reversals. One of the specimens, TW2, had a T-shaped cross-section and sustained out-of-plane buckling after spalling of the concrete cover. The configuration and detailing of specimen TW2 are shown in Figure B-4.



(a)



(b)



(c)

Figure B-4 Configuration and detailing of T-shaped wall specimen TW2: (a) isometric; (b) cross-section; and (c) detail (Thomsen and Wallace, 2004).

Specimen TW2 had an aspect ratio $h_u/b \approx 24/4 = 6$. From Equation B-9, this specimen should be stable to peak tensile strains on the order of $\varepsilon_{sm} = 0.21$. As expected, specimen TW2 remained stable through large lateral deformations, but it buckled laterally during cycles in which lateral drifts reached 2.5% of the wall height,

with peak tensile strain of approximately 0.05 (Thomsen and Wallace, 1995). The buckled section is shown in Figure B-5.

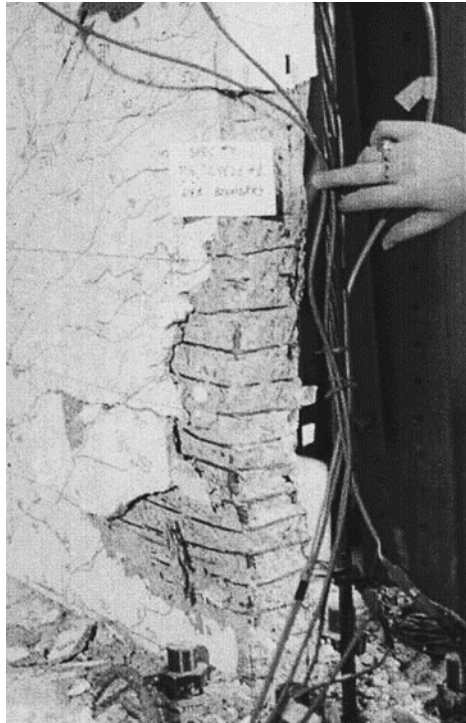


Figure B-5 Out-of-plane buckling observed in T-shaped wall specimen TW2 (Thomsen and Wallace, 1995).

Notably, at this stage of testing, the cover concrete has completely spalled from the confined core, leaving a more slender boundary element ($h_u/b \approx 24/2.75 \approx 9.6$). If Equation B-9 is applied to the core only, buckling would be expected for peak tensile strains of about $\epsilon_{sm} = 0.08$, which is on the order of the measured strain of 0.05. Thus, buckling of specimen TW2 can be understood by applying the buckling model to the wall boundary using the thickness of the confined core.

B.3 Comparison of Theoretical Model to Wall Thickness Requirements in Codes and Standards

Considering the effects of low-cycle fatigue, the maximum usable tensile strain is approximately $\epsilon_{sm} = 0.05$. Substituting $\epsilon_{sm} = 0.05$ into Equation B-11 results in a critical slenderness ratio of $h_u/b_{cr} = 13$. Code-based designs do not necessarily limit maximum tensile strain directly. For $\epsilon_{sm} = 0.10$, which is the approximate upper limit for steel reinforcement, Equation B-11 results in $h_u/b_{cr} = 9$.

For seismic design, ACI 318-11, *Building Code Requirements for Structural Concrete and Commentary* (ACI, 2011) does not address slenderness of wall boundary elements, although the 1997 *Uniform Building Code* (ICBO, 1997) previously recommended $h_u/b \leq 16$. In discussing U.S. practice, NIST GCR 11-917-

11, *Seismic Design of Cast-in-Place Concrete Special Structural Walls and Coupling Beams: A Guide for Practicing Engineers* (NIST, 2011), recommends $h_u/b \leq 10$ within the intended plastic hinge region of walls, and $h_u/b \leq 16$ elsewhere.

Eurocode 8, *Design of Structures for Earthquake Resistance – Part 1: General Rules, Seismic Actions and Rules for Buildings* (CEN, 2004), specifies minimum wall thickness of 8 inches (200mm) for confined portions of walls. Moreover, if the length of the confined portion does not exceed the larger of $2b$ and $0.2l_w$ (where l_w is the length of the wall), b should be at least $l_u/15$; otherwise b should be at least $l_u/10$ (where l_u is the unsupported height of the wall).

In NZS 3101, *Concrete Structures Standard, Part 1 – The Design of Concrete Structures* (SNZ, 2006a), the thickness of the wall boundary, b_m , shall be at least:

$$b_m = \frac{\alpha_r k_m \beta (h_w / l_w + 2) l_w}{1700 \sqrt{\xi_r}} \quad (\text{B-12})$$

over the height of the plastic hinge (but not less than the height of the first story). In Equation B-12, $\alpha_r = 1$ for walls with two curtains of longitudinal reinforcement, $\alpha_r = 1.25$ for walls with one curtain, $\beta = 7$ for ductile plastic regions, and $k_m = 1$, except that for long walls, k_m can be defined as:

$$k_m = \frac{h_u}{(0.25 + 0.055 h_w / l_w) l_w} \leq 1.0 \quad (\text{B-13})$$

$$\xi_r = 0.3 - \frac{\rho_l f_y}{2.5 f_c} \geq 0.1 \quad (\text{B-14})$$

where ρ_l refers to the local longitudinal reinforcement ratio in the wall boundary.

These equations result in wall slenderness ratio h_u/b ranging from about 8 for slender, heavily reinforced walls, to about 30 for squat, lightly reinforced walls.

Study of Solid Walls Above or Below Vertically Aligned Openings

This appendix presents detailed information on the approaches and assumptions used in investigating discontinuity regions in solid walls above or below vertically aligned openings in Section 4.3. A study was conducted to calculate shear stress in discontinuity regions and a design approach is proposed.

A total of four Chilean buildings were selected to calculate the shear stress in the discontinuity region and compare with shear capacity and observed damage to validate the proposed shear stress equation.

C.1 Introduction

Coupled walls are defined by two or more solid walls interconnected by beams or slabs aligned over the height of the building, creating a vertically aligned series of openings. The stack of openings often extends over the entire building height, though in some buildings, stacks of openings terminate in solid wall panels below or above the stack, or both.

The solid panel constitutes a discontinuity region that can be subjected to large shear stresses when the coupled walls are loaded laterally. Several examples of damage to this discontinuity region were observed following the 2010 Maule earthquake. Similar damage was observed in the United States following the 1989 Loma Prieta earthquake.

Figures C-1 through C-5 show examples of characteristic damage to solid panels above or below a stack of openings. Figure C-1 is a crack map from a building in Northern California following the 1989 Loma Prieta earthquake. Figures C-2 through C-5 show damage map and photographs of buildings damaged in the 2010 Maule earthquake.

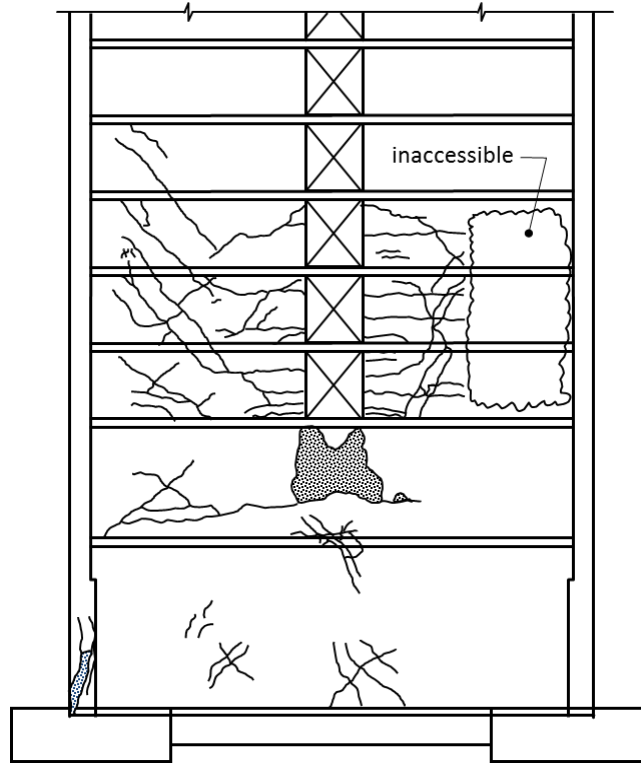


Figure C-1 Damage map from a building in Northern California damaged in the 1989 Loma Prieta earthquake (image courtesy of Jack Moehle).

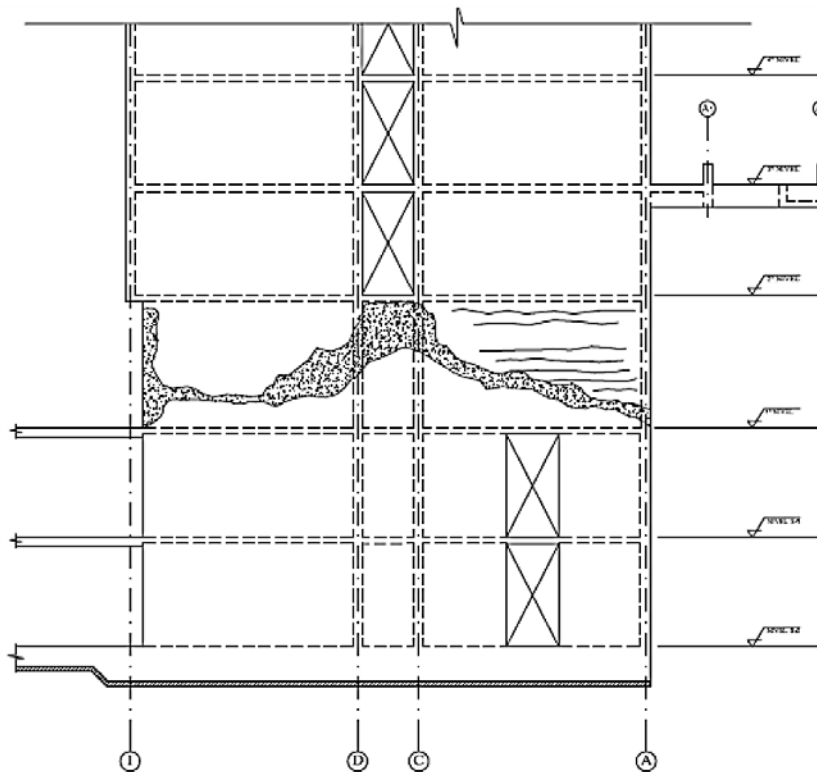


Figure C-2 Damage map of the Alto Rio Building in Concepción, Chile following the 2010 Maule earthquake at Grid 8 (IDIEM, 2010).



Figure C-3 Damage observed in solid panels at the top and bottom of a stack of openings in the Torre Mayor building in Chillán, Chile following the 2010 Maule earthquake (photo courtesy of EERI Chile earthquake reconnaissance team).



Figure C-4 Damage observed in solid panel at the bottom of a stack of openings in the Centro Mayor building in Concepción, Chile following the 2010 Maule earthquake (photo courtesy of EERI Chile earthquake reconnaissance team).



Figure C-5 Damage observed in solid panel at the bottom of a stack of openings in the Marina del Sol building in Viña del Mar, Chile following the 2010 Maule earthquake (photo courtesy of Patricio Bonelli).

C.2 Simulation of Response in Discontinuity Region

Tanyeri and Moehle (2013) explored local stresses in the discontinuity region of the Alto Rio building. This 15-story structure in Concepción collapsed during the 2010 Maule earthquake, overturning onto its side. Forensic studies (IDIEM, 2010) provide details of the collapse. Extensive damage to the discontinuity regions immediately below stacks of openings was observed (Figure C-2). A nonlinear model of a portion of the seismic force-resisting system along Grids 8 and 13 (Figure C-6) was constructed using the nonlinear finite element analysis software PERFORM-3D, *Nonlinear Analysis and Performance Assessment for 3D Structures* (CSI, 2013c), in order to simulate the response.

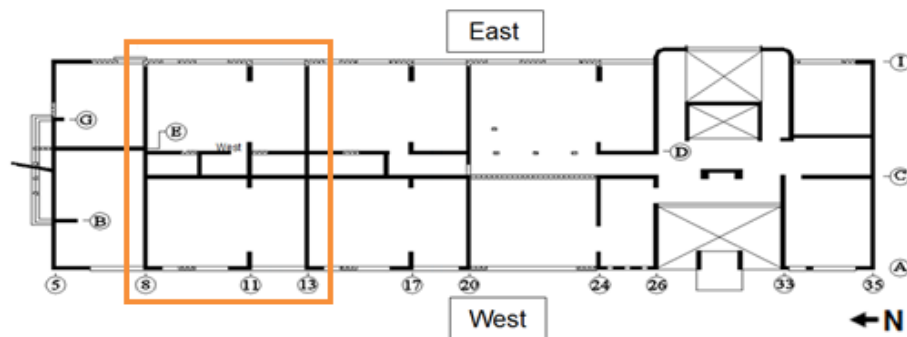


Figure C-6 Plan view of PERFORM-3D model slice for the Alto Rio building.

The area of study selected was deemed representative of the main portion of the seismic force-resisting system of the building. Similar to that shown in Figure C-2, the framing system along each of the axes comprised structural walls with a stack of openings terminating in a solid wall panel in the first story above grade.

Perpendicular wall segments connecting to these walls along both sides of the stack of openings were assumed fully effective as flanges. This approach is likely to exaggerate the shear on the discontinuity region in comparison with the actual shear. Structural walls were modeled using four-noded shear wall elements with fiber cross sections. In the first and second stories, where inelastic actions were expected to concentrate, shear wall elements were meshed so that each element had a height of $2b_w$, where b_w is wall thickness. An inelastic shear material was used for the walls, with nominal shear strength of $1.5V_n$, where V_n is the nominal shear strength defined in ACI 318-11, *Building Code Requirements for Structural Concrete and Commentary* (ACI, 2011).

The discontinuity regions beneath the stack of openings were modeled two different ways. In one model, the regions were modeled with an elastic shear material having effective shear stiffness defined as $G_c A_w = 0.4E_c A_w / 20$ in accordance with PEER/ATC-72-1 report, *Modeling and Acceptance Criteria for Seismic Design and Analysis of Tall Buildings* (ATC, 2010), where G_c is the shear modulus, E_c is Young's modulus and A_w is the web area. In the second model, the discontinuity regions were modeled using a bilinear shear material having initial stiffness $0.4E_c A_w$, with the break point at shear stress equal to $4\sqrt{f'_c}$ (psi), followed by a strain-hardening branch to $1.5V_n$. The model was loaded statically with expected gravity loads followed by progressively increasing lateral forces.

Figure C-7 shows the calculated average shear stress to roof drift ratio relationship for the discontinuity region below the stack of openings (solid line) and the entire wall cross-section (dashed line), for the model in which the discontinuity region is modeled as linear-elastic. The average stress in the discontinuity region is approximately three times the average stress acting across the entire wall section. This result is consistent with the results reported by Naeim et al. (1990).

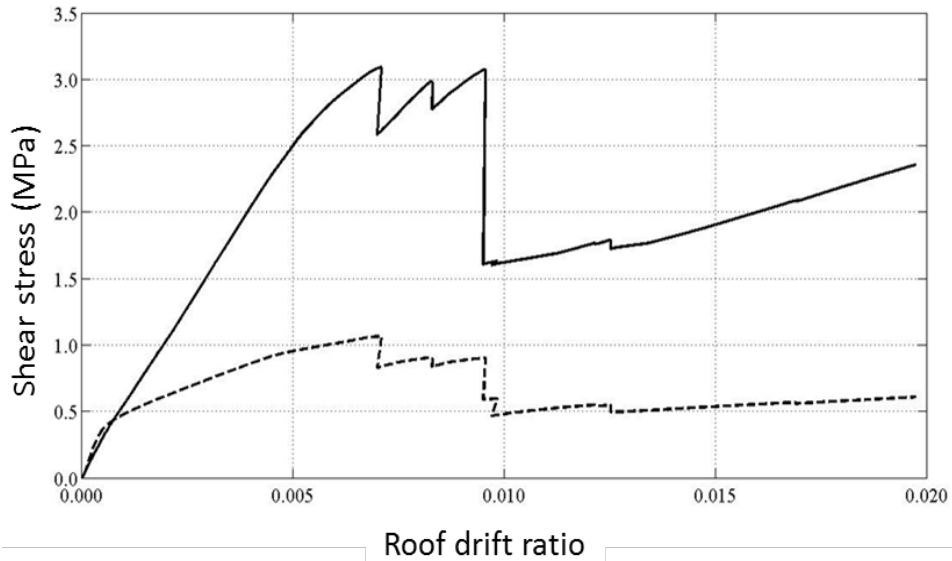


Figure C-7 Relationship of shear stress to roof drift ratio of discontinuity region (solid line) and of average for entire wall (dashed line), using a linear model for the discontinuity region. Stress for the discontinuity region is the average value over the height of the story below the stack of openings.

Figure C-8 shows the calculated relationship between shear stress and shear strain in the discontinuity region for the model in which the discontinuity region is modeled using an inelastic shear material. Inelastic response of the region is apparent.

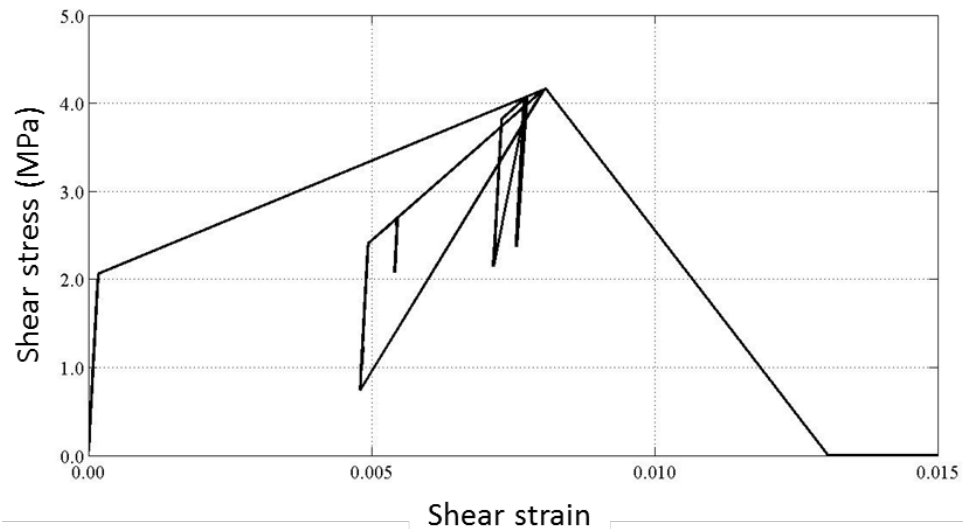


Figure C-8 Shear stress–strain relationship of the discontinuity region, using an inelastic shear material.

Overall, calculated results are consistent with reported damage, which shows cracking or destruction of the discontinuity region (see, for example, Figure C-2).

C.3 Calculation of Shear Stress in Discontinuity Region

Story-by-story analysis, as is commonly done in design, might miss the high stresses that occur in the discontinuity region. For example, section cut 1-1 in Figure C-9a would identify the need for boundary reinforcement at both sides of the openings, but section cut 2-2 just below the openings might suggest that the solid panel requires boundary reinforcement only at the exterior edges. Given this interpretation of the design actions, a common solution is to terminate the interior boundary bars a distance below the stack of openings equal to the tension development length, l_d , calculated for tensile stress $1.25f_y$. This short development length for the bars can result in high shear stress within the discontinuity region between the developed bars, as shown in Figure C-9b.

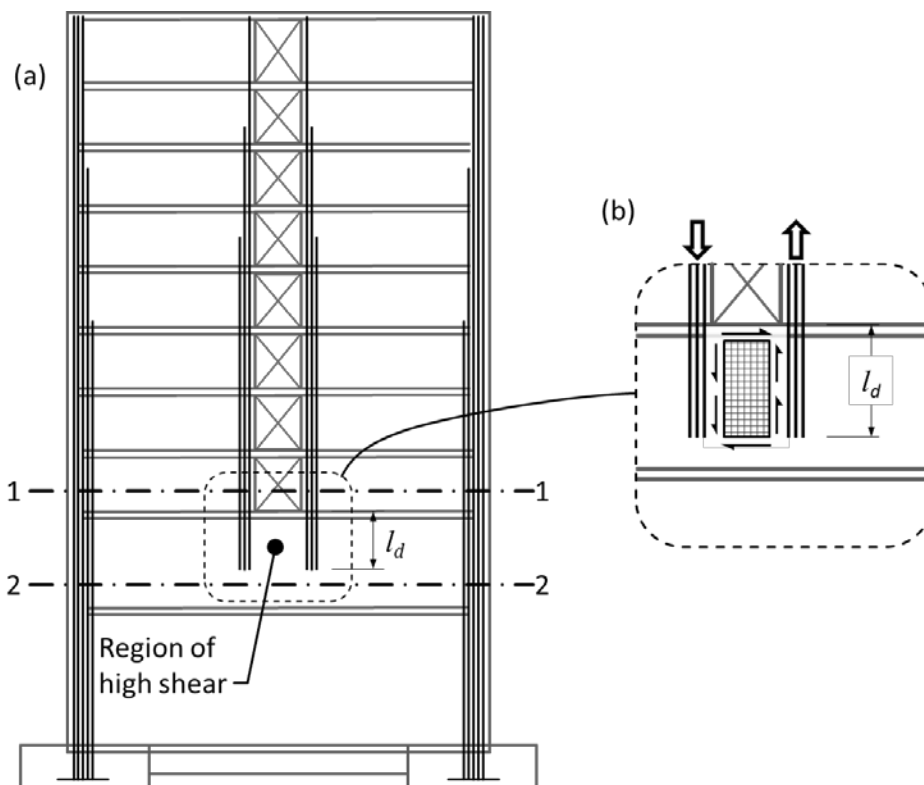


Figure C-9 Illustrations of: (a) minimum development length for wall boundary reinforcement; and (b) resulting shear stresses in the discontinuity region.

The internal forces in and around the discontinuity region can be approximated using equilibrium of the tension and compression forces from the boundary elements that flank the stack of openings. As shown in Figure C-10, if tension and compression forces T_1 and C_1 are at least partially resolved within panel zone **abcd**, this will result in a panel shear stress, v_1 . Moment equilibrium of panel **abcd** requires stress v_1 to act along both the vertical and the horizontal faces of **abcd**. Furthermore, equilibrium of the horizontal shear stress acting along **ab** requires reinforcement along and anchored beyond **ab**. The shear stress along **cd** can either be transferred to

the panel below or can be dragged out by reinforcement along and anchored beyond **cd**. It may be convenient to define panel zone dimensions, such that the horizontal tension and compression drag forces T_2 and C_2 are resisted by reinforcement in floor slabs located just below the stack of openings and one level lower. If this results in shear stresses beyond the available stress capacity, it may be necessary to distribute the forces deeper within the solid wall.

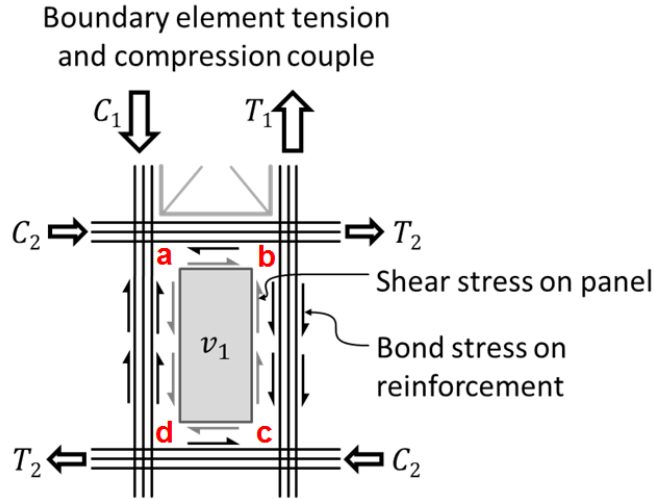


Figure C-10 Panel zone shear and tension/compression chords.

It is of interest to estimate the portion of total boundary element force that is resisted by the discontinuity region **abcd**, versus the portion resisted by the adjacent segments **efgh** and **ijkl** (Figure C-11). Tension and compression forces T_2 and C_2 identified in Figure C-11 need to be resolved in adjacent wall panels.

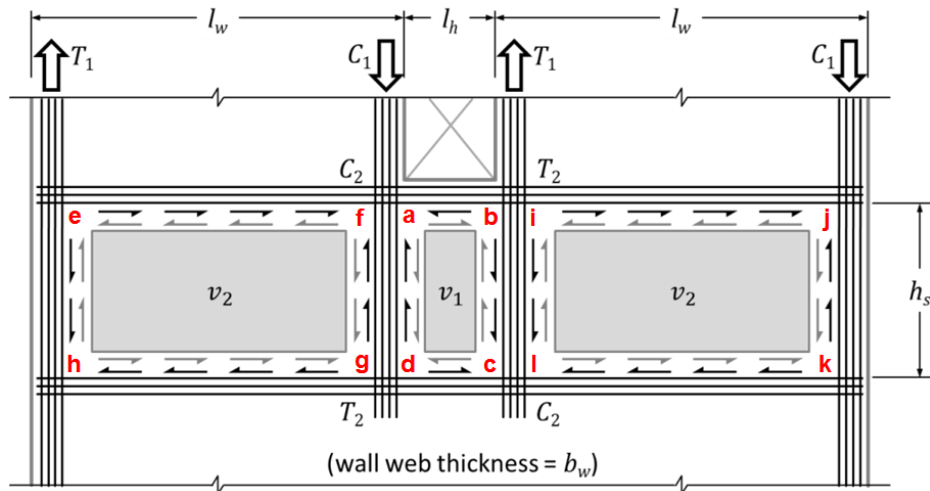


Figure C-11 Idealized resolution of basement wall forces beneath coupled walls.

One useful solution is obtained by assuming the coupled walls are weightless, lightly coupled, and of equal length, l_w (Figure C-11). Shear forces coming from the walls above are also ignored. Assuming $T_2 = C_2$, horizontal force equilibrium of the chord

along **ab** requires $T_2 = C_2 = v_1 l_k b_w / 2$. Horizontal force equilibrium of chords along **ef** and **ij** likewise requires $T_2 = C_2 = v_2 l_k b_w$. Equating these relations and rearranging, results in $v_2 = \frac{l_h}{2l_w} v_1$.

Turning attention to the vertical chords at the boundaries of the openings, vertical force equilibrium of the tension chord requires $T_1 = (v_1 + v_2) h_s b_w = \left(1 + \frac{l_h}{2l_w}\right) v_1 h_s b_w$. Solving for v_1 , the shear stress in panel zone **abcd** is calculated as:

$$v_1 = \frac{1}{1 + l_h / 2l_w} \left(\frac{T_1}{h_s b_w} \right) \quad (\text{C-1})$$

Considering typical geometries $l_h = 1.8$ m (6 feet) and $l_w = 6.1$ m (20 feet), the multiplier on average shear stress in Equation C-1 is 0.9. Thus, most of the shear is resolved in the panel zone beneath the stack of openings, with much lower shear stress in the wider panels to either side.

This proposed solution satisfies equilibrium within the stated limitations, but it does not recognize required deformation compatibility among adjacent wall segments. Importantly, shear distortion of panel **abcd** likely would result in shear transfer to the panel immediately below. Thus, a good design solution would be to extend some of the vertical boundary bars below panel **abcd** to engage additional depth of the solid wall.

Flanged walls sometimes occur adjacent to stacks of openings. A common example is where the stack of openings coincides with a building corridor, in which case the corridor walls act as flanges. For this condition, a portion of the wall flange contributes to shear in the discontinuity region. No studies have been found to document the use of effective flange width for this purpose. A reasonable assumption is that the effective flange width extends laterally on both sides of the web a distance, b_{eff} , equal to the height, h , of the discontinuity region assumed to resist the panel shear (Figure C-12). By this assumption, the effective width increases as the design shear is spread deeper into the solid wall section below the stack of openings. The effective width need not extend further than the available width, nor further than half the distance to an adjacent wall web.

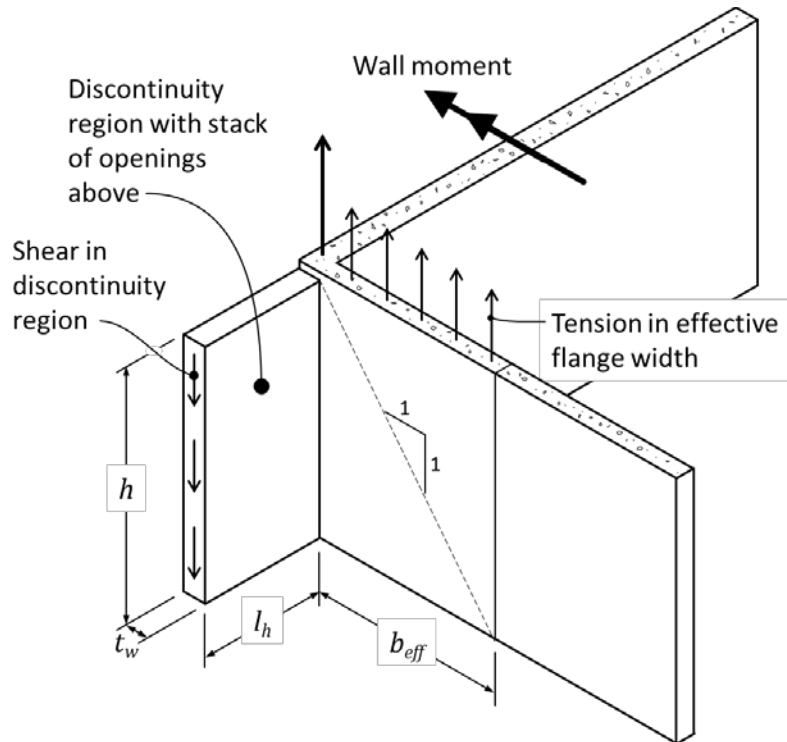


Figure C-12 Effective width of flanged wall loading a discontinuity region below a stack of openings.

C.4 Comparison of Shear Demand and Capacity in Discontinuity Region

The proposed Equation C-1 was applied to selected discontinuity regions of four buildings damaged in the 2010 Maule earthquake to calculate the shear stress in the region and compare with shear capacity and observed damage.

The following four buildings were studied:

1. The Alto Rio building was described in Section C.2.
2. Torre Mayor is a 17-story structure located in the city of Chillán. The building did not collapse during the 2010 Maule earthquake, but suffered damage along a discontinuity region below a stack of door openings (Figure C-3).
3. Centro Mayor is a 16-story structure located in the city of Concepción. The building did not collapse during the 2010 Maule earthquake, but suffered extensive damage in the first four stories, including damage to a wall below a stack of opening (Figure C-4).
4. Marina del Sol is a 20-story structure located in the city of Viña del Mar. The building did not collapse during the 2010 Maule earthquake, but suffered damage to a first floor wall below a stack of openings (Figure C-5).

In the Alto Rio building, the boundary reinforcement, including reinforcement in the flanges, was continuous from the bottom of the stack of openings to the foundation level. In the other three buildings studies the boundary reinforcement terminate at a distance past the discontinuity region but before the foundation level. Figures C-3 through C-5 show that even when the boundary reinforcement is anchored well past the discontinuity region, that region is vulnerable to shear damage as a result of force transfer that occurs near the discontinuity.

The following comparisons were made:

- The effective height, h , of a discontinuity region is taken equal as the lesser of the provided development length, l_d , of the main boundary reinforcement or the height $1.5l_h$ below the stack of openings, where l_h is the width of opening. The value of $1.5l_h$ is based on the observed depth of high stress (Naeim et al., 1990).
- Cracking shear strength of a discontinuity region is taken equal to $V_{cr} = v_{cr} t_w h$, where $v_{cr} = 4\sqrt{f'_c}$ psi (Sozen et al., 1992).
- Expected shear capacity is taken equal to nominal strength calculated in accordance with ACI 318-11 for squat walls, but using expected material properties. Specifically, shear strength is estimated as $V_n = v_n t_w h$, where $v_n = \left(3\sqrt{f'_c} + \rho_t f_{yt}\right)$ psi.
- Shear demand is calculated using Equation C-1 with the tension capacity of the boundary reinforcement, plus reinforcement within the effective flange width, b_{eff} , defined in Figure C-12. Tension capacity is based on the expected yield strength of the vertical reinforcement.

C.4.1 Findings

Results of the case studies are summarized in Table C-1.

Table C-1 Estimated Shear Demand and Capacity at Discontinuity Region

Building Wall	Steel Area, A_s , in. ²		f_y , ksi (f_{yt} , ksi)	Vertical Shear, $A_s f_y$, kips	Panel Dimensions		v_1 , psi	f'_c , psi	ρ_t	V_{cr} , psi	V_n , psi	v_1/V_n
	Boundary	Flange			Thickness, in.	Height ($\min l_d, 1.5l_h$), in.						
Alto Rio Grid 8	2.36	2.18	71 (71)	323	7.87	83	446	5,660	3.9×10^{-3}	301	502	0.89
Alto Rio Grid 13	2.36	5.94	71 (71)	591	7.87	83	813	5,660	2.5×10^{-3}	301	405	2.0
Torre Mayor	2.36	N/A	71 (71)	168	7.87	49.2	434	4,350	5.2×10^{-3}	264	567	0.77
Centro Mayor	7.61	N/A	71 (71)	540	7.87	63.0	1090	5,050	3.1×10^{-3}	284	433	2.5
Marina del Sol	9.13	N/A	71 (71)	648	9.84	59.1	1,120	5,220	4.2×10^{-3}	289	515	2.2

In the Alto Rio building, boundary element reinforcement was continuous to the base of the building without bar cutoffs. Therefore, the effective height of the discontinuity region is taken equal to the provided development length, l_d , of the main boundary reinforcement or $1.5l_h$ below the stack of openings. The estimated shear stresses are well above the cracking strength. Calculated shear stresses are 89% of the nominal strength along Grid 8 and 200% of nominal strength along Grid 13.

In the Torre Mayor building, boundary bars were discontinued 49.2 inches below stacks of openings (Figure C-13). Calculated shear stresses are above the cracking strength, and 77% of calculated nominal strength.

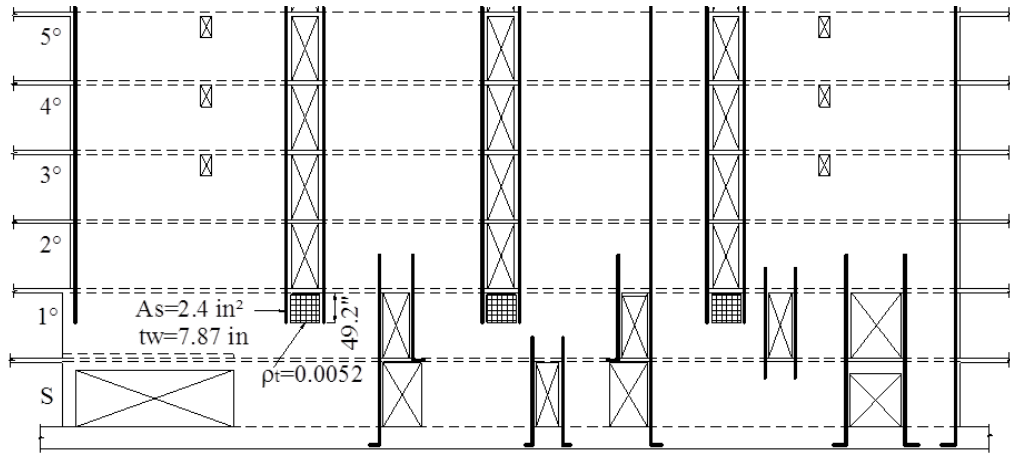


Figure C-13 Torre Mayor building reinforcement details around panel zone of interest.

In the Centro Mayor building, boundary bars are discontinued 63 inches below stacks of openings (Figure C-14). Calculated shear stresses are well above the cracking and nominal strengths.

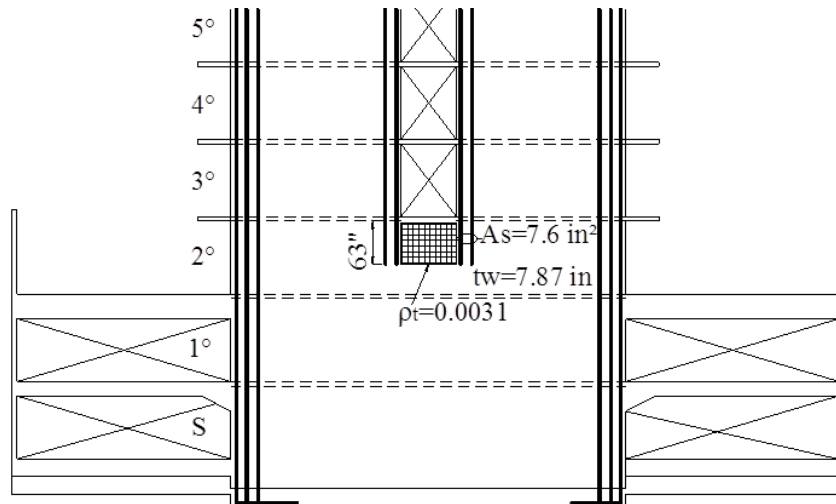


Figure C-14 Centro Mayor building reinforcement details around panel zone of interest.

In the Marina del Sol building, boundary bars are discontinued 59.1 inches below stacks of openings (Figure C-15). Calculated shear stresses are well above the cracking and nominal strengths.

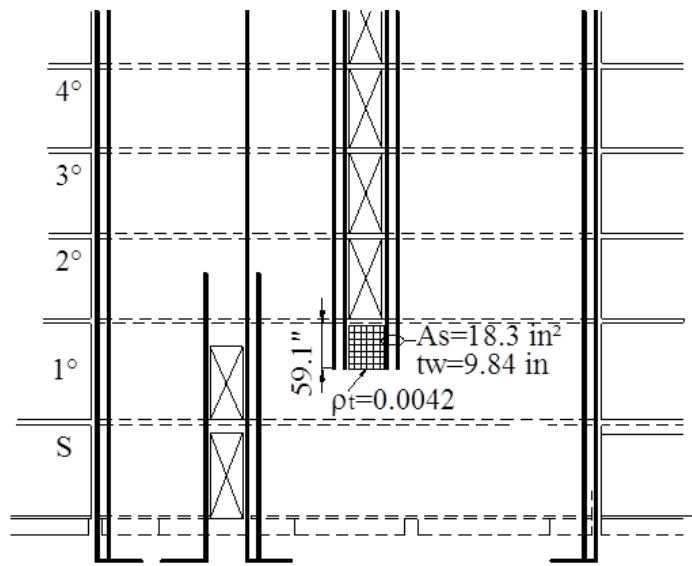


Figure C-15 Marina del Sol building reinforcement details around panel zone of interest.

C.4.2 Discussion

In two out of five cases, the calculated shear stress in the discontinuity region was marginally below the calculated nominal strength, such that the observed failures would not have been anticipated. In three other cases, the calculated stress exceeded nominal strength, consistent with the observed failures. Although the calculation procedures could be adjusted to improve the results for the two cases in which failure occurred but was not anticipated, such adjustments seem unwarranted considering the overall approximate nature of the procedures and the limited database.

The case study analyses adopted a depth for the discontinuity region equal to the lesser of the provided development length l_d and $1.5l_h$. The latter quantity is based on the linear analysis results of Naeim et al. (1990). For design purposes, it is more practical to consider the depth of the discontinuity region to be equal to the story height for the story below (or above) the stack of openings. This depth is not significantly different from $1.5l_h$ in typical construction. With this depth, the horizontal chords required for equilibrium of the panel (Figure C-9) can be located within the floor slabs. If the entire panel is reinforced for required shear stresses, it should be possible to use the entire height h_s to resist shear without overstressing the more highly stressed region immediately adjacent to the stack of openings.

Three of the four case study buildings had boundary reinforcement that was terminated l_d into the discontinuity region. In each of these cases, the failure was

clearly demarked by the length l_d . The preferred design solution is to always extend the bars at least l_d but not less than full story height h_s into the discontinuity region.

It is noteworthy that the Alto Rio building showed signs of distress in the discontinuity regions even though all reinforcement extended from the level with the stack of openings all the way to the foundation. This suggests that force transfer between the reinforcement and the discontinuity region occurs in the highly stressed portion of the discontinuity region immediately adjacent to the stack of openings, regardless of the provided development length. In the Alto Rio building, however, the complete collapse of the building obscured the initiation of various failure modes, such that the role of the damage in the discontinuity region is uncertain. Furthermore, there are no other known cases of damage in buildings with reinforcement continuous to the foundation. Thus, it is not fully clear how this condition should be considered in design. The conservative approach would be to assume full force transfer within the story immediately adjacent to the stack of openings, and design for this force to the extent practicable.

Appendix D

Study of Vertical Discontinuities

This appendix presents detailed information on the approaches and assumptions used in investigating issues related to vertical discontinuities in Chapter 4, Section 4.4. A study was conducted to explore the extent to which commonly used evaluation tools capture configuration issues by comparing observed damage related to vertical discontinuities with damage predicted using the available evaluation procedures.

A total of five buildings were evaluated using the procedures in ASCE/SEI 31-03, *Seismic Evaluation of Existing Buildings* (ASCE, 2003), and ASCE/SEI 41-06, *Seismic Rehabilitation of Existing Buildings* (ASCE, 2007). Tier 1, Tier 2, and Tier 3 Evaluations were conducted on these buildings to varying levels of detail. All five buildings were evaluated using Tier 1, three buildings were evaluated using Tier 2, and one building was evaluated using Tier 3. A study was also performed on wall discontinuities to investigate possible correlation between damage and a proposed new measure of the severity of local wall discontinuities.

D.1 Building Descriptions

Five buildings were studied as a part of the building configuration studies. In the sections that follow, a brief description of each building is provided, along with photos showing the exterior of the structure. For most buildings, sketches of floor plans are provided that indicate the level of damage observed in the lower stories. Brief descriptions of the damage levels, including the color used to indicate the damage in the floor plans, are provided in Table D-1. Additional details of the buildings are available in Birely (2012).

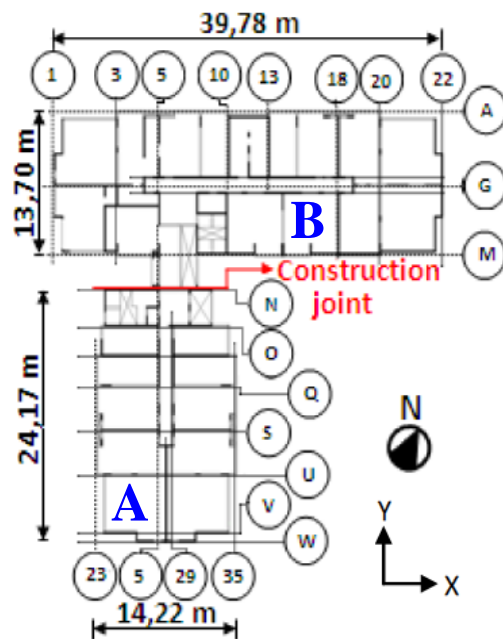
Table D-1 Descriptions of Identified Damage Levels

Damage Level Name (Number)	Color	Description
None (0)		No visible damage
Minor (1)		Minor cracks
Moderate (2)		Initial spalling
Severe (3)		Exposed reinforcement; Initial bar buckling and/or concrete crushing
Total (4)		Extensive bar buckling and concrete crushing

D.1.1 Plaza del Rio Building A

Plaza del Rio Building A (PR-A), located in Concepción, is a 12-story structure. The typical floor plate measures 24 m (79 feet) by 14 m (47 feet) with the longitudinal axis oriented approximately in the north-south direction. Figure D-1 shows the exterior of the building and typical floor plans; also shown in Figure D-1 is the adjacent Plaza del Rio Building B (see Section D.1.2). Walls are typically 150 mm (6 inches) thick and slabs are typically 130 mm (5 inches) thick. The foundation is a mat foundation approximately 400 mm (16 inches) thick, with a small basement under the elevator core. The soil at the site is on the boundary of site classes D and E per ASCE/SEI 7-10 designations. The design concrete strength is 25 MPa (3.6 ksi).

Damage was concentrated on the first two floors and included the following: (1) concrete damage to walls in the east-west (transverse) direction, including cracking, concrete spalling, bar buckling, bar fracture, crushing of core concrete, and global buckling of wall piers; (2) heaved soil around the foundation; and (3) damage to elevator shaft walls and coupling beams. Figure D-2 shows the layout of the walls on the first two floors, with the damage level indicated by the colors specified in Table D-1. The most severe damage occurred in the pair of Z-shaped walls located at the south end of the building and the pair of T-walls oriented in the east-west direction in the center of the building.



(a) Exterior view of both towers (Cerda, 2011)

(b) Typical floor plan (Westenenk et al., 2012)

Figure D-1 Overview of Plaza del Rio Buildings A and B. The two buildings form an “L” shape and are separated by a construction joint. Building A is the stem of the L-shaped building and Building B is the flange.

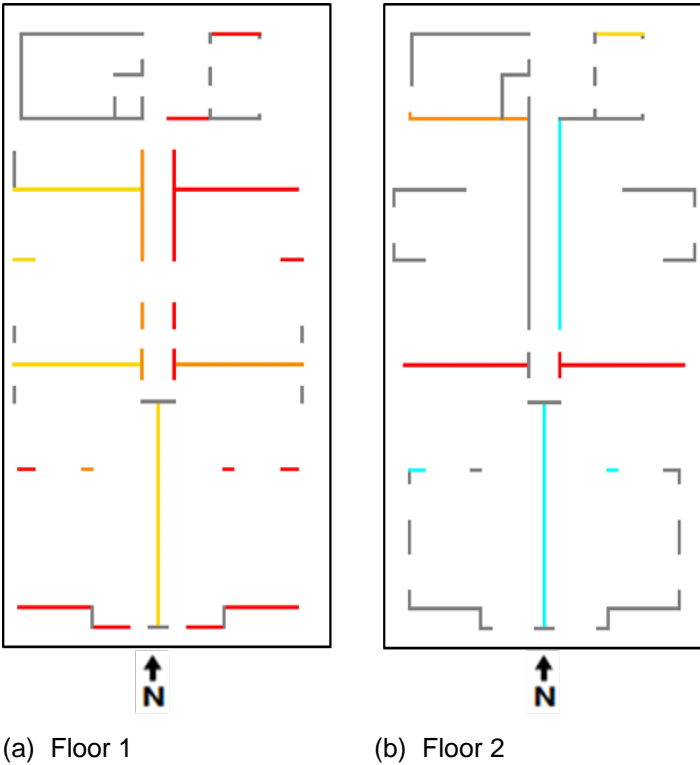


Figure D-2 Layout of first and second story walls of Plaza del Rio Building A (beams and slabs are not shown). Color indicates the level of damage.

D.1.2 Plaza del Rio Building B

Plaza del Rio Building B (PR-B), located in Concepción, is a 13-story structure with no basement. The typical floor plate measures 40 m (131 feet) by 14 m (45 feet) with the longitudinal axis oriented approximately in the east-west direction. Figure D-3 shows the exterior of the building and typical floor plans; also shown in Figure D-3 is the adjacent Plaza del Rio Building A (see Section D.1.2). Walls are typically 150 mm (6 inches) thick and slabs are typically 130 mm (5 inches) thick. The foundation is a mat foundation approximately 400 mm (16 inches) thick. The soil at the site is on the boundary of site classes D and E per ASCE/SEI 7-10 designations. The design concrete strength is 25 MPa (3.6 ksi).

Only minor damage (wall diagonal cracking) in the first story was observed following the earthquake. Figure D-6 shows the layout of the walls on the first two stories, with the damage level indicated by the colors specified in Table D-1.

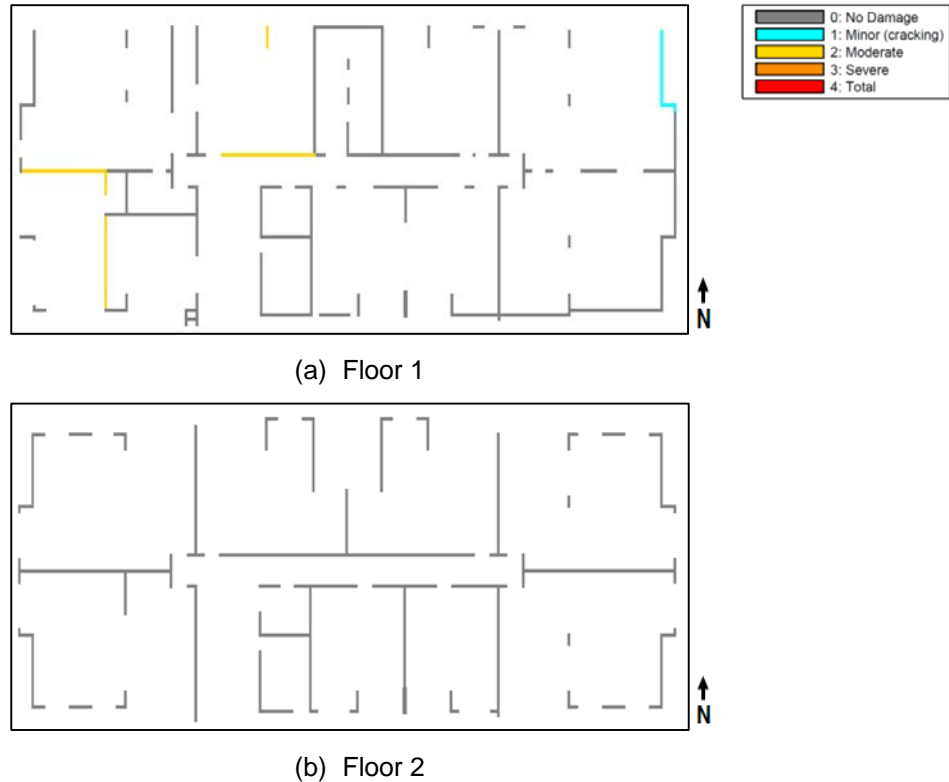


Figure D-3 Layout of walls for lower two floors of Plaza del Rio Building B (beams and slabs are not shown). Color indicates the level of damage.

D.1.3 Centro Mayor

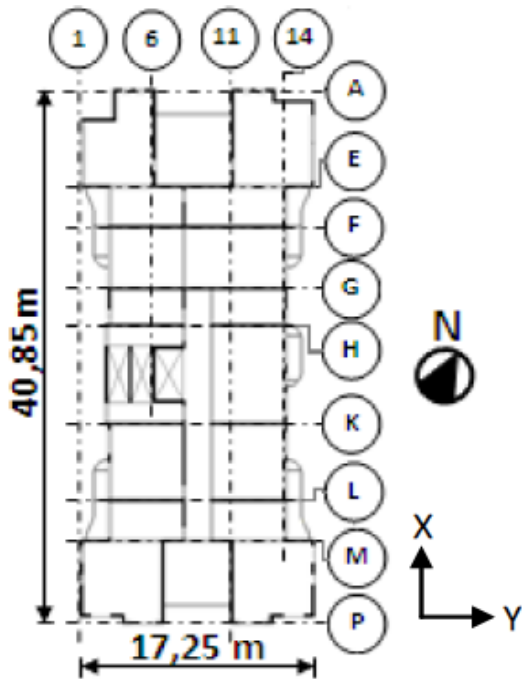
The Centro Mayor building, located in Concepción, is a 17-story structure with two basement levels. The typical floor plate measures 41 m (134 feet) by 17 m (57 feet) for most floors. Figure D-4 shows the exterior of the building and typical floor plans. Walls are typically 200 mm (8 inches) thick and slabs were typically 6 inches thick. The foundation is a mat foundation. The soil at the site is on the boundary of site classes D and E per ASCE/SEI 7-10, *Minimum Design Loads for Buildings and Other Structures* (ASCE, 2010), designations. The design concrete strength is 25 MPa (3.6 ksi).

Damage to the structure included: (1) severe concrete damage in walls in the east-west direction in the second and third stories and basement; (2) concrete damage extending diagonally through multiple piers separated by openings; (3) concrete and reinforcing steel damage in wall piers; (4) diagonally oriented damage to horizontal wall segments/coupling beams; (5) extensive concrete damage in T-, L-, and D-shape walls; and (6) slab damage. Figure D-5 shows the layout of the walls on the basement floors and first two above grade floors, with the damage level indicated by the colors specified in Table D-1.



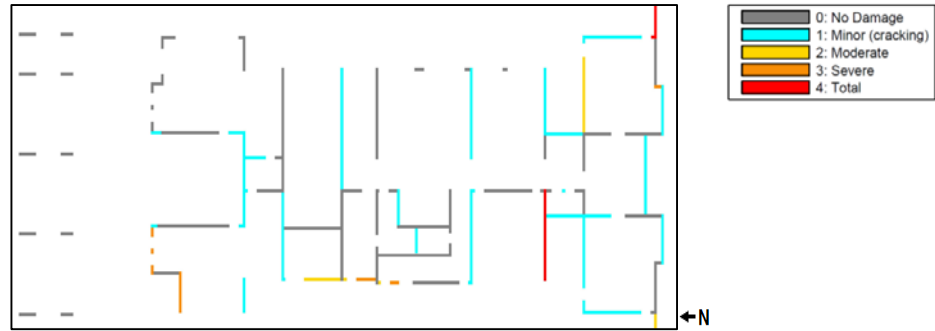
(a) North-south view (from DICTUC, 2010a)

(b) East-west view (from DICTUC, 2010b)

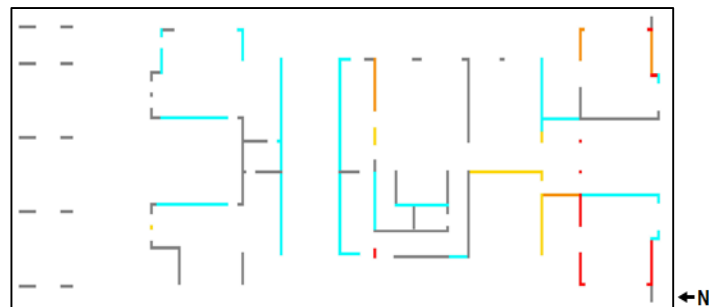


(c) Typical floor plan (from Westenenk et al., 2012)

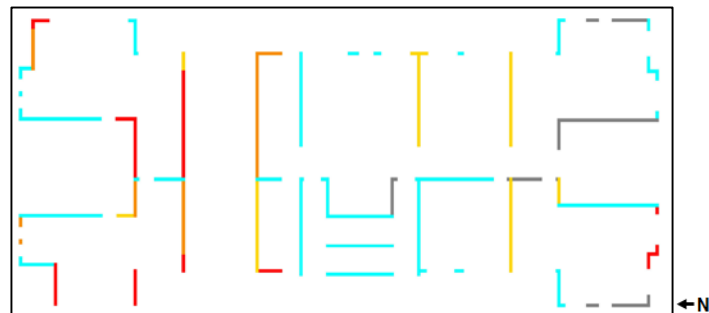
Figure D-4 Overview of Centro Mayor building.



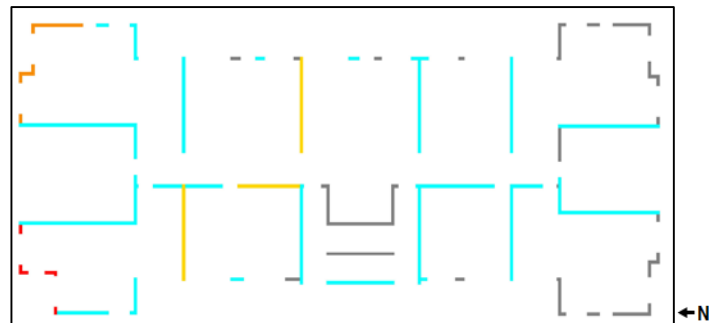
(a) Lower basement walls. Note that the lines on the left of the building depict walls that exist only in the basement levels and do not continue above the ground floor.



(b) Basement walls. Note that the lines on the left of the building depict walls that exist only in the basement levels and do not continue above the ground floor.



(c) First floor walls



(d) Second floor walls

Figure D-5 Layout of walls for the lower four floors of Centro Mayor building (beams and slabs are not shown). Color indicates the level of damage according to Table D-1.

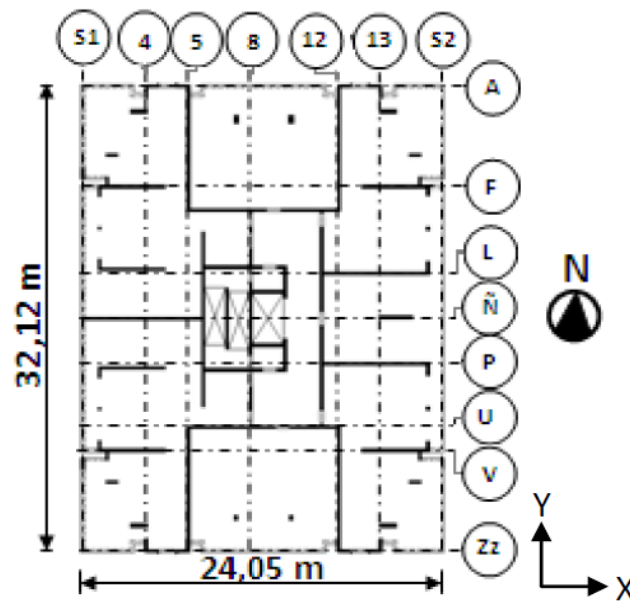
D.1.4 Alto Huerto

Alto Huerto (AH), located in San Pedro de la Paz, is a 15-story structure with two basement levels. The typical floor plate measures 32 m (105 feet) by 24 m (80 feet) for most floors. Figure D-6 shows an exterior view of the building and the plan of a typical floor. Walls are typically 200 mm (8 inches) thick and slabs are typically 6 inches thick.

During the earthquake, the walls sustained crushing and moved out-of-plane in the first story and basement. Localized damage occurred in discontinuous walls in the fifteenth story and other continuous walls in upper stories. Many flag-shaped walls were damaged. Floor plans indicating damage level are not available.



(a) Exterior



(b) Typical floor plan (from Westenenk et al., 2012)

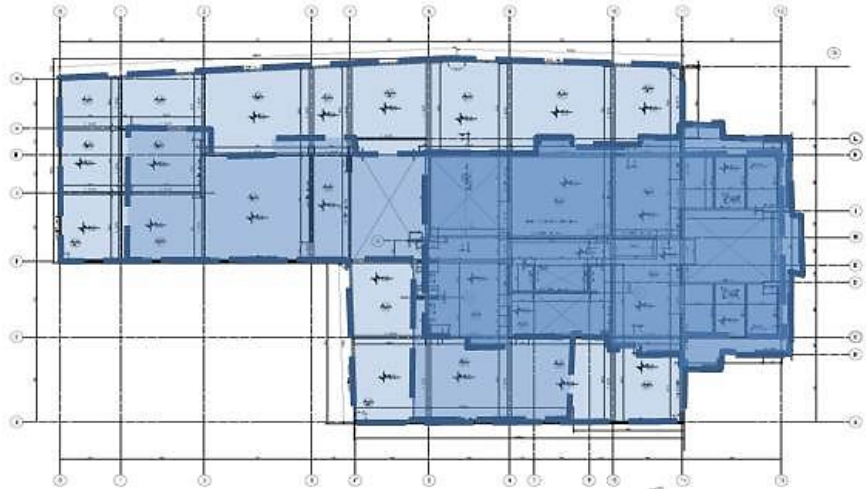
Figure D-6 Overview of Alto Huerto building.

D.1.5 Concepto Urbano

Concepto Urbano (CU), located in Concepción is a 22-story structure with two basement levels. The typical floor plate ranges from 52 m (170 feet) by 29 m (94 feet) in the basement and first floor to 49 m (159 feet) by 23 m (75 feet) for second through tenth floor and to 29 m (96 feet) by 17 m (57 feet) for eleventh floor and higher. Figure D-7 shows an artist's rendering of the exterior of the building, as well as a floor plan for the building at different levels. Most walls were between 200 mm (8 inches) and 300 mm (12 inches) thick, with thicker walls in the lower floors and decreased thickness in upper floors. Slabs are typically 150 mm (6 inches) thick. The foundation is a mat foundation approximately 400 mm (16 inches) thick. The

soil at the site is on the boundary of site classes D and E per ASCE/SEI 7-10 designations. The design concrete strength was 25 MPa (3.6 ksi).

No damage was reported following the earthquake. Figure D-8 shows the layout of the walls on the first two floors, with all walls indicating no damage by the colors specified in Table D-1.



(a) Exterior view
(from <http://www.boulevardimobiliario.cl/proyectos/54/>, last accessed March 7, 2014)

(b) Floor plan. The different shades indicate the plan at different levels of the structure.

Figure D-7 Overview of Concepto Urbano.

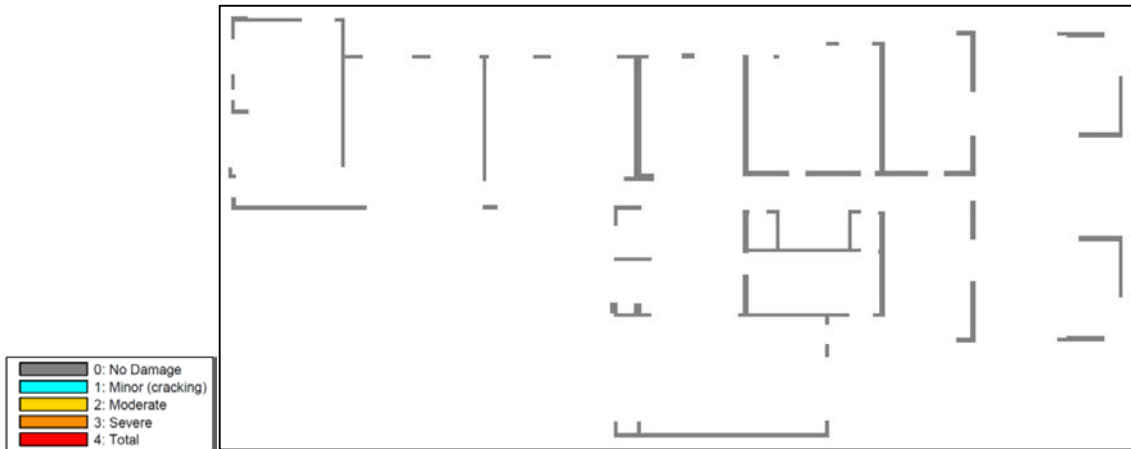


Figure D-8 Layout of walls for a typical floor of Concepto Urbano building (beams and slabs are not shown). The gray color indicates no observed damage.

D.2 ASCE/SEI 31-03 Tier 1 Evaluations

Conducting ASCE/SEI 31-03 Tier 1 Evaluations involves the completion of a series of checklists. Basic and supplemental checklists are provided in ASCE/SEI 31-03

and are specific to the building system considered. All five buildings are classified as building type C2, concrete shear wall buildings with rigid or stiff diaphragms. Accordingly, the basic structural checklist for building type C2, provided in ASCE/SEI 31-03 Section 3.7.9 was used. Completion of the checklists involves evaluating a series of criteria to determine if each statement is compliant, non-compliant, or not applicable. Any criterion determined to be non-compliant is subject to further evaluation in Tier 2.

D.2.1 Summary of Tier 1 Evaluation Results

Table D-2 provides a summary of the checklist statements identified as non-compliant for the five buildings studied.

Table D-2 Summary of ASCE/SEI 31-03 Checklist Items Identified as Non-Compliant (NC)

Checklist Item	Building Name				
	<i>Alto Huerto</i>	<i>Centro Mayor</i>	<i>Plaza del Rio A</i>	<i>Plaza del Rio B</i>	<i>Concepto Urbano</i>
Weak story	NC	NC	NC		NC
Soft story	NC	NC	NC	NC	NC
Geometry (changes in horizontal dimension of LFRS by more than 30% between stories)		NC			NC
Vertical discontinuities (discontinuous walls)	NC	NC	NC	NC	NC
Mass (change by more than 50% between stories)		NC			
Shear stress check (in concrete walls)		NC	NC	NC	
Reinforcing steel (ratio less than 0.0025 for wall horizontal reinforcement)					NC
Foundation dowels (not able to develop strength of walls or foundation)	(2)	NC ⁽¹⁾	(2)	NC	(2)
Overturning (walls with aspect ratio greater than 4:1)	NC ⁽¹⁾	NC ⁽¹⁾	NC ⁽¹⁾	NC ⁽¹⁾	(2)
Confinement reinforcing (lacking closely-spaced boundary ties)	NC ⁽¹⁾	NC ⁽¹⁾	NC ⁽¹⁾	NC ⁽¹⁾	(2)
Reinforcing at openings (lacking trim bars)			NC ⁽¹⁾	NC ⁽¹⁾	(2)
(Diaphragm) Openings at shear walls	NC	NC	NC	NC	(2)
(Diaphragm) Plan irregularities (limited reinforcement at re-entrant corners)		NC ⁽¹⁾	NC ⁽¹⁾	NC ⁽¹⁾	(2)

⁽¹⁾ Non-compliance for Immediate Occupancy performance level only

⁽²⁾ Condition not known

In comparing observed damage with Tier 1 Evaluation results across all buildings, the following general observations were made: (1) the shear-stress check did not correlate well with damage; (2) a significant change in stiffness or strength between two adjacent stories is more critical if the lower story is more flexible or weaker; and

(3) the weak story check was a marginally better predictor of a higher likelihood of damage than the soft story check.

D.3 ASCE/SEI 31-03 Tier 2 Evaluations

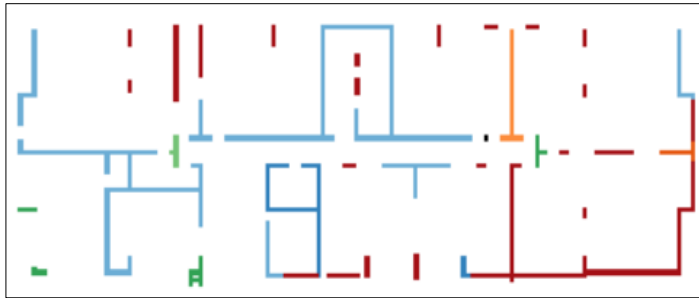
ASCE/SEI 31-03 Tier 2 Evaluations were completed for the Centro Mayor building and Plaza del Rio Buildings A and B. Tier 2 Evaluations involve computation of demand-capacity ratios (DCRs) for individual components using linear analysis results. In this study, Tier 2 Evaluations were conducted using the Linear Dynamic Procedure (LDP) detailed in ASCE/SEI 41-06. Demands were determined using three different response spectra to compare results:

1. ASCE/SEI 7-10, *Minimum Design Loads for Buildings and Other Structures* (ASCE, 2010), spectrum for Site Class D in a region of high seismicity in the United States (with site coefficients $F_a = 1.0$; $F_v = 1.5$, and spectral response acceleration parameters $S_s = 2.0$, $S_l = 1.0$) for the design earthquake (DE) and the maximum considered earthquake (MCE),
2. Chilean spectra based on the code in effect at the time the building was designed and as currently proposed, using Soil Type III (equivalent to Site Class D per ASCE/SEI 7-10), and
3. Response spectra generated from ground motion recordings at the Concepción and the Concepción-San Pedro de la Paz stations.

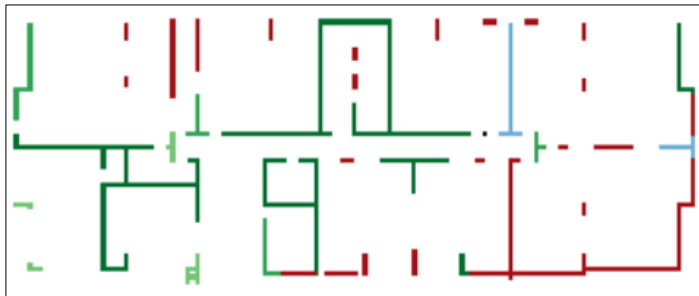
D.3.1 Summary of Tier 1 Evaluation Results

Evaluation results and conclusions for Plaza del Rio Building A are presented in Chapter 4. Summary results for Centro Mayor and Plaza del Rio Building B are provided here. Additional details for all building evaluations are presented in Birely (2012).

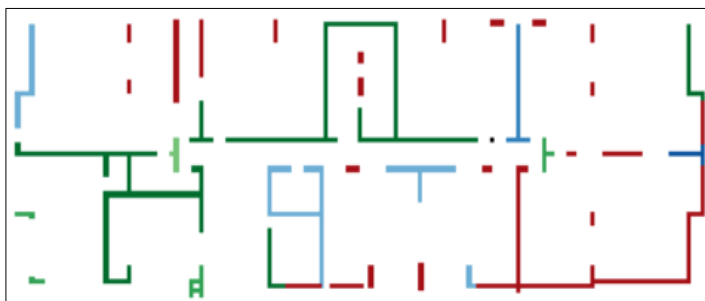
Figures D-9 through D-12 show unfactored DCR values (DCR_u) and controlling response for the critical story of the Centro Mayor building and Plaza del Rio Building B. Evaluation of these data in addition to the data for Plaza del Rio Building A presented in Chapter 4 show the following: (1) for all of the buildings, DCR_u values exceeded 2.0 for most of the primary lateral-load resisting walls for the ASCE/SEI 7-10 and San Pedro de la Paz response spectra; (2) for the Centro Mayor building and Plaza del Rio Building B, DCR_u values exceeded 2.0 for many of the primary lateral-load resisting walls for the Concepción response spectrum; and (3) for all buildings and all response spectra, the controlling mechanism for almost all primary lateral load-resisting walls was found to be flexure or shear; Centro Mayor building and Plaza del Rio Building B were found to have more shear-critical than flexure-critical walls.



(a) ASCE response spectrum



(b) Concepción response spectrum



(c) San Pedro de la Paz response spectrum

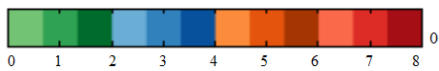
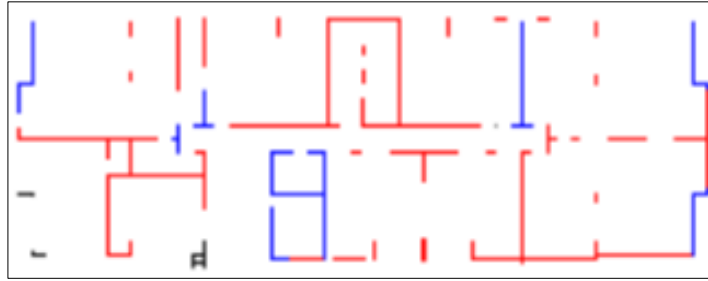
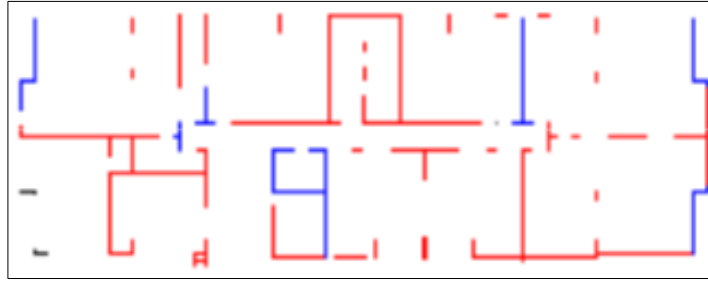


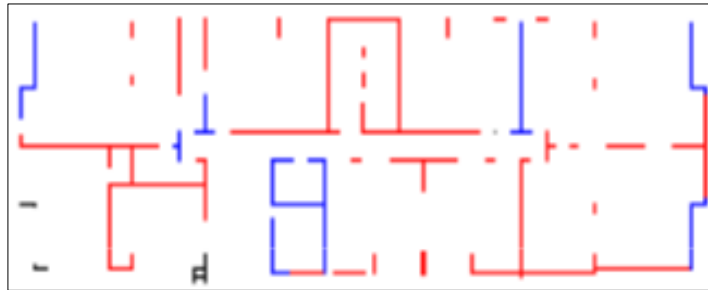
Figure D-9 Maximum DCR_u values for first story walls at Plaza del Rio Building B. Values range from 0 (light green) to 8 (dark red).



(a) ASCE response spectrum



(b) Concepción Response Spectrum



(c) San Pedro de la Paz response spectrum

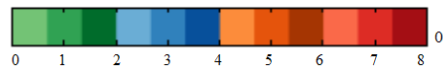
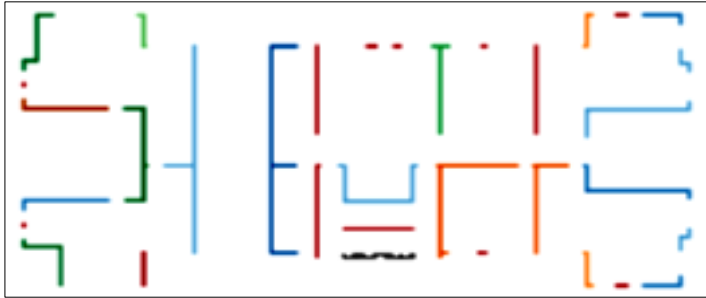
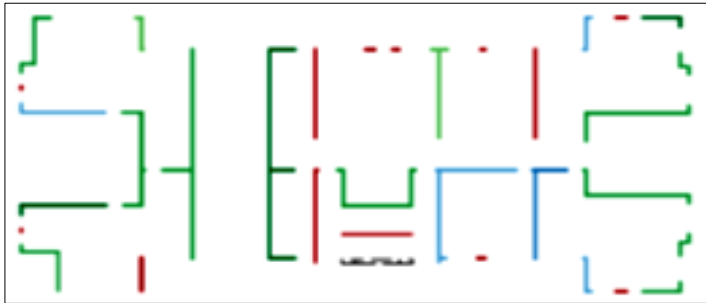


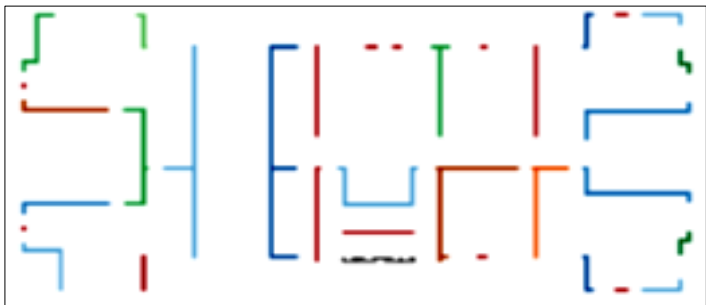
Figure D-10 Controlling response determined by largest DCR_u value for first story walls at Plaza del Rio Building B. Blue indicates flexure mechanism; red indicates shear mechanism; black indicates axial mechanism.



(a) ASCE response spectrum



(b) Concepción response spectrum



(c) San Pedro de la Paz response spectrum

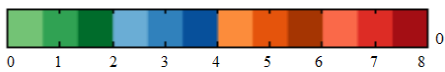
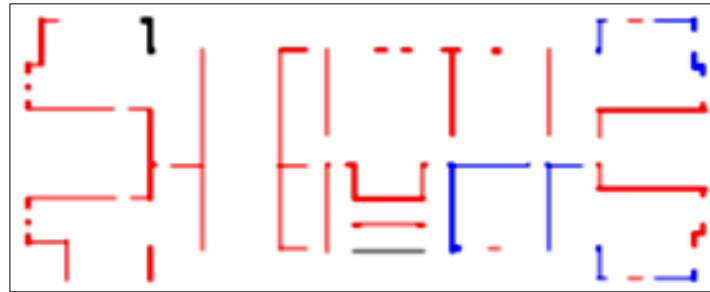
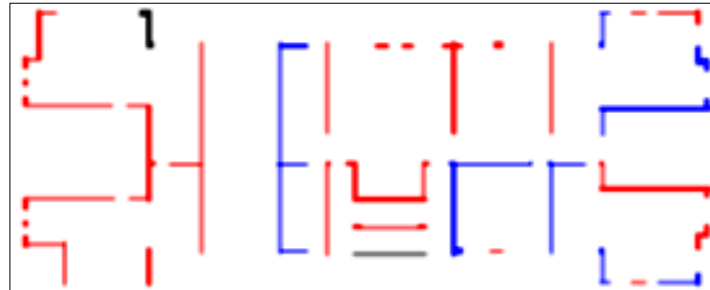


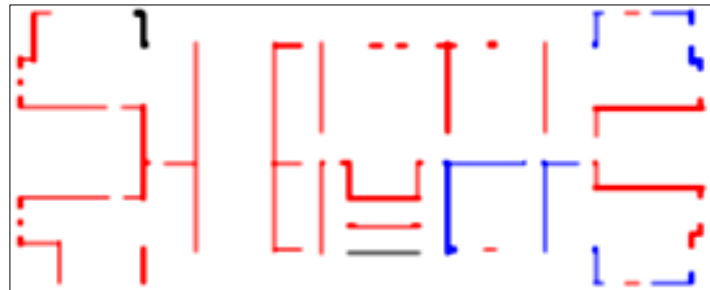
Figure D-11 Maximum DCR_u values for first story walls at Centro Mayor building. Values range from 0 (light green) to 8 (dark red).



(a) ASCE response spectrum



(b) Concepción response spectrum



(c) San Pedro de la Paz response spectrum

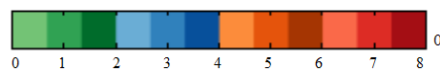


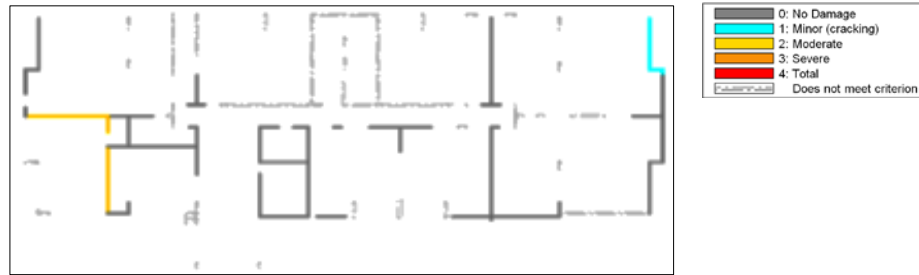
Figure D-12 Controlling response determined by largest DCR_u value for first story walls at Centro Mayor building. Blue indicates flexure mechanism; red indicates shear mechanism; black indicates axial mechanism.

ASCE/SEI 31-03 Tier 2 evaluation results also provide an opportunity to compare the severity of observed damaged with the predicted damage and resulting performance level. If the DCR_u values are less than 2, factored demand-capacity ratios (DCR_f) from linear analysis results can be used to predict the performance of the structure. The DCR_u values in Figures D-9 and D-11 indicate that evaluation using linear analysis results and DCR_f values is not appropriate, and nonlinear analysis should be performed. However, evaluation on the basis of DCR_f values was conducted to investigate the correlation between DCR_f values and damage. DCR_f values were computed for all of the spectra discussed above with m -factors provided in ASCE/SEI 41-06.

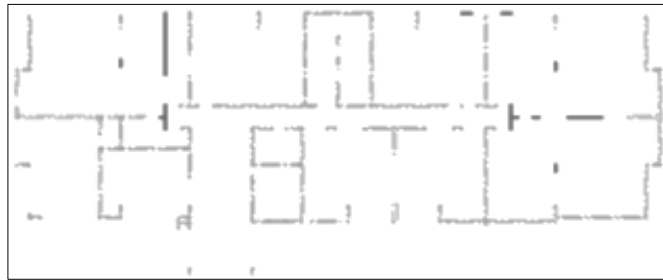
For design spectra, DCR_f were computed for the critical floor of each building and the building was assessed for three performance objectives: (1) Collapse Prevention at the MCE level (CP-MCE); (2) Life Safety at the DE level (LS-DE); and (3) Immediate Occupancy at the DE level (IO-DE). Similarly, for demands determined from recorded acceleration histories, DCR_f were computed for the unscaled, as-recorded motions (GM); in this case, performance objects were identified as CP-GM, LS-GM and IO-GM.

Figures D-13 and D-14 show these data for the ASCE/SEI 7-10 response spectrum for the Centro Mayor building and Plaza del Rio Building B. The data in these figures show the following for the ASCE/SEI 7 response spectrum scaled to the DE and MCE: (1) for Plaza del Rio Building B, most primary lateral load-resisting walls are inadequate for all performance objectives, though some are adequate for life safety for DE; (2) for the Centro Mayor building, about 50% of the walls are adequate for various performance objectives and about 50% are inadequate for all performance objectives; and (3) there appears to be little correlation between adequacy per ASCE/SEI 31-03 Tier 2 Evaluation and observed damage.

DCR_f data such as those in Figures D-13 and D-14 were also evaluated by counting the number of walls in heavily loaded lower stories expected and not expected to meet performance objectives and by identifying the severity of observed damage for the walls in each category. The height of the bars in Figures D-15 and D-16 show the number of first story walls in Plaza del Rio Building B and second story walls in the Centro Mayor building with calculated DCR_f values below and above one. Colors indicate the severity of observed damage for the walls in each category. Dashed gray lines indicate walls that do not meet the criterion for that panel. It is observed from the figures that there is little correlation between the predictions for individual components from the ASCE/SEI 31-03 Tier 2 procedure and the observed damage.



(a) Inadequate for all performance objectives



(b) Adequate for CP-DE

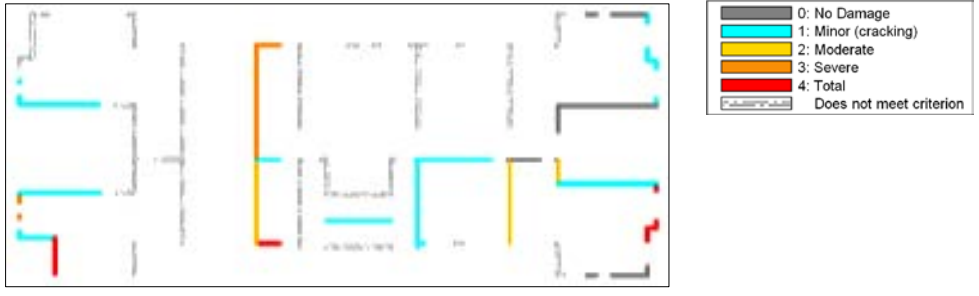


(c) Adequate for LS-DE

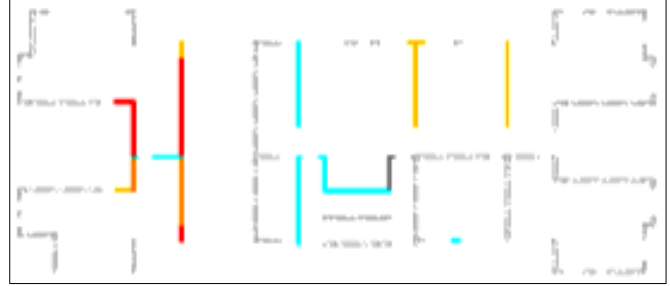


(d) Adequate for IO-DE

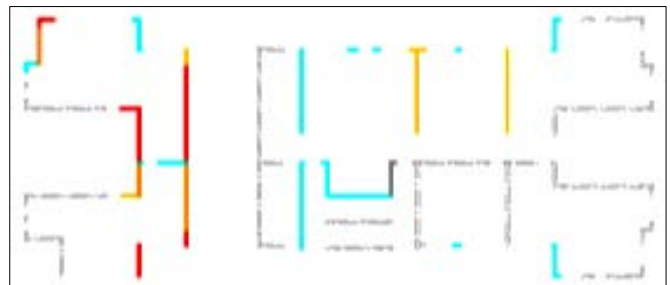
Figure D-13 First story walls of Plaza del Rio Building B expected to achieve ASCE/SEI 41-06 performance levels for the Design Earthquake. A colored wall indicates that the DCR_f is such that it is deemed adequate for the performance level and the fill color indicates the severity of the observed damage. Dashed gray lines indicate walls that do not meet the criterion for that panel.



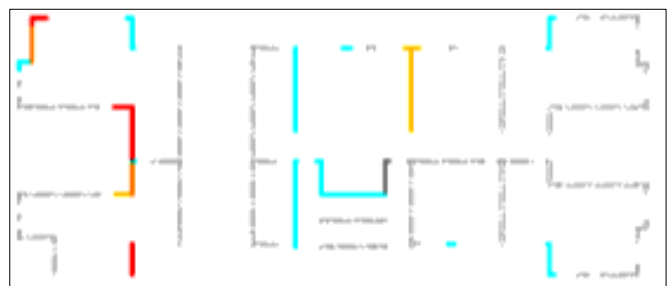
(a) Inadequate for all performance objectives



(b) Adequate for CP-DE

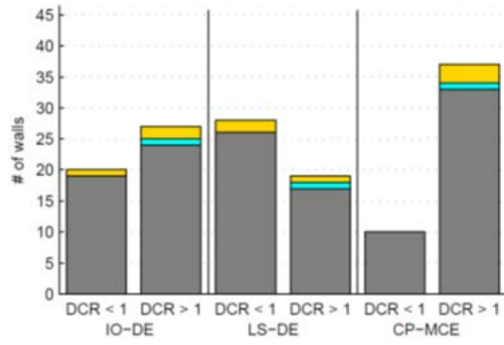


(c) Adequate for LS-DE

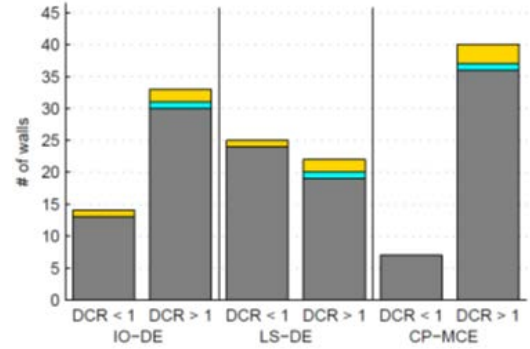


(d) Adequate for IO-DE

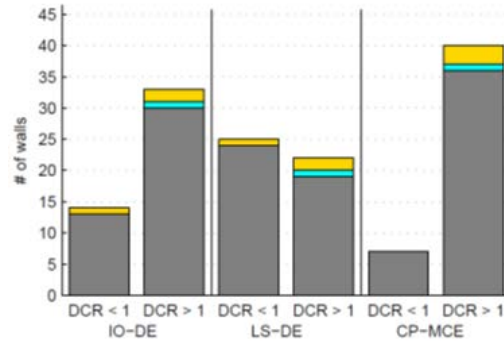
Figure D-14 Second story walls of the Centro Mayor building expected to achieve ASCE/SEI 41-06 performance levels for the Design Earthquake. A colored wall indicates that the DCR_f is such that it is deemed adequate for the performance level and the fill color indicates the severity of the observed damage. Dashed gray lines indicate walls that do not meet the criterion for that panel.



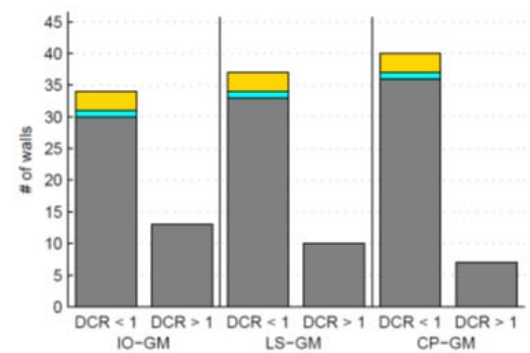
(a) ASCE response spectrum



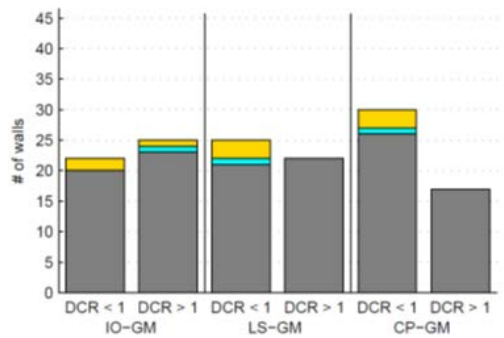
(b) Chilean response spectrum



(c) Proposed Chilean response spectrum



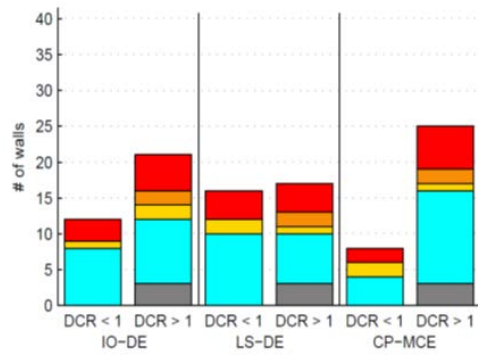
(d) Concepción response spectrum



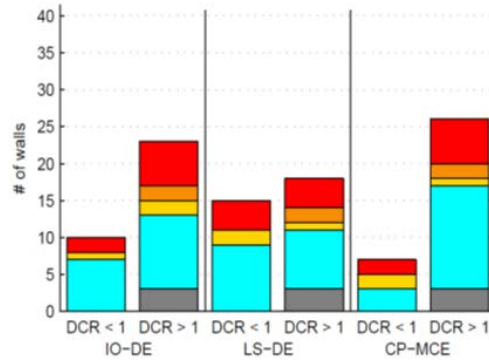
(e) San Pedro de la Paz response spectrum



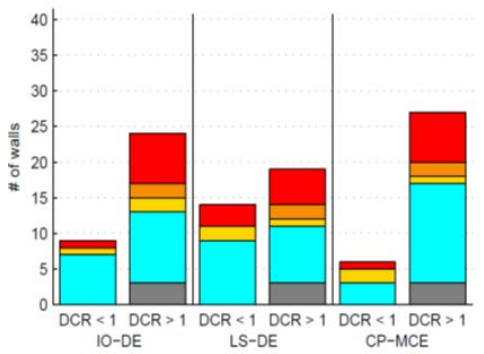
Figure D-15 Number of first story walls in Plaza del Rio Building B meeting and not meeting various performance objectives; colors indicate the severity of observed damage for walls in each category.



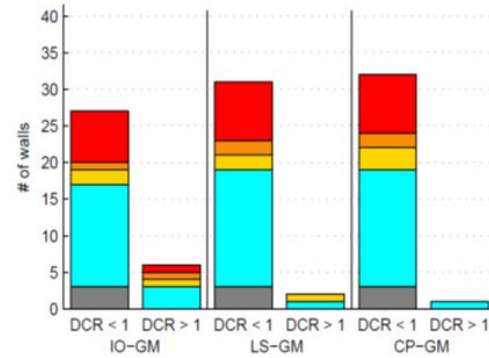
(a) ASCE response spectrum



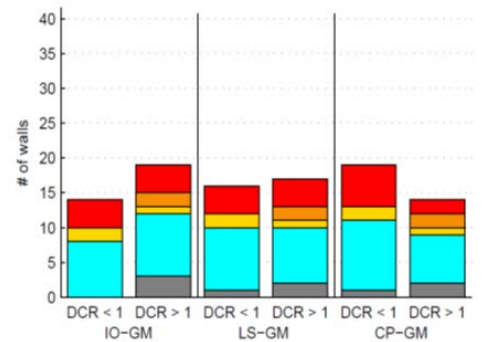
(b) Chilean response spectrum



(c) Proposed Chilean response spectrum



(d) Concepción response spectrum



(e) San Pedro de la Paz response spectrum

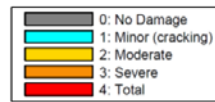


Figure D-16 Number of second story walls in the Centro Mayor building meeting and not meeting various performance objectives; colors indicate the severity of observed damage for walls in each category.

D.4 ASCE/SEI 31-03 Tier 3 Evaluations

In ASCE/SEI 31-03, detailed evaluation is conducted under Tier 3. The Tier 3 Evaluation procedure involves computation of maximum deformation demands and comparison with deformation capacities using nonlinear analysis. In this study, the Nonlinear Dynamic Procedure (NDP) specified in ASCE/SEI 41-06 was used. Plaza del Rio Building A was selected as the best candidate for conducting a Tier 3

nonlinear analysis, and investigating wall discontinuity effects using ASCE/SEI 41-06 (and other) criteria.

The ASCE/SEI 31-03 Tier 3 evaluation procedure comprises nonlinear dynamic analysis to compute maximum deformation demands for individual components, and comparison of maximum deformation demands with deformation capacities. If deformation demands exceed deformation capacities for various performance levels, then the component is deemed noncompliant for that performance level.

Deformation demands were computed for a suite of seven ground motions in Chile, scaled to match the ASCE/SEI 7-10 target spectrum for Site Class D in a region of high seismicity in the United States. Demands were also computed for the unscaled Concepción and Concepción-San Pedro de la Paz ground motions, with the objective of comparing calculated results with observed damage.

Nonlinear dynamic analyses were completed using the OpenSees, *Open System for Earthquake Engineering Simulation*, analysis platform (OpenSees, 2013) and PERFORM-3D, *Nonlinear Analysis and Performance Assessment for 3D Structures* (CSI, 2013c) Version 5.0.0. Three different approaches were used to determine the deformation capacity of structural wall components and assess performance (or the predicted level of damage):

- Rotation limits for wall components responding in flexure and shear, as provided in ASCE/SEI 41-06. These deformation capacities are a function of axial load and shear force demands, as well as wall design characteristics, and are used to assess acceptance for the Immediate Occupancy (IO), Life Safety (LS), and Collapse Prevention (CP) performance levels.
- Deformation limits from empirical fragility functions for slender walls responding in flexure from Birely (2012). These limits were used to determine the predicted damage state of wall components.
- Usable strain limits for concrete and longitudinal reinforcement, steel yield strain, concrete spalling strain, and concrete crushing strain, as provided in ASCE/SEI 41-06. These limits were used to assess material damage.

D.4.1 Nonlinear Modeling and Analysis

The following sections describe the OpenSees and PERFORM-3D numerical model development, present analysis results, summarize the results of the Tier 3 Evaluation, and compare predicted damage with damage observed following the 2010 Maule earthquake.

D.4.1.1 Gravity Loads

For both the OpenSees and PERFORM-3D models, gravity loads were estimated in accordance to the self-weight of structural members (including slab, walls, and

coupling beams). Gravity load was assumed equal to 170 psf including member self-weight. An additional dead load of 20 psf and a seismic live load of 12 psf were added to the slab. Seismic mass was applied at the center of mass of each diaphragm level based on output from SAP2000, *Integrated Software for Structural Analysis and Design*, Version 15 (CSI, 2013b).

D.4.1.2 Seismic Demands

Nonlinear dynamic analyses were performed for the case of the unscaled Concepción and San Pedro de la Paz records and for a suite of seven other Chilean ground motions (including the Concepción and San Pedro de la Paz records) scaled per ASCE/SEI 7-10 procedures to the minimum target spectra for the ASCE/SEI 7-10 DE and MCE spectra for Site Class D in a region of high seismicity in the United States (with parameters $F_a = 1.0$, $F_v = 1.5$, $S_s = 2.0$, $S_t = 1.0$). Figure D-17 shows the square root of the sum of the squares (SRSS) combination of the motions from the orthogonal directions of the unscaled records and the records scaled to the ASCE/SEI 7-10 DE minimum target spectrum. Using the OpenSees model, analyses were performed for all of the records and scaling described above; using the PERFORM-3D models, analyses were performed only for the unscaled Concepción and San Pedro de la Paz records.

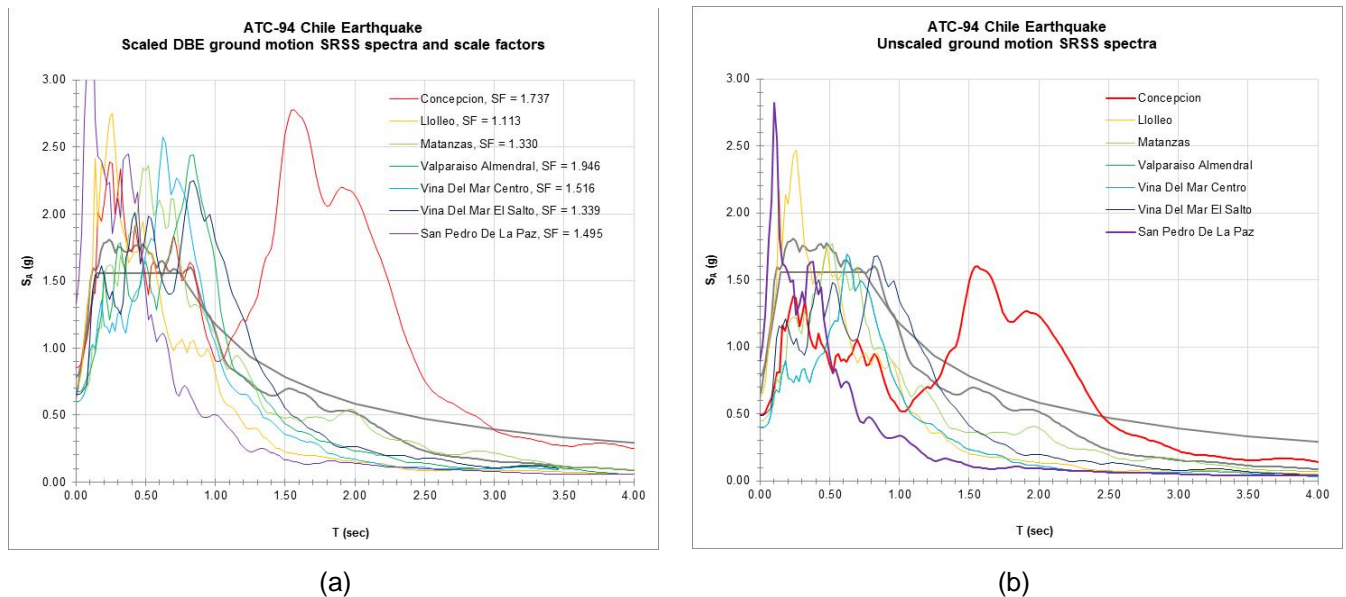


Figure D-17 SRSS response spectra of selected ground motion records from the 2010 Maule earthquake: (a) scaled; and (b) unscaled.

The available measured acceleration histories were defined in the north-south, east-west, and vertical directions. As the transverse direction of the Plaza del Rio Building A approximately coincided with the east-west direction and the longitudinal direction of the Plaza del Rio Building A approximately coincided with the north-

south direction, acceleration records were applied to the building without rotating. The vertical component of the ground acceleration was also used in the analyses.

D.4.2 OpenSees Nonlinear Analysis Model

A model of the Plaza del Rio Building A was created using the OpenSees platform. The model included only the walls; slabs, coupling beams and foundation elements were not included in the model. Walls were connected at the floor level via a rigid diaphragm constraint. The fiber-type force-based beam-column element available in the OpenSees platform was used to simulate the nonlinear response of the concrete walls. Rayleigh damping was used for the dynamic analysis with 2% critical damping defined at the elastic frequency of the first and third modes; in defining the damping matrix at each time step, the stiffness matrix from the previous converged state was used. P-delta effects were included in the analysis. The OpenSees model is presented in detail in Birely (2012); the model is described briefly below.

The fiber-type force-based beam-column element is a two-node line element. In the numerical model, this line element was located at the centroid of each wall. Birely (2012) documents how individual walls were defined. Where the centroid of a wall changed from one story to the next, an essentially rigid beam element was used to connect wall elements and provide force transfer. For each wall, one element with five integration points was used at each story; this was found by Pugh (2012) to provide accurate simulation of response.

The fiber-type force-based beam column element employs a fiber-type section model to simulate nonlinear flexural response. This section model comprises multiple concrete and steel fibers; a one-dimensional stress-strain model is used to simulate the response of these fibers. Fiber dimensions were approximately 0.4 inches by 1.2 inches. In defining the fiber-type section model, the recommendations of Pugh (2012) were employed. This included the level of discretization employed in the model and concrete and steel material models. Pugh (2012) shows that to accurately simulate loss of lateral load-carrying capacity in walls, it is necessary to “regularize” concrete and steel response using a mesh-dependent characteristic length and a measure of the energy dissipated in material softening. Without regularization of concrete and steel material response, the drift at which strength loss occurs is simulated inaccurately and is a function of the number of integration points used in the fiber-type beam-column element.

To enable simulation of nonlinear shear response, the fiber-type section model was combined with a shear section model. Figure D-18 shows the shear force versus shear strain model employed. The backbone curve for the model was developed using experimental data from planar wall tests (Lowe et al., 2012). The model was implemented in OpenSees using the hysteretic material model available in OpenSees, which can simulate a trilinear backbone curve and a pinched hysteretic response.

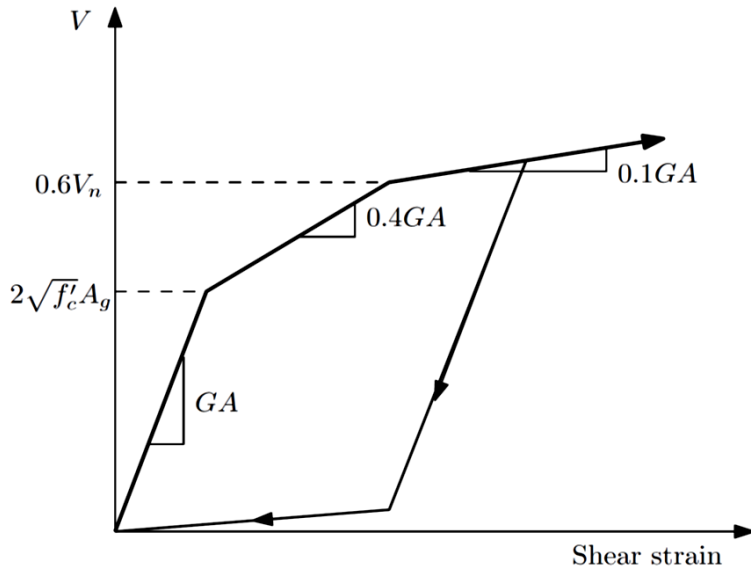


Figure D-18 Shear strength versus strain model employed in OpenSees analyses.

D.4.3 PERFORM-3D Nonlinear Analysis Models

Two models of Plaza del Rio Building A were created using PERFORM-3D. Figure D-19 shows the discretization of walls and coupling beams in the PERFORM-3D models.

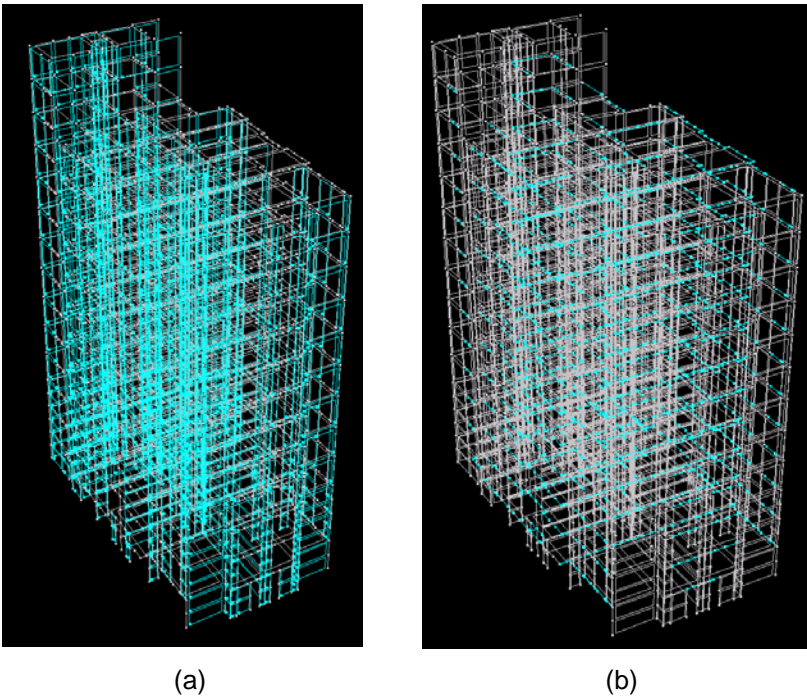


Figure D-19 Isometric view of PERFORM-3D model highlighting: (a) shear wall; and (b) coupling beams.

In one case, the building was modeled as having a fixed base (referred to as the “Perform Basic” model); in the second case, the building was modeled as having a flexible foundation (referred to as the “Perform SSI” model). For dynamic analyses under earthquake loading, both models included shear walls and coupling beams; walls were connected at the floor level via a rigid diaphragm constraint. Concrete slabs were included in the model and the rigid diaphragm concrete weight was removed for the gravity load analysis. P-delta effects were included in the dynamic analyses. Rayleigh damping was used for dynamic analysis with 2% critical damping defined at the elastic frequency of the first and third modes.

D.4.3.1 PERFORM-3D Modeling of Concrete Shear Walls

Concrete shear walls were modeled using the four-node shear wall shell element available in the PERFORM-3D software. Using this model, flexural response of the wall is simulated via a fiber-type discretization of the wall cross section; shear response is simulated via a user-defined one-dimensional shear stress versus strain model. Individual walls were discretized horizontally into several elements depending on the wall geometric configuration and discontinuities along the building height, as well as intersecting walls and beams. The walls were discretized vertically into 2 elements per story for the bottom portion of the building (stories 1 to 3), which experienced severe structural damage, while a single wall element per story was used for each of the remaining stories (stories 4 to 12). The aspect ratio of the wall elements (in either horizontal or vertical directions) was limited to 1:5 according to the recommendations in *User Guide PERFORM-3DTM Nonlinear Analysis and Performance Assessment for 3D Structures, Version 5* (CSI, 2011).

Using the wall element, nonlinear response due to flexural loading was simulated using a fiber-type discretization of the wall horizontal cross-section. A single integration point located at mid-height of the wall element was used. For the bottom three stories of the building, wall elements were discretized horizontally into eight concrete and steel fibers. For the remaining stories of the building, four concrete and steel fibers were used. The area of the concrete fiber was defined by the wall thickness (typically 150 mm; 6 inches) and the wall length represented by the element. Steel fiber area was defined by a longitudinal reinforcement ratio (typically 0.33% as defined by structural drawings). For the bottom three stories, one-dimensional material response models used for concrete and steel fibers included multi-linear envelopes with strength degradations at large strain demands, as described below; for the remaining stories in which nonlinear material response was expected to be limited, bilinear material models with no strength loss were used.

Concrete material behavior is defined on the basis of expected material strength. Because little confining reinforcement was provided in the walls (8 mm (0.3 inches) diameter bars at 500 mm (19.7 inches) on center, even in boundary element regions),

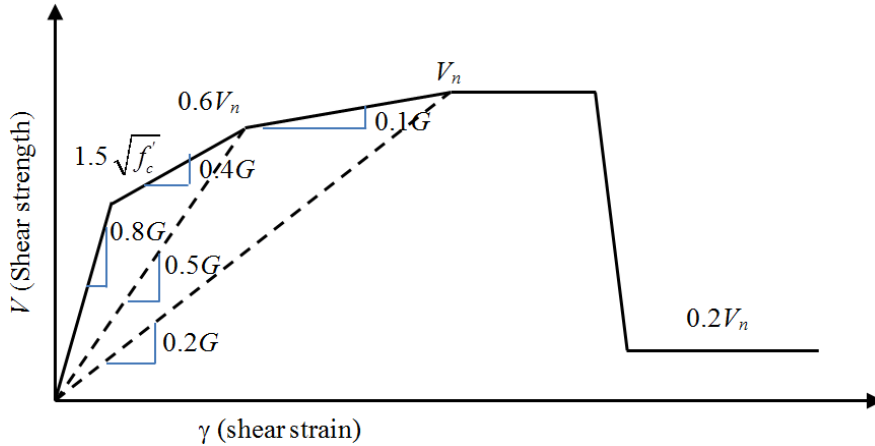
all concrete was modeled as unconfined. Concrete material response was defined using the Inelastic 1D Concrete Material option in PERFORM-3D. In compression, concrete response was defined by a trilinear stress-strain curve to the point of strength loss, linear strength loss to a residual strength of 10% of maximum strength, and complete loss of strength at the failure strain, DX , of -0.005 (ASCE/SEI 41-06 Supplement No. 1 Section 6.3.3.1 (ASCE, 2008)). The nominal concrete compressive strength (concrete material was specified as H25 in the construction drawings) of $f'_c = 25$ MPa (3.63 ksi) was increased by a factor of 1.5 to obtain the expected strength, $f'_{ce} = 37.5$ MPa (5.36 ksi) per ASCE/SEI 41-06. Pre- and post-peak stress-strain responses were defined using Mander (1988). Concrete was modeled as having no tensile capacity; no degradation in strength due to cyclic loading was simulated.

Steel material response was also defined on the basis of expected material strength. The steel material was defined using the inelastic steel material, non-buckling option with symmetrical trilinear curve in tension and compression, with no strength loss and no cyclic degradation. The steel yield strength, $F_y = 420$ MPa (60 ksi) was increased by a factor of 1.25 to obtain expected strength, $F_{ye} = 525$ MPa (75 ksi). In tension, the expected ultimate tensile strength, F_{ue} , was used with a factor of 1.25 and a value of 788 MPa (113 ksi). The strain values were defined using nominal properties for ASTM A706 steel and the ASCE/SEI 41-06 Supplement No. 1 limiting strains of -0.02 and 0.05 for compression and tension, respectively. These strain limits were defined as DL, the strain at which strength loss initiates. Steel strength degradation behavior is defined by following these strain limits with a residual strength of 10% of the peak strength in tension and compression.

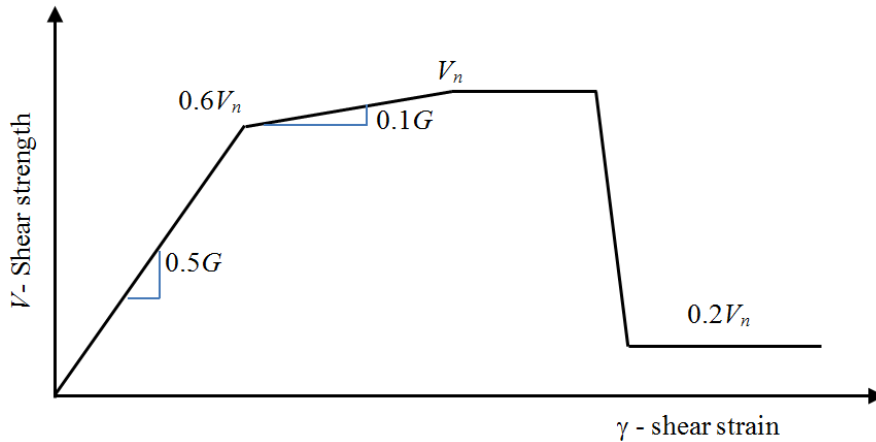
For the bottom three stories of the building, a nonlinear shear model was combined with the fiber-type flexural model; an elastic model with an effective shear modulus equal to 50% of the concrete elastic shear modulus, $G_c = 0.4E_c$, was used in combination with the fiber-type flexural model for the remainder of the building. The backbone curve for the nonlinear shear model was defined on the basis of experimental data (Lowe et al., 2012; Birely, 2012), recommendations in PEER/ATC-72-1, *Modeling and Acceptance Criteria for Seismic Design and Analysis of Tall Buildings* (ATC, 2010), and the ASCE/SEI 41-06 backbone curve for flexure-controlled walls (using Table 6-18 in ASCE/SEI 41-06 Supplement No. 1).

First an idealized multi-linear backbone curve was developed (Figure D-20a), then this idealized curve was simplified for use in PERFORM-3D (Figure D-20b), which only supports use of a trilinear curve to the point of strength loss. Note that the backbone curves shown in Figure D-20 are defined in terms of shear strength, $V = A_{cv} \tau$, where A_{cv} is the nominal shear area of the wall and τ is the shear stress (not shear strain, γ). The idealized model (Figure D-20a) employs a slightly reduced

shear modulus, $G_{eff} = 0.8G_c$, up to a strength of $1.5\sqrt{f'_c}$ psi, which is considered to be the cracking strength of the wall. A second slope equal to $0.4G_c$ is defined from the first yield up to shear strength of $0.6V_n$. The resulting secant stiffness of these two branches is $0.52G_c$, given the concrete compressive strength for the building. The final slope is defined as $0.1G_c$ up to the nominal shear strength, V_n .



(a) Multilinear idealized curve developed from experimental data based on PEER/ATC-72-1 and ASCE/SEI 41-06



(b) Simplified curve used in PERFORM-3D

Figure D-20 Shear backbone curves shown as shear strength versus shear strain.

The PEER/ATC-72-1 criteria for tall building design recommends use of an effective shear stiffness for lightly-reinforced shear walls of $GA_{g,eff}$ equal to 0.05 to 0.10 times $GA_{v,gross}$ for nonlinear response history analysis. This is consistent with the tangent stiffness of the backbone curve from $0.6V_n$ to $1.0V_n$. Post-peak response was defined per ASCE/SEI 41-06 for flexure-controlled walls and included a shear strain of 0.0075 at initiation of shear strength loss, a residual strength equal to 20% of peak shear strength, and a shear strain at complete loss of lateral load carrying capacity of 0.01. Shear strength was defined per ACI 318-11, *Building Code Requirements for Structural Concrete and Commentary* (ACI, 2011); since walls act as bearing walls,

shear strength was defined using nominal (lower-bound) concrete compression strength.

PERFORM-3D does not provide a mechanism for simulating the pinched hysteretic response typically observed for reinforced concrete walls and planar elements subjected to shear loading (Figure D-18). To capture the effect of the pinched hysteretic response on energy dissipation, cyclic degradation of unloading-reloading stiffness is included in the shear model. The ratio of the unloading stiffness to the initial stiffness, G_{unload}/G_o , was defined as 1.0 up to strength of $0.6V_n$, or approximately the elastic limit, as shown in Figure D-21. The post-peak unloading stiffness at different shear strains demands was determined by equating the area of the desired pinched hysteresis and the equivalent non-pinched hysteresis.

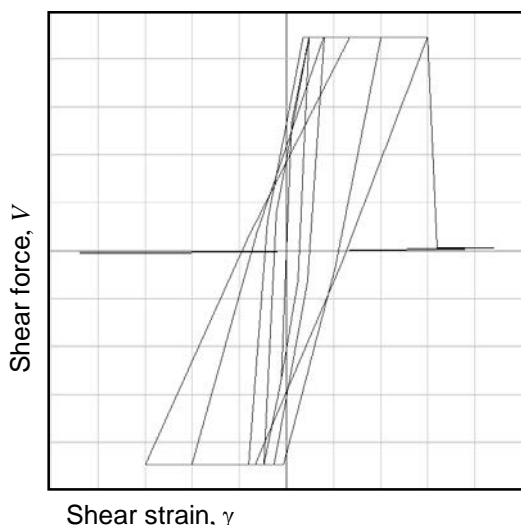


Figure D-21 Cyclic shear stress-strain model used in PERFORM-3D analysis.

D.4.3.2 PERFORM-3D Modeling of Coupling Beams

Preliminary analyses indicated that coupling beams would respond in shear rather than flexure. This observation is also consistent with observed damage in the building. Thus, coupling beams were modeled in PERFORM-3D using nonlinear shear hinges located at the beam mid-span and connected via elastic beam-column element at each side. The shear hinge behavior was defined using ASCE/SEI 41-06 Table 6-19 for shear-controlled walls or coupling beams, assuming high shear stress demand, and non-conforming transverse reinforcement. Shear capacity was defined using expected material properties and Chapter 21 equation in ACI 318. The elastic beam-column element behavior was defined using expected reinforced concrete material properties and nominal dimensions. The effective flexural stiffness was defined as $EI_{eff} = 0.05EI_{gross}$ based on review of coupling beam tests (Mohr, 2007); this was considered to be similar to the $EI_{eff} = 0.15EI_{gross}$ recommended in PEER/ATC-72-1. The effective shear stiffness was defined as $GA_{v,eff} = 0.25GA_{v,gross}$

per PEER/ATC-72-1. Young's and shear moduli were not modified and represented expected material properties of H25 concrete. A torsional release was applied to the beams, accounting for the lack of capacity and reduced dimensions in the transverse direction of the beams. Coupling beam elements with zero mass and increased flexural stiffness were defined within the wall elements to simulate the continuity of coupling beams at the wall supports and the transfer of coupling beam forces and moments into the wall.

D.4.3.3 PERFORM-3D Modeling foundation flexibility

The Perform SSI model of the Plaza del Rio Building A was created with a flexible foundation. In this model, foundation elements shown in the construction drawings were modeled and flexible soil springs were distributed along the length of the foundation elements. Only vertical foundation flexibility was modeled; lateral translational restraints were provided at the foundation-soil spring interface. Kinematic effects (filtering of the ground motions transmitted to the structure based on the geometry and properties of the foundation) and foundation damping effects (dissipation of energy through radiation and hysteretic soil damping) were not included in the analysis.

To model foundation flexibility, a short basement level was added to bring the base of the walls to the level of the mat foundation's centerline, wall elements were used to model grade beams, quadrilateral shell elements were used to model the mat foundation, and soil springs were added at the nodes of the mat foundation elements. Figure D-22 shows an idealization of the mesh including the foundation elements and soil springs according to the *User Guide*; note that sliding shear elements were not included in the model.

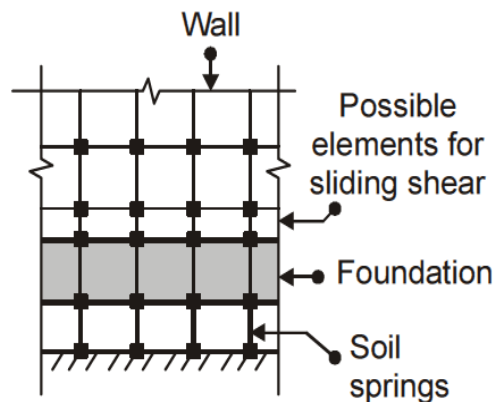


Figure D-22 Possible foundation models in PERFORM-3D (CSI, 2011).

Figure D- 23 shows foundation elements of the Perform SSI model for the Plaza del Rio Building A. The PERFORM-3D fiber wall element was used to extend walls below grade to the centerline of the mat foundation and to model grade beams. Wall

element material response was defined as for the walls in the upper stories of the building. Wall and grade beam material properties, geometry and reinforcement ratios as provided in the structural drawings were used. The thickness of the mat foundation elements was defined per the structural drawings; the effective stiffness of these elements was defined as $EI_{eff}=0.33EI_{gross}$ per ASCE/SEI 41-06 for cracked non-prestressed slabs. Nodal masses representing the basement extension of the walls and the mat foundation elements were added to the model. Horizontal restraints were provided at each node of the mat foundation.

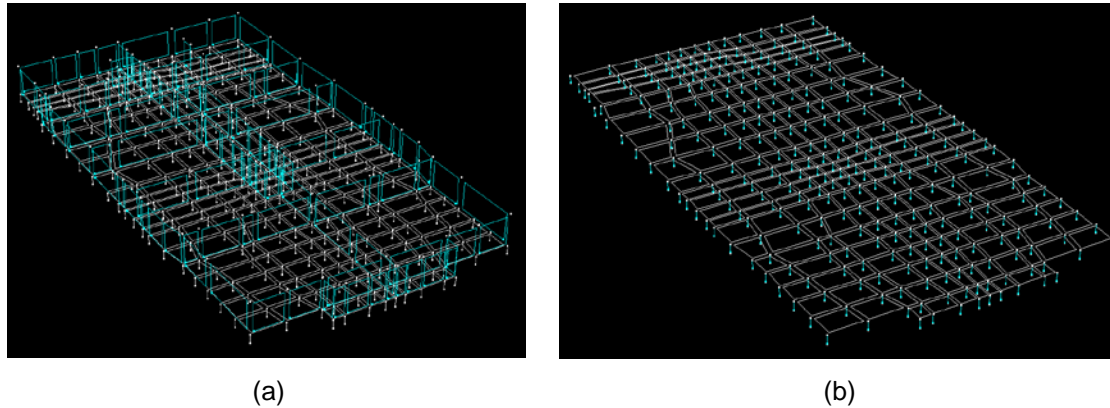


Figure D-23 Foundation level of building Plaza del Rio Building A modeled in PERFORM-3D (Perform SSI model): (a) wall elements are added to extend walls to centerline of mat foundation and wall elements used to model grade beams are highlighted; and (b) mat foundation elements are shown and soil springs are highlighted.

Two PERFORM-3D element types were considered for simulating soil flexibility: support spring and nonlinear elastic gap-hook bar. Both elements are defined by an elastic stiffness, k_v , determined using a fixed subgrade modulus, k , and a tributary area of the mat foundation, A_{trib} . Support spring elements can be defined to have different elastic stiffnesses in tension and compression; gap-hook elements can be defined to represent compression-only elastic behavior and thereby simulate foundation uplift. *Concrete Floors on Ground* (PCA, 2008) presents typical subgrade modulus values, k , for different soil types. For coarse grained soil, the subgrade modulus is typically in the range of 100 pci to 400 pci; for fine grained soils, the subgrade modulus is typically in the range of 20 pci to 150 pci. A subgrade modulus of 20 pci was assumed here as it represented a lower bound on foundation flexibility. Initial analyses were conducted using the gap-hook bar element with zero tensile capacity; however, dynamic analysis results for the Concepción ground motion record indicated minimal nonlinear action in the building with significant displacement due to foundation uplift; this was likely because the weight of the soil above the foundation elements was not included in the analyses. Subsequent analyses were conducted using the support spring element with equal stiffness in tension and compression. This was considered to represent an improvement over the

fixed-base model and an approximate representation of the expected behavior in which foundation uplift would occur only after the weight of the soil overburden had been overcome.

D.4.4 Analysis Results

A large quantity of analysis data were evaluated as part of this study. At the building level, data included the initial periods and mode shapes for the building, as well as roof displacement and acceleration, and story drift histories and maxima. For concrete walls in the first and second stories (where significant inelastic action was observed), moment-rotation and moment-curvature, equivalent plastic hinge rotation, shear stress-strain, and concrete and steel stress-strain histories and maxima were considered. For coupling beams, beam chord rotations, and beam-hinge shear force-deformation histories and maxima were considered. For the Perform SSI model, rotation and displacement of foundation elements was evaluated.

D.4.4.1 Modal Analysis Results

Table D-3 describes mode shapes and lists periods for the primary response modes of the building as determined using the OpenSees, PERFORM-3D, and SAP2000 models of the building. For the OpenSees model, the periods obtained for the primary modes are substantially longer than those obtained using SAP2000; this is attributed to exclusion of the slabs and coupling beams from the OpenSees model. For the Perform Basic model, the periods obtained for the primary modes are equal to or slightly exceed the results obtained using SAP2000 with cracked-section properties. This is due to the use of lower initial shear stiffness for walls and coupling beams in the Perform Basic model than were used in the SAP2000 model. For the Perform SSI model, the addition of foundation flexibility resulted in periods for the primary modes that are significantly larger than those obtained using any of the other models. Figure D-24 displays the relationship between building period and foundation flexibility, k , according to each mode.

Table D-3 Summary of Modal Periods for Plaza del Rio Building A

Modal Period	OpenSees	Basic Perform	Perform SSI	SAP2000	
				Gross section properties (uncracked)	Effective section properties (cracked)
Transverse translation	0.96s	0.71s	1.42s	0.48s	0.65s
Torsion	0.63s	0.56s	0.89s	0.41s	0.56s
Longitudinal translation	0.60s	0.49s	0.74s	0.29s	0.38s

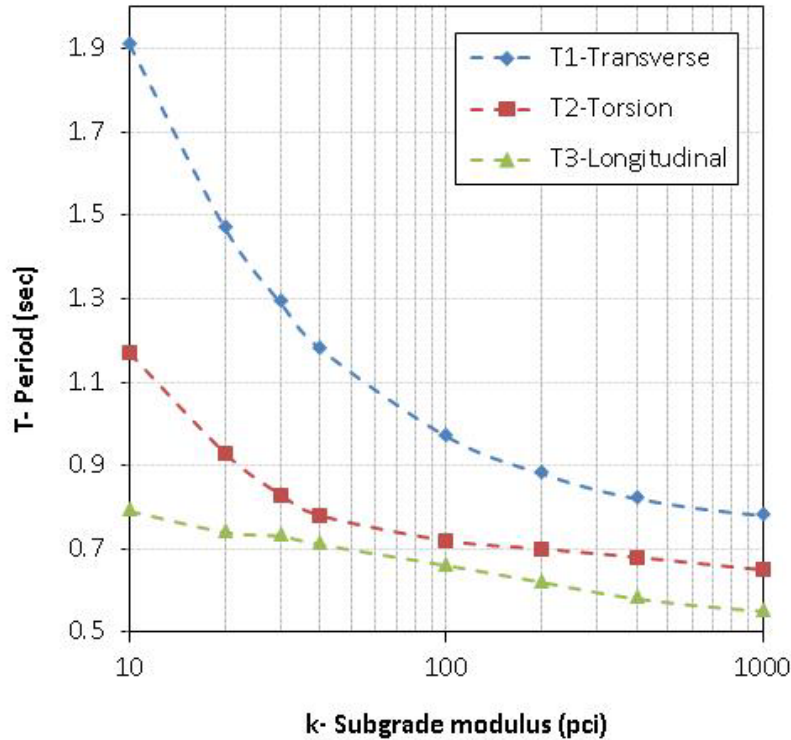


Figure D-24 Building period versus foundation flexibility, k .

D.4.5 OpenSees Nonlinear Dynamic Analysis Results

Analyses were performed for demands defined by the unscaled Concepción and San Pedro de la Paz records, as well as for the suite of seven Chilean ground motion records scaled to the DE and MCE demand levels. Performance prediction using demands calculated at the DE and MCE hazard levels coupled with ASCE/SEI 41-06 acceptance criteria at the Life Safety and Collapse Prevention performance levels representative of a typical ASCE/SEI 31 Tier 3 Evaluation that conducted in practice.

Most time-history analyses were fully completed in OpenSees; however, four analyses failed to converge prior to the end of the earthquake motion. The analyses that failed to converge were: (1) Concepción scaled to the DE (failed at 12 seconds of 141 seconds); (2) Concepción scaled to the MCE (failed at 13 seconds of 141 seconds); (3) San Pedro de la Paz scaled to the DE (failed at 31 seconds of 202 seconds); and (4) San Pedro de la Paz scaled to the MCE (failed at 27 seconds of 202 seconds). These convergence failures were due to failure of individual force-based beam-column elements to find a converged solution state (unlike displacement-based elements, force-based elements require an intra-element solution at each time step).

Table D-4 presents simulated maximum and residual roof drifts in the transverse and longitudinal directions for each of the ground motions considered. Results for the seven scaled records are averaged and compared to the unscaled Concepción record in Table D-5. Results show the following: (1) maximum drifts in the transverse

direction exceeds drifts in the longitudinal direction; (2) residual drifts were negligible; and (3) the suite of seven motions scaled to the DE level produced roof drifts that were on the order of drifts from the unscaled Concepción record (MCE-scaled motions produced higher drifts than the unscaled Concepción record).

Table D-4 Maximum and Residual Roof Drifts for Plaza del Rio Building A from OpenSees Analyses

Record		Maximum		Residual	
<i>Name</i>	<i>Scale</i>	<i>Trans. %</i>	<i>Long. %</i>	<i>Trans. %</i>	<i>Long. %</i>
Concepción	Unscaled	0.82	0.60	0.09	0.01
	DE	0.74*	0.45*	-	-
	MCE	2.01*	0.94*	-	-
San Pedro	Unscaled	0.94	0.59	0.02	0.01
	DE	1.33	0.81	-	-
	MCE	2.49	1.03	-	-
Llolleo	DE	0.54	0.47	0.00	0.00
	MCE	0.82	0.60	0.00	0.00
Matanzas	DE	1.46	0.68	0.17	0.00
	MCE	1.20	0.79	0.05	0.01
Valparaiso	DE	0.88	0.76	0.02	0.01
	MCE	1.17	1.02	0.11	0.07
Viña del Mar - Centro	DE	0.82	0.70	0.00	0.01
	MCE	1.13	0.95	0.04	0.02
Viña del Mar - El Salto	DE	1.05	1.05	0.00	0.01
	MCE	1.27	1.38	0.02	0.04

* Maximum displacement prior to "failure to converge."

Table D-5 Summary of Roof Drifts for Plaza del Rio Building A from OpenSees Analyses

	E-W (Transverse) Direction		N-S (Longitudinal) Direction	
	<i>Max.</i>	<i>Residual</i>	<i>Max.</i>	<i>Residual</i>
	Unscaled Concepción Record	0.82%	0.09%	0.60%
Average for 7 motions scaled to DE	0.88%	0.00%	0.70%	0.01%
Average for 7 motions scaled to MCE	1.20%	0.04%	0.95%	0.02%

Table D-6 shows similar data for calculated drifts in the first and second stories. These data show the following: (1) second story drifts typically exceed first story drifts; (2) a wide variation in drifts is observed for the suite of motions; and (3) very

large drifts are observed for the Concepción and San Pedro de la Paz records scaled to the DE and MCE levels.

Table D-6 Maximum and Residual First and Second Story Drifts for Plaza del Rio Building A from OpenSees Analyses

<i>Record</i>		Maximum Story Drift			
		<i>First Story</i>		<i>Second Story</i>	
<i>Name</i>	<i>Scale</i>	<i>Trans. %</i>	<i>Long. %</i>	<i>Trans. %</i>	<i>Long. %</i>
Concepción	Unscaled	0.12	0.17	0.51	0.35
	DE	0.12	0.16	0.35	0.31
	MCE	0.63	0.63	1.63	0.87
San Pedro	Unscaled	0.20	0.25	0.48	0.41
	DE	0.38	0.46	0.80	0.65
	MCE	2.16	0.97	2.23	1.00
Llolleo	DE	0.16	0.17	0.30	0.25
	MCE	0.22	0.22	0.39	0.32
Matanzas	DE	0.17	0.25	0.97	0.51
	MCE	0.22	0.28	0.72	0.60
Valparaiso	DE	0.17	0.29	0.47	0.51
	MCE	0.22	0.63	0.32	0.81
Viña del Mar - Centro	DE	0.14	0.25	0.41	0.43
	MCE	0.19	0.31	0.59	0.51
Viña del Mar - El Salto	DE	0.18	0.36	0.52	0.70
	MCE	0.23	0.40	0.66	0.73

Analysis results were used to determine if walls met or exceeded different performance levels using several different performance criteria, and predicted performance was compared with observed damage. The following criteria were used to determine predicted performance: (1) ASCE/SEI 41-06 rotation limits for walls responding in flexure, used to assess IO, LS, and CP performance levels; (2) fragility functions developed in Birely (2012) for planar walls, used to determine the predicted damage state; and (3) usable strain limits provided in ASCE/SEI 41-06 for concrete and longitudinal reinforcement, steel yield strain, concrete spalling strain, and concrete crushing strain, which were used to assess material damage.

ASCE/SEI 41-06 deformation limits and Birely (2012) fragility functions utilize “hinge rotation” criteria as a measure of response, which can be directly determined from a lumped plasticity model. Because the OpenSees model utilizes a distributed plasticity model, calculation of an equivalent hinge rotation was necessary to employ these criteria (described in Birely, 2012).

Figures D-25 through D-27 show performance predicted for the San Pedro de la Paz ground motion record, using the various performance criteria identified above, for the first and second story walls of Plaza del Rio Building A (results for the Concepción record are provided in Chapter 4). In these plots wall color indicates whether observed damage was less than, equal to, or greater than predicted. Figures D-25 through D-27 also show walls that were expected to exhibit shear failure, determined by $V_u > 1.1V_n$. Data in these figures show that:

- Most walls could be expected to exhibit shear failure;
- Most primary lateral load-carrying walls were predicted to have damage exceeding the LS or CP performance levels per ASCE/SEI 41-06 deformation capacities;
- All primary lateral load-carrying walls were predicted to have damage exceeding DS 4 (Damage State 4, which requires replacement of the wall) per fragility functions developed in Birely (2012);
- Most primary lateral load carrying walls were predicted to have strains in excess of those causing concrete spalling but not concrete crushing per ASCE/SEI 41-06 usable strain limits; and
- Predicted damage was not highly correlated with observed damage for demands determined by the San Pedro de la Paz ground motion record.

Results across all analyses and different performance criteria are summarized in Table D-7.

Table D-7 Summary of Predicted and Observed Performance Levels for Primary Lateral Load-Carrying Walls using Different Performance Criteria

Demand	ASCE/SEI 41-06 Criteria		Fragility Function Criteria		Usable Strain Criteria	
	<i>Trans.</i>	<i>Longit.</i>	<i>Trans.</i>	<i>Longit.</i>	<i>Trans.</i>	<i>Longit.</i>
Unscaled Concepción	LS/CP – CP	LS/IO – LS	DS4	DS4	Yield/Spall – Spall	Yield
DE	LS – LS/CP	LS/CP – CP	DS4	DS4	Yield – Yield/Spall	Yield – Yield/Spall
MCE	LS/CP – CP	CP	DS4	DS4	Yield/Spall - Spall	Spall
Observed Damage	CP	LS/CP	DS3/DS4	DS3/DS4	Crushing	Spall/Crushing

The data in Figures D-25 through D-27 were compiled into the bar chart shown in Figure D-28, which shows the number of walls in the first and second story of the building exceeding each of the considered performance states. Bars in Figure D-28 are colored to show the number of walls with observed damage that was less than, equal to, or greater than predicted. The range of colors in each bar indicate that there is little correlation between observed and predicted damage, however, the small

proportion of the bars in the figure that are colored red indicate that the criteria are producing a generally conservative assessment (for this case study building).

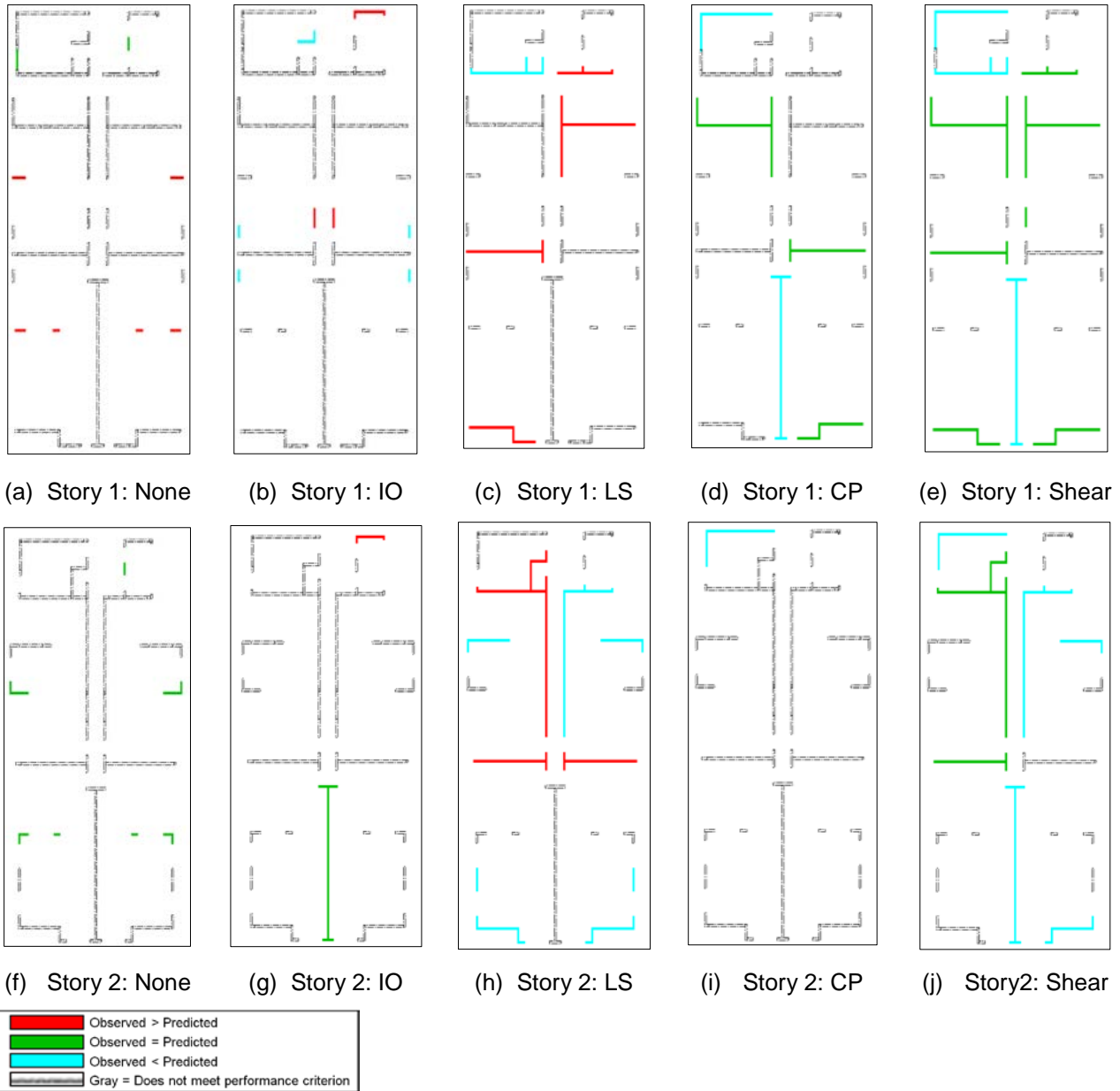


Figure D-25 Response of first and second story walls in Plaza del Rio Building A to unscaled San Pedro de la Paz ground motion. Colored walls indicate walls that exceed ASCE/SEI 41-06 acceptance criteria for each performance level. Colors indicate whether observed damage is less than, approximately equal to, or greater than predicted damage. Walls colored in the “shear” plan view are considered to have failed in shear with $V_u > 1.1 V_n$. Dashed gray walls indicate walls that do not meet the performance criterion for that panel.

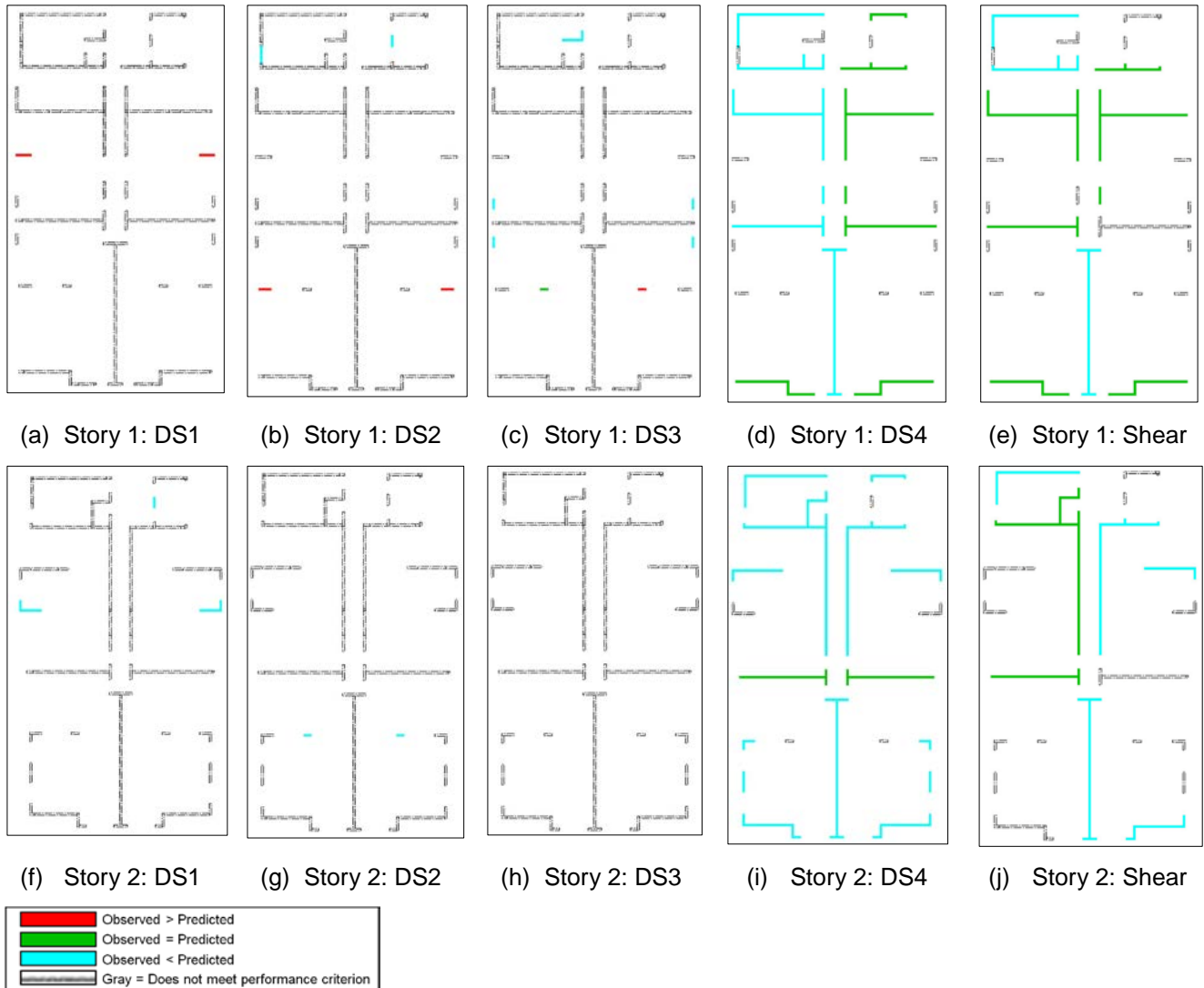


Figure D-26

Response of first and second story walls in Plaza del Rio Building A to unscaled San Pedro de la Paz ground motion. Colored walls indicate walls that exceed median drift at onset of damage states by Birely (2012). Colors indicate whether observed damage is less than, approximately equal to, or greater than predicted damage. Walls colored in the “shear” plan view are considered to have failed in shear with $V_u > 1.1 V_n$. Dashed gray walls indicate walls that do not exceed the median drift for that damage state.

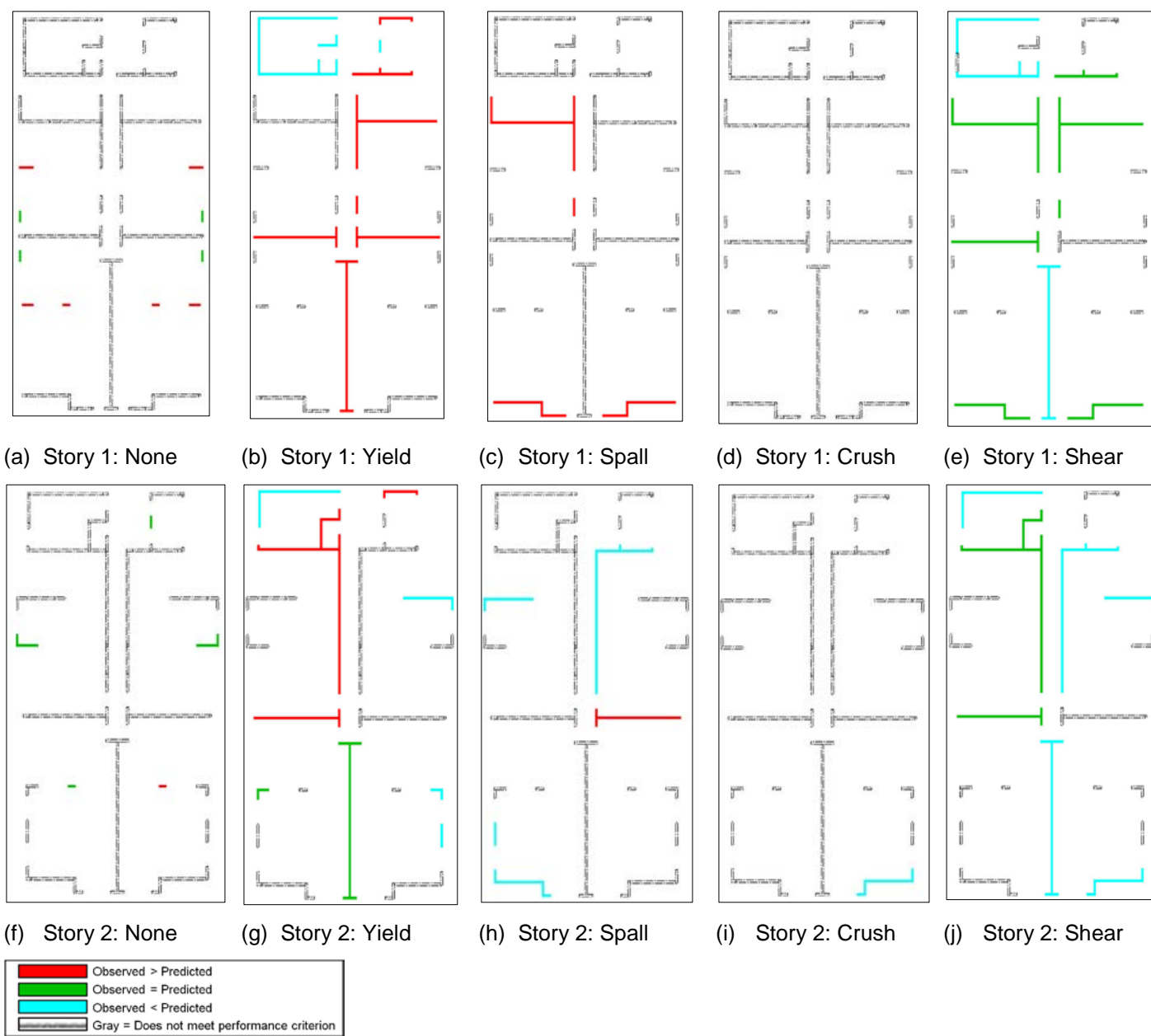


Figure D-27 Response of first and second story walls in Plaza del Rio Building A to unscaled San Pedro de la Paz ground motion. Colored walls indicate walls exceed strain at onset of steel yielding and concrete spalling and crushing. Colors indicate whether observed damage is less than, approximately equal to, or greater than predicted damage. Walls colored in the “shear” plan view are considered to have failed in shear with $V_u > 1.1 V_n$. Dashed gray walls indicate walls that are not predicted to fail in shear.

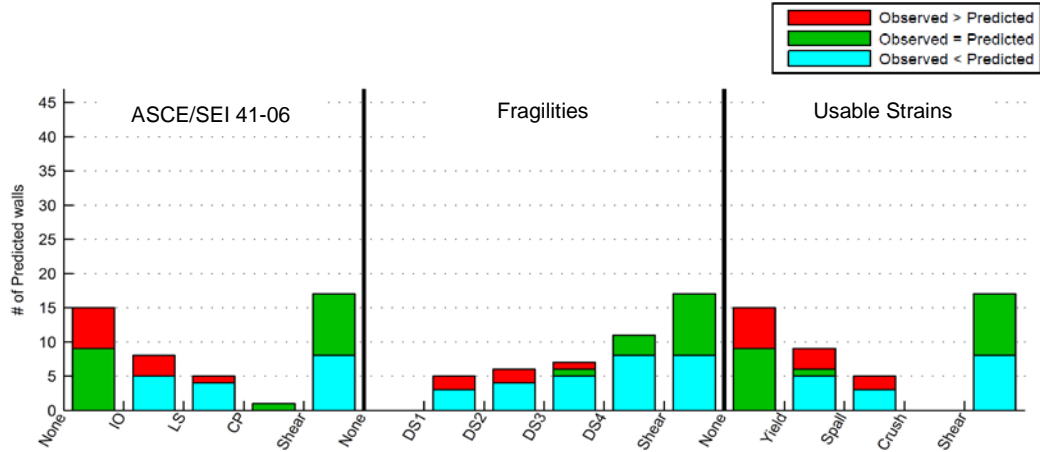


Figure D-28 Number of walls in Plaza del Rio Building A exceeding acceptance criteria for each performance measure.

D.4.6 PERFORM-3D Nonlinear Dynamic Analysis Results

Analyses were conducted in PERFORM-3D using the Perform Basic and Perform SSI models and the unscaled San Pedro de la Paz and Concepción ground motion records. Table D-3 shows the periods for the primary modes of response, as predicted using these models. All initial periods are 0.5 seconds or greater and inelastic action could be expected to elongate these periods substantially. The SRSS response spectra for the unscaled San Pedro de la Paz and Concepción records in Figure D-17 show that for periods in excess of 0.5 seconds, spectral accelerations for the Concepción record are greater, and at longer periods much greater, than the San Pedro de la Paz record. Given these data, it could be expected that simulated demands for the Concepción record would be substantially larger than demands for the San Pedro de la Paz record, which was indeed the case.

From an analysis using the Perform Basic model subjected to the unscaled San Pedro de la Paz ground motion record, the resulting maximum roof drifts in the transverse and longitudinal directions were, respectfully, 0.3% and 0.2%, corresponding to maximum roof displacements of 103 mm (4.1 inches) and 70 mm (2.8 inches) in each direction. Residual drifts were essentially zero. Consistent with these results, the analysis predicted minimal inelastic action occurring in the building. Hysteretic damping represented 30% of the total damping, with 70% of the damping attributed to Rayleigh damping. Hysteretic damping was due to inelastic action in walls and coupling beams; however deformation demands in the elements did not exceed ASCE/SEI 41-06 limits for Life Safety or Collapse Prevention. Small force and deformation demands associated with the San Pedro de la Paz record were attributed to the relatively low spectral values for this record in the mid- to long-period range. Given the limited inelastic response predicted using the San Pedro de la Paz record, as well as the relatively low spectral values for this record in the period range of

interest, additional analyses were not conducted using the Perform SSI model and the San Pedro de la Paz record.

Both the Perform Basic and Perform SSI models were subjected to the unscaled Concepción ground motion record. Results in Table D-8 summarize maximum and residual drifts calculated in the transverse and longitudinal directions for both models. Large drifts were predicted in the longitudinal direction in the first story at approximately 30 seconds into the earthquake motion, following several cycles with large acceleration demands. These large drifts were attributed to shear failure of the primary longitudinal walls. Because these drifts exceeded 3%, the drift at which symmetric flanged walls have been shown to lose lateral load carrying capacity (Birely, 2012), analysis results were considered to indicate failure of the building. Despite shear failure of the primary longitudinal walls, flexural capacity of primary longitudinal walls (which is decoupled in the Perform model so shear failure does not result in flexural failure) along with flexural and shear capacity of secondary walls enabled the structure to remain stable and return to approximately zero displacement in the longitudinal direction. Ultimately, a residual roof drift of less than 0.1% and a residual first story drift of less than 0.4% were predicted in the longitudinal direction.

Table D-8 Plaza del Rio Building A Maximum and Residual Drifts for the Concepción Ground Motion

	E-W (Transverse) Direction						N-S (Longitudinal) Direction					
	Maximum Drifts			Residual Drifts			Maximum Drifts			Residual Drifts		
	<i>Roof</i>	<i>1st Story</i>	<i>2nd Story</i>	<i>Roof</i>	<i>1st Story</i>	<i>2nd Story</i>	<i>Roof</i>	<i>1st Story</i>	<i>2nd Story</i>	<i>Roof</i>	<i>1st Story</i>	<i>2nd Story</i>
Perform Basic	2.31%	0.50%	1.93%	0.50%	0.06%	0.52%	0.74%	>3.0%	0.68%	0.05%	0.35%	0.10%
Perform SSI	2.80%	1.48%	2.52%	1.48%	0.23%	0.63%	1.09%	>3.0%	1.08%	0.03%	0.30%	0.07%

It is noted that in the case of the actual structure, the presence of the adjacent Plaza del Rio Building B would have limited large drift excursions to the north, and pounding damage observed following the earthquake suggests that this did occur. For the Perform Basic model, maximum and residual drifts in the transverse direction were concentrated in the second story. For the Perform SSI model, maximum and residual drifts were larger in the second story, but first story drifts were significant. For both models, large second story drifts in the transverse direction were the result of inelastic flexure and shear actions in the primary walls. Large first story drifts in the Perform SSI model were the result of shear failure in the primary walls.

Figures D-29 and D-30 show walls and coupling beams that experienced deformation demands in excess of the ASCE/SEI 41-06 Collapse Prevention limit states and usable material strains. These figures show that for many coupling beams, rotation demands exceeded the ASCE/SEI 41-06 limit for Collapse Prevention and, thus, many coupling beams could be considered to have failed.

Comparison of results from the Perform Basic and Perform SSI models indicates that foundation flexibility significantly affected simulation of structural response and assessment of performance.

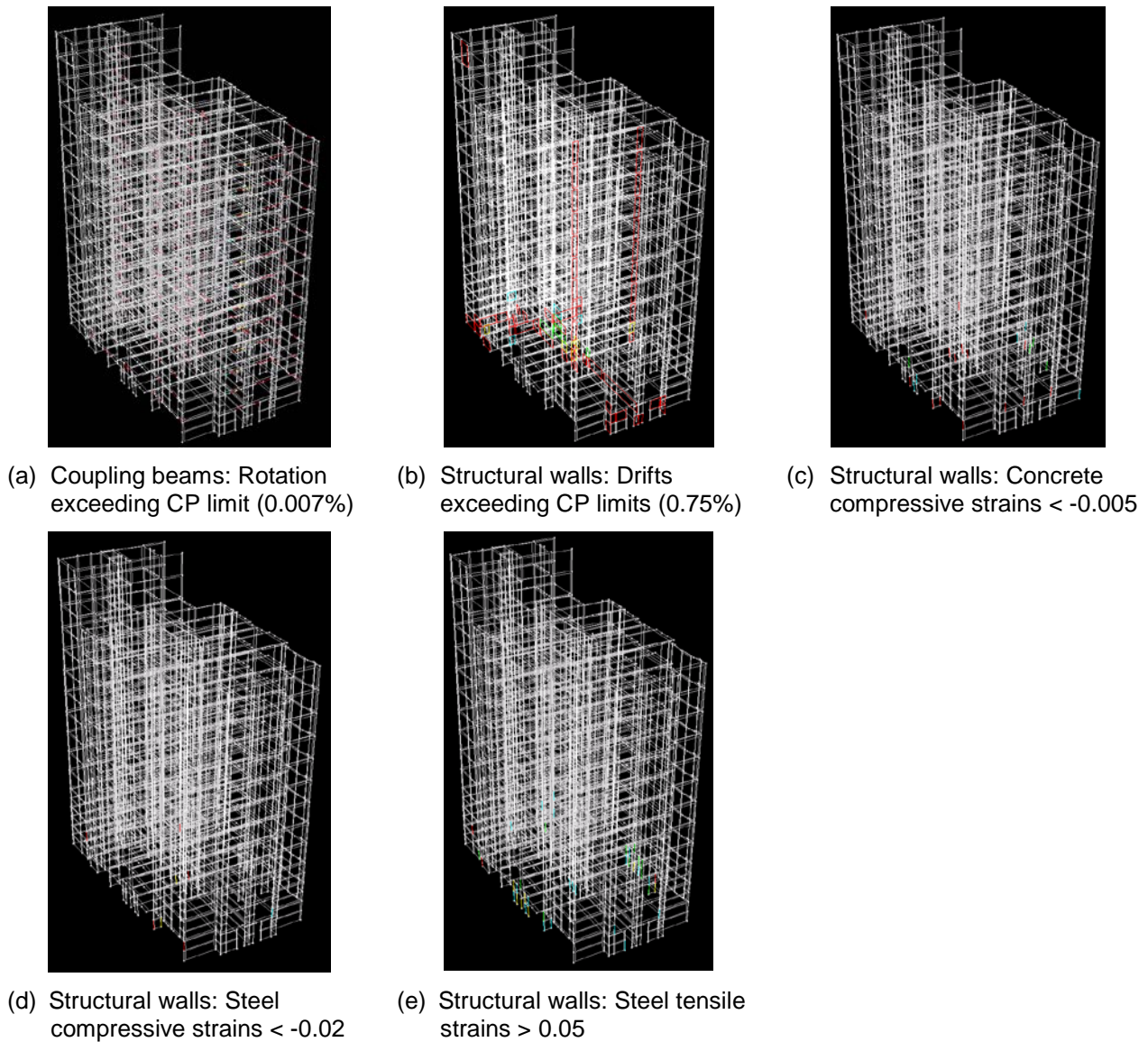
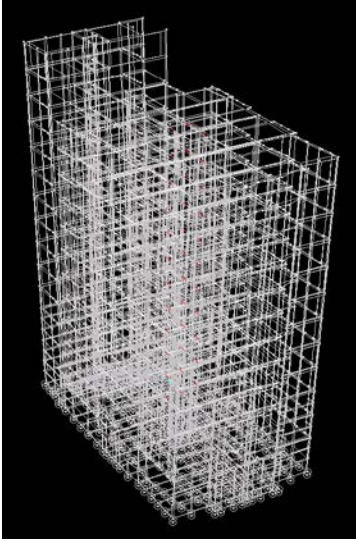
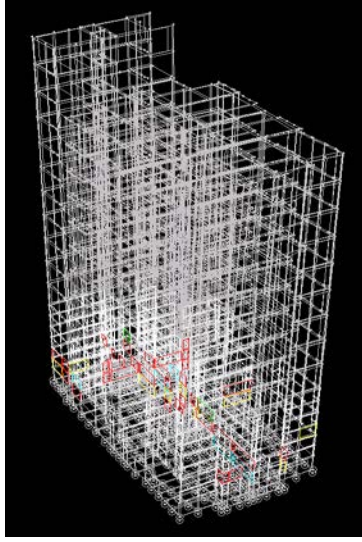


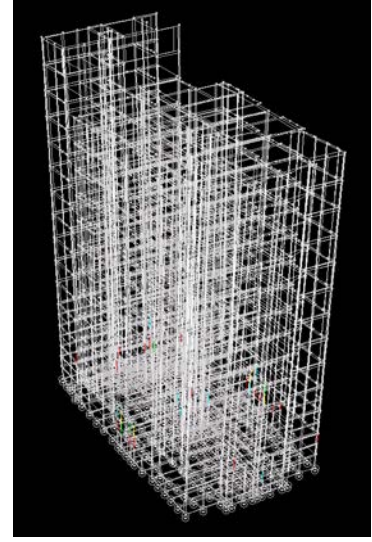
Figure D-29 Perform Basic model results showing damage exceeding Collapse Prevention limits in shear walls (shear and flexure models) and coupling beams for the Concepción record.



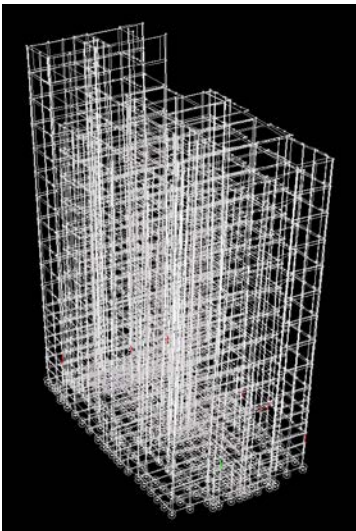
(a) Coupling beams: Rotation exceeding CP limit (0.007%)



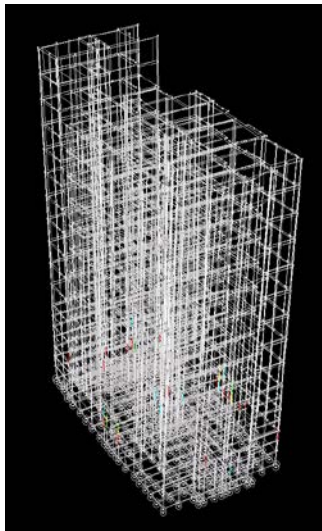
(b) Structural walls: Drifts exceeding CP limits (0.75%)



(c) Structural walls: Concrete compressive strains < -0.005



(d) Structural walls: Steel compressive strains < -0.02



(e) Structural walls: Steel tensile strains > 0.05

Figure D-30 Perform SSI model results showing damage exceeding Collapse Prevention limits in shear walls (shear and flexure models) and coupling beams for the Concepción record.

D.5 Investigation of Local Vertical Discontinuities in Walls

ASCE/SEI 31-03 Tier 1 checklists consider vertical discontinuities in buildings by considering the load path, verifying that all lateral load resisting elements are continuous to the foundation, and by considering the stiffness and strength of a story relative to the stories above and below. However, studies of mid-rise walled buildings damaged in the 2010 Maule earthquake suggests that local changes in the stiffness and strength of individual building components may be correlated with

damage, and that checks of total story strength and stiffness do not necessarily capture these effects.

This study was undertaken to quantify local discontinuities observed in walls of four case study buildings, and to determine if there is any significant correlation between observed damage and different measures of these local discontinuities. The four buildings included in this study were Plaza del Rio Buildings A and B, Centro Mayor, and Concepto Urbano.

For the purpose of this study, a local wall discontinuity was considered to be any location where the cross-section of a wall in a given story (referred to as the upper wall) changes in the story below (referred to as the lower wall). In the four buildings studied, discontinuities typically fell into one of the following categories:

- Termination – discontinuation of an upper wall, so that no lower wall exists in the story below.
- Opening – the presence of a new opening in a lower wall (Figure D-31a).
- Shift – a change in the centroid of a wall cross-section, including a change in the dimension or location of a wall flange (Figure D-31b).
- Flag – a change in the dimension of the web of a wall in which the upper wall is larger than the lower wall (Figure D-31c).

The colors shown in Figure D-31 indicate the level of damage observed in walls that exhibited the identified local discontinuity.

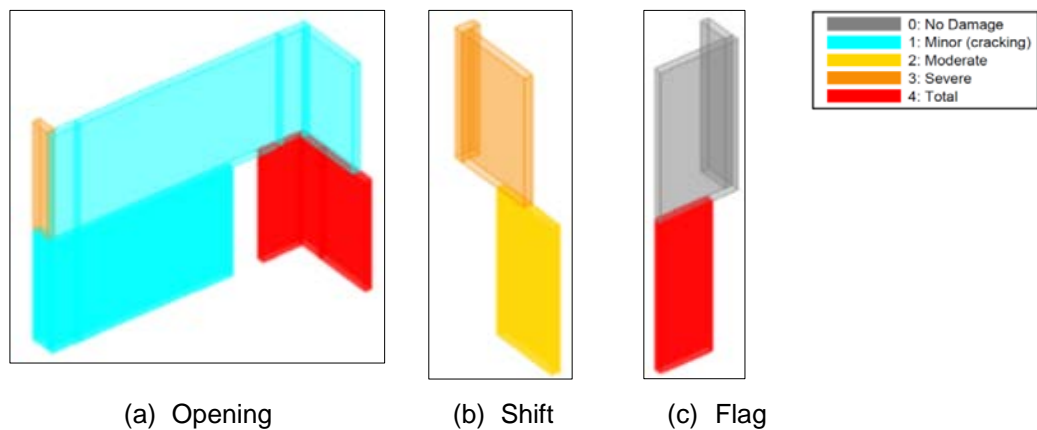


Figure D-31 Typical local wall discontinuities observed in case study buildings.

The complexity of discontinuities in the case study buildings ranged from simple, isolated flag-shaped walls, for which damage was easily attributed to the reduced wall length and area, to walls with multiple adjacent discontinuities, for which damage was not easily attributed to any individual discontinuity. To incorporate

uncertainty associated with the presence of multiple complex discontinuities into the study, each discontinuity was assigned a quality ranking based on: (1) simplicity of the geometry; (2) confidence that the observed damage is associated with the discontinuity; (3) the presence of other local discontinuities associated with either or both of the lower and upper walls; and (4) the importance of the discontinuity to the overall performance of the building, considering factors such as location within the building and the percentage of total shear carried by the wall.

Quality rankings ranged from 0 for a high quality data point, to 6 for a low quality data point. Figure D-32 shows the number of local discontinuities at each quality ranking in each of the four case study buildings. Correlation between local discontinuity measures and observed damage was investigated using “high-quality” data points with quality rankings of 0 or 1.

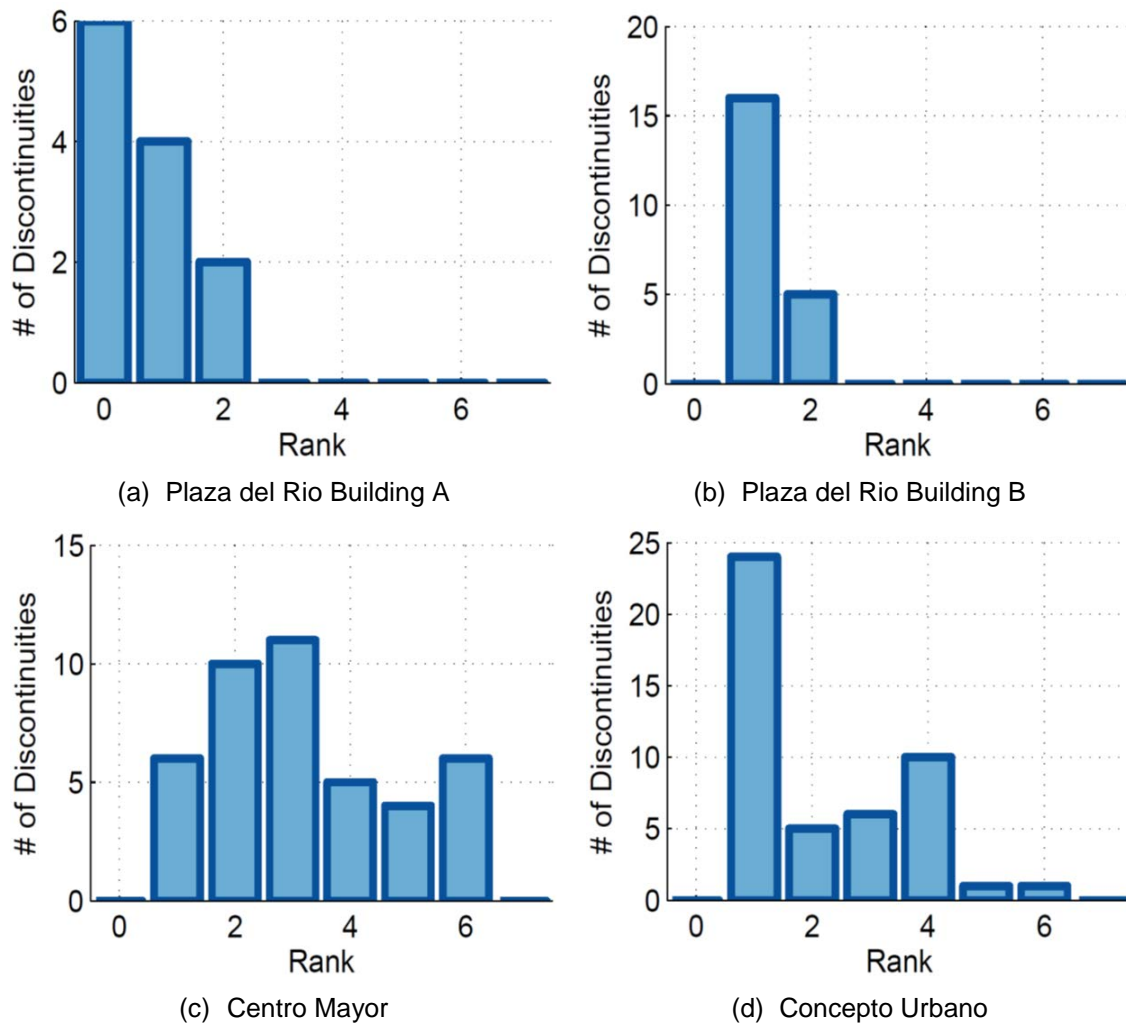


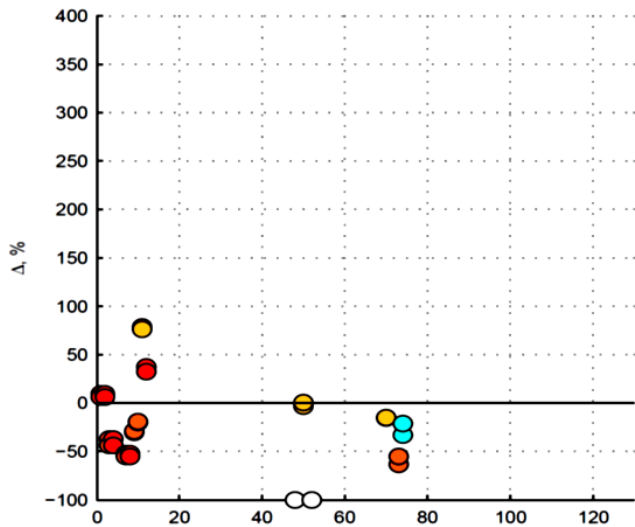
Figure D-32 The number of local discontinuities at each quality ranking in each of the four case study buildings.

The following measures were used to quantify local discontinuities observed in the walls of the case study buildings:

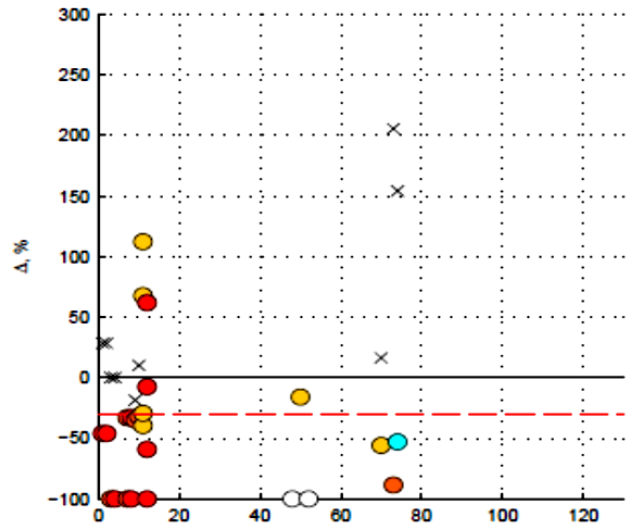
- Change in area ($\Delta A/A^{upper}$) – A change in wall area, normalized by the area of the upper wall, reported as a percentage.
- Change in dimension ($\Delta L_x/L_x^{upper}$ and $\Delta L_y/L_y^{upper}$) – A change in the maximum x- and y-dimensions of the wall, normalized by the dimension of the upper wall in that direction, reported as a percentage. This is calculated by the dimensions of the rectangle in which the wall is inscribed.
- Change in centerline length ($\Delta L_{cl}/L_{cl}^{upper}$, $\Delta L_{cl,x}/L_{cl,x}^{upper}$, and $\Delta L_{cl,y}/L_{cl,y}^{upper}$) – A change in the centerline length of the wall, normalized by the centerline length of the upper wall, reported as a percentage. The centerline length, L_{cl} , of the wall is the total length of wall as measured along the centerline of the cross-section. A distinction can be made to evaluate the change in centerline length in the x- and y-directions.
- Change in centroid ($\Delta x_c/L_x^{upper}$ and $\Delta y_c/L_y^{upper}$) – A change in the in-plane coordinates of the geometric centroid of the wall, normalized by the length of the wall in the direction of the coordinate, reported as a percentage. This number is always reported as a negative number to facilitate comparison with the other measures defined above.

Approximately 120 discontinuities were identified in the case study buildings and each was assigned an ID number. Figure D-33 shows plots of the magnitude of the discontinuity (% change) versus discontinuity ID number for each of the local discontinuity measures considered. Values shown are for discontinuity ID numbers with a quality ranking of 0 or 1 in severely damaged case study buildings (Centro Mayor and Plaza del Rio Building A). The color of each data point indicates the level of earthquake damage observed in the building in the vicinity of the discontinuity.

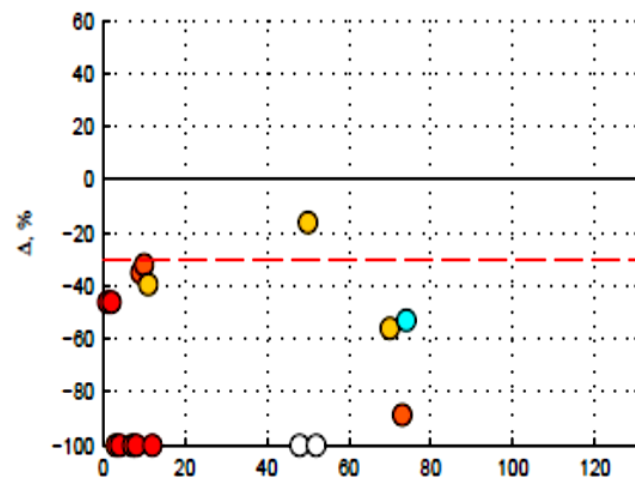
Correlation between the discontinuity measure and observed damage can be seen in the way that data points in the figure change to red (i.e., damage becomes more severe) as the magnitude of the discontinuity (% change) increases. Based on the information shown in Figure D-33, it was concluded that damage was correlated with a change that exceeded 30% in the centerline length or centroid location of a wall (identified by the dashed lines in the figure). Correlation was strongest when the controlling directional properties (i.e., maximum values between two directions) were considered (Figure D-33c). A modification to the ASCE/SEI 31-03 Tier 1 Evaluation in the form of a new checklist statement was developed to capture this result.



(a) Global properties:
Area ($\Delta A/A^{upper}$); Centerline Length ($\Delta L_{cl}/L_{cl}^{upper}$)



(b) Directional properties:
Centerline Length ($\Delta L_{cl,x}/L_{cl,x}^{upper}$,
 $\Delta L_{cl,y}/L_{cl,y}^{upper}$);
Centroid ($\Delta x_c/L_x^{upper}$, and $\Delta y_c/L_y^{upper}$)



(c) Controlling directional properties (i.e., max. of):
Centerline Length ($\Delta L_{cl,x}/L_{cl,x}^{upper}$, $\Delta L_{cl,y}/L_{cl,y}^{upper}$);
Centroid ($\Delta x_c/L_x^{upper}$, $\Delta y_c/L_y^{upper}$)

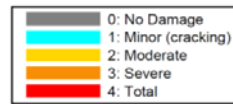


Figure D-33 Magnitude of discontinuity measure for each discontinuity ID (color indicates the level of earthquake damage observed in the building in the vicinity of the discontinuity).

Appendix E

Study of a Pier-Spandrel System

This appendix presents detailed information on the study of a pier-spandrel system to illustrate the concepts of evaluating the expected mechanism of behavior for a structural system, using hand calculations.

E.1 Case Study Building

The O'Higgins building, located in Concepción, was selected for study of pier-spandrel system behavior. The building in Concepción suffered severe damage and partial collapse in the 2010 Maule earthquake. Although not necessarily the cause of collapse, shear failure in wall piers constrained between stronger spandrels, and flexural hinging in spandrels at heavier piers, was observed in the building. An exterior elevation after the 2010 Maule earthquake and an idealized representation of the pier-spandrel shear wall system are provided in Figure E-1. The geometry, reinforcement details, and specified material properties were obtained from available structural drawings for the building, and expected material properties for concrete and steel reinforcement were estimated based on the PEER/ATC-72-1, *Modeling and Acceptance Criteria for Seismic Design and Analysis of Tall Buildings* report (ATC, 2010).

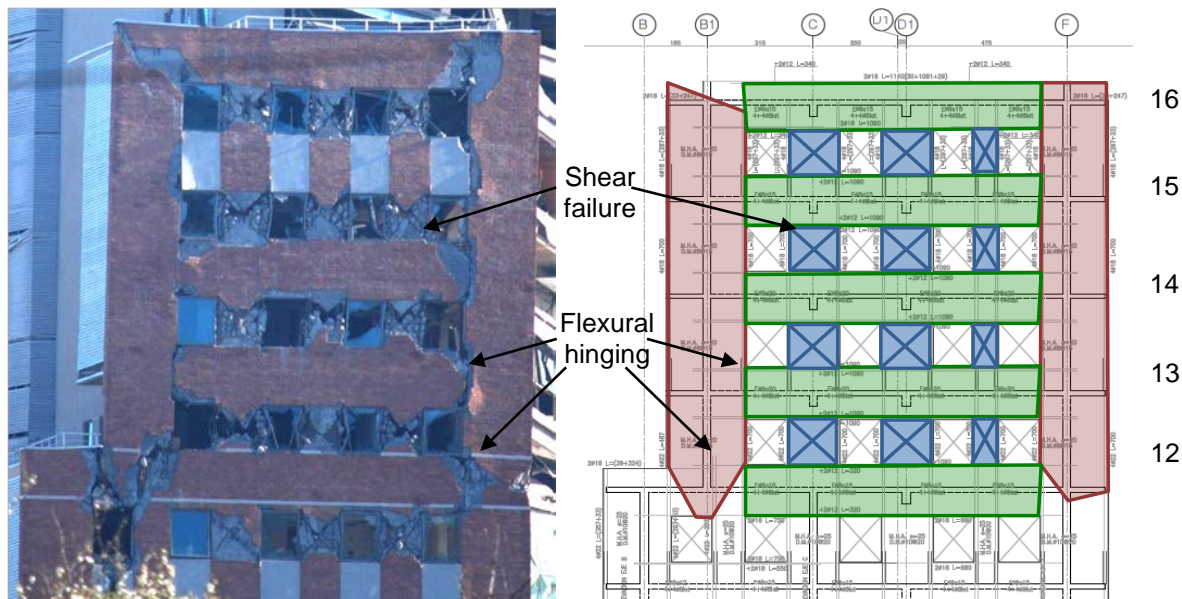


Figure E-1 Exterior elevation of the O'Higgins building after the 2010 Maule earthquake (photo courtesy of PEER), and idealized pier spandrel system.

E.2 Identification of Controlling Behavior

The FEMA P-306 report, *Evaluation of Damaged Concrete and Masonry Walls Buildings* (FEMA, 1999), provides a method for determining component and system response mechanisms that identifies the controlling behavior for each component, and then employs joint equilibrium and the principles of virtual work to determine the expected system response mechanism.

Axial loads were calculated based on tributary area, self-weight, and typical dead and live loads defined for a residential building in Chilean Norma NCh433Of.96, *Earthquake Resistant Design of Buildings* (INN, 1996). The resulting axial load ratio on the wall piers represents approximately 2% of their nominal axial capacity. Axial loads due to seismic forces were neglected.

The shear strength of each wall pier and spandrel was computed for: flexural yielding (per ACI 318-11); sliding shear (per FEMA P-306); and diagonal tension (per ACI 318-11, FEMA P-306 with both low- and high-displacement ductility demands) behaviors. Table E-1 presents a summary of the shear forces corresponding to each of the behavior modes considered for each wall pier and spandrel beam (as identified in Figure E-1b).

Table E-1 Wall Pier and Spandrel Beam Shear Strength and Expected Behavior Mode

Element			Behavior Modes Considered, and Corresponding Shear Force (kips)					
Type	Line	Level	Flexure	Sliding shear	Diagonal Tension			Controlling Behavior
					ACI 318	FEMA P-306, low ductility	FEMA P-306, high ductility	
External Pier	B1,F	12	290	435	280	230	139	Diagonal Tension
		13	235	372	280	228	137	
		14	235	372	280	226	134	
		15	235	372	280	224	132	
Internal Pier	C	12	401	365	206	182	115	Diagonal Tension
		13	318	318	206	179	113	
		14	318	318	206	177	110	
Internal Pier	D1	12	304	298	168	146	92	Diagonal Tension
		13	239	292	168	144	90	
		14	239	292	168	143	88	
Spandrel	B1-F	13-16	236	155	199	144	76	Diagonal Tension

The behavior mode with the lowest corresponding shear force is expected to govern the seismic response of the element. In the table it can be seen that the expected shear strength of individual piers is less than the shear that would correspond to flexural yielding. Results indicate that all components could be expected to sustain shear-induced damage.

E.3 Plastic Analysis

Next, the principle of virtual work was used to determine the maximum lateral force, applied at the top of the pier-spandrel system, corresponding to development of each of a series of system-level plastic mechanisms. In the plastic analysis of the four-story four-bay pier-spandrel system selected for this study, several plastic mechanisms were considered, including shear failure of intermediate piers (Figure E-2a), spandrel shear failure between pier lines (Figure E-2b), among others.

A system mechanism comprising shear damage to interior piers and flexural yielding at the end of the spandrels and exterior piers was found to have the lowest mechanism load and, thus, controls response. This mechanism is also consistent with the expected behavior and observed damage in the building.

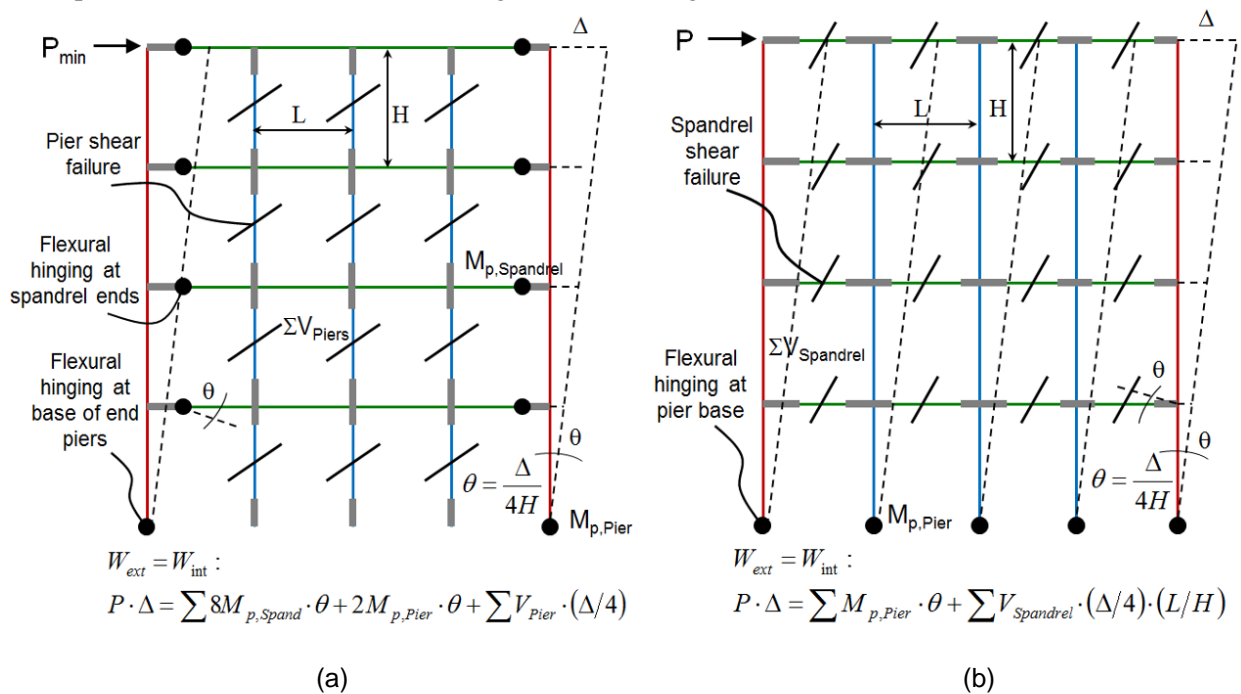


Figure E-2 Sample plastic mechanisms studied: (a) mechanism validated by calculation and post-earthquake observations; and (b) mechanism considered and shown by calculation not to govern.

Analysis of Wall Buildings

This appendix presents detailed information regarding testing configuration, material properties, and loading protocols used for the experiments used for calibration of analytical models presented in Chapter 5. Detailed information regarding the Alto Rio building, as well as summary of other work conducted on the Alto Rio building are provided.

F.1 Simulation of Acevedo and Moehle (2010) Tests

The specimen tested by Acevedo and Moehle (2010) was designed to represent the boundary element in the end regions of a concrete wall, based on the requirements for non-special boundary elements in Section 21.9.6.5 of ACI 318-08, *Building Code Requirements for Structural Concrete and Commentary* (ACI, 2008). Figure F-1 shows the dimensions and detailing of the specimen. The average concrete compressive strength was about 6 ksi (41 MPa) and the #6 reinforcing bars have a yield strength of about 67 ksi (462 MPa). A tension test on the wall was carried out first to develop 4% tensile strain on the specimen. Then the specimen was loaded in compression at a rate of about one kip per second until a buckling-like failure occurred (Figure F-2a) at a much lower load than the nominal capacity of the specimen.

In the LS-DYNA (LSTC, 2010) model the compressive strength of concrete was assumed to be 5.8 ksi (40 MPa). The yield strength and ultimate strength of steel were assumed to be 71.5 ksi (500 MPa) and 101 ksi (700 MPa) respectively.

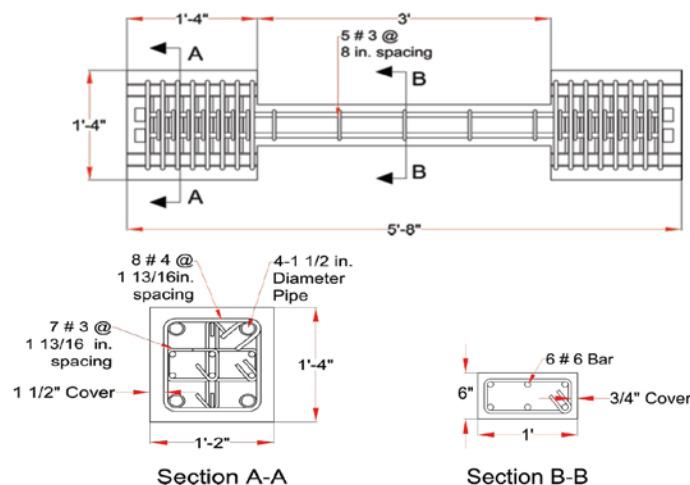


Figure F-1 Specimen dimension and detailing (Acevedo and Moehle, 2010).

F.2 Simulation of Rodriguez et al. (1999) Tests

The form of reinforcing bar specimen in the Rodriguez et al. (1999) buckling tests is illustrated in Figure F-2. The corresponding fiber beam analytical model is also shown. It comprises the total length, S_h , of bar having diameter, D , together with the $0.6D$ long transitions to the larger diameter threaded sections at each end. The 30mm gauge length is discretized into ten fiber beam elements.

Rodriguez et al. defined onset of buckling as when the difference in strain across the bar over a 30 mm (1.2 inches) gauge length exceeds 20% of the mean strain.

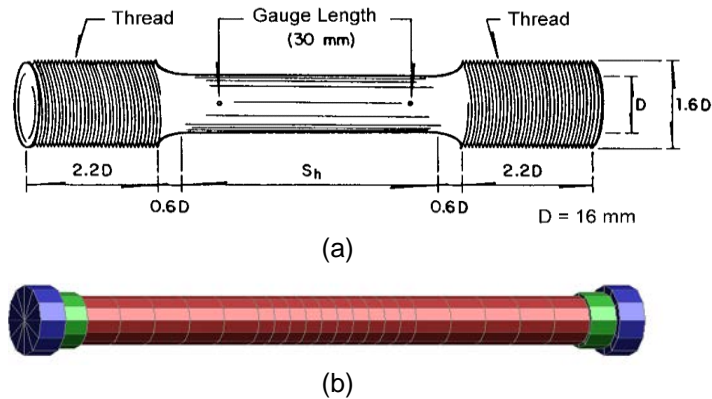


Figure F-2 Illustrations of: (a) test specimen; and (b) fiber beam model. Note: the 30 mm gauge length is not to scale.

Figure F-3 shows the applied average strain loading history applied to both the experiment and the simulation. The analytical and experimental results were compared to verify that the model is capable of capturing the initiation of buckling determined experimentally by considering the difference in longitudinal strain ϵ_1 and ϵ_2 at opposite sides of the bar over the gauge length. Figure F-4 compares the stress-strain hysteresis at the two sides of the bar in the test and simulation. The comparison shows that the analytical model captures well the hysteretic stress-strain relationship at two opposite sides of the test specimens.

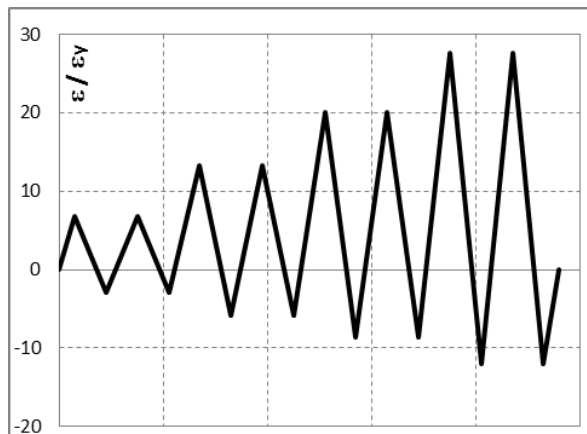


Figure F-3 Average strain loading history applied in Rodriguez et al. (1999).

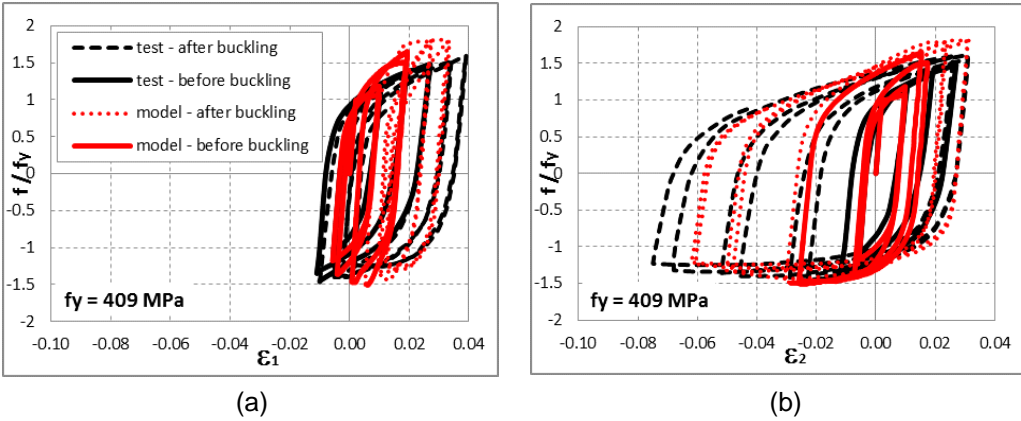


Figure F-4 Stress-strain hysteresis: (a) measured on one side of bar; and (b) measured on opposite side of bar.

The sensitivity of bar response to applied strain history was investigated by subjecting the analytical model to seven different loading protocols. Protocol “1” is that used by Rodriguez et al. (Figure F-3) in which the applied strain in tension and compression gradually increases cycle by cycle. Figure F-5 illustrates the remaining six loading protocols (labeled from “2” to “7”), in which loading cycles with maximum applied tensile strains of 4% and 5% and maximum compression strains are 1% and 2% are applied in different order (e.g., starting with large cycle in tension, followed by small cycle in tension).

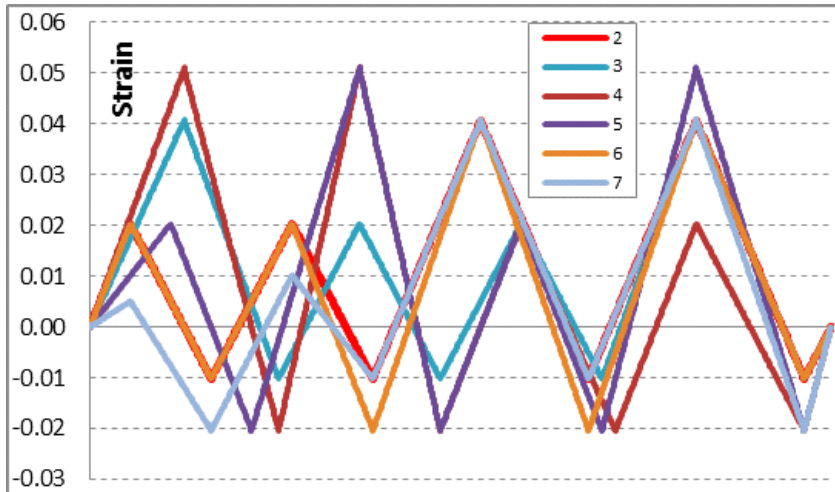


Figure F-5 Applied strain protocols 2 to 7.

F.3 Simulation of Lowes et al. (2011) Specimen PW4

F.3.1 Model Geometry and Material Properties

Figure F-6a shows the geometry and physical reinforcement arrangement in the cross-section of specimen PW4 used by Lowes et al. (2011), and Figure F-6b shows the considered boundary element.

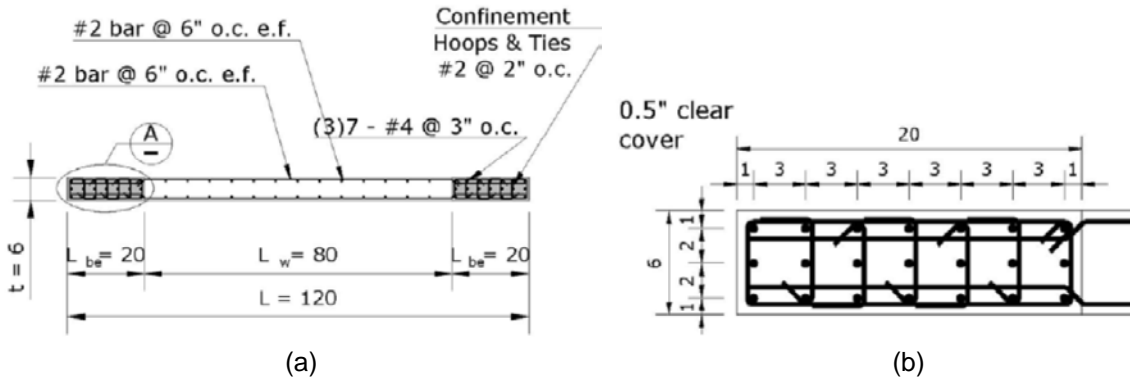


Figure F-6 Wall specimen PW4: (a) cross-section; and (b) boundary element (Lowe et al., 2011).

The vertical reinforcement in the boundary element comprised #4 bars with yield stress of 462 MPa (70 ksi) and ultimate stress of 755 MPa (109 ksi). Hoops in the boundary element were spaced vertically at 51 mm (2 inch) centers such that the S/D ratio equals 4. It should be noted that on the end face of the wall, one #4 bar is not mechanically restrained by a tie bar hook.

The monotonic stress-strain relationships for unconfined and confined concrete and #4 bar reinforcing steel are shown in Figure F-7. The strength of unconfined concrete is taken as $f'_c = 29.4$ MPa (203 ksi) based on cylinder tests. The effect of confinement is considered using confinement model developed by Mander (1988), and confined concrete was characterized with ultimate strength of $f'_{cc} = 47.1$ MPa (325 ksi).

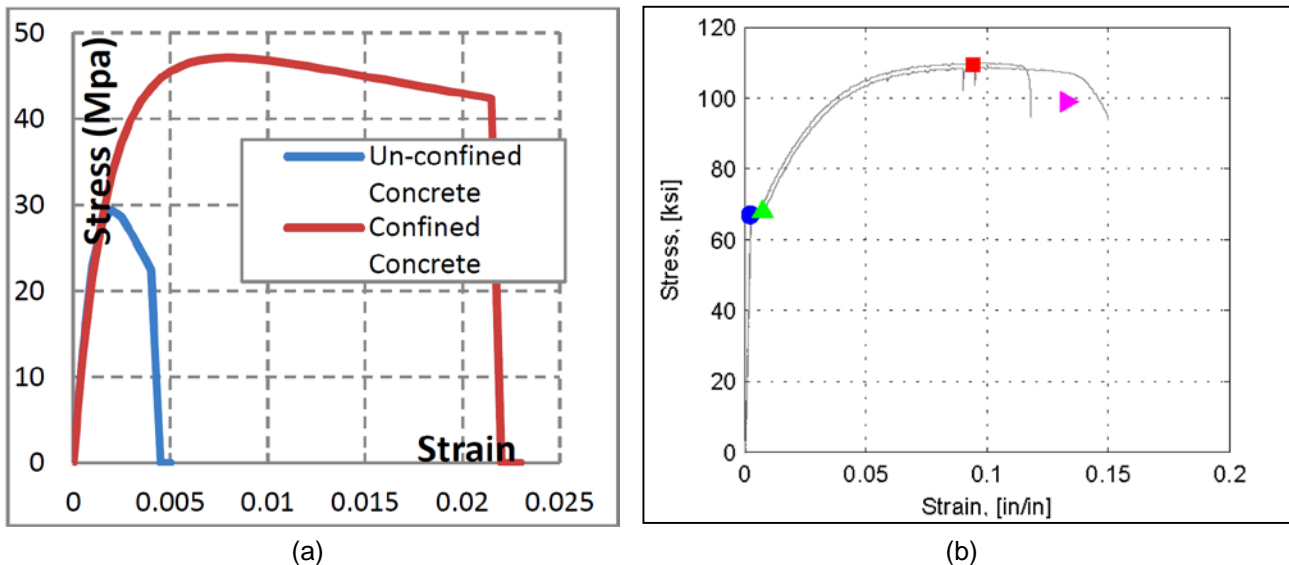


Figure F-7 Material properties of: (a) unconfined and confined concrete; and (b) reinforcing steel #4 bars in wall specimen PW4.

Figure F-8 compares an elevation of the wall model with the physical specimen PW4. The model comprises a mesh of 12 inches high shell elements. Each 20 inch

boundary length is divided into two elements, and the central zone is divided into eight equal element divisions.

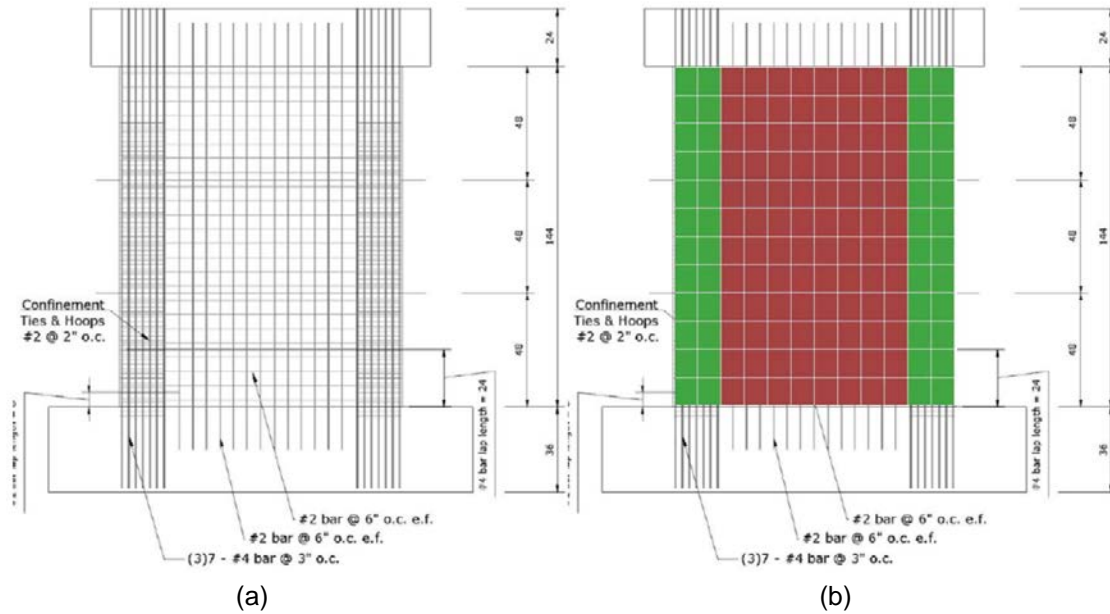


Figure F-8 Elevations of: (a) PW4 test specimen (from Lowes et al. 2011); and (b) LS-DYNA shell model.

Figure F-9 shows the plan section sandwich modeled in the boundary zones in the LS-DYNA model. The confined zone has a thickness of 113 mm (4.45 inches) measured from the outside of the horizontal reinforcement, and the vertical reinforcement bars in the middle of the section are distributed to the two outer curtains. Although this will slightly overestimate the out-of-plane bending and buckling resistance of the wall, overall wall buckling was not a mode of failure observed in the test. Figure F-10 shows the plan section sandwich in the web portion of the wall where all concrete is assumed unconfined.

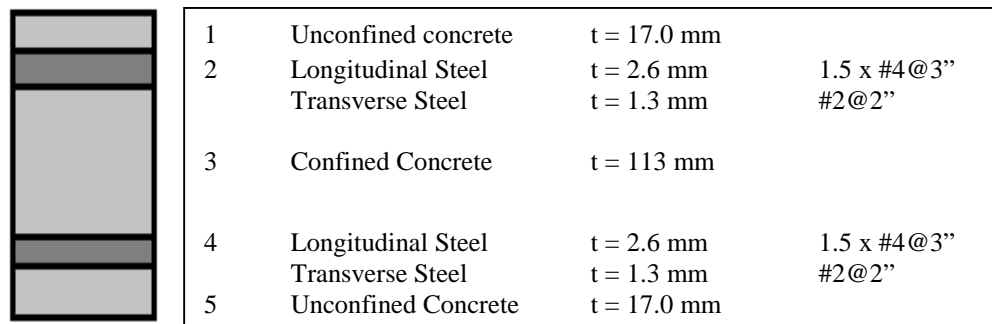


Figure F-9 LS-DYNA sandwich shell for confined zones of wall.



1	Unconfined concrete	t = 25.3 mm	
2	Longitudinal Steel	t = 0.203 mm	#2@6"
	Transverse Steel	t = 0.203 mm	#2@6"
3	Unconfined Concrete	t = 101 mm	
4	Longitudinal Steel	t = 0.203 mm	#2@6"
	Transverse Steel	t = 0.203 mm	#2@6"
5	Unconfined Concrete	t = 25.3 mm	

Figure F-10 LS-DYNA sandwich shell for central unconfined zone of wall.

The material properties for rebar and concrete (confined and unconfined) were based upon the test results associated with the PW4 wall specimen, and were described in Section F.2.2.

F.3.2 Loading Protocol

The loading protocol for PW4 wall specimen is a hybrid scheme involving lateral loads and moment applied at the top, with additional shear forces applied at two lower levels controlled to match a target lateral displacement history at the control point (at the top of the clear wall). A constant vertical load is also maintained.

For simulation, the loading history was approximated by a lateral displacement control with constant vertical load applied. A single lateral displacement was applied to a rigid extension above the top of the wall at an elevation such that the ratio of applied shear force to moment would be approximately correct at the base of the wall. In the initial simulation, it was assumed that the lateral deflection at the analysis loading point was a constant ratio of the reference displacement at the top of the wall in the physical test.

F.3.3 Simulation with Bar Buckling

A detailed study was performed to examine bar buckling at the confined boundary region of the PW4 shear wall specimen by modeling the reinforcing bar with a refined mesh of fiber beam elements as in the simulation of the Rodriguez et al. tests. In this case, because the middle bar on the end face of the wall is not restrained by a hook, the entire rebar cage of the end of the wall was modeled with fiber beam elements, as shown in Figure F-11a. This model was subjected to the average vertical strain history predicted at this boundary in the initial LS-DYNA simulation of PW4 specimen (Figure F-11b). The reinforcement cage was restrained such that bars could not deflect into the core of the wall, but could deflect outwards as would be the case if the cover concrete had spalled. Figure F-11c shows the shape of the rebar cage after buckling. The middle (untied) bar buckles first, followed by the corner bars.

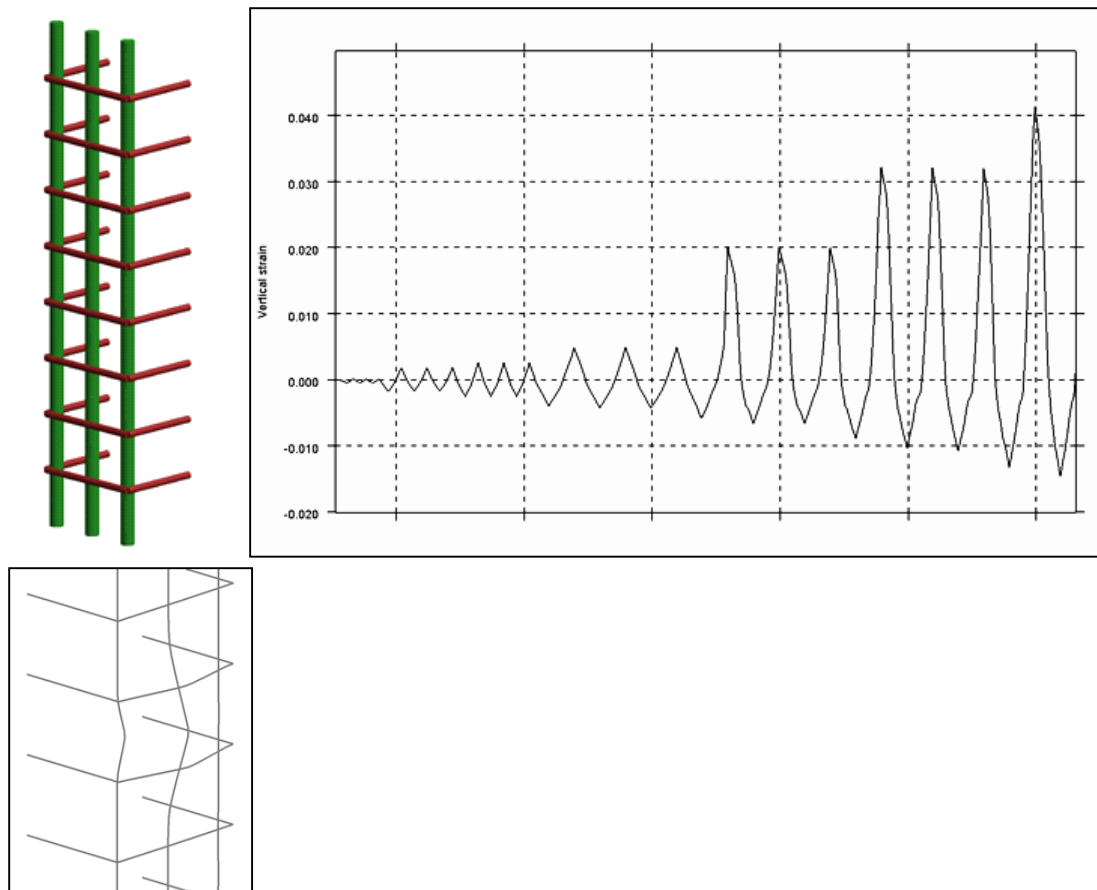


Figure F-11 Simulation of reinforcement cage buckling at PW4 wall specimen.

An attempt was made to represent the reinforcing bar hysteresis predicted from the fiber-beam model by adjusting parameters in the reinforcing bar model available in the LS-DYNA shell element. As shown in Figure F-12, the hysteretic behavior of the shell model does not exactly match that of the more detailed fiber beam simulation, and the differences between the middle and corner bars are not captured; however, the overall hysteresis behavior is reasonably well-matched.

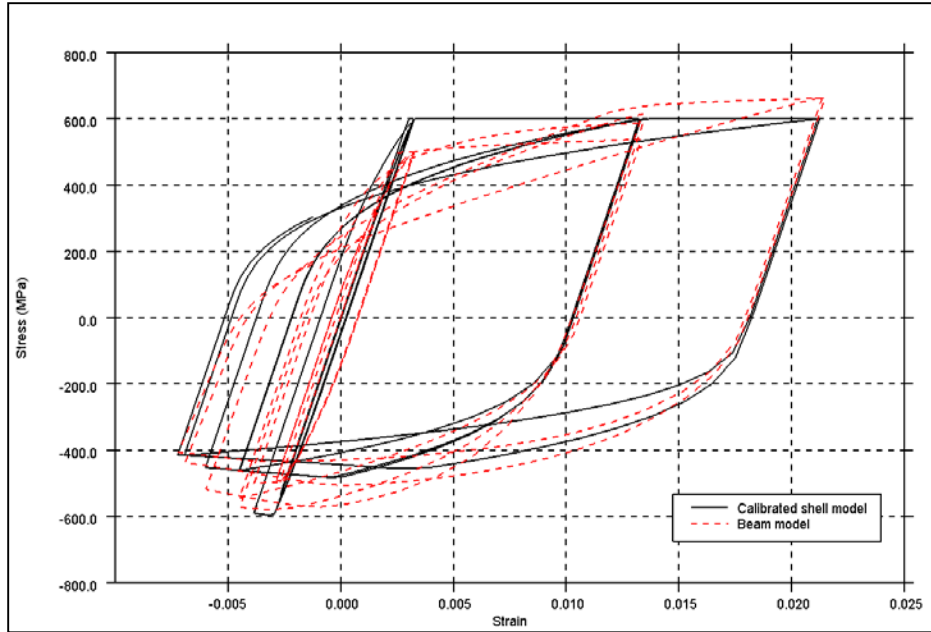


Figure F-12 Comparison of shell element reinforcing bar model to match stress-strain hysteresis of fiber-beam model of reinforcing bar cage of PW4 wall specimen.

F.4 Alto Rio Building

F.4.1 Building Information

The Alto Rio building was 15 stories above grade with two basement levels below grade, supported by a mat foundation on alluvial soil. A longitudinal elevation of the building is provided in Figure F-13. The LS-DYNA analysis model comprised a representative three-dimensional slice of the building.

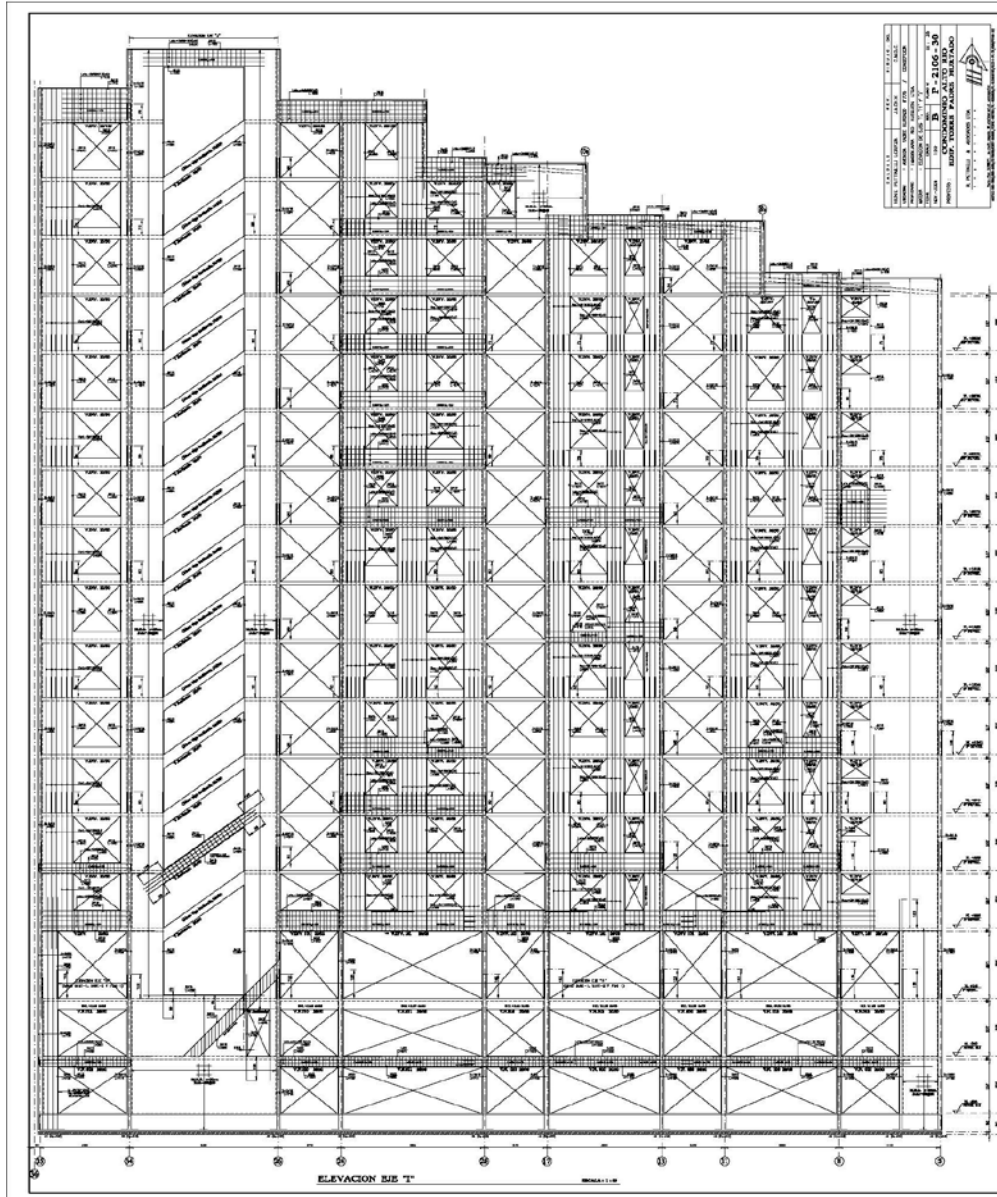


Figure F-13 Alto Rio Building longitudinal section (courtesy of Patricio Bonelli).

F.4.2 Material Properties

The specified design cube strength of the concrete was 4.4 ksi (30 MPa) below the second floor and 3.6 ksi (25 MPa) above the second floor. These correspond to cylinder strengths of 3.6 ksi (25 MPa) and 2.9 ksi (20 MPa), respectively. The specified design yield and ultimate strengths of the reinforcing steel were 60 ksi (420 MPa) and 90 ksi (630 MPa), respectively.

Based upon testing of 4 inch (100 mm) core samples from the building after the collapse the mean concrete cube strength over 29 samples from the entire building was 7.1 ksi (48.7 MPa) (with coefficient of variation 0.15); the mean cube strength of

the eight samples taken from the critical first story walls was 6.8 ksi (46.6 MPa) (IDEM 2010). The corresponding mean cylinder strength values are 6.3ksi (43.7 MPa) and 6.0 ksi (41.6 MPa), respectively.

The mean yield stress of 27 samples of reinforcing bars was 70 ksi (480 MPa) (with coefficient of variation 0.088) and mean ultimate strength of 100 ksi (720 MPa) (coefficient of variation 0.043).

The mean measured density of the concrete cores was 147 pcf (2,350 kg/m³).

F.4.3 Ground Motions

Concepción experienced strong ground shaking, with recorded spectral acceleration exceeding 1.0g. Horizontal response spectra from accelerations recorded near the Alto Rio building show peaks at approximately 1.5 to 2.0 seconds (Figure F-14), presumably due to some site amplification. The acceleration histories (Figure F-15) show that the first strong pulses occur about 10 seconds into the record.

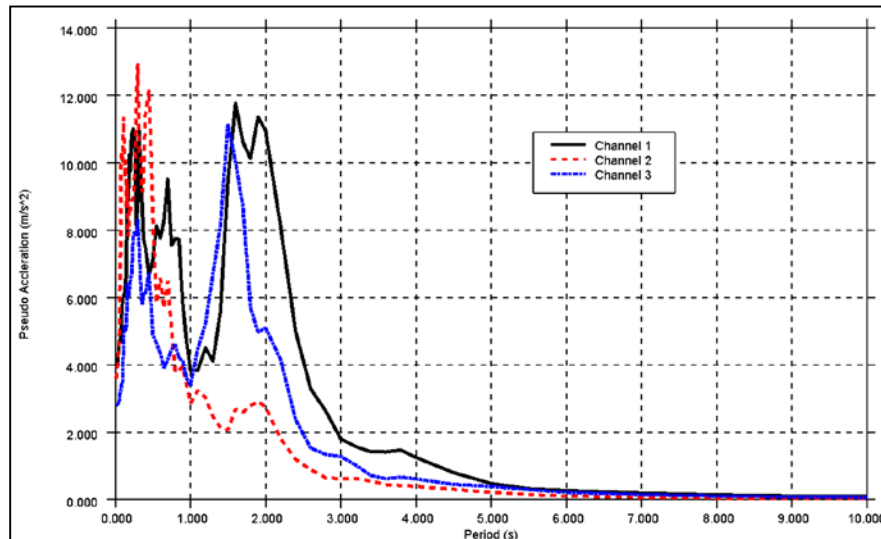


Figure F-14 Spectra of triaxial Concepción records.

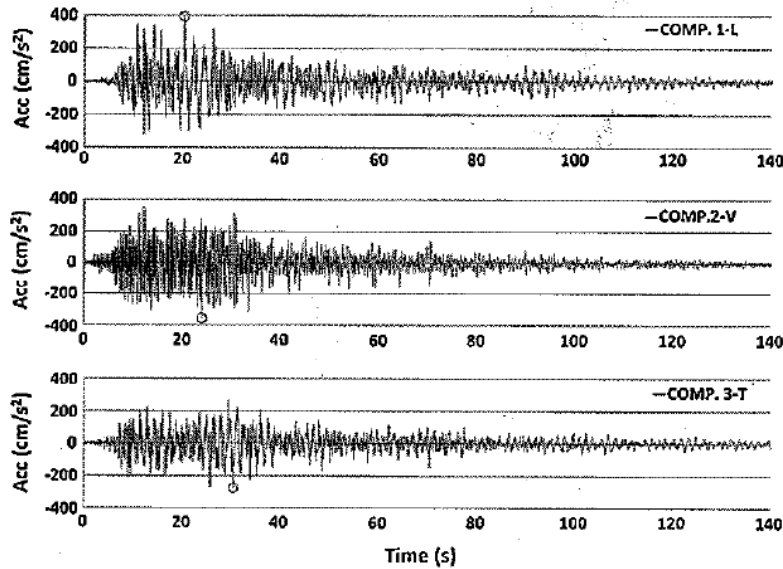


Figure F-15 Acceleration time histories of the Concepción record (Boroschek et al., 2012).

F.4.4 Gravity Loads

For the purposes of analysis, the density of reinforced concrete was assumed to be 156 pcf (2,500 kg/m³) to allow for reinforcement and wall finishes. The assumed added floor mass was 12.5 pcf (200 kg/m²).

Figure F-16 illustrates the vertical stresses in the walls of the modeled portion of the building due to gravity. At grade level the average stress is 260 psi (1.8 MPa), or 0.04A_gf'_c, and the maximum stress is about 725 psi (5 MPa), or 0.12A_gf'_c.

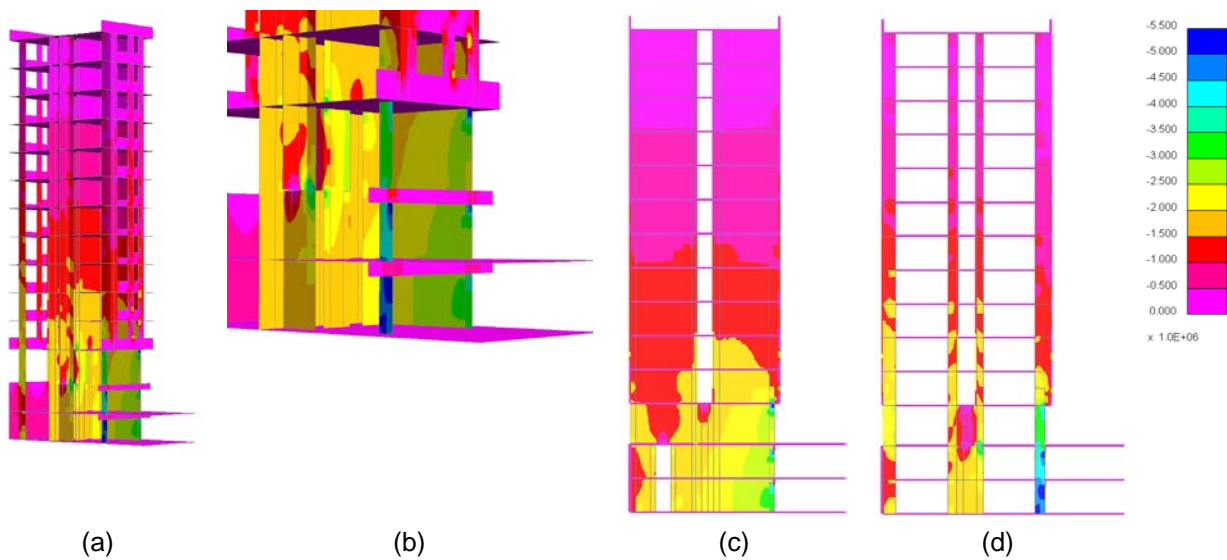


Figure F-16 Gravity stresses (MPa) in LS-DYNA model (1 MPa = 145 psi): (a) perspective view; (b) close-up of basement, first, and second floors; (c) elevation at Grid 13; and (d) elevation at Grid 17.

F.4.5 Natural Period

The natural period of the building slice model depends on a number of assumptions. Key parameters include the following:

- Whether cracked or uncracked section properties are assumed: Natural periods for small strain behavior (uncracked walls) are compared in this section.
- The Young's modulus of concrete, E : The possible range of concrete modulus is related to the range of potential concrete strengths. For f'_c values of 4.1 ksi (28 MPa) to 6.7 ksi (46MPa), the range of E values is taken as 25GPa to 32GPa.
- The conditions assumed at the building base: This study considers: (1) a rigid basement case where it is assumed that the external boundaries of the model below grade are fully restrained; and (2) a flexible basement case where the external basement walls are unrestrained.
- The effectiveness of the coupling between the main transverse walls provided by the corridor slabs: This comparison considers: (1) a case where the slabs are assumed to have uncracked stiffness properties; and (2) a case where the slabs are assumed to have zero flexural stiffness.
- The seismic imposed load is assumed to be 40 psf (200 kg/m²) for this study.

The range of natural periods predicted by LS-DYNA in the small strain range is summarized in Table F-1.

Table F-1 Natural Periods of the LS-DYNA Alto Rio Building Model Based on Stiffness Assumptions

Concrete Modulus E , ksi (GPa)	Basement	Period	
		<i>Slab Coupling Uncracked</i>	<i>Slab Coupling Zero</i>
3,625 ksi (25 GPa)	Rigid	0.48 s	0.52 s
3,625 ksi (25 GPa)	Flexible	0.57 s	0.60 s
4,640 ksi (32 GPa)	Rigid	0.41 s	0.46 s
4,640 ksi (32 GPa)	Flexible	0.50 s	0.53 s

For comparison, Song et al. (2012) predict a first mode period of 0.5 seconds using a three-dimensional elastic shell model of the entire building in SAP2000, *Integrated Software for Structural Analysis and Design* (CSI, 2013b) assuming $E = 4,700$ ksi (32.4 GPa) and a rigid basement. The periods of the LS-DYNA slice model appear consistent with this, considering that the model by Song et al. includes the taller zone of the building.

F.4.6 Intrinsic Damping

Intrinsic small-strain energy dissipation not captured by nonlinear material hysteresis was represented by incorporating a material damping ratio in LS-DYNA.

An intrinsic damping ratio of 1% of critical was specified over the frequency range of the principal modes (0.1 Hz to 10.0 Hz), which decreases (in the adopted formulation) to about 0.5% at 30 Hz and 0.2% at 100 Hz. Although this is lower than values traditionally used for seismic response analysis, it is considered appropriate for this building because:

- It is consistent with measurements of small-strain damping of reinforced concrete material, bare concrete wall structures, and concrete chimneys.
- There are no significant nonstructural components (all external and internal walls are concrete structural walls).
- Frame action is absent, so infill window and door frames will not shear significantly.

F.5 Alto Rio Building Simulation Results

F.5.1 Nonlinear Analysis Results for Expected and Measured Material Properties

A comparison of nonlinear analysis results for the Alto Rio building with expected and measured material properties under triaxial excitation is provided in Figures F-17 through F-21. Here, the expected f'_c is taken as 30MPa, and measured f'_c as 43MPa.

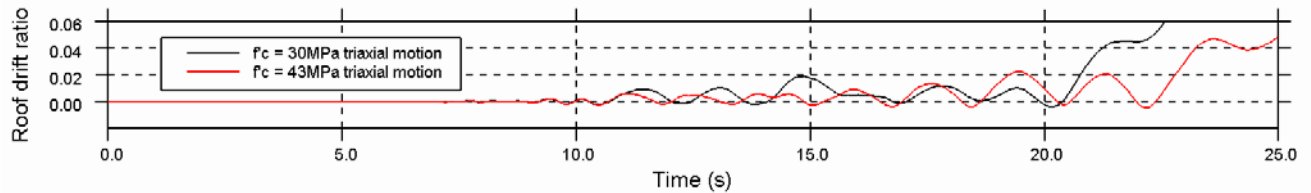


Figure F-17 Roof drift ratio time-history of the wall on Grid 13 with expected (black) and measured (red) properties.

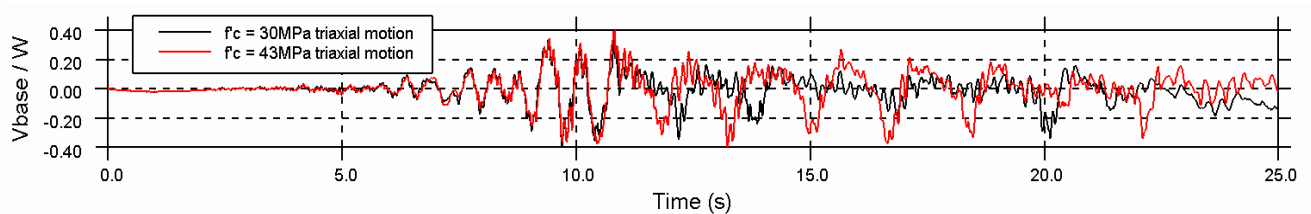


Figure F-18 Base shear ratio time-history of the wall on Grid 13 with expected (black) and measured (red) properties.

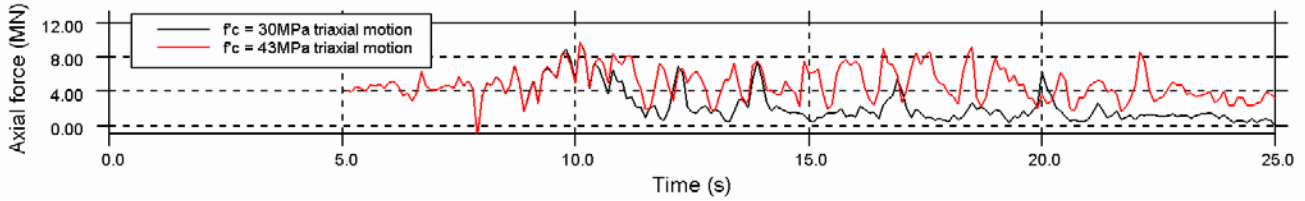


Figure F-19 Axial force time-history of the wall on Grid 13 with expected (black) and measured (red) properties.

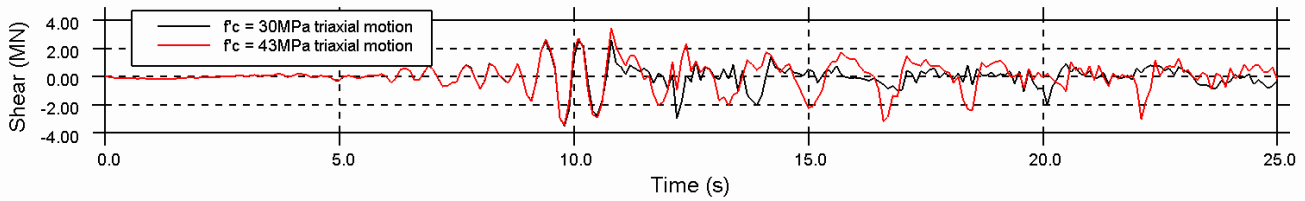


Figure F-20 Shear force time-history of the wall on Grid 13 with expected (black) and measured (red) properties.

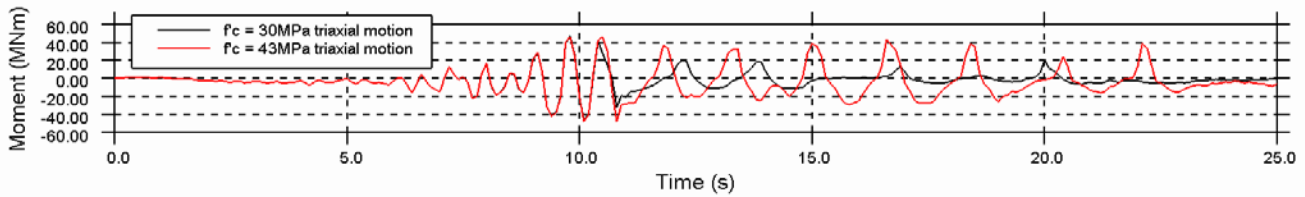


Figure F-21 Moment time-history of the wall on Grid 13 with expected (black) and measured (red) properties.

F.5.2 Simulation Results with Basement Assumptions

Figure F-22 and Figure F-23 below show the roof drift ratio and the base shear ratio time histories for $f'_c = 4.4$ ksi (30 MPa) for the two basement support assumptions.

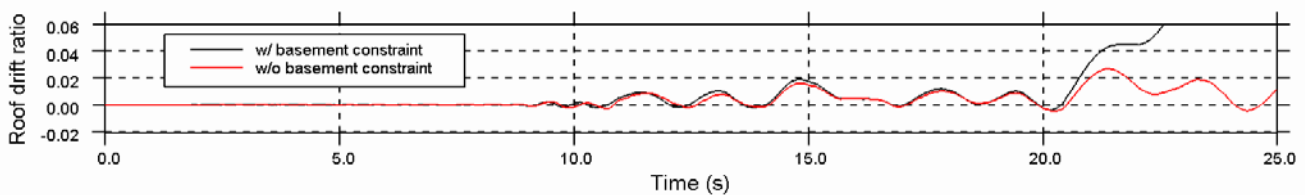


Figure F-22 Roof drift ratio time-history of the wall on Grid 13 with (black) and without (red) basement constraint.

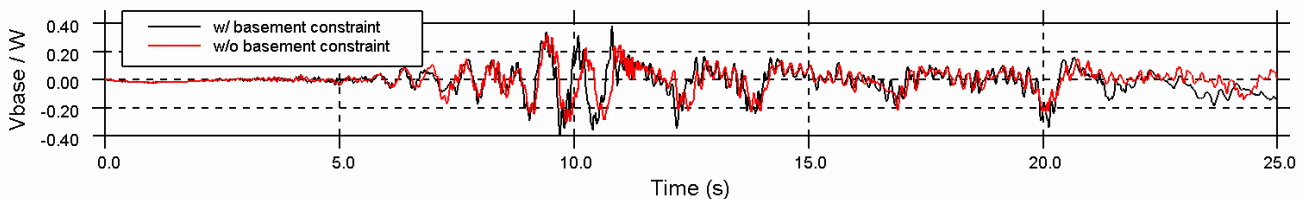


Figure F-23 Base shear ratio time-history of the wall on Grid 13 with (black) and without (red) basement constraint.

F.6 Other Analyses of the Alto Rio Building

F.6.1 Tuna and Wallace (2012)

Tuna and Wallace performed an analysis of a similar slice of the building in PERFORM-3D, using fiber beam cross sections with uniaxial stress versus strain relations for concrete and steel having expected material strengths of $f'_c=4.7$ ksi (32.5 MPa) and $f_y=70$ ksi (491 MPa) (1.3 and 1.17 times the design strength, respectively). The effect of rebar buckling was represented by decreasing the stress sustained by the rebar in compression for strains greater than 0.003 by a factor depending on the slenderness ratio of bars.

The shear behavior of the walls was modeled using a tri-linear relation similar to that recommended by *Supplement No.1 to ASCE 41-06* (ASCE, 2008) (Figure F-24), with shear force-deformation relations derived from recent experimental studies as outlined in the PEER/ATC-72-1 report (ATC, 2010). The uncracked shear modulus was taken as $0.4E_c$ and shear (diagonal) cracking was assumed to occur at $0.25f'_c$ (MPa) but not greater than $0.5nV$, where nV is the ACI 318-08 nominal wall shear strength. Tensile strength of concrete is ignored.

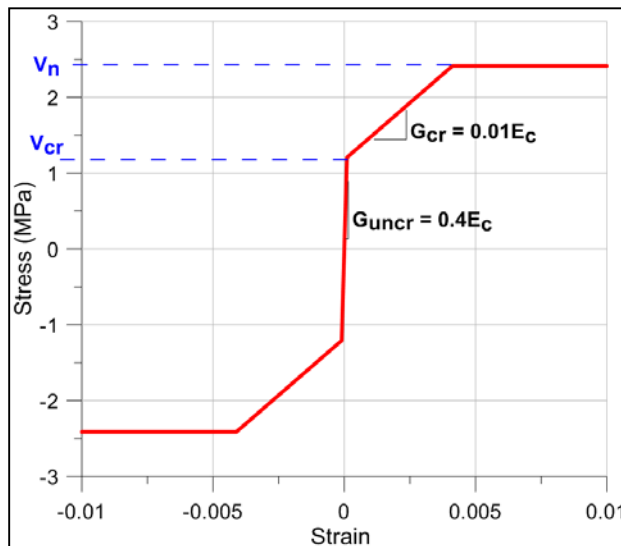


Figure F-24 Shear model used by Tuna and Wallace (2012).

The natural period of the model in the transverse direction was 0.70 seconds (with slab coupling) and 0.77 seconds (without slab coupling). This latter period compares with 0.60 seconds from the LS-DYNA model of an adjacent slice (with flexible basement) and concrete with $E = 4060$ ksi (28 GPa). Following the application of gravity loading, the analytical model was subjected to the east-west component of the ground motion recorded in Concepción. Rayleigh damping was specified as 2.5% of critical at $0.2T$ and $1.0T$, where T is the first mode period.

F.6.2 Song et al. (2012)

Song et al. (2012) analyzed a three-dimensional model of the entire building in SAP2000 using a relatively coarse mesh of shell elements assuming uncracked concrete with $E = 4.7$ ksi (32.4 GPa) and assuming the building fully fixed at ground level. A first mode natural period of 0.5 seconds with participation factor 1.6 is reported. Based on Sozen (2003), the expected roof drift ratio was estimated as 1%.

No response history analysis was performed in this study. However, the authors concluded that collapse of the building must have required some brittle mechanisms to have occurred, which may have included:

- Shear failures beneath the stacks of wall openings such as described in Chapter 4 of this report,
- Compressive stress concentrations at discontinuities,
- Fracture of vertical bars, and
- Bond failure along unconfined lap splices.

F.6.3 Kohrangi et al. (2012)

Kohrangi et al. (2012) analyzed a three-dimensional model of the entire building in SAP2000 in which the walls were modeled as vertical beams with cracked sections ($0.5E_cI_g$), and coupling between connected wall segments was accomplished with stiff horizontal arms. The basement stories were laterally restrained. First mode periods of 1.09 seconds and 1.07 seconds in the long and the transverse directions, respectively, were observed. It is noted that these natural periods are more than twice the natural periods determined by Song et al.

No response history analysis was performed in this study. Vulnerability assessments were made by the linear static and nonlinear static procedures of FEMA 356, *Prestandard and Commentary for the Seismic Rehabilitation of Buildings* (FEMA, 2009) but the findings are inconclusive. Based on pushover analyses, the authors predicted the building to be more vulnerable to collapse in the longitudinal direction than the transverse. They also expressed concern that large tensile forces in walls due to coupling action could have contributed to the failure.

References

- Acevedo, C., and Moehle, J., 2010, *Seismic Vulnerability of Non-Special Boundary Element of Shear Wall Under Axial Force Reversals*, June 2010 Presentation, Pacific Earthquake Engineering Research Center Internship Program, University of California, Berkeley, California.
- ACI, 2008, *Building Code Requirements for Structural Concrete and Commentary*, ACI 318-08, American Concrete Institute, Farmington Hills, Michigan.
- ACI, 2010, *Specification for Tolerances for Concrete Construction and Materials*, ACI 117-10, American Concrete Institute, Farmington Hills, Michigan.
- ACI, 2011, *Building Code Requirements for Structural Concrete and Commentary*, ACI 318-11, American Concrete Institute, Farmington Hills, Michigan.
- ASCE, 2003, *Seismic Evaluation of Existing Buildings*, ASCE/SEI 31-03, American Society of Civil Engineers, Reston, Virginia.
- ASCE, 2007, *Seismic Rehabilitation of Existing Buildings*, ASCE/SEI 41-06, American Society of Civil Engineers, Reston, Virginia.
- ASCE, 2008, *Supplement No. 1 to ASCE 41-06*, American Society of Civil Engineers, Reston, Virginia, <http://www.asce.org/sei/supplements/>.
- ASCE, 2010, *Minimum Design Loads for Buildings and Other Structures*, ASCE/SEI 7-10, American Society of Civil Engineers, Reston, Virginia.
- ATC, 2010, *Modeling and Acceptance Criteria for Seismic Design and Analysis of Tall Buildings*, PEER/ATC-72-1 report, prepared by the Applied Technology Council for the Pacific Earthquake Engineering Research Center, Redwood City, California.
- Bae, S., and Bayrak, O., 2008, "Plastic hinge length of reinforced concrete columns," *Structural Journal*, Vol. 105, No. 3, pp. 290-300.
- Baker, A.L.L., and Amarakone, A.M.N., 1965, "Inelastic hyperstatic frame analysis," *Special Publication 12: Flexural Mechanics of Reinforced Concrete*, American Concrete Institute, Farmington Hills, Michigan.
- Birely, A., 2012, *Seismic Performance of Slender Reinforced Concrete Walls*, Ph.D. Dissertation, University of Washington, Seattle, Washington.
- Boroschek, R., and Contreras, V., 2012, "Strong ground motion from the 2010 M_w 8.8 Maule Chile earthquake and attenuation relations for Chilean Subduction Zone interface earthquakes," *International Symposium on Engineering*

- Lessons Learned from the 2011 Great East Japan Earthquake*, Japan Association for Earthquake Engineering, Tokyo, Japan, Vol. 1, pp. 1722-1733.
- Boroschek, R., Contreras, V., Kwak, D.-Y., and Stewart, J.P., 2012, “Strong ground motion attributes of the 2010 M_w 8.8 Maule, Chile, earthquake,” *Earthquake Spectra*, Vol. 28, No. S1, pp. S19-S38.
- Boroschek, R., Soto, P., and Leon, R., 2010, *Maule Region Earthquake, February 27, 2010, $M_w = 8.8$* , RENADIC Report 10/08 Rev. 2, University of Chile, Santiago, Chile.
- Buckle, I., Hube, M., Chen, G., Yen, W.-H., and Arias, J., 2012, “Structural performance of bridges in the offshore Maule earthquake of 27 February 2010,” *Earthquake Spectra*, Vol. 28, No. S1, pp. S533-S552.
- CEN, 2004, *Eurocode 8: Design of Structures for Earthquake Resistance – Part 1: General Rules, Seismic Actions and Rules for Buildings*, EN 1998-1:2004:E, European Committee for Standardization, Brussels, Belgium.
- Cerda, M.J., 2011, *Análisis de Daños del Edificio Plaza del Río, Provocados por el Terremoto del 27 de febrero del 2010*, Memoria de titulación de Ingeniero Civil, Universidad Técnica Federico Santa María, Departamento de Obras Civiles, Valparaíso, Chile.
- Chai, Y.H., and Elayer, D.T., 1999, “Lateral stability of reinforced concrete columns under axial reversed cyclic tension and compression,” *Structural Journal*, Vol. 96, No. 5, pp. 780-789.
- Comerio, M.C., 2013, *Housing Recovery in Chile: A Quantitative Mid-Program Review*, Report No 2013-01, Pacific Earthquake Engineering Research Center, Berkeley, California.
- Corley, W.G., Fiorato, A.E., and Oesterle, R.G., 1981, “Structural walls,” *Structural Journal*, Vol. 72, No. 4, pp. 77-132.
- Cowan, H., Beattie, G., Hill, K., Evans, N., McGhie, C., Gibson, G., Lawrance, G., Hamilton, J., Allan, P., Bryant, M., Davis, M., Hyland, C., Oyarzo-Vera, C., Quintana-Gallo, P., and Smith, P., 2011, “The M8.8 Chile Earthquake, 27 February 2010,” *New Zealand Society of Earthquake Engineering Bulletin*, Vol. 44, No. 3, pp. 123-166.
- CSI, 2011, *User Guide PERFORM-3DTM Nonlinear Analysis and Performance Assessment for 3D Structures, Version 5*, Computers and Structures, Inc., Berkeley, California.

- CSI, 2013a, *Extended Three Dimensional Analysis of Building Systems*, ETABS, Computers and Structures, Inc., Berkeley, California, <http://www.csiamerica.com/etabs2013>.
- CSI, 2013b, *Integrated Software for Structural Analysis and Design*, SAP2000, Computers and Structures, Inc., Berkeley, California, <http://www.csiamerica.com/sap2000>.
- CSI, 2013c, *Nonlinear Analysis and Performance Assessment for 3D Structures*, PERFORM-3D, Computers and Structures, Inc., Berkeley, California, <http://legacy.csiamerica.com/perform3d/overview>.
- DICTUC, 2010a, *Informe de Levantamiento de Daños Edificio Centro Mayor, Concepción*, Informe No. 906576/10-056-EE-01-R0, División Ingeniería Estructural y Geotécnica, Área Ingeniería Estructural, filial de la Pontificia Universidad Católica de Chile, Santiago, Chile.
- DICTUC, 2010b, *Verificación de Correcta Ejecución de las Obras Conforme a Diseño Edificio Centro Mayor, Concepción*, Informe No. 906576/10-056-EN-01-R0, División Ingeniería Estructural y Geotécnica, Área Ingeniería Estructural, filial de la Pontificia Universidad Católica de Chile, Santiago, Chile.
- DICTUC, 2010c, *Inspección Visual de Daños Estructurales Tras Sismo Del 27 de Febrero de 2010 Edificio Plaza del Rio Torre A, Salas 1343 Concepción*, Informe No. 879068, División Ingeniería Estructural y Geotécnica, Área Ingeniería Estructural, filial de la Pontificia Universidad Católica de Chile, Santiago, Chile.
- DICTUC, 2010d, *Inspección Visual y Levantamiento de Daño Edificio Alto Huerto*, Informe No. 906575/10-056-EE-01-R0, División Ingeniería Estructural y Geotécnica, Área Ingeniería Estructural, filial de la Pontificia Universidad Católica de Chile, Santiago, Chile.
- DICTUC, 2010e, *Contrastación de la Existencia en Terreno de Elementos de Confinamiento de Borde y del Plano de Algunos Muros Versus Especificaciones de Planos Estructurales Tras Sismo del 27 Febrero de 2010*, Informe No. 878055, División Ingeniería Estructural y Geotécnica, Área Ingeniería Estructural, filial de la Pontificia Universidad Católica de Chile, Santiago, Chile.
- EERI, 2010, "The Mw 8.8 Chile Earthquake of February 27, 2010," *EERI Newsletter*, June 2010, Vol. 44, No. 6, Earthquake Engineering Research Institute, Oakland, California.

- EERI, 2011, "The M 6.3 Christchurch, New Zealand, Earthquake of February 22, 2011," *EERI Special Earthquake Report*, May 2011, Earthquake Engineering Research Institute, Oakland, California.
- Elnashai, A.S., Gencturk, B., Kwon, O.-S., Hashash, Y., Kim, S.J., Jeong, S.-H., and Dukes, J., 2012, "The Maule (Chile) earthquake of February 27, 2010: Development of hazard, site specific ground motions and back-analysis of structures," *Soil Dynamics and Earthquake Engineering*, Vol. 42, pp. 229-245.
- Engineers Association of Chile, 2010, *Informe Técnico Del Colegio De Ingenieros De Chile A.G. Sobre Los Efectos Del Terremoto En Edificaciones De Las Regiones Metropolitana, V Y VI*, Colegio de Ingenieros de Chile (Engineers Association of Chile), accessed June 30, 2012, http://www.ingenieros.cl/index.php?option=com_content&task=view&id=441&Itemid=451.
- FEMA, 1999, *Evaluation of Earthquake Damaged Concrete and Masonry Wall Buildings*, FEMA P-306, prepared by the Applied Technology Council for the Federal Emergency Management Agency, Washington, D.C.
- FEMA, 2000, *Prestandard and Commentary for the Seismic Rehabilitation of Buildings*, FEMA 356, prepared by the American Society of Civil Engineers for the Federal Emergency Management Agency, Washington, D.C.
- FEMA, 2009, *Quantification of Building Seismic Performance Factors*, FEMA P-695, prepared by Applied Technology Council for Federal Emergency Management Agency, Washington, D.C.
- GUC, 2010, "Terremoto Cauquenes 27 Febrero 2010," *Centro Sismológico Nacional*, Department of Geophysics, University of Chile, accessed April 23, 2012, <http://www.sismologia.cl/seismo.html>.
- Hines, E., Restrepo, J.I., and Seible, F., 2004, "Force-displacement characterization of well-confined bridge piers," *Structural Journal*, Vol. 101, No. 4, pp. 537-548.
- ICBO, 1997, *Uniform Building Code*, International Conference of Building Officials, Whittier, California.
- ICC, 2000, *International Building Code*, International Code Council, Washington, D.C.
- ICC, 2009, *International Building Code*, International Code Council, Washington, D.C.
- IDIEM, 2010, *Peritaje Estructural Edificio Alto Río, Ciudad de Concepción, Informe Final, Descripción de Caída y Factores Asociados al Colapso*, Informe No.

- 644.424-00, Centro de Investigación, Desarrollo e Innovación de Estructuras y Materiales (IDIEM), University of Chile, Santiago, Chile.
- INN, 1985, *Concrete – General Requirements*, NCh170.Of 1985, Instituto Nacional de Normalización, Santiago, Chile.
- INN, 1996, *Earthquake Resistant Design of Buildings*, NCh433.Of96, Instituto Nacional de Normalización, Santiago, Chile.
- INN, 2006, *Reinforcing Steel – Hot-Rolled Rebar for Reinforced Concrete*, NCh204.Of2006, Instituto Nacional de Normalización, Santiago, Chile.
- INN, 2008, *Reinforced Concrete Design and Analysis Requirements*, NCh430.Of2008, Instituto Nacional de Normalización, Santiago, Chile.
- Kabeyasawa T., Shiohara H., Otani S., and Aoyama H., 1983, “Analysis of the full-scale seven-story reinforced concrete test structure,” *Journal of the Faculty of Engineering*, University of Tokyo, Tokyo, Japan, Vol. 37, No. 2, pp. 431-478.
- Kohrangi, M., Sullivan, T.J., and Calvi, G.M., 2012, “Seismic assessment of a 15-story building damaged in the Chile Earthquake of February 27th 2010,” *15th World Conference on Earthquake Engineering*, Lisbon, Portugal, Paper No. 2840.
- Lagos, R., and Kupfer, M., 2012, “Performance of high rise buildings under the February 27th 2010 Chilean Earthquake,” *International Symposium on Engineering Lessons Learned from the 2011 Great East Japan Earthquake*, Japan Association for Earthquake Engineering, Tokyo, Japan, Vol. 1, pp. 1754-1765.
- LATBSDC, 2011, *An Alternative Procedure for Seismic Analysis and Design of Tall Buildings Located in the Los Angeles Region*, Los Angeles Tall Buildings Structural Design Council, Los Angeles, California.
- Lehman, D.E., Turgeon, J.A., Birely, A.C, Hart, C.R., Marley, K.P, Kuchma, D.A., and Lowes, L.N., 2013, “Seismic behavior of a modern coupled wall,” *Journal of Structural Engineering*, Vol. 139, Special Issue NEES 2: Advances in Earthquake Engineering, pp. 1371-1381.
- Lemnitzer, A., Skolnik, D.A., Massone, L., de la Lerra, J.C., and Wallace, J.W., 2012, “Seismic monitoring of reinforced concrete buildings following the M_w 8.8 Feb 27th, 2010 offshore Maule Earthquake in Chile,” *15th World Conference on Earthquake Engineering*, Lisbon, Portugal, Paper No. 4515.
- Lowes, L., Lehman, D., Birely, A., Kuchma, D., Hart, C., and Marley, K., 2011, “Behavior, analysis, and design of complex wall systems: planar wall test

- program summary document,” *NEESHub*, published on October 17, 2011, <http://nees.org/resources/3677>.
- Lowes, L.N., Lehman, D.E., Birely, A.C., Kuchma, D.A., Marley, K.P., and Hart, C.R., 2012, “Earthquake response of slender planar concrete walls with modern detailing,” *Engineering Structures*, Vol. 43, October 2012, pp. 31-47.
- LSTC, 2013, *LS-DYNA*, Livermore Software Technology Corporation, Livermore, California, <http://www.lstc.com/products/ls-dyna>.
- Maffei, J., Comartin, C., Kehoe, B., Kingsley, G., and Lizundia, B., 2000, “Evaluation of earthquake damaged concrete and masonry wall buildings,” *Earthquake Spectra*, Vol. 16, Iss. 1, pp. 263-283.
- Mander, J., Priestley, M., and Park, R., 1988, “Theoretical stress - strain model for confined concrete.” *Journal of Structural Engineering*, Vol. 114, No. 8, pp. 1804-1826.
- Massone, L.M., Bonelli, P., Lagos, R., Luders, C., Moehle, J., and Wallace, J.W., 2012, “Seismic design and construction practices for RC structural wall buildings,” *Earthquake Spectra*, Vol. 28, No. S1, pp. S245-S256.
- Mattock, A.H., 1967, “Discussion of rotational capacity of hinging regions in reinforced concrete beams,” *Journal of the Structural Division*, Vol. 93, No. ST2, pp. 519-522.
- Mohr, D., 2007, *Nonlinear Analysis and Performance Based Design Methods for Reinforced Concrete Coupled Shear Walls*, Master’s Thesis, University of Washington, Seattle, Washington.
- Naeim, F., Schindler, B., Martin, J.A., and Lynch, S., 1990, “Hidden zones of high stress in seismic response of structural walls,” *Proceedings*, Structural Engineers Association of California Convention, pp. 402-422.
- Nagae, T., Tahara, K., Matsumori, T., Shiohara, H., Kabeyasawa, T., Kono, S., Nishiyama, M., Wallace, J.W., Ghannoum, W., Moehle, J.P., Sause, R., Keller, W., and Tuna, Z., 2011, *Design and Instrumentation of the 2010 E-Defense Four-Story Reinforced Concrete and Post-Tensioned Concrete Buildings*, Report No 2011-104, Pacific Earthquake Engineering Research Center, Berkeley, California.
- NIST, 2011, *Seismic Design of Cast-in-Place Concrete Special Structural Walls and Coupling Beams: A Guide for Practicing Engineers*, NIST GCR 11-917-11 REV-1, prepared by the NEHRP Consultants Joint Venture, a partnership of the Applied Technology Council and the Consortium for Universities for

Research in Earthquake Engineering, for the National Institute of Standards and Technology, Gaithersburg, Maryland.

NIST, 2012, *Comparison of U.S. and Chilean Building Code Requirements and Seismic Design Practice 1985-2010*, NIST GCR 12-917-18, prepared by the NEHRP Consultants Joint Venture, a partnership of the Applied Technology Council and the Consortium for Universities for Research in Earthquake Engineering, for the National Institute of Standards and Technology, Gaithersburg, Maryland.

OpenSees, 2013, *Open System for Earthquake Engineering Simulation*, OpenSees, Pacific Earthquake Engineering Research Center, Berkeley, California, <http://opensees.berkeley.edu>.

Orakcal, K., and Wallace, J.W., 2006, "Flexural modeling of reinforced concrete walls-experimental verification," *Structural Journal*, Vol. 103, No. 2, pp. 196-206.

Panagiotakos, T.B., and Fardis, M.N., 2001, "Deformations of reinforced concrete members at yielding and ultimate," *Structural Journal*, Vol. 98, No. 2, pp. 135-148.

Parra, P.F., and Moehle, J.P., 2014, *Lateral Buckling in Reinforced Concrete Walls*, Report UCB/SEMM-2014/01, University of California, Berkeley, California.

Paulay, T., and Priestley, M.J.N., 1993, "Stability of ductile structural walls," *Structural Journal*, Vol. 90, No. 4, pp. 385-392.

PCA, 2008, *Concrete Floors on Ground*, EB075.03, Fourth Edition, Portland Cement Association, Skokie, Illinois.

Pugh, J., 2012, *Numerical Simulation of Walls and Seismic Design Recommendations for Walled Buildings*, Ph.D. Dissertation, University of Washington, Seattle, Washington.

Rodriguez, M.E., Botero, J.C., and Villa, J., 1999, "Cyclic stress-strain behavior of reinforcing steel including effect of buckling," *Journal of Structural Engineering*, Vol. 125, No. 6, pp. 605-612.

Sawyer, H.A., 1965, "Design of concrete frames for two failure stages," *ASCE-ACI Proceedings of the International Symposium on Flexural Mechanics of Reinforced Concrete*, Miami, Florida, Vol. 12, pp. 405-431.

Sheikh, S.A., and Khoury, S.S., 1993, "Confined concrete columns with stubs," *Structural Journal*, Vol. 90, No. 4, pp. 414-431.

Shimazaki, K., and Sozen, M.A., 1984, "Seismic drift of reinforced concrete structures," *Research Reports*, Hazama-Gumi, Ltd., Minato, Tokyo, Japan, pp. 145-166.

- SNZ, 2006a, *Concrete Structures Standard, Part 1 – The Design of Concrete Structures*, NZS 3101: Part 1: 2006, Standards New Zealand, Wellington, New Zealand.
- SNZ, 2006b, *Concrete Structures Standard, Part 2 – Commentary*, NZS 3101: Part 2: 2006, Standards New Zealand, Wellington, New Zealand.
- Song, C., Pujol, S., and Lepage, A., 2012, “The collapse of the Alto Río building during the 27 February 2010 Maule, Chile, earthquake,” *Earthquake Spectra*, Vol. 28, No. S1, pp. S301-S334.
- Sozen, M.A., Monteiro, P., Moehle, J.P., and Tang, H.T., 1992, “Effects of cracking and age on stiffness of reinforced concrete walls resisting in-plane shear,” *Proceedings, Fourth Symposium on Current Issues Related to Nuclear Power Plant Structures, Equipment and Piping*, Orlando, Florida.
- Tabata, T., Nishihara, H., and Suzuki, H., 2003, “Ductility of reinforced concrete shear walls without column shape,” *Proceedings of the Japan Concrete Institute*, Vol. 25, No. 2, pp. 625-630 (in Japanese).
- Takahashi, S., Yoshida, K., Ichinose, T., Sanada, Y., Matsumoto, K., Fukuyama, H., and Suwada, H., 2011, “Flexural drift capacity of reinforced concrete walls with limited confinement,” *Structural Journal*, Paper S-2011-062, Vol. 110, No. 1, pp. 95-104.
- Tanyeri, A.C., and Moehle, J.P., 2014, *Collapse of a Concrete Wall Building in the 2010 Chile Earthquake*, Report UCB/SEMM-2014/02, University of California, Berkeley, California.
- Thomsen IV, J.H., and Wallace, J.W., 1995, *Displacement-Based Design of RC Structural Walls: An Experimental Investigation of Walls with Rectangular and T-Shaped Cross-Sections*, Report No. CU/CEE-95/06, Department of Civil and Environmental Engineering, Clarkson University, Potsdam, New York.
- Thomsen IV, J.H., and Wallace, J.W., 2004, “Displacement-based design of slender reinforced concrete structural walls – Experimental verification,” *Journal of Structural Engineering*, Vol. 130, No. 4, pp. 618-630.
- Tran, T.A., 2012, *Experimental and Analytical Studies of Moderate Aspect Ratio Reinforced Concrete Structural Walls*, Ph.D. Dissertation, Department of Civil and Environmental Engineering, University of California, Los Angeles, California.
- Tuna, Z., 2012, *Seismic Performance, Modeling, and Failure Assessment of Reinforced Concrete Shear Wall Buildings*, Ph.D. Dissertation, University of California, Los Angeles, California.

- Tuna, Z., and Wallace, J.W., 2014 (in press), "Collapse assessment of the Alto Rio building in the 2010 Chile Earthquake," *Earthquake Spectra* (accepted for publication in 2014).
- Turgeon, J., 2011, *The Seismic Performance of Coupled Reinforced Concrete Walls*, Master's Thesis, University of Washington, Seattle, Washington.
- Uribe, F.Y., and Ruiz, E.S., 2010, "Descripción de caída y factores asociados al colapso," *Peritaje Estructural Edificio Alto Rio*, Centro de Investigación, Desarrollo e Innovación de Estructuras y Materiales (IDIEM), University of Chile, Santiago, Chile, pp. 34-35.
- University of Chile, 2012, "2010 1002271 Terremoto del Maule," *Terremotos de Chile / Earthquakes of Chile*, accessed March 22, 2012, <http://terremotos.ing.uchile.cl/registros/164>.
- USGS, 2010, "Offshore Maule, Chile, Earthquake," *National Strong-Motion Project*, United States Geological Survey, last updated May 5, 2010, http://nsmp.wr.usgs.gov/data_sets/20100227_0634.html.
- USGS, 2011, *Pager - M 8.8 - Offshore Maule, Chile*, United States Geological Survey, last updated September 19, 2011, <http://earthquake.usgs.gov/earthquakes/pager/events/us/2010tfan/index.html>.
- USGS, 2013a, *Historic World Earthquakes*, United States Geological Survey, last updated March 06, 2013, http://earthquake.usgs.gov/earthquakes/world/historical_country.php.
- USGS, 2013b, *Magnitude 8.8 - Offshore Bio-Bio, Chile*, United States Geological Survey, last updated May 08, 2013, <http://earthquake.usgs.gov/earthquakes/eqinthenews/2010/us2010tfan/#summary>.
- Wallace, J.W., 1996, "Evaluation of UBC-94 provisions for seismic design of RC structural walls," *Earthquake Spectra*, Vol. 12, No. 2, pp. 327-348.
- Wallace, J.W., and Ibrahim, Y.A., 1996, *BIAX: A Computer Program for the Analysis of Reinforced Concrete and Reinforced Masonry Cross Sections*.
- Wallace, J.W., and Moehle, J.P., 1992, "Ductility and detailing requirements of bearing wall buildings," *Journal of Structural Engineering*, Vol. 118, No. 6, pp. 1625-1644.
- Wallace, J.W., and Orakcal, K., 2002, "ACI 318-99 provisions for seismic design of structural walls," *Structural Journal*, Vol. 99, No. 4, pp. 499-508.
- Westenenk, B., de la Llera, J.C., Besa, J.J., Jünemann, R., Moehle, J.P., Lüders, C., Inaudi, J.A., Elwood, K.J., and Hwang, S.-J., 2012, "Response of reinforced concrete buildings in Concepción during the Maule earthquake," *Earthquake Spectra*, Vol. 28, No. S1, pp. S257-S280.

Zhang, D., Federico, G., Telleen, K., Schellenberg, A., Fleischman, R., and Maffei, J., 2011, "Structural analysis to replicate observed damage to engineered buildings from the January 2010 Haiti Earthquake," *Proceedings, Structures Congress 2011*, Las Vegas, Nevada.

Project Participants

National Institute of Standards and Technology

John (Jack) R. Hayes, Jr.
Engineering Laboratory (MS8604)
National Institute of Standards and Technology
100 Bureau Drive
Gaithersburg, Maryland 20899
www.NEHRP.gov

Steven L. McCabe
Engineering Laboratory (MS8604)
National Institute of Standards and Technology
100 Bureau Drive
Gaithersburg, Maryland 20899
www.NEHRP.gov

NEHRP Consultants Joint Venture

APPLIED TECHNOLOGY COUNCIL
201 Redwood Shores Parkway, Suite 240
Redwood City, California 94065
www.ATCouncil.org

CONSORTIUM OF UNIVERSITIES FOR
RESEARCH IN EARTHQUAKE ENGINEERING
1301 S. 46th Street, Building 420
Richmond, California 94804
www.CUREE.org

Joint Venture Management Committee

James R. Harris
J.R. Harris & Company
1775 Sherman Street, Suite 2000
Denver, Colorado 80203

Christopher Rojahn
Applied Technology Council
201 Redwood Shores Parkway, Suite 240
Redwood City, California 94065

Robert Reitherman
Consortium of Universities for Research in
Earthquake Engineering
1301 S. 46th Street, Building 420
Richmond, California 94804

Andrew Whittaker
University at Buffalo
Dept. of Civil, Structural, and Environ. Engin.
230 Ketter Hall
Buffalo, New York 14260

Joint Venture Program Committee

Jon A. Heintz (Program Manager)
Applied Technology Council
201 Redwood Shores Parkway, Suite 240
Redwood City, California 94065

William T. Holmes
Rutherford + Chekene
55 Second Street, Suite 600
San Francisco, California 94105

Michael Constantinou
University at Buffalo
Dept. of Civil, Structural, and Environ. Engin.
132 Ketter Hall
Buffalo, New York 14260

Jack Moehle
University of California, Berkeley
Dept. of Civil and Environmental Engineering
325 Davis Hall – MC 1792
Berkeley, California 94720

C.B. Crouse
URS Corporation
1501 4th Avenue, Suite 1400
Seattle, Washington 98101

James R. Harris (ex-officio)
Andrew Whittaker (ex-officio)

Project Technical Committee

Joseph Maffei (Project Director)
Maffei Structural Engineering
148 Hermosa Avenue
Oakland, California 94618

Patricio Bonelli
Patricio Bonelli y Asociados LTDA.
Montana 853, Of. 401
Viña del Mar, Chile

Dominic J. Kelly
Simpson Gumpertz & Heger, Inc.
41 Seyon Street
Building 1, Suite 500
Waltham, Massachusetts 02453

Dawn E. Lehman
University of Washington
Dept. of Civil and Environmental Engineering
214 B More Hall
Seattle, Washington 98195

Laura N. Lowes
University of Washington
Dept. of Civil and Environmental Engineering
233 C More Hall
Seattle, Washington 98195

Project Review Panel

S.K. Ghosh
S.K. Ghosh Associates, Inc.
334 East Colfax Street
Palatine, Illinois 60067

Tara Hutchinson
University of California, San Diego
Dept. of Structural Engineering
9500 Gilman Drive
La Jolla, California 92093

Working Group Members

Begoña Aguirre
Av. Blanca Estela 1661
Lomas de Montemar, Concón
V region, Chile

Jack Moehle
University of California, Berkeley
Dept. of Civil and Environmental Engineering
325 Davis Hall – MC 1792
Berkeley, California 94720

Karl Telleen
Maffei Structural Engineering
148 Hermosa Avenue
Oakland, California 94618

John W. Wallace
University of California, Los Angeles
Dept. of Civil and Environmental Engineering
731C Boelter Hall
Los Angeles, California 90095

Michael Willford
Arup North America Ltd.
560 Mission Street, Suite 700
San Francisco, California 94105

Derrick Roorda
Buro Happold
140 Geary Street, 8th Floor
San Francisco, California 94108

Mete Sozen
Purdue University
Lyles School of Civil Engineering
550 Stadium Mall Drive
West Lafayette, Indiana 47907

Ady Aviram
Simpson Gumpertz & Heger, Inc.
100 Pine Street, Suite 1600
San Francisco, California 94111

Anna Birely
Texas A&M University
Department of Civil Engineering
3136 TAMU
College Station, Texas 77843

Chris Hilson
University of California, Los Angeles
3710 Midvale Avenue, #203
Los Angeles, California 90034

Yuli Huang
Arup North America Ltd.
560 Mission Street, Suite 700
San Francisco, California 94105

Pablo Parra
University of California, Berkeley
435 Davis Hall
Berkeley, California 94720